BIOSCORODITE:

Biological crystallization of scorodite for arsenic removal

Thesis committee

Thesis supervisor
Prof. dr. ir. C.J.N. Buisman
Professor of Biological Recovery and Reuse Technology
Wageningen University

Thesis co-supervisor
Dr. ir. J. Weijma
Researcher at the sub-department of Environmental Technology
Wageningen University

Other members
Prof. dr. P.C. de Ruiter, Wageningen University
Prof. dr. G.J.W. Euverink, University of Groningen
Dr. G. van Weert, Oretome Limited, Caledon East, Canada
Dr. ir. J.L. Huisman, Paques B.V., Balk

This research was conducted under the auspices of the Graduate School SENSE (Socio-economic and Natural Sciences of the Environment).

BIOSCORODITE:

Biological crystallization of scorodite for arsenic removal

Paula Andrea Gonzalez Contreras

Thesis

submitted in fulfilment of the requirements for the degree of doctor
at Wageningen University
by the authority of the Rector Magnificus
Prof. dr. M.J. Kropff,
in the presence of the
Thesis Committee appointed by the Academic Board
to be defended in public
on Friday 22 June 2012
at 11 a.m. in the Aula.

Paula Andrea Gonzalez Contreras
Bioscorodite: Biological crystallization of scorodite for arsenic removal, 206 pages.

Thesis, Wageningen University, Wageningen, NL (2012)
With references, with summaries in Dutch and English.
ISBN: 978-94-6173-294-1

"Every search begins with beginner's luck and ends with the victor's being severely tested"

Paulo Coelho (from The Alchemist)

CONTENTS

Chapter 1

General Introduction

1.1 INTRODUCTION

1.1.1 Arsenic chemistry and mineralogy

Arsenic is a metalloid that is found in four oxidation states -3 (arsine), 0 (arsenic), 3 (arsenite) and 5 (arsenate). Arsenic has only one stable isotope (^{75}As) and is the 47th in abundance among the 88 naturally occurring elements [86, 163].

Minerals containing arsenic can be classified in elemental arsenic, arsenide, arsenosulfide, arsenites and arsenates. Arsenic, arsenide and arsenosulfides are associated with anoxic hydrothermal ore deposits and metamorphic and intrusive igneous rocks [86, 131]. Once these minerals are exposed to oxygen and water under surface or near-surface conditions, they weather to arsenite and arsenate minerals. In Table 1.1, several common arsenic-bearing minerals are classified by their origin: hydrothermal deposits or weathering product.

TABLE 1.1 Common arsenic-bearing minerals occurring in nature classified by their origin (adapted after [86, 131])

Origin: hydrothermal deposits			**Origin: weathering product**		
Mineral	Formula	Mineral Group	Mineral	Formula	Mineral Group
Arsenic	As(0)	Elemental	Arsenolite	As_2O_3	Arsenite
Arsenopyrite	FeAsS	Arsenosulfide	Claudetite	As_2O_3	Arsenite
Cobaltite	(Co,Fe)AsS	Arsenosulfide	Mansfieldite	$AlAsO_4 \cdot 2H_2O$	Arsenate
Orpiment	As_2S_3	Arsenosulfide	Olivenite	Cu_2OHAsO_4	Arsenate
Realgar	AsS (As_4S_4)	Arsenosulfide	Pharmaco-siderite	$Fe_3(AsO_4)_2(OH)_3 \cdot 5H_2O$	Arsenate
Enargite	Cu_3AsS_4	Arsenic sulfosalts	Scorodite	$FeAsO_4 \cdot 2H_2O$	Arsenate

In contrast to heavy metals, the aqueous chemistry of arsenic cannot be used to control its mobilization. Arsenic species are mobile in a wide pH range, at both reduced or oxidized conditions by biological activity [86].

In oxygenated environments, arsenic is mainly found in the oxidation state of +5. Arsenic (As^{5+}) appears as H_3AsO_4 at pH values below 2. In the pH range from 2 to 11 H_3AsO_4 dissociates to $H_2AsO_4^-$ and $HAsO_4^{2-}$ [86]. At low Eh values arsenic is found in the oxidation state +3 as H_3AsO_3. Up to pH 9 H_3AsO_3 does not dissociate. At higher pH values it appears as $H_2AsO_3^-$, $HAsO_3^{2-}$ and AsO_3^{3-} [86].

In reduced environments (at redox potential below -250 mV), arsenic compounds such as orpiment (As_2S_3) can be formed in the presence of sulphur or hydrogen sulphide [16]. Arsine and elemental arsenic are formed under very strong reducing conditions [16, 86].

1.1.2 Arsenic toxicity

Humans may be exposed to inorganic arsenic via air, drinking water, food and soil. The effects of arsenic exposure include a variety of skin cancer, internal cancers, cardiovascular, peripheral vascular disease, diabetes and adverse reproductive outcomes [92]. In the case of arsenic, toxicity is related to its speciation. The most toxic form of arsenic is arsine gas (AsH_3), followed by arsenic trioxide, sodium arsenite, sodium arsenate, monomethylarsonic acid, dimethylarsinic acid and trimethylarsine [16, 61, 163].

The pathophysiology of arsenic is complex. At high dosage levels, arsenic disrupts the fundamental functioning of cells [163]. Ingested arsenic is quickly absorbed from the gastrointestinal tract and reduced from pentavalent to trivalent arsenic forms. These reduced species are then methylated to monomethylarsonic acid (MMA) and to dimethylarsinic acid (DMA). This methylation process is considered the detoxification pathway of inorganic arsenic, as MMA and DMA are less toxic species [16, 92]. Although methylation facilitates arsenic excretion from the body, not all the arsenic is completely methylated. Around 70% of the arsenic intake is excreted with the urine within 2 days [61]. The average fractions of arsenic metabolites in urine are 15-25% inorganic arsenic, 10-15% MMA and 70-80% DMA [61, 92]. Normal levels of arsenic in the urine of people with no known high exposure are in the range of 5-50 μg As L^{-1}. However, the consumption of seafood may increase concentrations up to 1 mg As L^{-1} [61].

1.1.3 Biological transformations of arsenic

Although arsenic is toxic to humans, some organisms have evolved to tolerate this metalloid up to 20 g L^{-1} [39, 80, 114, 135, 158, 161]. Organisms can oxidize, reduce, methylate and demethylate arsenic. Two main microorganism groups that metabolize arsenic are the dissimilatory arsenate-reducing prokaryotes (DARPs) and the arsenite-oxidizing prokaryotes (AOs) [135].

The DARPs couple arsenate reduction to the oxidation of organic matter. Representative organisms of this group include proteobacteria, Gram positive bacteria, thermophilic Eubacteria and Crenarchaea [135]. These microorganisms can use several electron donors including, between hydrogen and acetate, formate, pyruvate, butyrate, citrate, succinate, fumarate, malate and glucose [115, 135].

On the other hand, AOs carry out arsenite oxidation. This group includes heterotrophic arsenite oxidizers (HAOs) and chemolithoautotrophic arsenite oxidizers (CAOs). Arsenite oxidation by HAOs is regarded as a detoxification reaction, which converts As^{3+} to As^{5+}, a less toxic form. CAOs couple arsenite oxidation to the reduction of electron acceptors such as oxygen or nitrate. The obtained energy is used to fix CO_2 into organic cellular material [115, 135]. Several researches demonstrated that arsenite can be oxidized by meso-acidophiles [32, 46, 47] and by neutro-thermophilic microorganisms such as

Thermus [70]. There is also evidence of arsenite oxidation occurring at extreme conditions. For example, Sehlin and Lindstrom reported that *Sulfolobus acidocaldarius* strain BC oxidizes arsenite at 65°C and pH 2 [152].

1.2 ARSENIC CONTAMINATION

1.2.1 Natural arsenic contamination

Arsenic is present in over 320 minerals [16, 85]. Volcanic eruptions and other processes may naturally releasing high arsenic concentrations in the environment [16].

In ground waters (pH 6.5-8.5), arsenic mobilization occurs at oxidized and reduced redox conditions [61]. Arsenic contamination in groundwater (0.1 to 5 mg L^{-1}) affects millions of people in Bangladesh, India and Pakistan [92, 121, 127]. In addition, large populations (0.3-1 million) are potentially exposed to arsenic in Nepal, China, Argentina, Chile and Mexico [92, 121, 127].

Potential health impact of naturally occurring arsenic contamination has promoted international organizations to decrease the recommended values for arsenic limit in drinking water. Thus in 2006, the WHO reduced the maximum contaminant level of arsenic from 50 to 10 μg L^{-1} in drinking water [168]. This value has been adopted by the European Union, the United States, Japan and many other countries.

1.2.2 Anthropogenic arsenic contamination sources

During the 20th century, arsenic mainly as arsenic trioxide and metal arsenic was used in feed supplements, semiconductors, wood preservatives and medicines [90]. Arsenic trioxide is mainly used to produce arsenate-based preservatives to protect wood from microorganisms (Fig. 1.1). Those include chromated copper arsenate (CCA), ammoniacal copper arsenate and ammoniacal copper zinc arsenate [90]. At the end of the century, the recognized widespread arsenic poisoning in Bangladesh and the improper disposal of arsenic-bearing waste led in some countries to establish stricter legislations. As a consequence, arsenic use was banned for several applications. Since 1990s, USA has discontinued the use of pesticides containing arsenic and since 2003, the use of CCA has been banned for a large variety of products [90]. As a consequence of these mitigation actions, arsenic trioxide consumption has decreased from 25 to 5 thousand metric tons in the last decade [100].

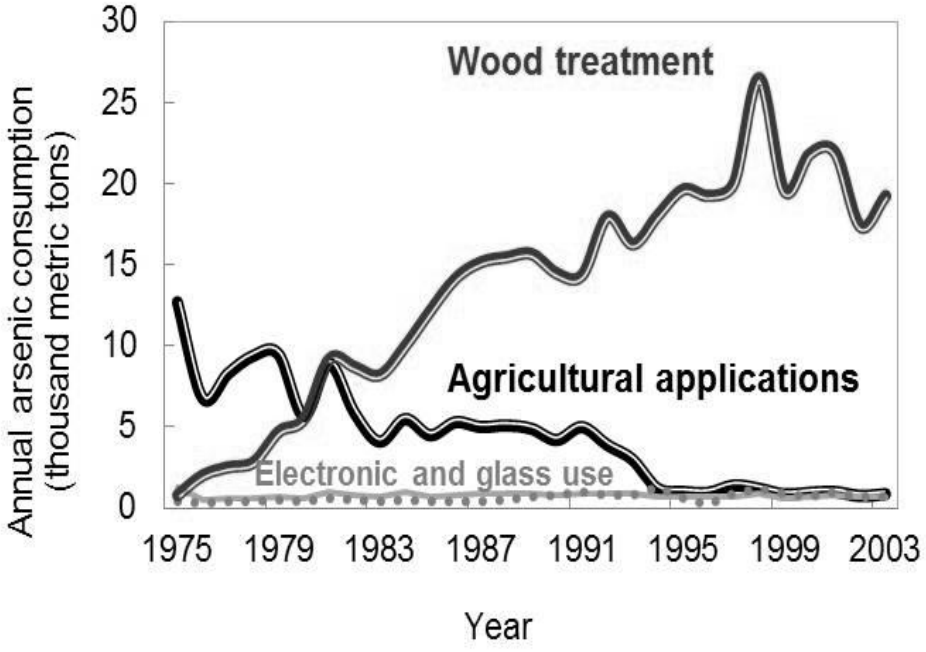

FIGURE 1.1 Arsenic (arsenic trioxide and metal arsenic) end-use in wood treatment, agricultural chemicals, glass and electronics. Data are available until 2003 (modified after ref.[100]).

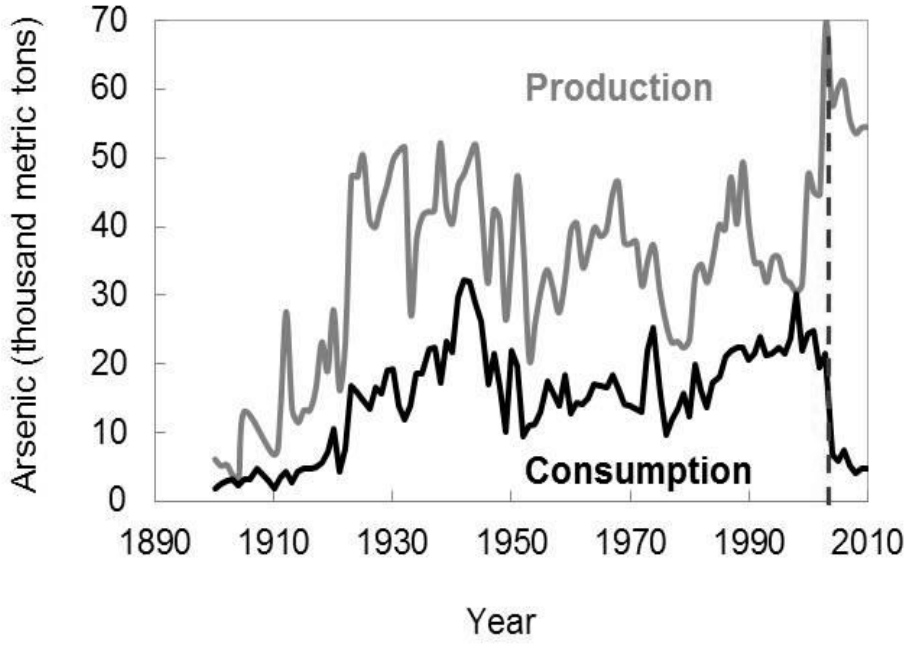

FIGURE 1.2 Arsenic production and consumption (arsenic trioxide) during the last century. Dashed line indicates arsenic consumption reduction occurred in 2004 (modified after ref.[100]).

More than 50% arsenic of worldwide arsenic consumption is used in the wood preservative industry for non-residential use [23]. The treated wood is a potential contaminant source as arsenic may be released from weathering of CCA-treated wood or from the landfilling, incineration, or recycling of wood debris [90]. In 2005 during the Hurricane Katrina, 1470 metric tons of arsenic were released from wood debris [45, 52].

Recently, gallium arsenide (GaAs) and indium arsenide (InAs) have become important materials in semiconductors being widely used in computers, electronics, such as solar cells and space research [23, 61]. The waste generated after the end user of these electronic contains arsenic mixed with other metals. For example, a mobile telephone typically contains GaAs in its circuitry (arsenic content below 1 milligram) [23]. Every new 3G cell phone and i-phone will require more GaAs in their circuits. Inappropriate recycling of electronic waste containing arsenic is a potential source of anthropogenic arsenic contamination.

Human activity has strongly influenced arsenic contamination. The disposition of industrial waste, smelting of arsenic bearing minerals and burning of fossil fuels contribute continuously to arsenic contamination spread [16, 90]. For example, during the last decade mineral processing has increased arsenic trioxide production. In 2004, arsenic trioxide production reached 70 thousand tons (Fig. 1.2). In 2010, about 55 thousand tons were worldwide produced as a by-product in China (45%), Chile (20%), Morocco (14%) and Peru (8%) [23, 100]. Arsenic trioxide that is not sold is accumulated and stored until suitable technologies for its safe disposal are developed. Current world reserves are thought to be more than one million ton [23].

The processing of minerals also contributes to the release and contamination at mine sites producing annually 20000-25000 t of solid waste of arsenic [116].

Worldwide, there are 253 sites reported in literature as arsenic contaminated sites. From these sites, 161 are contaminated due to anthropogenic source and 147 are exclusively related to mineral processing and mining waste (Table 1.2) [87]. It is clear that anthropogenic arsenic contamination is a worldwide occurring problem far away from being solved. Arsenic can be recycled but its use is being banned for all applications except in electronics. Existing arsenic waste disposal products like orpiment and arsenic trioxide are unstable solid materials. These unstable materials containing arsenic can contribute to new arsenic pollution scenarios.

TABLE 1.2 Worldwide identified/reported locations of significant arsenic contamination due to anthropogenic sources (modified after [87]). Sources considered are: (A) mining waste and processing, (B) coal mining, (C) smelter and industrial complex. Only countries having more than one contaminated site are listed.

Locations with significant anthropogenic arsenic contamination	A	B	C	Total locations
Asia: Japan (2), Malaysia (3), Philippines (3), Russia (2)	17	3	1	21
Australia (3), New Zealand (2), and the south-western pacific	5	1	1	7
Africa	5	-	-	5
Europe and Turkey: Czech Republic (2), France (3), Germany (7), Greece (4), Italy (2), Poland (2), Spain (5), Sweden (3), Turkey (2), Ukraine (2)	41	1	4	46
Canada: Ontario (8)	20	-	-	20
United States of America: California (6), Colorado (7), Montana (5), Nevada (5), New Mexico (3), Utah (3)	40	1	2	43
Central America and the Caribbean: Mexico (7)	7	-	-	7
South America: Argentina (2), Brazil (6), Chile (2)	12	-	-	12
Total	147	6	8	161

1.2.3 Arsenic legislation

Increasing environmental awareness is leading to stricter regulations in order to protect human health. During the last decades, several countries have decreased the arsenic limit in drinking water. Global regulations values for arsenic fluctuate between 5 and 50 μg L^{-1} (Table 1.3). Despite stricter legislations for drinking water, arsenic limit values for solid and liquid wastes have not decreased. Most countries follow the US-EPA recommendations and use the Toxicity Characteristic Leaching Procedure (TCLP) test [53]. TCLP test is the most used procedure with the purpose to identify arsenic bearing waste. This test involves the evaluation of solid waste at a concentration of 50 g L^{-1} in a buffered acetic acid solution (pH 5) simulating landfill disposition. The dissolution of elements is measured after 20 hours of reaction. The arsenic limit concentration in the solution is 5 mg L^{-1} below which a material is classified as “non-hazardous”. Arsenic limit concentration of the TCLP test is 500 times higher than the drinking water regulations.

TABLE 1.3 Worldwide limits for arsenic in various water/waste stream (modified after [88]).

	Drinking water (µg L^{-1})	Natural surface and groundwater (µg L^{-1})	Solid/liquid wastes (µg L^{-1})
US: New Jersey	5	-	-
Australia	7	50	-
US	10	150[a]-340[b]	5000[c]
EU	10	-	-
World Health Organization	10	-	-
Canada	10	-	-
Japan	10	10	100
Taiwan	10	-	500
Mexico	35	-	-
Bangladesh	50	-	200[d]
Argentina, Chile, China, Croatia, Ecuador, Ghana, India, Nepal, Thailand, Vietnam	50	50	-

a) Dissolved arsenic CCCs (criteria continuous concentration), b) dissolved arsenic CMC (criteria maximum concentrations), c) EPA-TCLP test and d) arsenic discharged into inland surface waters or used to irrigate land.

1.3 ARSENIC TREATMENT IN THE METALLURGICAL INDUSTRY

1.3.1 Arsenic problem in the metallurgical industry

Mining can release high concentrations of arsenic by the oxidation of sulphide minerals, either by roasting of arsenical ores or by acid mine drainage. During pyrometallurgical operations, arsenic trioxide dust is produced in the smelting and roasting of sulphides concentrates. These processes usually operate at temperatures higher than 700°C, which leads to volatize arsenic. Arsenic is mobilized as arsenic oxide with the exhaust gases. Arsenic removal from flue gases is mostly achieved by arsenic trioxide collection in electrostatic precipitators or wet gas scrubbers (up to 30%wt arsenic) and recovered as arsenic trioxide (As_2O_3). Significant amounts of arsenic can also be recovered in the acid plant tail gas with sulphuric acid. In copper electrorefineries, arsenic is a major impurity and bleed streams are commonly recycled to concentrate arsenic in the electrolyte to 20 g L^{-1} [119, 144].

Elevated arsenic concentrations are commonly found in tailings and sulphidic mine waste of gold, copper-gold, tin, lead-zinc, and some uranium ores [116]. Arsenic in mine waters is generally originated from the oxidation of arsenopyrite (FeAsS), orpiment

(As_2S_3), realgar (AsS), enargite (Cu_3AsS_4) and tennanite ($(Cu, Fe)_{12}As_4S_{13}$) [116]. Flotation tailings usually contain residual arsenic bearing sulphides and these compounds may become soluble as a result of pH changes brought about by acid mine drainage or algal activity [144].

1.3.2 Precipitation systems for arsenic removal

Mining and metallurgical activities result in the generation of large volumes of arsenic solid waste. Arsenic is removed by precipitation systems into calcium and ferric arsenates [143]. In the past century, calcium arsenate precipitation was the most used method to remove arsenic. Calcium arsenate precipitation is discontinued because it has a high instability. Calcium arsenate sludge can leach up to 900-4400 mg As L^{-1} under the TCLP test (maximum allowance test 5 mg As L^{-1}) [144].

A second precipitation system is arsenic precipitation in ferrihydrite. Arsenical ferrihydrite precipitation has been chosen by the US EPA as the best demonstrated available technology (BDAT) (Fig.1.3). Ferrihydrite has been widely used despite of the high iron consumption and neutralizing agent associated to its precipitation. Arsenical ferrihydrite precipitation requires a high iron consumption with respect to arsenic, i.e. Fe/As > 4 and therefore large amounts of waste material are produced [143, 159]. Riveros *et al.* [144] describe examples of the use of arsenical ferrihydrite in the metallurgical industry denoting a high iron consumption. Not only Fe/As molar ratio higher than 4 are used for arsenical ferrihydrite precipitation, but also Fe/As molar ratio higher than 10 are used [144]. The excessive use of iron leads to large sludge production. For example, around 40 ton per day of residue are produced by arsenical ferrihydrite precipitation, which only contains between 300-500 kg As per day [144].

In addition to iron consumption, arsenical ferrihydrite precipitation also consumes neutralizing agent (lime) to adjust the pH value between 3 and 4 and later is adjusted to pH value between 7 and 9 [144].

Arsenical ferrihydrite precipitates contain around 0.5-2%wt of arsenic with a maximum solid content of 20-25%wt, which difficult the solid-liquid separation [143]. The disposal and storage of these compounds is not entirely safe as they easily undergo physical and chemical changes with time, resulting in arsenic releases into the environment. Even EPA still has concerns about the stability of arsenic bearing ferrihydrite precipitates under long term storage conditions [143, 157, 159]. Arsenic adsorption in ferrihydrite can also be affected by ions as phosphate, sulphate, carbonate, and dissolved organic species, affecting the removal of arsenic and the relative long term stability of ferrihydrite [159]. Some authors suggest that arsenical ferrihydrite can be considered stable when an Fe/As molar ratio higher than 4 is provided, a pH slightly acidic is kept and the contact with

reducing substances such as reactive sulphides or reducing conditions as deep water, bacteria or algae is avoided [144].

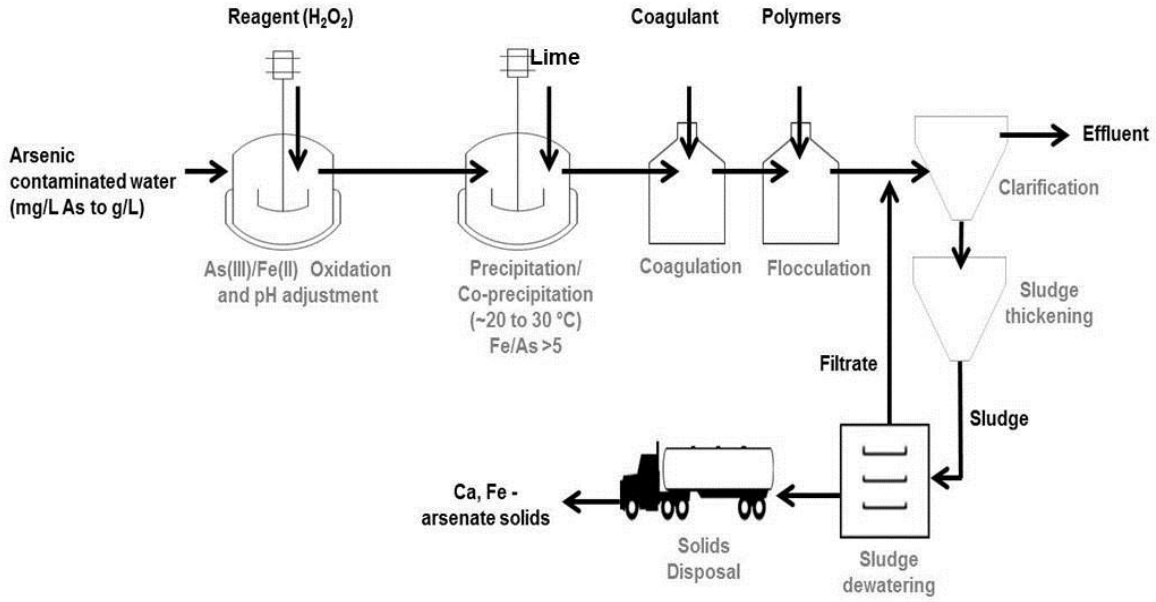

FIGURE 1.3 Scheme for general iron precipitation system for arsenic treatment (modified after ref. [89]).

1.3.3 Scorodite precipitation

Crystalline ferric arsenate, known as scorodite ($FeAsO_4 \cdot 2H_2O$), is a naturally occurring secondary supergene arsenic mineral. Scorodite formation and dissolution can be important in controlling arsenic mobility in acid mine drainage, hot springs, surface and near-surface waters. Because its low solubility, high arsenic content (25-30%wt.), high stability and compactness, scorodite presently is considered an attractive medium for arsenic stabilization and the safest storage material [42, 105, 106, 128, 145].

Hydrothermal scorodite crystallization has been applied for arsenic immobilization from metallurgical streams. This process employs acid pressure oxidation with temperatures above 150°C and oxygen overpressures of up to 2000 kPa [37, 48, 59, 143, 144]. Initially, hydrothermal scorodite was produced at pH 0.7 in ferric nitrate medium and temperatures of 125°C (ideally 160°C) were needed to ensure good crystallinity [144]. The pH range between 0.2 and 1.8 did not affect the structure or composition of scorodite, but arsenic concentrations (As^{5+}) higher than 15 g L^{-1} were required to obtain a pure product [144]. Because hydrothermal scorodite crystallization requires autoclave systems at high temperature and high pressure, the technology is not widely applied.

Atmospheric scorodite precipitation at lower temperatures (T<95°C) has been considered as an alternative to hydrothermal crystallization. The feasibility of atmospheric scorodite precipitation was demonstrated by Demopoulos and co-workers at McGill University in Canada [36]. The method is based on the concept of saturation control, which is the primary crystallization parameter that controls the nucleation-growth process. Saturation control was achieved by step wise neutralization of the supersaturated solution. Ambient-pressure crystallization of scorodite was demonstrated using arsenic concentrate solutions (>10 g As^{5+} L^{-1}) and stepwise neutralization from pH 0.9 to 4 [38, 154, 155]. The maintenance of a low saturation level in combination with the addition of seed materials effectively resulted in lowering the crystallization temperature to 80-95°C (Fig. 1.4) [38, 154, 155]. Atmospheric scorodite crystallization needs the addition of seed crystals. With this purpose, hydrothermally produced parent seeds and gypsum crystals have been used. Streams containing ferrous iron (Fe^{2+}) and arsenite (As^{3+}) have been also used. After chemical oxidation to ferric and arsenate, scorodite is produced by step wise neutralization as described above [26, 65].

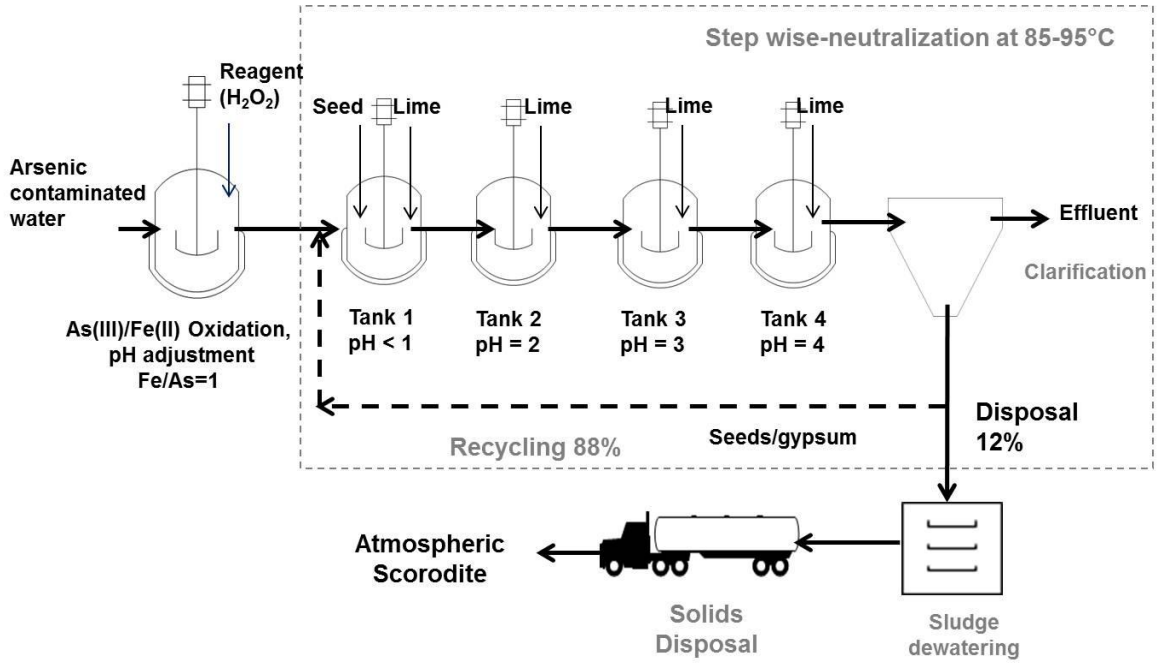

FIGURE 1.4 Scheme for atmospheric scorodite precipitation system for arsenic treatment (based on [38, 154, 155]).

The majority of the metallurgical streams have diluted arsenic concentrations, commonly ranging from 1 to 3 g As L^{-1}. In contrary to the relatively dilute arsenic concentrations found in metallurgical streams, most studies conducted on atmospheric

scorodite precipitation use arsenic concentrations ranging from 10 to 50 g As L^{-1} [38, 65, 154]. There is only one study that demonstrates scorodite precipitation using dilute arsenic streams up to 2 g L^{-1} at 95°C [27]. The feasibility of scorodite precipitation using diluted arsenic streams depended on scorodite seed addition and recycling of seed material (30 to 40 g L^{-1} scorodite). In this process, arsenic efficiency removal was depended of the seed recycling. No seeds recycling resulted in no removal of arsenic.

The formation of scorodite is expensive because it has traditionally required high temperatures which are normally obtained by the use of autoclave technology. Feasibility of the scorodite process can be significantly improved with the precipitation at atmospheric temperature (90°C) decreasing the cost. The use of seeds and neutralizing agents for step wise neutralization systems may become a bottle neck in the atmospheric crystallization of scorodite. The occurrence of atmospheric precipitation of scorodite would significantly lower the cost and would make scorodite an obvious option for arsenic disposal.

1.4 BIOHYDROMETALLURGY PROCESSESS

Many microbial metal and mineral transformations have a potential application for the treatment of environmental pollution. Some biological processes, such as bioheap leaching and stirred tank bioleaching of mineral, are well-established technologies in the mining industry. In 1980, the first commercial application of copper heap bioleaching was initiated [40, 133].

Another extensive commercial application of biohydrometallurgy is bio-oxidation of refractory sulfidic gold ores. In this process, the microorganisms oxidize pyrites, arsenianpyrites or arsenopyrites to expose gold occluded within the sulphide minerals matrix. BIOX process is an example of a robust stirred-tank bioleaching process of refractory gold concentrates [161]. The establishment of bioleaching technology in metallurgical processes as a robust process is evidenced by the several established BIOX bioleaching plants commissioned during the last 20 years (Table 1.6). The bacteria of BIOX process are mesophile (40-45°C) and acidophile (pH 1.2-1.8) microorganisms and also these bacteria are tolerant to high arsenic concentrations up to 20 g As^{5+} L^{-1} and up to 6 g As^{3+} L^{-1} [161].

Thermophile bioleaching have also acquired a prominent role in the processing refractory copper sulphides such as chalcopyrite ($CuFeS_2$). It has been demonstrated that bioleaching of copper from chalcopyrite concentrate is increased to 90% under thermophile bioleaching (60°C) compared to 12% under mesophilic bioleaching (22°C) [21, 22, 138].

TABLE 1.6 Commercial BIOX stirred-tank reactor bioleach plants for pre-treatment of gold concentrates (modified after [133, 161]).

Mine	Country	Concentrate treatment capacity (t/day)	Reactor size (m^3)	Date of commissioning
Fairview	South Africa	62	340	1986
Sao Bento	Brazil	150	550	1990
Harbour Lights	Australia	40	160	1991-1999
Wiluna	Australia	158	480	1993
Ashanti	Ghana	960	900	1994
Sansu	Ghana	960	900	1994
Tamboraque	Peru	60	262	1998-2002
Fosterville	Australia	211	900	2005
Suzdal	Kazakhstan	196	650	2005
Bogoso	Ghana	820	1500	2006
Jinfeng	China	790	1000	2006
Kokpatas	Uzbekistan	1069	900	2008

1.5 THE NEXT STEP: BIOMINERALIZATION PROCESSESS FOR ENVIRONMENTAL PURPOSES

The most stable end-product for arsenic immobilization is produced through its precipitation in scorodite crystals. Scorodite precipitation for arsenic removal is however not applied in the mining industry because the high cost associated to the technology but also because several steps are required. Furthermore, most scorodite studies are carried out in batch tests, using very high arsenic concentrations. This excludes the treatment of diluted arsenic metallurgical streams or acid mine drainages (1-5 g L^{-1}).

As microorganisms are used in biohydrometallurgy to oxidize minerals, minerals can be produced with the aid of microorganisms, i.e. through biomineralization.

1.5.1 Biomineralization

Biomineralization refers to the processes by which organisms form minerals. There are two types of biomineralization: biologically controlled or biologically induced biomineralization [117]. The first one, controlled biomineralization is completely regulated by the microorganisms with a physiological purpose [12]. Thus, the organism exerts a degree of control over the nucleation and growth of the mineral particles. Therefore, the biominerals synthesized are well-ordered (not amorphous), with a narrow size distribution and a consistent particle morphology [12]. Magnetosomes are the most recognized biomineral controlled by magnetotactic bacteria [11].

The second mechanism is indirect biomineralization. In this mechanism, minerals are formed as a by-product of the cell's metabolic activity or through its interactions with the aqueous environment [63, 117]. Thus, indirect biomineralization is an unintended result of metabolic activities. These biominerals are characterized by poor crystallinity, broad particle-size distributions and lack of specific crystal morphologies probably due to a lack of saturation control that induce more amorphous materials. In general, during indirect biomineralization the mineral nucleates in solution or forms from poorly crystallized mineral species already present. Also bacterial surfaces, such as cell walls or polymeric materials (exopolymers) produced by bacteria, can act as important sites for the adsorption of ions, mineral nucleation and growth [63]. Examples of indirect biominerals are orpiment, jarosite, struvite, calcite [167].

Biomineralization, especially indirect mechanism, can be directed for specific environmental purposes. The aim of this thesis is to study the possibility of scorodite crystallization with the aid of microorganisms, i.e. indirect biomineralization of scorodite.

1.5.2 Bioscorodite crystallization

The aim of the work described in this thesis is to develop a controlled process for biological crystallization of scorodite from metallurgical streams. In the "bioscorodite process", scorodite is crystallized with the aid of ferrous iron oxidizing bacteria (Fig. 1.5). The biological process has three main advantages: (1) low cost of the oxidizing chemical (oxygen in air), (2) the supersaturation level is controlled on microscale by controlling the rate of biological oxidation, resulting in higher crystallinity and (3) low iron consumption and therefore low sludge production (Table 1.7).

To balance the rates of oxidation and crystallization, the parameters that affect these rates are of importance. The oxidation rate is influenced by the type of bacteria used, the retention of biomass in the reactor, oxygen supply and environmental conditions (pH, temperature and metal concentration). The crystallization rate is mainly influenced by the temperature, crystal concentration in the reactor, and the supersaturation level.

The research focuses on the influence of the abovementioned parameters on biological oxidation and crystallization. The starting point of this thesis is the proof of principle of bioscorodite formation with the purpose of selecting suitable microorganisms and process conditions such as arsenic concentration, temperature and pH value.

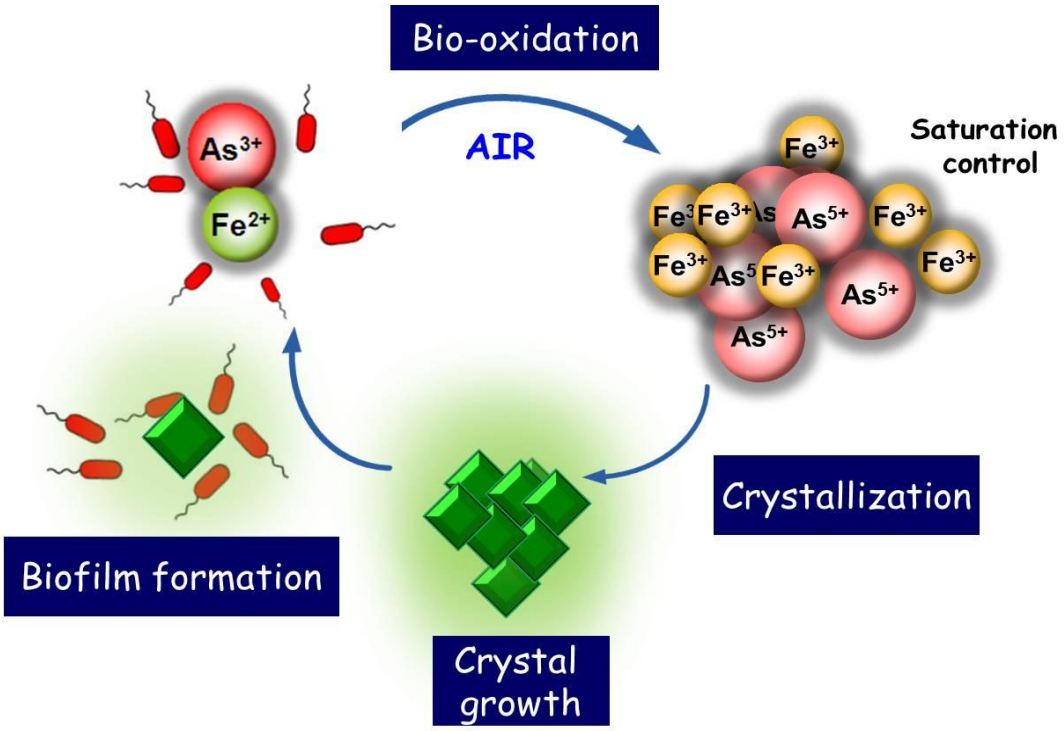

FIGURE 1.5 Theoretical concept of bioscorodite crystallization

The bioscorodite process is patented by Paques B.V (Balk, The Netherlands) as the ARSENOTEQ™ process. In this thesis, the proof of principle, reactor selection and operational conditions of bioscorodite crystallization are described. The main advantages of the bioscorodite process are summarized in Table 1.7a and 1.7b.

TABLE 1.7a Bioscorodite process compared to traditional processes to remove arsenic.

	Bioscorodite (this thesis)	**Arsenical ferrihydrite precipitation**	**Calcium arsenate precipitation**
Temperature requirement	72°C	30-50°C	30°C
Arsenic content (%)	30%wt As	0.5-2%wt As	~35%wt As
Iron/Calcium consumption	Fe/As =1	Fe/As >5	Ca/As > 1 to 2
Oxidant	Air (O_2)	O_2/H_2O_2	O_2/H_2O_2
Arsenic leaching concentrations (mg As L^{-1})	0.013-1	1-2	1600-3600
Seeds addition	-	-	-

TABLE 1.7b Bioscorodite process compared to scorodite chemical precipitation.

	Bioscorodite (this thesis)	Atmospheric scorodite	Hydrothermal scorodite
Temperature requirement	72°C	85°C	>150°C
Arsenic content (%)	30%wt As	30%wt As	30%wt As
Iron consumption (Fe/As)	1	1	1
Oxidant	Air (O_2)	O_2/H_2O_2	O_2/H_2O_2
Arsenic leaching concentrations (mg As L^{-1})	0.013-1	0.1-13	0.1-5
Seeds addition	-	Gypsum or scorodite	-

1.6 SCOPE AND OUTLINE OF THE THESIS

This thesis is part of the project "Bioscorodite Crystallization for Safe Arsenic Disposal". The research was financially supported by the Dutch Ministry of Economic Affairs/Agentschap NL through the INNOWator programme, Paques B.V (Balk, The Netherlands) and Nystar (Budel-Dorplein, the Netherlands).

The aim of the current research is to biocrystallize scorodite for simultaneous arsenic removal and immobilization. **Chapter 2** describes the analysis and speciation of inorganic arsenic from samples containing high iron and sulphate concentrations. In **Chapter 3**, the proof of principle of bioscorodite crystallization is described. The iron oxidation kinetics of a mixed thermoacidophilic culture at suboptimal growth pH (optimal pH for scorodite formation) is presented in **Chapter 4.** In this chapter, the feasibility of continuous cultivation of iron oxidizing microorganisms for bioscorodite crystallization is studied. In **Chapter 5**, the biomineralization mechanism of bioscorodite is studied at pH 1.2 and 75°C, using a mixed thermoacidophilic culture. In **Chapter 6**, factors that influence the stability of bioscorodite crystals are studied. In this chapter also the stability of bioscorodite crystals in long-term leaching tests (1 year) is investigated. **Chapter 7** describes a follow-up study from Chapter 6. In this chapter, the structural changes that bioscorodite crystals undergo during one year of storage are studied. Chapter 6 and 7 also present a detailed characterization of bioscorodite crystals. Continuous bioscorodite crystallization in CSTRs at pH 1.2 and 72°C is presented in **Chapter 8**. The use of an airlift reactor for continuous arsenic removal and bioscorodite production at pH 1.2 and 72°C is described in **Chapter 9**. In **Chapter 10** the stability of bioscorodite crystals is evaluated and an approach for long/term disposal of bioscorodite crystals is presented. In this chapter also the properties of bioscorodite are compared to those of mineral scorodite and chemically synthesized scorodite. Finally, **Chapter 11** combines the results to discuss

the applications of the bioscorodite process. In this chapter also an economical cost comparison is presented. A complete overview of this thesis is given in Fig.1.6.

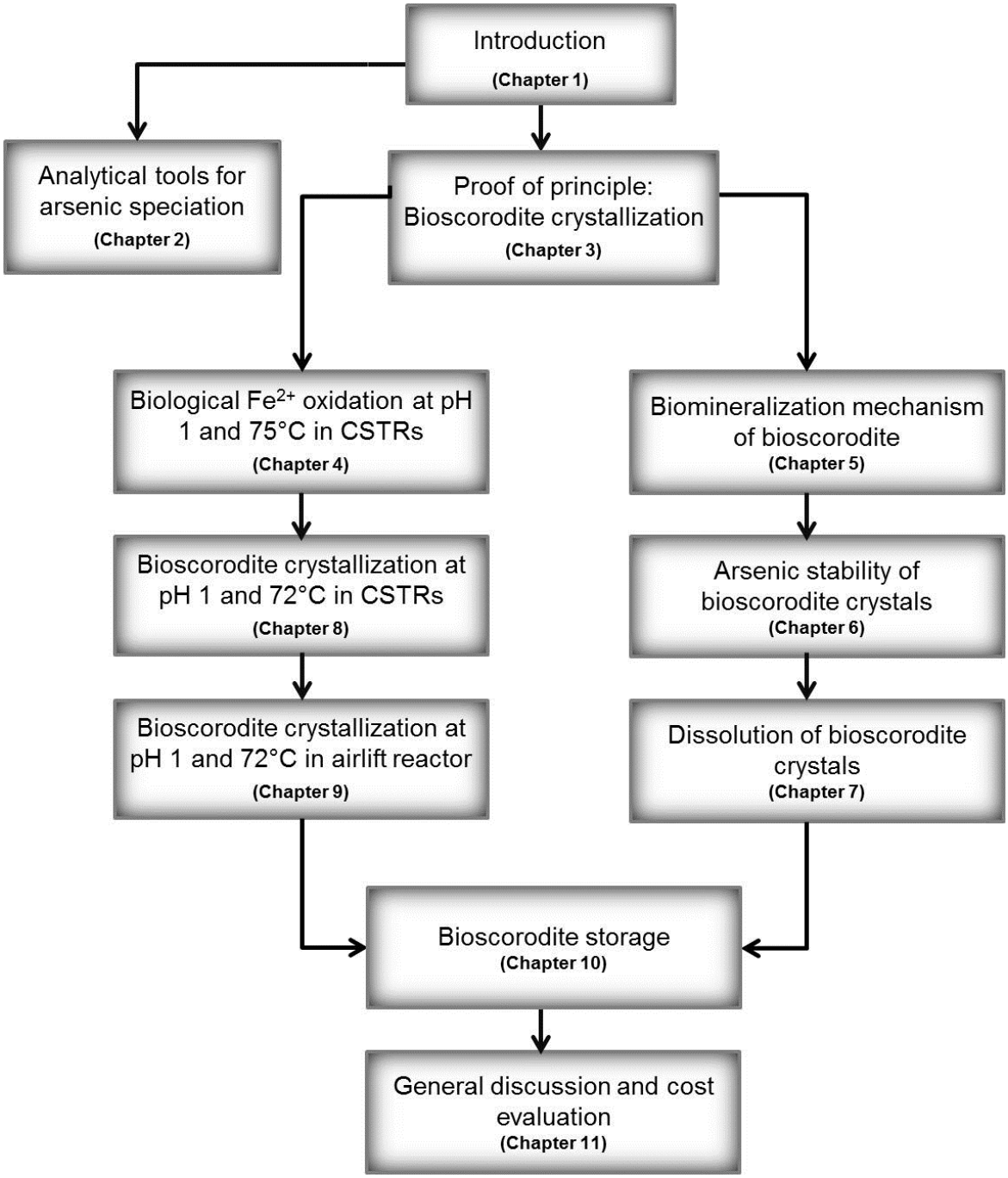

FIGURE 1.6 Overview of this thesis.

Chapter 2

Arsenic speciation

Abstract

To monitor the oxidation of arsenite to arsenate in oxidizing and bioleaching reactors, speciation analysis of the inorganic arsenic compounds is required. Existing arsenic speciation analysis techniques are based on the use of liquid chromatography columns coupled to detector equipment such as inductively coupled plasma optical emission spectrometry (ICP-OES). These techniques are fairly complex and expensive. Therefore, for analysis of arsenic speciation in our studies on thermophilic iron and arsenic oxidation, we developed a simple (and inexpensive) method. The method is based on anionic ion exclusion chromatography using sulphuric acid as mobile phase, followed by UV detection. The detection limit was 0.1 mg L^{-1} of arsenite (As^{3+}) and 0.1 mg L^{-1} of arsenate (As^{5+}). The method was validated with samples from an iron-oxidizing bioreactor containing 0.12 mol L^{-1} H_2SO_4, 1 g L^{-1} arsenic, and 3 g L^{-1} iron. Samples from arsenopyritic gold concentrates by partial bio-oxidation and leaching samples were analysed, showing the usefulness of the method for arsenic contained in environmental compartments. We also describe the apparent effect of the arsenic valence state on ICP-OES detection for total arsenic.

This chapter has been published as:

Gonzalez-Contreras, P; Gerrits-Benneheij, I, Weijma, J, Buisman, C.J.N., HPLC inorganic arsenic speciation analysis of samples containing high sulphuric acid and iron levels. *Toxicological and Environmental Chemistry* **2011,** *93* (3), pp. 415 - 423.

2.1 INTRODUCTION

Aqueous samples from (bio) hydrometallurgical processes and acid mine drainage often contain sulphuric acid as the oxidation product from the sulphur which is present in most metal ores [20]. Such samples characteristically also contain dissolved (heavy) metals and metalloids originating from the ore. Because arsenic is a major constituent of most ores, it is commonly found as dissolved arsenite or arsenate.

A number of methods for arsenic speciation analysis have been proposed which can be found in several reviews [3, 4, 9, 25, 62, 76, 107]. The tendency in arsenic speciation analysis is the use of selective liquid chromatography of many arsenic species coupled to element-specific detectors with a low detection system. The major species analysed from environmental and clinical samples are arsenite As (III), arsenate As (V), dimethylarsinate (DMA), monomethylarsonate (MMA), arsenobetaine (AsB) and arsenocholine (AsC) [3, 4, 9, 25, 62, 76, 107]. The most used detectors for arsenic speciation are Inductively Coupled Plasma Mass Spectrometry (ICP-MS) and Inductively Coupled Plasma Optical Emission Spectrometry (ICP-OES). Both detectors are accurate in the microgram per litre range, especially ICP-MS (below 1 μg L^{-1}) compared to ICP-OES (50 μg L^{-1}) [3, 4, 62, 132]. Others researchers have observed some errors in arsenic analysis (as arsenite) as quantified by ICP-OES [170]. They assumed that the speciation effect must have occurred between steps of aerosol transportation from the spray chamber to the plasma, droplet desolvation and vaporization near or within the plasma, and analyte atomization in the plasma [170].

In the current study we first evaluated the conditions to use ICP-OES to measure total arsenic in samples that contain mixtures of arsenite and arsenate. Secondly, we assessed the speciation of inorganic arsenic (arsenite, arsenate) in samples from an iron-oxidizing bioreactor. This bioreactor is used in our current studies on bioscorodite ($FeAsO_4 \cdot 2H_2O$) crystallization, which we studied in small batch reactors (Chapter 3). The aqueous samples from this bioreactor contained ferrous iron (Fe^{2+}) and ferric iron (Fe^{3+}) in a dilute sulphuric acid medium with inorganic arsenic concentrations up to 1 g L^{-1} as arsenic. We used a HPLC system with sulphuric acid as the mobile phase for the speciation analysis of inorganic arsenic. The high arsenic concentration in our samples, as opposed to the micrograms per litre concentrations typically found in ground water samples, enable the use of a detector system much more simple than, for example, ICP-OES. Because of its simplicity of detection, we opted for the use of a UV detector instead of ICP-OES.

2.2 EXPERIMENTAL SECTION

2.2.1 Instrumentation

The HPLC system consisted of an on-line Elite degassing system (Atech, The Netherlands), a gradient pump Gynkoteck M480 (Dionex, The Netherlands), an autosampler Midas 830 (Separations, H.I. Ambacht, The Netherlands), a chromatography oven compartment module coupled to a column thermostat (Separations, The Netherlands). The HPLC system was connected to a UV photometer Ultimate VWD 3400 (Dionex, The Netherlands).

A Varian Vista-MPX Simultaneous Inductively Coupled Plasma Optical Emission Spectroscopy (ICP-OES) system with CCD detector was used with a plasma flow of 15 L min^{-1}, auxiliary flow of 1.5 L min^{-1} and a nebulizer flow of 0.9 L min^{-1}. The generator power was 1.3 kW and the nebulizer pressure 200 kPa. Argon was used as the optic purge gas. The instrumental LOC was established in the ICP-OES.

2.2.2 Chemicals and standards

MilliQ water with a resistivity of 18.2 MΩ cm^{-1} was used for the preparation of the solutions. The calibration of ICP-OES was made with dilutions of the arsenic acid (H_3AsO_4) ICP standard (1 g L^{-1} as As) in nitric acid 2-3% (Merck, Germany). The total iron ICP standard used was 1 g L^{-1} diluted in 2-3% HNO_3 (Merck, Germany). Arsenite (As^{3+}) ICP standard was used as arsenic trioxide (1 g L^{-1} as As) diluted in 0.3% NaOH, 0.5 % (v/v) HCl, 0.06% $NaHCO_3$; and arsenate (As^{5+}) ICP standard was arsenic oxide hydrate 1 g L^{-1} in water (Inorganic Ventures, Lakeweood, N.J. United States). Standard solutions for HPLC were prepared in 10 mmol L^{-1} sulphuric acid. The arsenic species were prepared from disodium hydrogen arsenate heptahydrate ($Na_2HAsO_4 \cdot 7H_2O$) (Fluka, Switzerland) and a sodium arsenite standard solution Tritipur (0.05 mol L^{-1} ± 0.1% $NaAsO_2$) (Merck, Germany). Arsenate standard solution was standardized by comparing its value with the measures by ICP-OES against the ICP standard for arsenate (As^{5+}). The ICP-OES gave a value for the standard solution of 1.005 (0.0033 ± 0.0032), (RSD ± 95% CI), n=5.

2.2.3 Chromatography conditions

We tested two columns for ion exclusion in HPLC. The columns are specified for organic acid separation using sulphuric acid as mobile phase. The columns used were the OA-1000 organic acid H^+, 6.5 x 300 mm (Altech) and the Rezex ROA organic acid H^+ (8%) 300 x 7.8 mm (Phenomenex). A pre-column of Carbo-H 4 x 3.0 mm was prior to each column. The mobile phase used for both columns was sulphuric acid 10 mmol L^{-1}

with an isocratic flow rate of 0.4 mL min^{-1}. The sample loop used was 20 µL. The temperature of the columns was set at 70°C.

The UV detector wavelength was selected based on the reported maximum absorption of 197 nm for arsenite and 192 nm for arsenate [120]. The UV detector was set to 195 nm for the selection of the most suitable column. Once the most suitable column was selected, the maximum UV absorption was evaluated at 192 nm, 195 nm, and 197 nm.

2.2.4 ICP-OES conditions

The default method parameters used in ICP-OES are Replicated Read Time (RRT) of 10 s, Instrument Stabilization Delay (ISD) of 20 s, and Rinse Time (RT) of 10 s. All the standards dilutions were prepared in milliQ water and with 1% nitric acid in the final solution. At these conditions, a sample set with various standard concentrations of As^{3+} and As^{5+} was prepared and analysed. The calibration curve for ICP-OES was made with the total Arsenic ICP standard.

2.2.5 Bioreactor samples

Samples were taken from an iron-oxidizing reactor which was operated at pH 1.2 and a temperature of 75°C in 0.12 mol L^{-1} sulphuric acid. The samples contained 100 mg L^{-1} ferrous iron (Fe^{2+}) and 3000 mg L^{-1} ferric iron (Fe^{3+}); biomass and nutrients were present in the medium as well (Chapter 3). The maximum arsenic concentration present in the bioreactor was 1000 mg L^{-1} and the minimum was dependent on reactor performance. Before analysis, samples were filtered over a 0.2 µm cellulose acetate membrane filter Spartan 30 (Whatman, Germany) and diluted with 10 mmol L^{-1} sulphuric acid.

2.3 RESULT AND DISCUSSIONS

2.3.1 Evaluation of ICP-OES for total arsenic measurement from samples containing As^{3+} and As^{5+}

It was observed that total arsenic was not fully quantified by ICP-OES in samples with diluted arsenite standard, with a deviation of up to 19% (Fig. 2.1). The rinse was made with the same diluted acid as blank to detect the remaining arsenic. It was found that the blank injected after standards contained high arsenic concentrations, apparently remaining from previous injections. The blanks after the analysis of 1 mg L^{-1} As^{3+} analysis contained 0.084 mg L^{-1} ± 0.055 and after the analysis of 1 mg L^{-1} As^{5+} contained 0.019 mg L^{-1} ± 0.0008. By contrast, total arsenic was well correlated to the arsenate standard concentrations (data not shown). Therefore, for analysis with ICP-OES of total arsenic in samples containing arsenite, we chemically oxidized As^{3+} using hydrogen peroxide. It was

found that a 6% hydrogen peroxide solution was needed to fully oxidize 10 mg L^{-1} of As^{3+} with a reaction time of 10 min as shown in Figure 2.2. With such a treatment total arsenic was accurately analysed by ICP-OES in samples containing As^{3+}, as shown in Figure 2.1. The presence of iron up to 1 g L^{-1} and 0.12 mol L^{-1} sulphuric acid in the samples had no effect on the analysis of total arsenic.

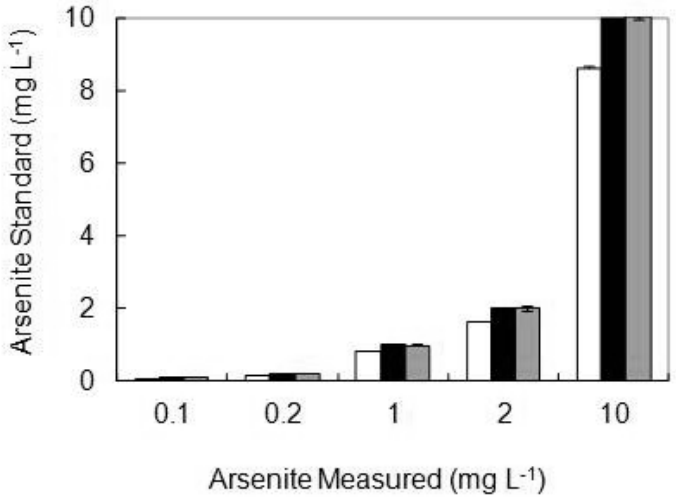

FIGURE 2.1 Total arsenic measurements with ICP-OES of samples containing As^{3+} after treatment with hydrogen peroxide. Before analysis, samples were diluted in milliQ water. The first bar shows the As^{3+} sample without any treatment, the second bar shows the theoretically expected concentration, and the third bar shows the As^{3+} concentration after treatment with hydrogen peroxide.

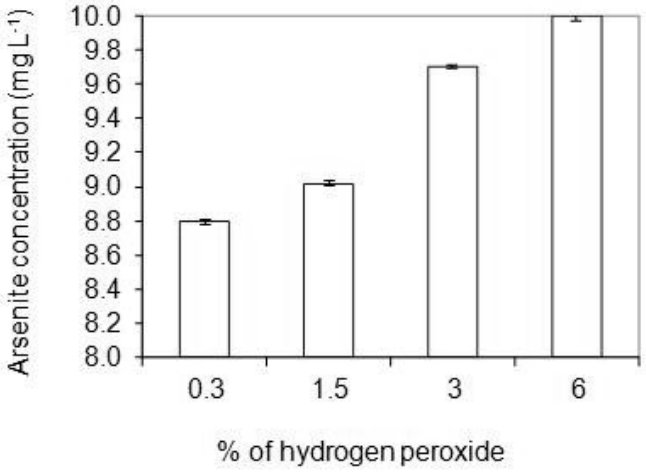

FIGURE 2.2 Chemical oxidation of arsenite (10 mg L^{-1}) with hydrogen peroxide in a reaction time of 10 min.

2.3.2 Evaluation of inorganic arsenic speciation with ion exclusion chromatography (HPLC) and UV detection

Two ion exclusion columns normally used for organic acids were tested for analysis of As^{3+} and As^{5+}. We selected the Rezex ROA column because the sulphate peak did not interfere with the arsenic peaks as occurred with the OA-1000 column. The retention time for the arsenic analytes was different in the columns as can be seen in Figure 2.3. Also As^{3+} and As^{5+} peaks are separated by a large time in the Rezex ROA column. The peak at 10 min in the Rezex ROA column resulted from the sulphate in the medium. The OA-1000 column separated As^{3+} and As^{5+} less effectively. The maximum absorption of both arsenic analytes was observed at 192 nm as can be seen in Figure 2.4.

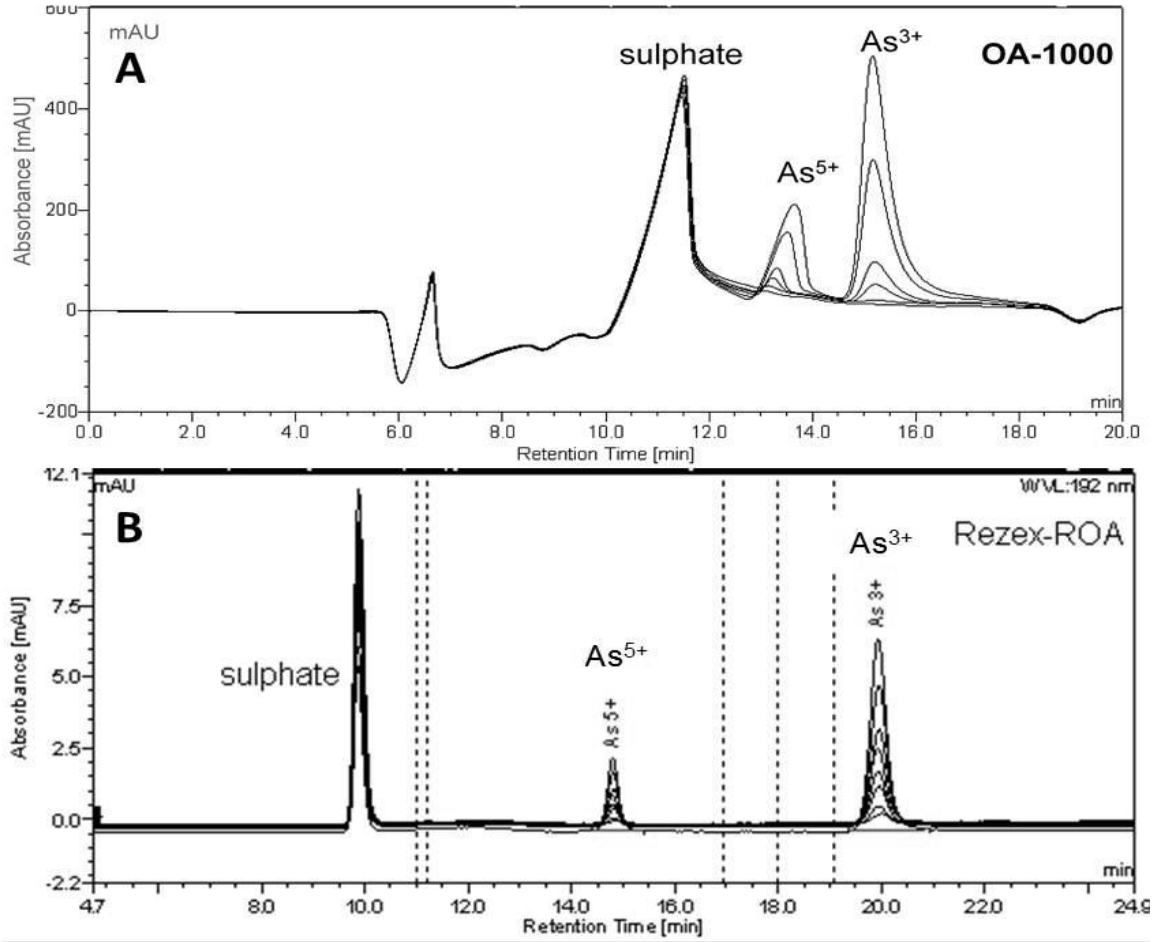

FIGURE 2.3 Arsenic speciation of As^{3+} and As^{5+} in Ion exclusion columns with UV detection at 195 nm using 10 mmol L^{-1} sulphuric acid as mobile phase in the OA-1000 column (A) and Rezex ROA column (B).

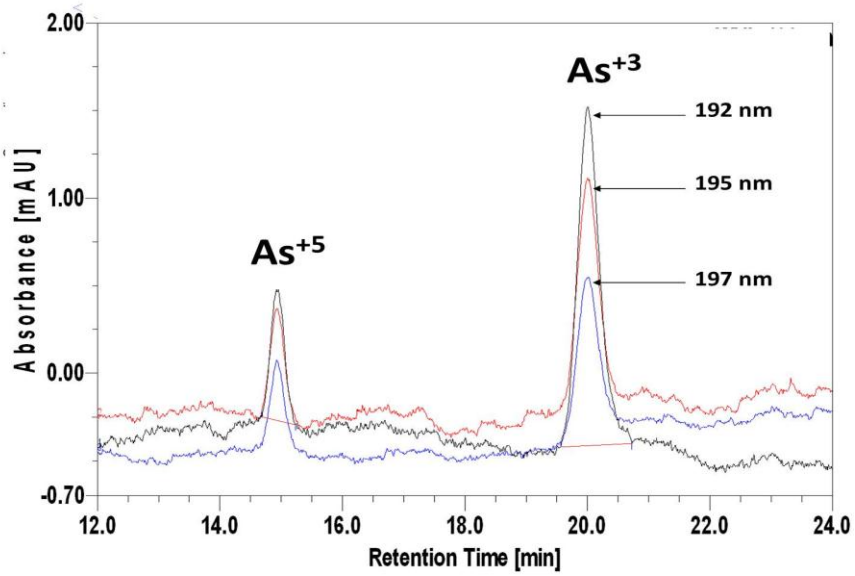

FIGURE 2.4 Arsenic UV absorption of 0.4 mg As^{3+} L^{-1} and 0.4 mg As^{5+} L^{-1} using an Ion exclusion Rezex ROA column with 10 mmol L^{-1} sulphuric acid as mobile phase at 192, 195, and 197 nm.

When adequate peak separation with a sufficiently low detection limit in the Rezex column was obtained we proceeded to evaluate the calibration curve and reproducibility of the method. The calibration curves for As^{3+} and As^{5+} range from 0.1 to 2 mg L^{-1} allowing high dilution of our bioreactor samples.

The reproducibility of the method was evaluated using a set of standards containing 1 mg As^{3+} L^{-1} and 1 mg As^{5+} L^{-1}. The one sample t-test (2 tailed) was used to assess the statistical significance of the data. The hypothesis tested was the standard concentration of 1 mg L^{-1}. The t critical is $t_{0.005,19} = 2.811$ was compared with the experimental values to hold the hypothesis of $t_{(19)} = 3.6$ for arsenite and of $t_{(19)} = 5.0$ for arsenate. The statistical analysis shows that the values obtained are highly significant and that both experimental samples tested (arsenite and arsenate) were equal to the hypothesis with an error of less than 1%. The recovery of both analytes was highly acceptable with 100.2% of As^{3+} and 103.3% of As^{5+}.

2.3.3 Evaluation of iron-oxidizing reactor and leaching samples by Ion exclusion Rezex ROA column and UV detection

Bioreactor samples were analysed immediately after they were taken from the reactor. The sulphuric acid medium present in the samples preserved the As^{3+} analyte for two weeks. Only 2.5 mg As^{3+} L^{-1} was oxidized (0.25%) by chemical oxidation in the samples after two weeks of storage in the dark at 5°C (Fig. 2.5).

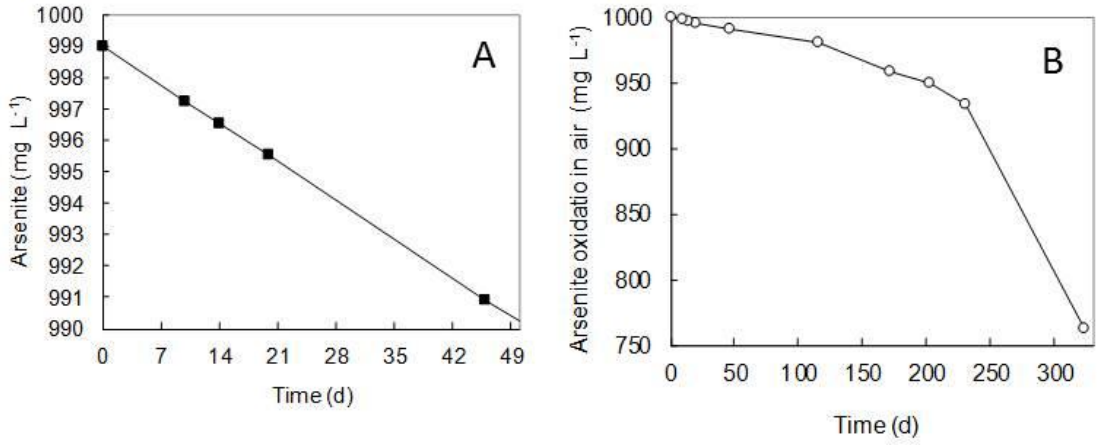

FIGURE 2.5 Chemical oxidation of the standards stored in the dark at 5°C. Left: detail of the first seven weeks of storage. Right: Almost one year of storage.

The samples had a pH of 1.2 in 0.12 mol L^{-1} sulphuric acid containing 100 mg L^{-1} ferrous iron (Fe^{2+}) and 3000 mg L^{-1} ferric iron (Fe^{3+}). Figure 2.6 shows the analysis of samples from the bioscorodite reactor in batch operation. The analysis of arsenic speciation in this bioreactor is critical to monitor the biological arsenic oxidation. Once arsenite oxidation has started, arsenate (As^{5+}) becomes available for precipitation.

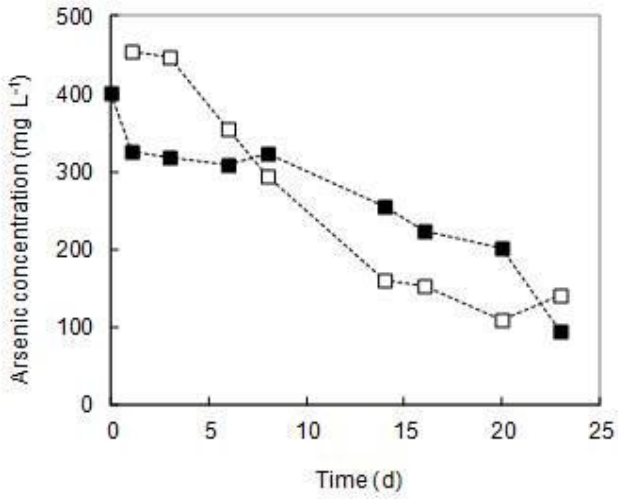

FIGURE 2.6 Arsenic speciation (As^{3+} and As^{5+}) in a batch bioscorodite reactor by analysis with Ion exclusion Rezex ROA column with UV detection at 192 nm using sulphuric acid 10 mmol L^{-1} as mobile phase. Legend: ■ As^{3+} □ As^{5+}.

We evaluated the applicability of the method with two additional environmental samples. The first sample originated from leaching tests of scorodite mineral. The leaching

solution of this test was acetic acid at pH 5. Figure 2.7 shows the chromatogram of this sample. Scorodite contains arsenate in its structure therefore arsenite was not expected to be found in these samples. The acetic acid is identified by the method but does not interfere with the peaks of arsenic and does not affect the determination of low arsenic concentrations.

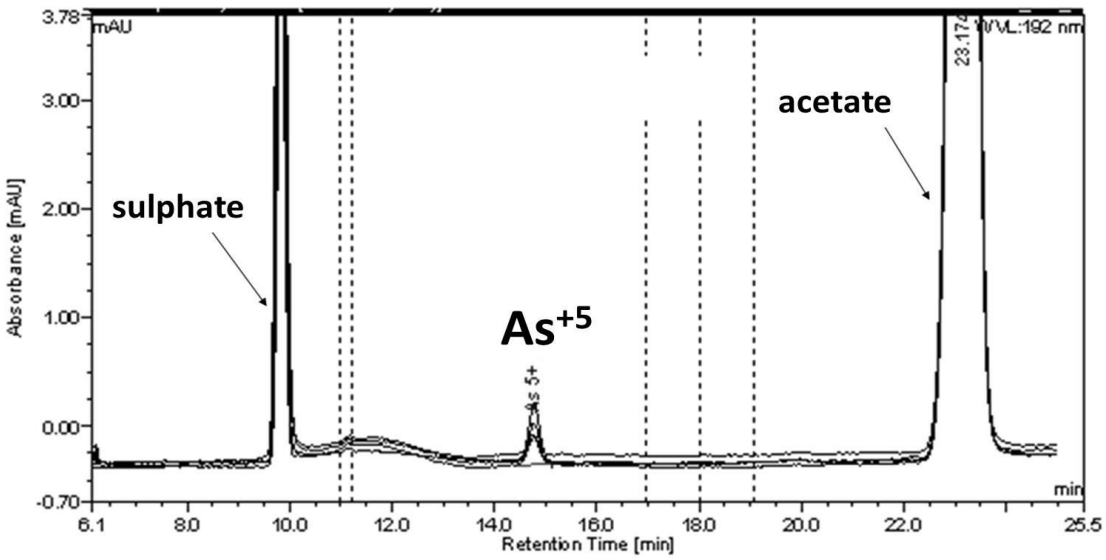

FIGURE 2.7 Evaluation of samples of leached scorodite mineral. The leaching solution consists of acetic acid at pH of 5. Scorodite mineral contains arsenate in its structure, therefore arsenite was not expected to be found in this sample, which was confirmed by the analysis.

The second sample was obtained from the processing of arsenopyrite gold concentrates by partial bio-oxidation reactors followed by bio-reduction [91]. Figure 2.8 shows results for the second sample containing both arsenic species and sulphate, the analysis was not affected by any of the leaching products from the mineral present in the reactor.

The use of sulphuric acid as eluent increases the retention time due to a strong stimulation of diffusion of the analyte into the stationary phase. In addition, the suppliers of the columns have indicated that when strong acids are used as mobile phase, the column is self-regenerating; therefore, special regeneration steps are not required. Although the total run time of column Rezex-ROA is longer than those on the other columns (20 min instead of 8 min), the method fulfilled our objectives. We were able to determine the arsenite and arsenate concentrations in iron-oxidizing bioreactors, arsenopyrite gold concentrates leaching bioreactor and from leaching tests without the interferences produced by sulphate as observed in other columns.

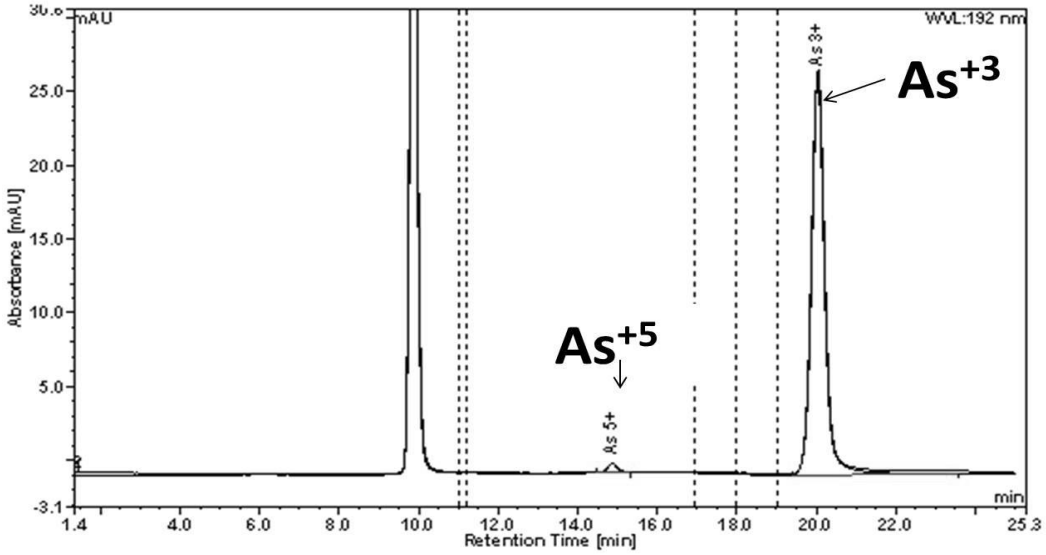

FIGURE 2.8 Evaluation of bioleaching samples from the processing of arsenopyritic gold concentrates by partial bio-oxidation and bio-reduction.

2.4 CONCLUSION

The proposed method, simultaneous As^{3+} and As^{5+} analysis with a detection limit of 0.1 mg L^{-1} achieved by HPLC and UV detection, offers sufficient detection limits and reproducibility for the investigation of inorganic arsenic speciation in bioleaching studies and applications. The method was successfully applied to bioleaching samples in sulphuric acid matrix. This method therefore looks suitable for effluents from metallurgical processes and various environmental samples.

Acknowledgements

The authors acknowledge to A. Hol (WUR, The Netherlands), who kindly provide the bioleaching samples.

Chapter 3

Proof of principle: bioscorodite crystallization

Abstract

Scorodite is an arsenic mineral with the chemical formula $FeAsO_4 \cdot 2H_2O$. It is the most common natural arsenate associated with arsenic-bearing ore deposits. In the present study, we show that under mesophilic conditions bioscorodite does not precipitate. In thermophilic conditions, the iron-oxidizing archaeon *Acidianus sulfidivorans* is able to precipitate scorodite in the absence of any primary minerals or seed crystals, when grown on 0.7 g L^{-1} ferrous iron (Fe^{2+}) at 80°C and pH 0.8 in the presence of 1.9 g L^{-1} arsenate (H_3AsO_4). The simultaneous biologically induced crystallization of ferric iron (Fe^{3+}) and arsenic to scorodite prevented accumulation of ferric iron. As a result, crystal growth was favoured over primary nucleation which resulted in the formation of highly crystalline bioscorodite very similar to the mineral scorodite. Because mineral scorodite has a low water solubility and high chemical stability, scorodite crystallization may form the basis for a novel method for immobilization of arsenic from contaminated waters with high arsenic concentrations.

This chapter has been published as:

Gonzalez-Contreras, P.; Weijma, J, Buisman, C. J. N., Biogenic scorodite crystallization by *Acidianus sulfidivorans* for arsenic removal. *Environmental Science and Technology* **2010,** 44, 675-680.

Section 3.3.3 of this chapter has been published by the same authors as: Biological scorodite crystallization: Effect of high ferric concentration and foreign seeds. *Advanced Materials Research* **2009,** 71-73, 629-632.

3.1 INTRODUCTION

Scorodite is a naturally occurring arsenic mineral with chemical formula $FeAsO_4 \cdot 2H_2O$. In nature, scorodite is often found as a secondary supergene mineral associated with arsenic-bearing primary minerals such as arsenopyrite (FeAsS) [60, 151] or enargite ($CuAsS_4$) [110]. Scorodite formation is explained by assuming that weathering of the primary minerals results in incongruent dissolution of arsenate (AsO_4^{3-}) and ferric iron (Fe^{3+}) [42, 143]. This weathering includes chemical and biological oxidation mechanisms and in the latter case, scorodite formation could represent a form of biomineralization [42]. The formation of secondary scorodite is environmentally relevant as its solubility may control the concentration of arsenic in natural waters and drainage from arsenic–bearing ores which are exposed to the atmosphere [42, 143].

Although incongruent dissolution presumably results in the presence of scorodite in nature, chemical crystallization of scorodite from aqueous solutions is also a known phenomenon, as has been demonstrated in several laboratory studies. At a temperature of 140-150°C and low pH, scorodite crystallizes from solutions containing arsenate and ferric iron [37, 48, 59]. Scorodite can also be crystallized from metastable solutions at more moderate, atmospheric conditions, as was shown by a group of researchers at McGill University in Canada led by Demopoulos [38, 154, 155]. Scorodite was crystallized at 80-95°C from a solution containing 19 g L^{-1} arsenate and 7.2 g L^{-1} ferric iron by i) controlling the pH just below a value of 0.9 at which amorphous ferric arsenate precipitation initiates, ii) a slow stepwise neutralization, and iii) the addition of scorodite or foreign seeds to induce crystallization at low supersaturation level [38, 154, 155]. Instead of arsenate (AsO_4^{3-}) and ferric iron (Fe^{3+}), also arsenite (AsO_3^{3-}) and ferrous iron (Fe^{2+}) can be used as the source of arsenic and iron for scorodite crystallization. Then, the arsenite and ferrous iron are first chemically oxidized with peroxide or pure oxygen to the scorodite reactants [26, 65]. In nature, these strong oxidizing agents are absent, implying that a chemical crystallization of scorodite from solutions is unlikely.

Naturally occurring micro-organisms like *Acidianus sulfidivorans* [140] are able to oxidize ferrous iron (Fe^{2+}) to ferric iron (Fe^{3+}) under pH and temperature conditions that favour scorodite crystallization. These thermophilic micro-organisms use oxygen from air as the electron acceptor for ferrous iron oxidation. Thus, when these micro-organisms are grown in the presence of ferrous iron and arsenate, scorodite is expected to be crystallized. In this paper we explore the biologically induced crystallization of scorodite from solution in the absence of any primary mineral. This mechanism could be the basis of new methods to remove arsenic from contaminated water sources and industrial waste streams and immobilize it as scorodite. Contamination with arsenic arises from mining and metallurgical activities, especially when it concerns ores of Cu, Ni, Au, Pb and Zn [37,

144]. From this perspective, scorodite biologically induced crystallization could be of environmental significance, as scorodite up to today is an attractive medium for arsenic stabilization and the safest known storage material due to its low solubility, high stability and compactness [42, 105, 106, 128, 145]. Current methods for arsenic removal from such streams are mainly based on sorption onto iron oxides or precipitation as amorphous calcium arsenate and ferric arsenate. However, the disposal and storage of these compounds is not entirely safe as they easily undergo physical and chemical changes with time [157], resulting in arsenic release to the environment.

In the current study, we investigate the possible role of mesophilic and thermophilic iron oxidizing microorganisms in the crystallization of scorodite using atmospheric oxygen as freely available oxidant. It is aimed at keeping the supersaturation at a low level by slow biological oxidation of ferrous iron, to obtain a completely crystalline scorodite product. Gypsum seeds are added in order to decrease the saturation level of scorodite.

3.2 EXPERIMENTAL SECTION

3.2.1 Materials

Serum bottles of 100 mL closed with a butyl rubber stopper and crimped aluminium seal were used as reaction vessel and placed in a thermostat shaker incubator at 150 rpm at 35°C and 80°C. Experiments were carried out at least in duplicate. Experiments were carried out with seeds (20 and 80 g L^{-1}) and without seeds (gypsum). The ratio head space/liquid volume in the bottles was such that a 50% excess of oxygen (in air) was present relative to the stoichiometric amount needed for complete ferrous iron oxidation. Liquid samples were taken with a syringe, filtered and analysed for pH, iron and arsenic concentrations. Measurements of pH and redox potential were measured with glass electrodes QP181X and QR480X-Pt, respectively (Prosense, Netherlands). At the end of the experiment the solution was filtered and solids were washed several times with hot distilled water and dried at 70°C before characterization.

3.2.2 Medium and Inoculum

The defined growth medium used for the thermophilic acidophiles contained: 1 g L^{-1} $(NH_4)_2SO_4$, 0.1 g L^{-1} KCl, 0.5 g L^{-1} $MgSO_4 \cdot 7H_2O$, and 0.5 g L^{-1} K_2HPO_4 as described by Plumb *et al.* (2002) [139]. Micronutrients were added according to growth medium 150 (DSM 18786). All chemicals used were analytical-reagent grade. Iron (II) sulphate heptahydrate ($FeSO_4 \cdot 7H_2O$) was used as the ferrous iron source and was dissolved in 0.25 M sulphuric acid (H_2SO_4) before use. Arsenate was added as disodium hydrogen arsenate heptahydrate ($Na_2HAsO_4 \cdot 7H_2O$). All the solutions were adjusted to pH 0.8 with

concentrated sulphuric acid. Arsenate and ferrous iron were added to the bottles once the temperature of the medium reached 30 or 80°C.

Mesophilic microorganism *Thiobacillus ferrooxidans* (DSMZ 10321) and the thermophile archaeon *Acidianus sulfidivorans* (DSMZ 11091) were supplied by the German Collection of Microorganism and Cell Cultures (DSMZ, Braunschweig, Germany). *Thiobacillus* has an optimum temperature at 30°C and pH 1.4. These iron oxidizers were grown in medium 70 DSM with ferrous sulphate. *Acidianus* has a pH range of growth between 0.35 and 3.0, with optimal growth at pH 0.8-1.4. *Acidianus* cells grow at a temperature between 45 and 83°C, with optimum growth at 74°C [140]. In our experiments, *Acidianus sulfidivorans* was grown in medium 150 DSM 18786 with the pH adjusted to 0.8 at 80°C. A chemical control was prepared using ferric iron instead of ferrous iron. A chemical control (CC) without microorganisms and biological controls (BC) with the microorganisms without arsenic were prepared.

3.2.3 Methods

Iron speciation in aqueous phase. Iron species in the aqueous phase were measured using Dr.Lange Cuvette test LCK 320 for ferrous iron (Fe^{2+}) and ferric iron (Fe^{3+}) and a Xion 500 spectrophotometer (Hach-Lange, Germany).

Arsenic speciation was not carried out in these experiments. It is expected that biologically ferrous iron oxidation increases the redox potential from + 0.35 V in the medium to values at which arsenate is stable with ferrous iron above + 0.56 V (pH between 0 and 2) [164].

3.2.4 Structure characterization of solids

The total arsenic and total iron concentrations of aqueous and solid samples were measured with a Varian Vista-MPX Simultaneous Inductively Coupled Plasma Atomic Emission Spectroscopy (ICP-AES) system based on Standard Method 3120-B [30]. Liquid samples were filtered with a membrane 0.45 µm cellulose acetate filter to avoid interferences according to Standard Method 3500-Fe-B1 [31]. Solid samples were digested in HCl-HNO_3 solution prior to ICP-AES analysis.

X-Ray Diffraction (XRD) was used to identify the nature of the solid materials. Wide Angle X-ray Scattering (WAXS) powder diffractograms were recorded on a Philips PC-APD diffractometer in the reflection geometry in the angular range 5–50°(2θ), with a step size of 0.02°(2θ) and an acquisition time of 0.6 seconds per step. The CuKα1 radiation from the anode, generated at 40kV and 50mA, was monochromatized using a 15µm Ni foil (λ = 0.1542 nm). The diffractometer was equipped with a 1° divergence slit, a 0.2mm receiving slit and a 1° scatter slit.

The structural H_2O content of the solid phases was determined with a Thermo Gravimetric Analyser (Perkin-Elmer TGA7 equipped with Pyris software). The thermal gravimetrical analysis was performed with about 10 mg of air-dried powdered material at a heating rate of 10°C min^{-1} from 50°C to 400°C under air/nitrogen atmosphere.

Fourier Transform Infra Red (FT-IR) spectra of the solid samples were obtained on a Varian Scimitar 1000 FT-IR Spectrometer equipped with a DTGS-detector. The measurement resolution was set at 4 cm^{-1} and the spectra were collected in the range of 4000–400 cm^{-1} for KBr-disks and 4000-650 cm^{-1} for Attenuated Total Reflectance (ATR) with 64 co-added scans. KBr-sample disks were prepared from a mixture of 1 wt% of finely ground sample in KBr. The sample chamber was purged by N_2 gas for 10 min before scanning was started. ATR was performed on a PIKE MIRacle ATR equipped with a diamond w/ZnSe lens single reflection plate.

The crystal habit of the solids was investigated with Scanning Electron Microscopy (SEM). Samples were glued on a copper sample holder using conductive carbon tape and silver tape and sputter coated with 20 nm platinum (JFC 1200, JEOL, Japan). The surfaces were analysed with a FESEM (JEOL 6300 F, Tokyo, Japan) at room temperature, a working distance of 15 mm and SE detection at 3.5 kV. All images were recorded digitally (Orion, 6 E.L.I. sprl., Belgium) at a scan rate of 100 seconds (full frame) at a size of 2528 x 2030, 8 bit. Noise reduction and resizing of the images was done with Adobe Photoshop CS. Besides, SEM-Energy Dispersive X-ray Spectroscopy (EDS) (INCA energy, Oxford Instruments Analytical, High Wycombe, England) was used to measure the Fe/As ratio in the solid structure.

3.2.5 Calculation of the Ion Activity Product (IAP).

The IAP of bioscorodite crystals was calculated assuming that it has the same properties as mineral scorodite. The supersaturation in aqueous solutions is expressed by the IAP of the lattice ions in solution divided by the activity solubility product of the salt, K_a (IAP at saturation). The IAP of scorodite is defined as the product of the activities of ferric iron and arsenate in solution. Considering that K_a is a constant value for scorodite, the IAP can be used to monitor the supersaturation level of the solution. However, the values reported for K_a of scorodite depend on whether the scorodite used was mineral, hydrothermal crystallized, or atmospheric crystallized, and those were determined for different solution systems. These IAP values depend strongly on pH value and dissociation constants varying between -19 and -26 at different medium such as nitric acid and sulphuric acid [43, 96, 105, 106, 109, 146, 172].

Thus, the congruent dissolution of bioscorodite crystals is defined in equation 3.1[42, 105, 106]:

$$FeAsO_4 \cdot 2H_2O \ \ (Scorodite) \Leftrightarrow Fe^{3+} + AsO_4^{3-} + 2H_2O \qquad \text{(eq. 3.1)}$$

$$IAP_{SCORODITE} = \left(a_{Fe^{3+}}\right)\left(aAsO_4^{3-}\right) \qquad \text{(eq. 3.2)}$$

Equations 3.3 and 3.4 were used for the calculation of the activity of arsenate and ferric iron.

$$aAsO_4^{3-} = \frac{Arsenate_{total}}{1 + \frac{a_{H^+}}{K_3} + \frac{\left(a_{H^+}\right)^2}{K_2K_3} + \frac{\left(a_{H^+}\right)^3}{K_1K_2K_3}} \qquad \text{(eq. 3.3)}$$

$$aFe^{3+} = \frac{Ferric_{total}}{1 + \frac{K_1}{a_{H^+}} + \frac{K_1K_2}{\left(a_{H^+}\right)^2} + \frac{K_1K_2K_3}{\left(a_{H^+}\right)^3} + \frac{K_1K_2K_3K_4}{\left(a_{H^+}\right)^4}} \qquad \text{(eq. 3.4)}$$

The hydrolysis constants for arsenate and ferric iron are shown in Table 3.1.

TABLE 3.1 Hydrolysis constants of arsenate and ferric iron. The constants at 80°C were determined by van't Hoff and used for the IAP calculation.

Temperature of hydrolysis constants	pK (25°C)	pK (80°)	pK (80°)
Calculation method used	Literature [10, 42]	Van't Hoff [108]	HCS [1]
Arsenate			
$H_3AsO_4 = H_2AsO_4^- + H^+$	2.24	2.27	2.53
$H_2AsO_4^- = HAsO_4^{2-} + H^+$	6.86	6.95	6.81
$HAsO_4^{2-} = AsO_4^{3-} + H^+$	11.49	11.51	11.28
Ferric Iron			
$Fe^{3+} + H_2O = Fe(OH)^{2+} + H^+$	2.19	2.18	-
$Fe(OH)^{2+} + H_2O = Fe(OH)_2^+ + H^+$	3.48	3.47	-
$Fe(OH)_2^+ + H_2O = Fe(OH)_3 + H^+$	6.33	6.31	-
$Fe(OH)_3 + H_2O = Fe(OH)_4^- + H^+$	9.6	9.57	-

The effect of the temperature in the hydrolysis constant of arsenate and ferric iron was corrected using van't Hoff, assuming that the heat capacity of the reactions is zero. This means that the van't Hoff Equation was integrated assuming the enthalpy of the reaction as constant [108]. However this is only valid for temperatures up to 50°C [108]. The calculation of hydrolysis constants at 80°C was also determined by using HSC Chemistry® software [1]. HSC makes a Criss-Croble extrapolation for the heat capacity of aqueous species at elevated temperatures (>25°C to 300°C). Criss-Croble extrapolation is only used if the temperature coefficients of the heat capacity function are not given in the HSC database.

3.3 RESULTS AND DISCUSSION

3.3.1 Mesophilic experiments

Thiobacillus ferrooxidans oxidized ferrous iron at pH 1.3 and 30°C. A concomitant iron and arsenic removal from solution took place leading to precipitates formation. The precipitates had a characteristic yellow colour resembling rather ferrihydrite than scorodite (green pale colour). The yellow precipitates and those covering the gypsum seeds were identified as poorly crystalline ferric arsenate by XRD analysis (Fig. 3.1).

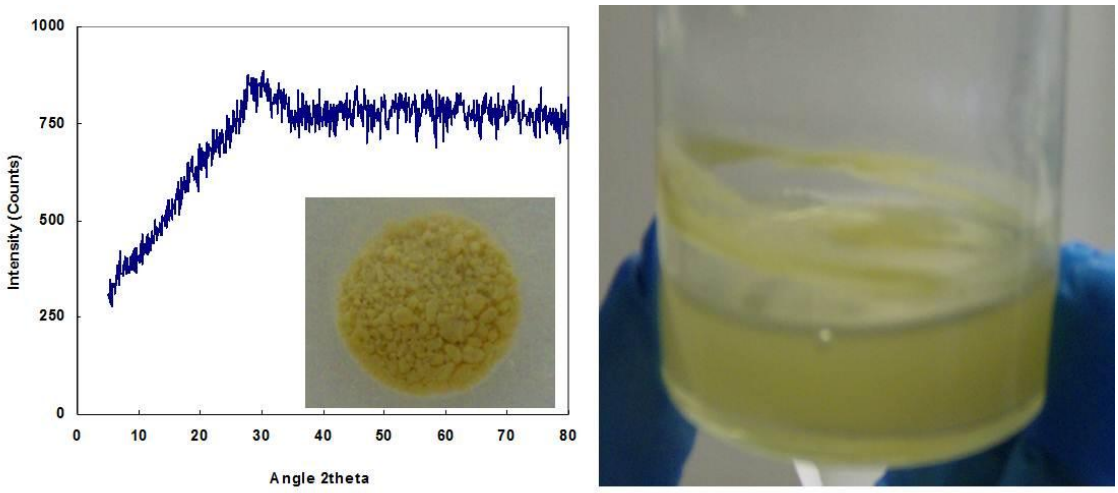

FIGURE 3.1 XRD analysis of poorly crystalline ferric arsenate precipitates at 30°C and pH 1.3 with *Thiobacillus ferrooxidans*.

3.3.2 Thermophilic experiments without seeds: control of scorodite supersaturation by biological ferrous iron oxidation

Experiments were carried out with solutions containing 0.75 g L^{-1} ferrous iron (Fe^{2+}) and 1.9 g L^{-1} arsenate (H_3AsO_4) equivalent to 1 g L^{-1} As^{5+}. The induction pH of this solution, i.e. the pH at which amorphous precipitates were formed, was determined at pH 1.2 in a chemical experiment. At this pH a yellow precipitate was formed. XRD of the precipitate exhibited one broad band at 29°2θ as occurred with the mesophilic precipitates described in section 3.3.1, which is characteristic for poorly crystalline ferric arsenate [112].

Ferrous iron oxidation and scorodite crystallization resulted in a slight fluctuation of the pH between 0.8 and 1.2 and an increase of the initial redox potential from +0.35 V to values of +0.6 V after day 4 was observed. In the chemical control the pH remained constant (data not shown). In biologically induced crystallization experiments, stoichiometric concentrations of 0.75 g L^{-1} Fe^{2+} and 1 g L^{-1} As^{5+} were used (molar ratio

Fe/As=1.1). Arsenic and ferrous iron concentrations decreased gradually during the experiment (Fig. 3.2). Ferrous iron oxidation rate was 0.04 g L^{-1} d^{-1}. The low ferric iron concentration during the experiment indicated that the biologically oxidized iron was removed by precipitation.

In the chemical control only little (2%) ferrous iron oxidation took place as shown in Figure 3.2. This indicates that in the biological experiments ferrous iron conversion was due to biological oxidation. In a separate chemical control using ferric iron instead of ferrous iron, nearly all ferric iron and 64% of the arsenate precipitated as poorly crystalline ferric arsenate (data not shown). The biological control indicated that the microorganisms were not affected by 1 g L^{-1} As^{5+} (data not shown).

The supersaturation of ferric arsenate was evaluated based on the Ion Activity Product (IAP) of ferric arsenate (Fig. 3.3). The IAP increased from day 5 until day 14, which coincided with the increase of arsenate activity. On day 9, greenish-grey solids appeared in the bottle, when the log IAP reached values close to -22. This IAP value is in the range of values for log K_a reported for scorodite [96, 105, 106, 109, 113, 128, 146].

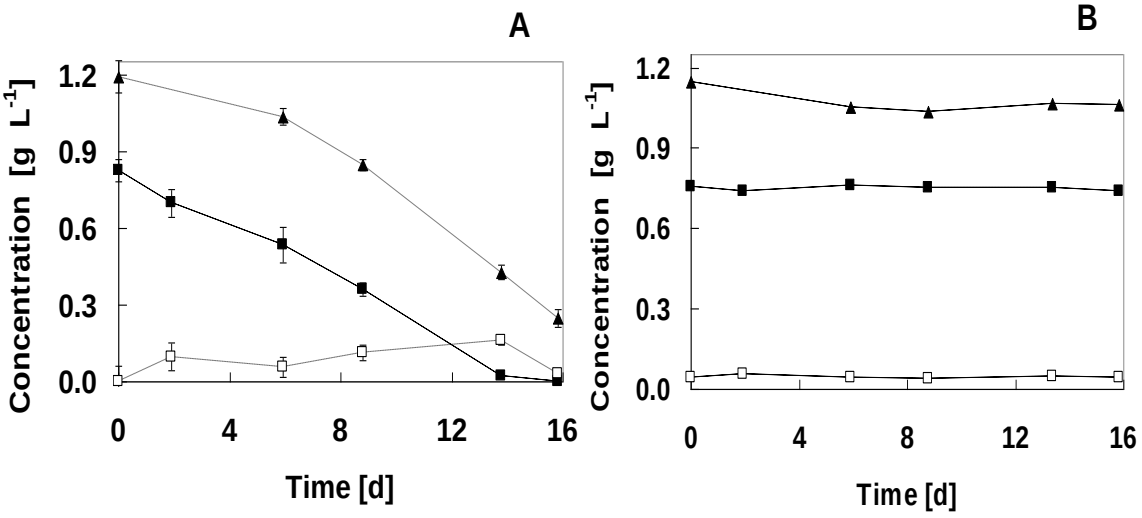

FIGURE 3.2-A Ferrous iron conversion and arsenic depletion in experiments with *Acidianus sulfidivorans* at 80°C, 1 g L^{-1} As^{5+} and 0.72 g L^{-1} Fe^{2+}. Fig. 3.2-B: Chemical Control. Legend: ■ Fe^{2+}, □ Fe^{3+}, ▲ As^{5+}.

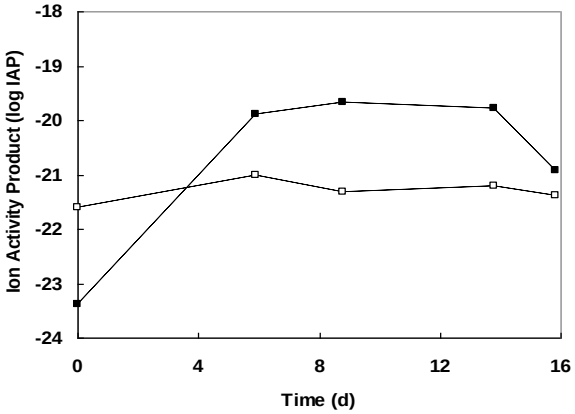

FIGURE 3.3 Ion activity product of scorodite in experiments with *Acidianus sulfidivorans* at 80°C, 1 g L^{-1} As^{5+}. Legend: ■ A1 Fe/As: 1/1, □ Chemical Control.

The downward trend of the IAP at day 14 resulted from the downward trend of ferric iron activity, whereas the fluctuation of arsenic activity resulted from the variation of pH and arsenic precipitation. Part of the solids adhered to the bottom surface of the bottle while the remainder was present in suspension.

At day 16, when the experiment was terminated, the arsenic removal was on average 80 ± 2 % (s.d.). It is noted that arsenic removal and solids formation had not stabilized yet.

3.3.3 Thermophilic experiments using gypsum seeds

In experiments using gypsum seeds, the ferrous oxidation rate was the same as observed in the experiments without gypsum seeds (section 3.3.2). The Ion Activity Product calculated for bottles using gypsum followed the same trend as in bottles without gypsum (Fig. 3.3). However, a high arsenic removal efficiency was obtained in experiments using the highest gypsum concentration, i.e. 80 g L^{-1} (Fig. 3.4).

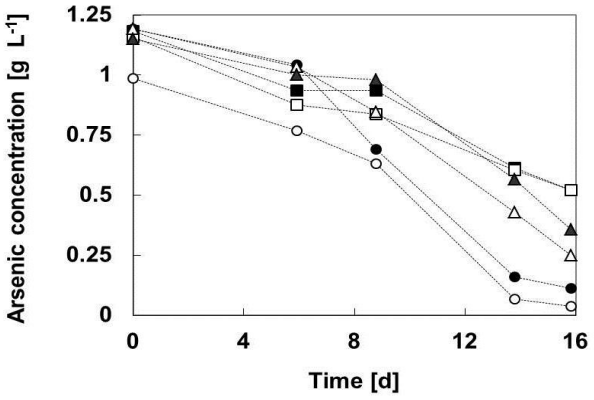

FIGURE 3.4 Arsenic depletion from solution in experiments with and without gypsum using an Fe/As molar ratio of 1 at pH 0.8 and 80°C. Legend: Δ, ▲ no gypsum addition; □, ■ 20 g gypsum L^{-1}; ○, ● 80 g gypsum L^{-1}.

The arsenic mass balance in the presence of gypsum seeds indicated that the amount of arsenic removed from the liquid phase does not match the amount of arsenic precipitated as bioscorodite. Adsorption of Arsenic on gypsum crystals was tested in separate experiments (data not shown). The results indicated that only 6% of arsenic from solution was adsorbed on 80 g gypsum L^{-1}. Therefore, more than 50% of arsenic from solution was not adsorbed on the gypsum nor precipitated as bioscorodite. It is possible that a high fraction of arsenic was removed by the formation of an amorphous phase, which may have been induced by the addition of gypsum seeds.

In the 80°C experiments, addition of external gypsum seeds did not improve the kinetics of biological scorodite crystallization. Higher arsenic removal rates were probably due to the formation of amorphous phases. Bioscorodite crystals formed in these experiments were observed on the surface of gypsum crystals (Fig. 3.5) but also in solution.

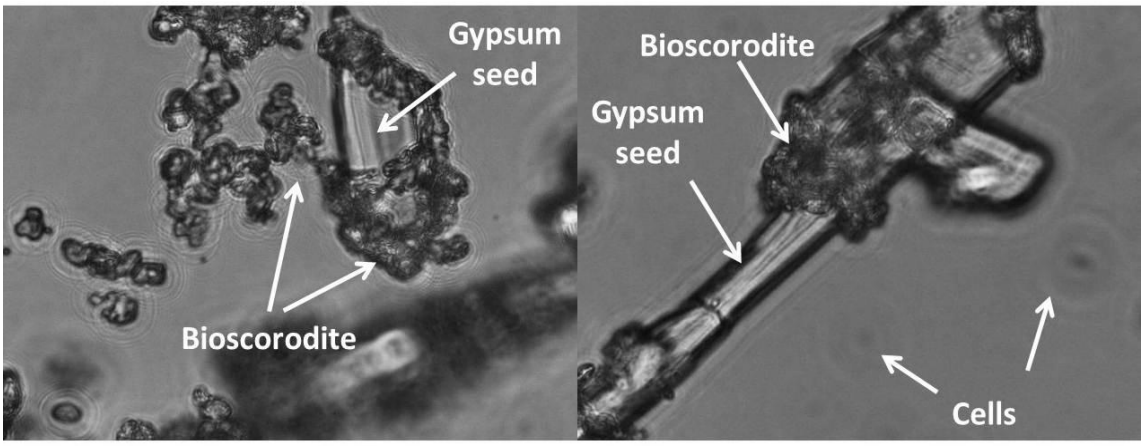

FIGURE 3.5 Bioscorodite formed on the surface of gypsum crystals at pH 0.8 and 80°C.

3.3.4 Characterization of obtained solids by biologically induced crystallization without gypsum

Solids were analysed by ICP-OES, SEM-EDX, XRD, TGA and FT-IR techniques, and the crystal habit by SEM. The characteristics of the scorodite from our experiments were compared with literature data available for mineral scorodite and scorodite produced by hydrothermal crystallization (Table 3.2).

The amount of arsenic removed from solution matched the amount of arsenic contained in the produced solid material. XRD diffraction showed that all the peaks belonged to the scorodite crystal pattern while other precipitates were not identified (Fig. 3.6).

The Fe/As molar ratio of bioscorodite crystals measured by ICP-OES was 0.98-1.28. However, SEM-EDX indicated an Fe/As molar ratio close to 1.0 (Fig. 3.7).

The TGA curve of the bioscorodite crystals showed that the inflection point started at 170° to 240°C. The weight loss measured by TGA was 15.1% (15.6% theoretical value for

mineral scorodite); however, between 240° and 400°C the structural water loss increased to 18.6% (Fig. 3.8). The TGA curve of bioscorodite crystals is in agreement with the TGA reported for hydrothermal scorodite. However, between 240 and 400°C, the weight loss was 3% and this suggests that the bioscorodite crystals were contaminated with organic matter that decomposes between 275 and 400°C.

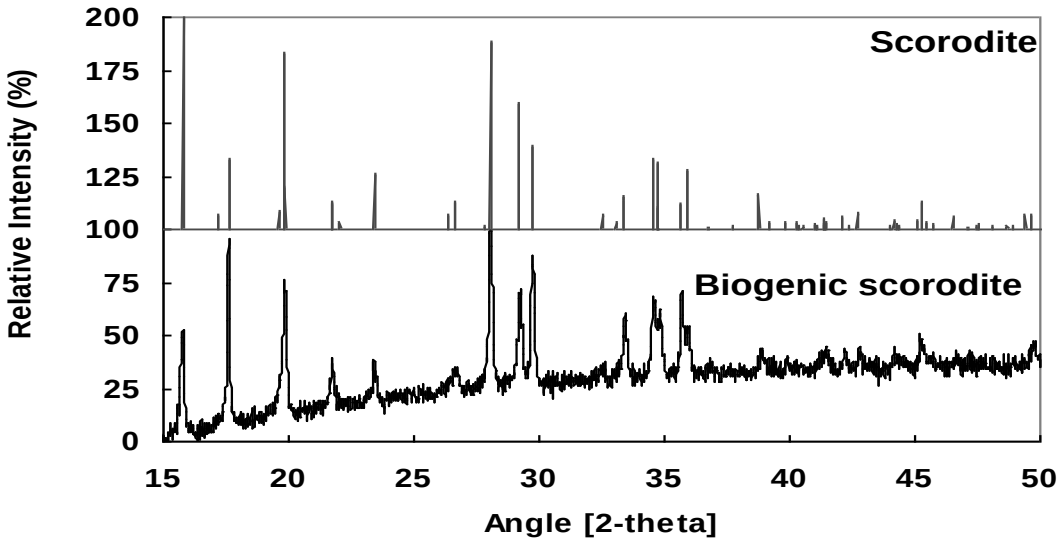

FIGURE 3.6 X-Ray Diffraction of bioscorodite crystals obtained at 80°C and 1 g $L^{-1}As^{5+}$ compared with the XRD pattern for natural scorodite [112, 166]. The solids in our experiments were identified as high crystalline scorodite and no other precipitates were identified in the samples.

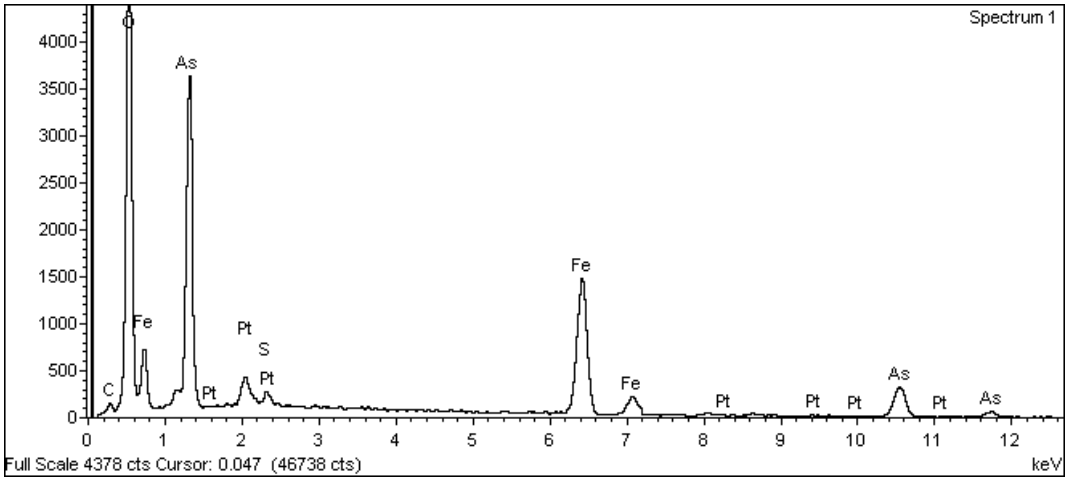

FIGURE 3.7 Typical SEM-EDX spectrum of bioscorodite crystals obtained at 80°C and 1 g L^{-1} As^{5+}.

Using FT-IR it was possible to identify the vibrations from As-O and O-H linkages of the scorodite and to assess whether other precipitates were incorporated in the structure of

scorodite. Arsenate stretching and bending bands at 424 and 819 cm^{-1} of bioscorodite crystals corresponded well with the bands reported for hydrothermal and mineral scorodite [97, 124, 141]. Also, the O-H stretching vibration was identified [97, 124]. Other vibration bands at 1025, 1054, and 2989 cm^{-1} could be due to contamination with phosphate or organic material [44, 134]. In our research, neither the vibration bands reported for sulphate [112, 141], hydrous iron oxides [124] or goethite (α-FeOOH) [124] were found in bioscorodite crystals, revealing that these contaminants were not present (Fig. 3.8).

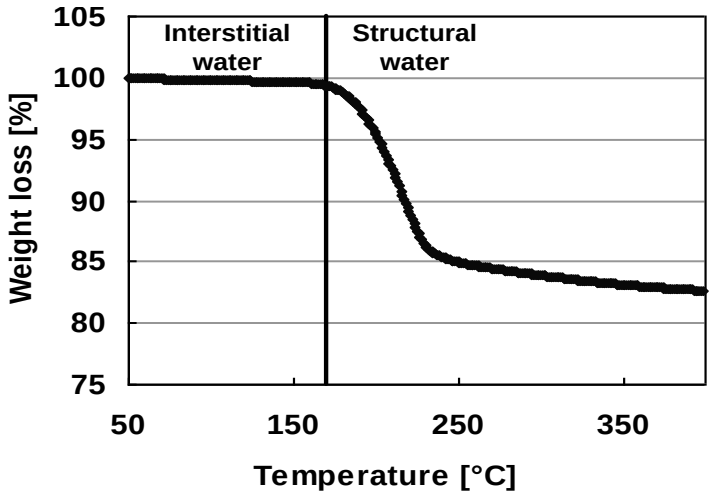

FIGURE 3.8 Evolution of Thermo Gravimetric Analyser (TGA) weight loss of bioscorodite crystals obtained at 80°C and 1 g L^{-1} As^{5+}. Up to 240°C, the TGA curve of bioscorodite crystals is in agreement with the TGA curve reported for hydrothermal scorodite [18, 48, 112, 113], with a sudden trend downward between 170 and 240°C which corresponds to 15.08% loss of structural water.

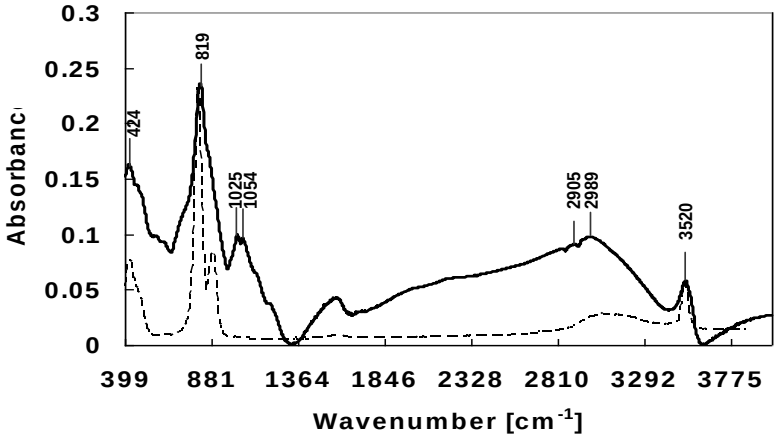

FIGURE 3.9 FT-IR of bioscorodite crystals obtained at 80°C and 1 g L^{-1} As^{5+} (KBr-mode, pellet of KBr with ~1 (wt.%) of scorodite) compared with the FT-IR pattern for natural scorodite [97, 124, 134, 148] in order to identify arsenate vibrations (424-819) and O-H linkages (3520) of bioscorodite.

TABLE 3.2 Comparison of bioscorodite formed in our experiments, using 1 g L^{-1} As^{5+} and 0.85 g L^{-1} Fe^{2+} at 80°C, with mineral (M) and hydrothermal (H) scorodite produced by chemical crystallization. The nature of the scorodite is indicated for each reference as M or H.

Characterization	Bioscorodite (This study)	Mineral/Hydrothermal Scorodite (Literature)
Colour	Pale Green	Pale green
Fe/As molar ratio (ICP-AES)	1.1 (0.98 to 1.28)	1[166]M, 1 (0.98 to 1.05) [112]M
Fe/As molar ratio (SEM-EDX)(Fig.3.7)	0.98 to 1	
As	31.5 %	32.4 % [166]M
Fe	28.1 %	24.2 % [166]M
XRD diffraction (Fig.3.6)		
Reflection angles	15.7, 17.6,19.8,23.4,28.1, 29.2, 29.7, 34.5, 34.8	15.7, 17.6, 19.8, 23.4, 28.1, 29.2, 29.7, 34.5, 34.7 [166]M, [44]M
TGA (Fig. 3.8)		
Weight loss % (170 to 240°C)	15.1 %	15.6 % [48]H, [112]H, [113]H, [18]H
Weight loss % (240 to 400°C)	3.5 %	-
FT-IR (Fig. 3.9)		
As-O vibrations – Bending	424 cm^{-1}	436 cm^{-1} [134]M
Stretching	819 cm^{-1}	820 cm^{-1} [134]M, [96]M, [124]M
O-H stretching vibrations	3520 cm^{-1}	3516 cm^{-1} [134]M, [148]H
SEM (Fig. 3.10-3.11)		
Crystal habit (I)	Crystal size: 1 µm. Octahedral habit. Smooth, ordered and uniform size of dipyramids crystals.	Crystal size: 2-4 µm [113]H, [18]H. Dipyramids that look like octahedrons [166]M, [112]M
Crystal habit (II)	Crystal size: 2-5 µm. Octahedral habit. Dense and uniform aggregate with irregular size of smooth crystals	

The habit and size of the crystals were investigated with SEM for the mix of the solids adhering to the bottom of the bottle and the part that remained in suspension. Two types of

precipitates could be distinguished, one less aggregated (habit I) and one more aggregated (habit II) (Fig. 3.10).

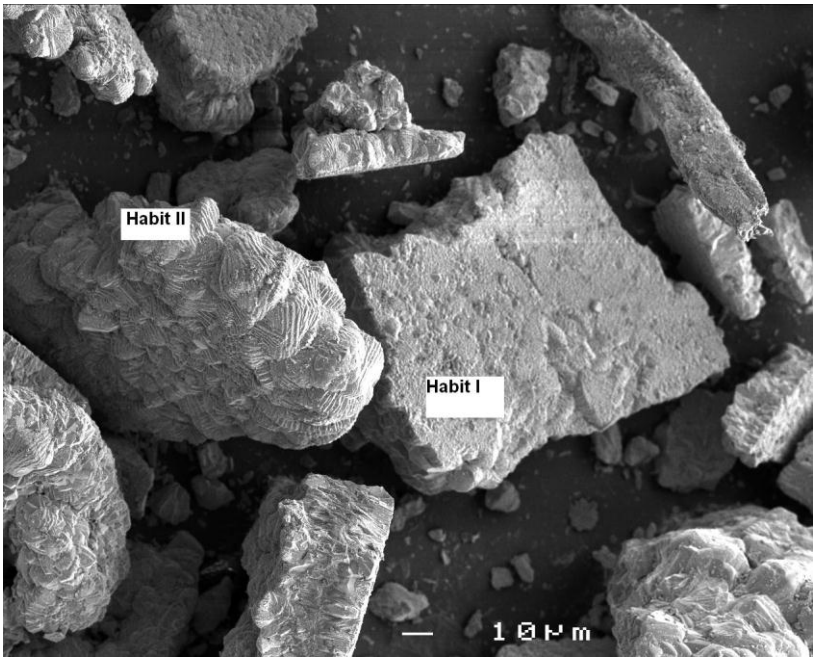

FIGURE 3.10 SEM photograph of the bioscorodite, crystal habit (I) and (II) obtained at 80°C and 1 g L^{-1} As^{5+}. Photograph with 400 x magnification and SE detection at 3.5 KV.

About equal amounts of habit (I) and (II) were present in the samples. The surface of crystal habit (I) consisted of well-defined dipyramid octahedrons displaying smooth surfaces, having a homogeneous size of around 1 μm of length (estimated value) as can be seen in Figure 3.11a and Figure 3.11b, which is the characteristic habit of mineral scorodite [44, 166].

On the surface of the bioscorodite crystals with habit (II) the crystal unit shape is less easily identified as dipyramid octahedron and has a more heterogeneous size distribution (Fig. 3.11c, d). Nevertheless, both crystal habits exhibit the same characteristics as shown in Table 3.2. Habit I and II were evaluated by SEM-EDX showing that both habits have the same elemental composition. Habit I had an Fe/As molar ratio of 0.98 as assessed in several points and habit II had a ratio of 0.90. The lower Fe/As molar ratio obtained in habit II of bioscorodite crystals was attributed to the morphology of the crystal (aggregate surface) which does not allow to operate with the proper angle of the EDX ray. Bioscorodite crystals did not show polycrystalline particles or small aggregates as has been reported for scorodite crystals produced by chemical crystallization [111, 113, 154, 155].

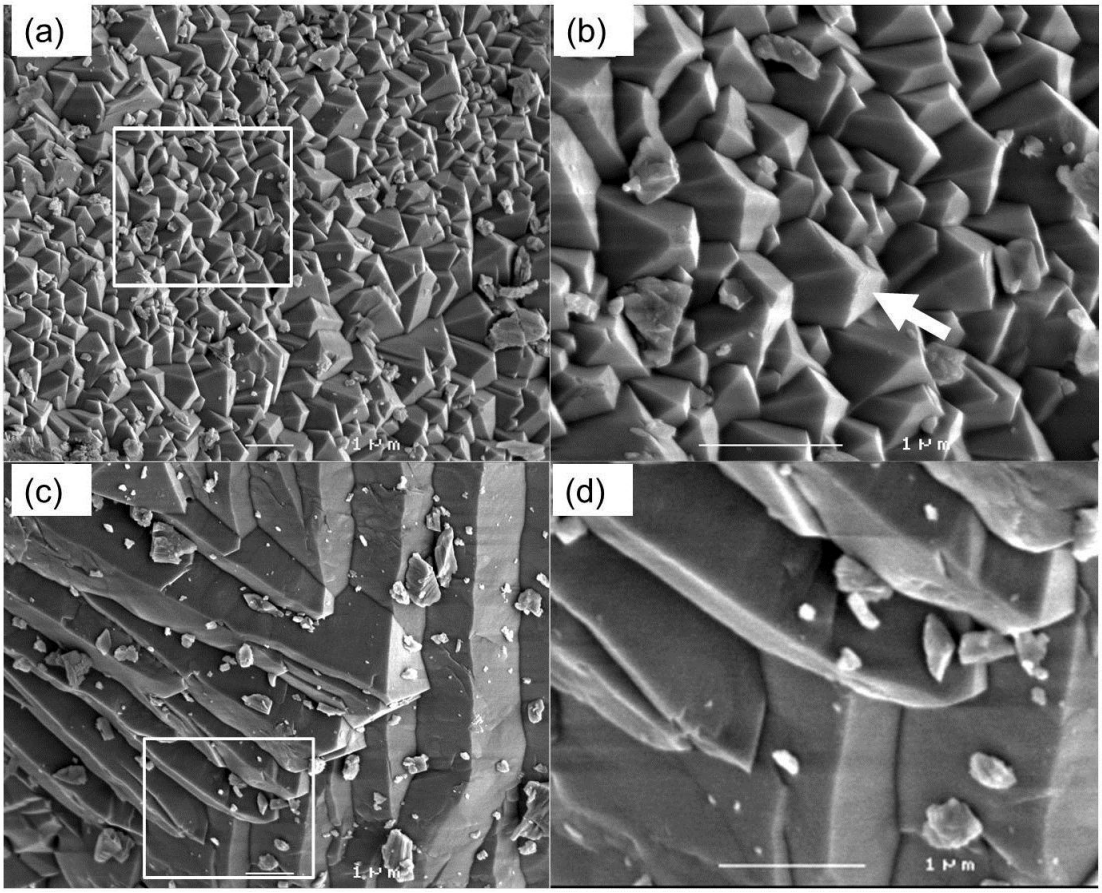

FIGURE 3.11. SEM photographs of bioscorodite crystals obtained at 80°C and 1 g L^{-1} As^{5+}. (a) crystal habit (I) with 1000 x magnification and (b) with 30000 x magnification. (c) crystal habit (II) with 1000 x magnification and (d) with 30000 x magnification. The arrow in Figure 3.11 indicates the typical octahedron habit of the crystal and the squares the selected area for high magnification. SEM performed with SE detection at 3.5 KV.

3.3.5 Environmental impact of biologically induced crystallization of scorodite crystals

In biologically induced crystallization of scorodite, biological oxidation and crystallization take place simultaneously. The crystallization rate is determined on microscale by the slow biological oxidation of ferrous iron.

It is expected that the highly crystalline scorodite formed in our experiments has a low solubility and high stability, which will be evaluated in future work. If the bioscorodite crystals have the same stability properties as the scorodite found in nature, biologically induced crystallization could be applied as an environmentally acceptable strategy for arsenic remediation and storage.

Biologically induced crystallization of scorodite has several advantages compared to chemical crystallization processes used for scorodite crystallization:

(1) the bioscorodite crystals features are very similar to the mineral;

(2) supersaturation is controlled on microscale by biological iron oxidation at 80°C without the use of seed material;

(3) the biological oxidation does not need the use of strong chemical oxidants;

(4) arsenic levels of at least of 1g L^{-1} can be treated (potential future applications of bioscorodite crystallization for metallurgical streams);

(5) crystal and agglomerates size enable an efficient solid-liquid separation.

Several analytical methods confirmed that bioscorodite crystals have the same properties as mineral scorodite and no other precipitates were produced or found in the structure of bioscorodite. This confirms the formation of a high crystalline scorodite without any contaminants. Bioscorodite crystals are similar to scorodite mineral and exhibited the same habit crystal: orthorhombic with a dipyramidal habit [166]. Other studies on scorodite chemical crystallization have not reported the dipyramidal habit of scorodite, instead these reported agglomeration of small undefined particles [154, 155].

Bioscorodite crystals resemble scorodite found in nature but it shows differences with scorodite produced by chemical crystallization. The similarity of bioscorodite crystal with natural scorodite suggests that biologically induced crystallization could be one of the mechanisms that also regulate the occurrence of scorodite in nature.

Chapter 4

Biological ferrous iron oxidation at pH 1 and 75°C by Archaea

Abstract

The extreme acid conditions required for scorodite ($FeAsO_4 \cdot 2H_2O$) biomineralization (pH below 1.3), are suboptimal for growth of most thermoacidophilic archaea. With the objective to develop a continuous process suitable for biomineral production, this research focuses on growth kinetics of thermoacidophilic archaea at low pH conditions. Ferrous iron oxidation rates were determined in batch-cultures at pH 1.1 and a temperature of 75 °C for *Acidianus sulfidivorans*, *Metallosphaera prunea* and a mixed *Sulfolobus* culture. Ferrous iron and CO_2 in air were added as sole energy and carbon source. The highest growth rate (0.066 h^{-1}) was found with the mixed *Sulfolobus* culture. Therefore, this culture was selected for further experiments. Growth was not stimulated by increase of the CO_2 concentration or by addition of sulphur as an additional energy source. In a CSTR operated at the suboptimal pH of 1.1, the maximum specific growth rate of the mixed culture was 0.022 h^{-1}, with ferrous iron oxidation rates of 1.5 g L^{-1} d^{-1}. Compared to pH 1.3, growth rates were strongly reduced but the ferrous iron oxidation rate remained unaffected. Influent ferrous iron concentrations above 6 g L^{-1} caused instability of Fe^{2+} oxidation, probably due to product (Fe^{3+}) inhibition. Ferric-containing, nano-sized precipitates of K-jarosite were found on the cell surface. Continuous cultivation stimulated the formation of an exopolysaccharide-like substance. This indicates that biofilm formation may provide a means of biomass retention. Our findings showed that stable continuous cultivation of a mixed iron-oxidizing culture is feasible at the extreme conditions required for continuous biomineral formation.

This chapter has been published as:
Gonzalez-Contreras, P; Weijma, J, Buisman, C. J. N., Kinetics of ferrous iron oxidation by batch and continuous cultures of thermoacidophilic Archaea at extremely low pH of 1.1-1.3. *Applied Microbiology and Biotechnology* **2012,** *93* (3), 1295-1303.

4.1 INTRODUCTION

Biomineral production has the potential to become an active field of research for the development of new materials and applications. Some of these applications require the adaptation of microorganisms to extreme conditions. This is the case for the biogenic production of scorodite by thermoacidophilic microorganisms, where temperatures above 60°C and a pH below 1.3 are needed to favour the formation of highly crystalline materials (Chapter 3). Scorodite biomineral formation needs at least 1 g L^{-1} of ferrous iron (Chapter 3). This implies that these thermoacidophilic microorganisms must sustain growth at below their optimal substrate concentrations and pHs.

Although previous efforts to produce biominerals using thermoacidophilic microorganisms were successful, more information about the involved microorganisms is needed for the application in a continuous process. Several studies in engineered bioleaching operations describe how *Sulfolobales* archaea mediate the oxidation of mineral sulphides through simultaneous sulphur and iron oxidation [39, 57, 118, 129, 130]. Thermophile conditions (60 – 80°C) in a tank bioleaching reactor are required when a significant portion of the copper is present as refractory primary copper sulphides such as chalcopyrite [138]. Growth parameters reported for *Sulfolobales* species are summarized in Table 4.1, which includes the dominant genera of *Sulfolobus*, *Metallosphaera* and *Acidianus* [93, 129, 142].

TABLE 4.1 Growth characteristics for thermoacidophilic *Sulfolobales* species.

Genus	Species	T_{opt} (°C)	T_{max} (°C)	$pH_{opt.}$	pH range	Specific growth rate μ (h^{-1})	Ref
Sulfolobus	*acidocaldarius*	75	85	2.5-3.5	1-5	0.072 (g)	[14, 83, 93]
	solfataricus	87	88	4	2-5	0.067 (g)	[14, 93]
	shibatae	80	85	3	3-7	-	[14, 93]
	metallicus	68	75	1.8	1-4	0.018-0.025 (p)	[93, 126, 129, 139]
Metallosphaera	*sedula*	75	80	2	1-4.5	0.13 (o)	[57, 93, 129]
	prunae	75	80	-	1-4.5	0.19 (p)	[64, 93]
Acidianus	*infernus*	88	95	2	1.5-5	0.028 (s)	[14, 93, 99]
	brierleyi	70	75	1.5-2	1-6	0.043 (f)	[35, 118]
	ambivalens		95	-	-	0.17 (s)	[93, 99]
	sulfidivorans	75	83	0.8-1.4	0.35-3	-	[140]

Notes: The substrate sources used to determine growth rates are indicated between brackets. (g) glucose, (p) pyrite, (o) ores, (s) elemental sulphur, (f) ferrous iron.

The low growth rate and low cell yield of thermoacidophilic cultures are known bottlenecks for their application in continuous bioreactors [14] and for bioleaching of sulphide minerals [93, 125]. In those applications, *Sulfolobales* species oxidized high ferrous iron concentrations of above 10 g L^{-1} Fe, at the optimum range pH for growth: pH 2-2.5. The iron oxidation rates for thermoacidophiles are about ten times as low as mesophiles iron oxidizing acidophiles [125]. Information concerning thermoacidophilic microorganisms growing at suboptimal conditions and only using a single energy source, such as ferrous iron, is only scarcely available.

The objectives covered in this research are: (1) to select a suitable thermoacidophilic culture for ferrous iron oxidation at extremely low pH of 1.1-1.3, for later use in biomineralization reactors. (2) To determine how the addition of co-substrates (sulphur, carbon dioxide enrichment) affects the microorganisms growing at suboptimal growth conditions, i.e., low pH and low ferrous iron concentration. (3) To determine the kinetics of biological oxidation of ferrous iron in batch tests and in continuous reactors. (4) To evaluate the stability of continuous reactors operated at suboptimal conditions during a period of one year.

4.2 MATERIALS AND METHODS

4.2.1 Microorganism and medium

The archaea *Acidianus sulfidivorans* (DSM 18786) and *Metallosphaera prunae* (DSM 10039) were obtained from the German Collection of Microorganism and Cell Cultures (DSMZ, Braunschweig, Germany). *A. sulfidivorans* originates from a sulphur-rich acidic edge of a hot spring [140]. *Metallosphaera prunae* originates from hot deposits in a slag heap of a uranium mine [64]. Selected physiological characteristics of *A. sulfidivorans* and *M. prunae* are shown in Table 4.1. The mixed culture, kindly provided by M. Gericke from Mintek (Randburg, South Africa), was collected from a hot, sulphur-rich coal dump [68]. The mixed culture has a reported optimum growth temperature of 70°C and a pH optimum of 1.8 [68]. The dominant archaeon in this culture was *Acidianus brierleyi* (98 - 99%). *Metallosphaera sedula* (1 - 2%) and very small numbers of *Sulfolobus* spp. were also present in the culture [39].

The defined growth medium used for the thermophilic acidophiles contained: 1 g L^{-1} $(NH_4)_2SO_4$, 0.1 g L^{-1} KCl, 0.5 g L^{-1} $MgSO_4 \cdot 7H_2O$, and 0.5 g L^{-1} K_2HPO_4 as described by Plumb *et al.* (2002) [139]. Micronutrients were added according to growth medium 150 (DSM 18786). All chemicals used were analytical-reagent grade. Ferrous iron stock solutions were prepared by dissolving iron (II) sulphate heptahydrate ($FeSO_4 \cdot 7H_2O$) at several concentrations in 0.1 mol L^{-1} sulphuric acid (H_2SO_4). Biologically produced elemental sulphur (biosulphur) was used as sulphur source. Biosulphur was obtained from

a full-scale biogas treatment facility (Eerbeek, the Netherlands) in which H_2S is biologically oxidized to elemental sulphur. Biosulphur contains approximately 5% organic matter [95]. Biosulphur particles are hydrophilic and therefore easily dispersible in water, as opposed to chemically produced sulphur [95].

4.2.2 Experimental procedures

Three series of batch experiments and two CSTR experiments were carried out. Serum bottles of 100 mL, closed with a butyl rubber stopper and a crimped aluminium seal were used as incubation vessels. One series of bottles was used for liquid sampling and another for gas sampling. The headspace/liquid volumetric ratio in the bottles was such that a 50% excess of oxygen (in air) was present relative to the stoichiometric amount needed for complete ferrous iron oxidation. The bottles were inoculated 10% v/v with the primary culture and incubated in a shaking incubator at 150 rpm and a temperature of 75°C. Ferrous iron oxidation was monitored by measuring ferrous iron depletion in the medium and oxygen depletion in the headspace. Liquid samples were taken with a syringe, filtered over a 0.45 μm cellulose acetate membrane filter (Spartan 30, Whatman, Germany) and analysed for pH, redox, cell count and ferrous and ferric iron concentration.

Batch experiment 1: selection of thermoacidophilic archaeal culture

For *A. sulfidivorans, M. prunae* and the mixed culture, ferrous iron oxidation rates were determined at 1 $g \cdot L^{-1}$. Bottles were incubated at 75°C. The mixed culture was also cultivated at 70°C (reported optimum temperature [39]).

Batch experiment 2: determination of ferrous iron oxidation rate by a thermoacidophilic mixed culture at 1 g L^{-1} ferrous iron

The growth of a mixed culture oxidizing ferrous iron at 75°C was evaluated at various conditions of pH, the presence of sulphur, carbon dioxide enrichment and ferrous and ferric concentrations. All bottles were incubated with 1 g L^{-1} Fe^{2+}, 5% v/v carbon dioxide enrichment and 100 mg L^{-1} of elemental sulphur as additional energy source and the initial pH was adjusted to 1.7. These conditions were kept the same for all bottles, except when a specific parameter was the subject of study.

Batch experiment 3: kinetics of ferrous iron oxidation by the thermoacidophilic mixed culture at 75°C

The ferrous iron kinetic experiments were carried out at pH 0.9 and 1.3. The ferrous iron oxidation rate was assessed at both pH conditions in a ferrous iron range between 0 and 11 g L^{-1}. Specific growth rate and cell yield on ferrous iron were determined as well.

CSTR reactors

Two aerated Continuous Stirred Tank Reactors (CSTR) were used, each with 1 L of working volume. The temperature was controlled at 75 ± 2°C. The reactors were equipped with electrodes for measurement of oxygen, pH, redox potential and temperature. The air flow to the reactors was controlled by mass flow controllers at a rate of 0.4 volume of air per volume of medium per minute, using a stainless diffuser. The effluent air was dehumidified with condensers and the condensate was returned to the CSTR. No evaporation was observed.

4.2.3 Methods

Iron species in the aqueous phase were measured using Dr. Lange Cuvette test LCK 320 for ferrous (Fe^{2+}) and ferric iron (Fe^{3+}) and a Xion 500 spectrophotometer (Hach-Lange, Germany). Redox potential and pH were measured with glass electrodes QR480X - Pt billed - S8 and QP181X - S8 (Prosense, The Netherlands), respectively. Slope calibration of pH electrode was made with pH 1 and pH 4 buffers. Dissolved oxygen was measured using an InPro 6800 oxygen sensor (Mettler Toledo, Germany) connected to a Stratos e2402-oxy meter (Knick, Germany). The oxygen sensor was calibrated at 0% with nitrogen and at 100% with water-saturated air. Cells were counted in a Bürker-Türk chamber (Brand, Germany). In addition, biomass concentration was measured as the difference between the amount of total nitrogen and the total nitrogen in centrifuged samples (15 min, 12000 rpm). The method is based on the absorbance of nitrophenol with the Dr. Lange cuvette test LCK238 (Hach-Lange, Germany).

Carbon dioxide and oxygen in the gas headspace of the bottles was determined with a gas chromatograph (Fisons Instruments GC 8000) equipped with two columns: 1.5 m x 1/8 inch teflon packed with Chromosorb 108 (60 - 80 mesh) and 1.2 m x 1/8 inch stainless steel packed with molecular sieve 5A (60 - 80 mesh). Both columns were connected in parallel with a split of 1:1. The carrier gas was helium, with a flow rate of 45 mL min^{-1}. Temperatures were 60°C for the column, 110°C for the injection port and 100°C for the thermal conductivity detector.

Autotrophic growth through elemental sulphur oxidation to sulphate was calculated by the difference between the oxygen consumed by ferrous iron oxidation and the consumption of total oxygen in the headspace of the bottles. The sulphate concentration was not measured as the concentration of sulphate in the medium (0.1 mol L^{-1} sulphuric acid medium) was too high to detect a small increase due to sulphur oxidation.

The morphology of the culture was investigated with scanning electron microscopy (SEM). Samples were prepared by mild centrifugation, after which pellets were fixed in glutaraldehyde 2.5% and dehydrated with a grades series of ethanol-water mixtures (70% to 100%). Then the samples were dried by the critical point method and glued on a copper

sample holder using conductive carbon tape and silver tape and sputter coated with 20 nm platinum (JFC 1200, JEOL, Japan). The surfaces were analysed with a FESEM (JEOL 6300 F, Tokyo, Japan) at room temperature, a working distance of 15 mm, and SE detection at 3.5 kV. All images were recorded digitally (Orion, 6 ELI sprl., Belgium) at a scan rate of 100 s (full frame) at a size of 2528 x 2030, 8 bit. Noise reduction and resizing of the images was done with Adobe Photoshop CS. Besides, SEM-Energy Dispersive X-ray Spectroscopy (EDS) (INCA energy, Oxford Instruments Analytical, High Wycombe, England) was used to measure several elements in the samples (C, N, O, and S).

Precipitates from the reactor were collected by filtration using paper filters (Schleicher & Schuell 589/1, pore size 12-25 µm), washed with 0.1 M sulphuric acid, and dried at 60°C. X-ray diffraction (XRD) was used to identify the nature of the solid materials. Wide angle X ray scattering (WAXS) powder diffractograms were recorded on a Philips PC-APD diffractometer in the reflection geometry in the angular range 5–50° (2θ), with a step size of 0.02° (2θ) and an acquisition time of 0.6 s per step. The CuKα1 radiation from the anode, generated at 40 kV and 50 mA, was monochromatized using a 15 µm Ni foil (λ = 0.1542 nm). The diffractometer was equipped with a 1° divergence slit, a 0.2 mm receiving slit, and a 1° scatter slit.

4.3 RESULTS

4.3.1 Batch experiment 1: selection of thermoacidophilic archaeal culture at 75°C, oxidizing 1 g L^{-1} of ferrous iron

The mixed culture and *M. prunae* had a higher ferrous iron oxidation rate (0.31 g L^{-1} d^{-1}) compared to *A. sulfidivorans* (0.01 g L^{-1} d^{-1}) (data not shown). Furthermore, the mixed culture had a higher ferrous iron oxidation rate at 75°C (0.5 g L^{-1} d^{-1}) than at the reported optimum temperature of 70°C (0.34 g L^{-1} d^{-1}) (data not shown). In previous experiments with *A. sulfidivorans* at the same conditions, we observed a higher ferrous iron oxidation rate of 0.04 g L^{-1} d^{-1} (Chapter 3) than in the experiments described here. The lower ferrous iron oxidation rate observed in the current experiments was probably because *A. sulfidivorans* needs an additional energy source such as sulphur or mineral sulphide [140]. The mixed culture was selected for further experiments because of its high ferrous iron oxidation rate at 75°C in comparison with the pure cultures.

4.3.2 Batch experiment 2: determination of ferrous iron oxidation rate by a thermoacidophilic mixed culture at 75°C and 1 g L^{-1} of ferrous iron

A summary of the results is shown in Figure 4.1.

pH effect

The favourable pH-range for the mixed culture was pH 1.4 to 2. At pH 1.2 a small drop in cell concentration was measured even though ferrous iron was completely oxidized. The microorganisms were inactive at pH 0.8.

Carbon dioxide enrichment in air

Air enriched with carbon dioxide up to 1.4% resulted in a small increase in the ferrous iron oxidation rate. However, it was observed that the ferrous iron oxidation rate decreased when carbon dioxide was increased up to 5%. The cell count did not substantially increase with respect to carbon dioxide addition. This was confirmed by the constant total biomass-nitrogen concentration of 1.5 mg N L^{-1}. These results imply that the microorganisms were not limited by carbon dioxide in the gas phase.

The effect of sulphur as a secondary energy source

In bottles supplied with 0.5 and 1 g L^{-1} of elemental sulphur, a pH drop from 1.63 to 1.54 was measured due to proton formation from sulphur oxidation ($2S° + 3O_2 + 2H_2O \rightarrow 2H_2SO_4$ [20]). Sulphur oxidation in the bottles was monitored by oxygen consumption. When oxygen depletion was only the result of oxidation of 0.96 to 0.99 mmol Fe^{2+} per bottle (~ 1 g L^{-1} Fe^{2+}), a stoichiometric oxygen consumption of 0.22 to 0.24 mmol O_2 per bottle was found. When sulphur was added, the total oxygen consumption increased to values of 0.33 to 0.48 mmol O_2 per bottle, i.e., oxygen was consumed by the microorganisms to oxidize sulphur. The supply of sulphur as an extra energy source did not increase the carbon dioxide consumption of 0.024 mmol nor the number of active cells of $3.2 \cdot 10^7$ cell mL^{-1} during the experiment.

The effect of ferric iron concentration

The addition of 5 or 10 g L^{-1} ferric iron resulted in a drop of the pH from 1.5 to 0.8, probably due to precipitation of ferric oxy-hydroxide which is an acid-generating reaction. As a consequence of the pH drop, the cells were inactive and a ferrous iron conversion of only 10% was observed.

4.3.3 Batch experiment 3: batch kinetics of ferrous iron oxidation by a thermoacidophilic mixed culture at 75°C

Two pH values were selected for the batch kinetics. A pH of 1.3 because this is the maximum for scorodite crystallization, and a pH of 0.9 because this is the minimum pH for growth. Both values are suitable for scorodite biomineralization, although the lower pH is preferable because it will minimize the formation of other iron precipitates (Chapter 3). Figure 4.2 shows that higher ferrous iron oxidation rates were obtained at a pH of 1.3 ± 0.07 than at a pH 0.9 ± 0.03. The specific growth rate and growth yield were calculated

from the amount of ferrous iron oxidized by the cells and the increase of biomass measured as number of cells per mL. The growth-substrate relationship is shown in Figure 4.3. The specific growth rate of cells in suspension was a function of limiting substrate concentration (ferrous iron) and pH (0.9 and 1.3). At ferrous iron concentrations below 1 g L^{-1}, linear growth was observed. This indicates that the substrate concentration was much lower than the saturation concentration according to Monod kinetics. At higher ferrous iron concentrations, exponential growth was observed. Despite the lower specific growth rate at inhibiting ferrous iron concentrations (above 8 g L^{-1}), cells were active as shown by the trend line in Figure 4.2.

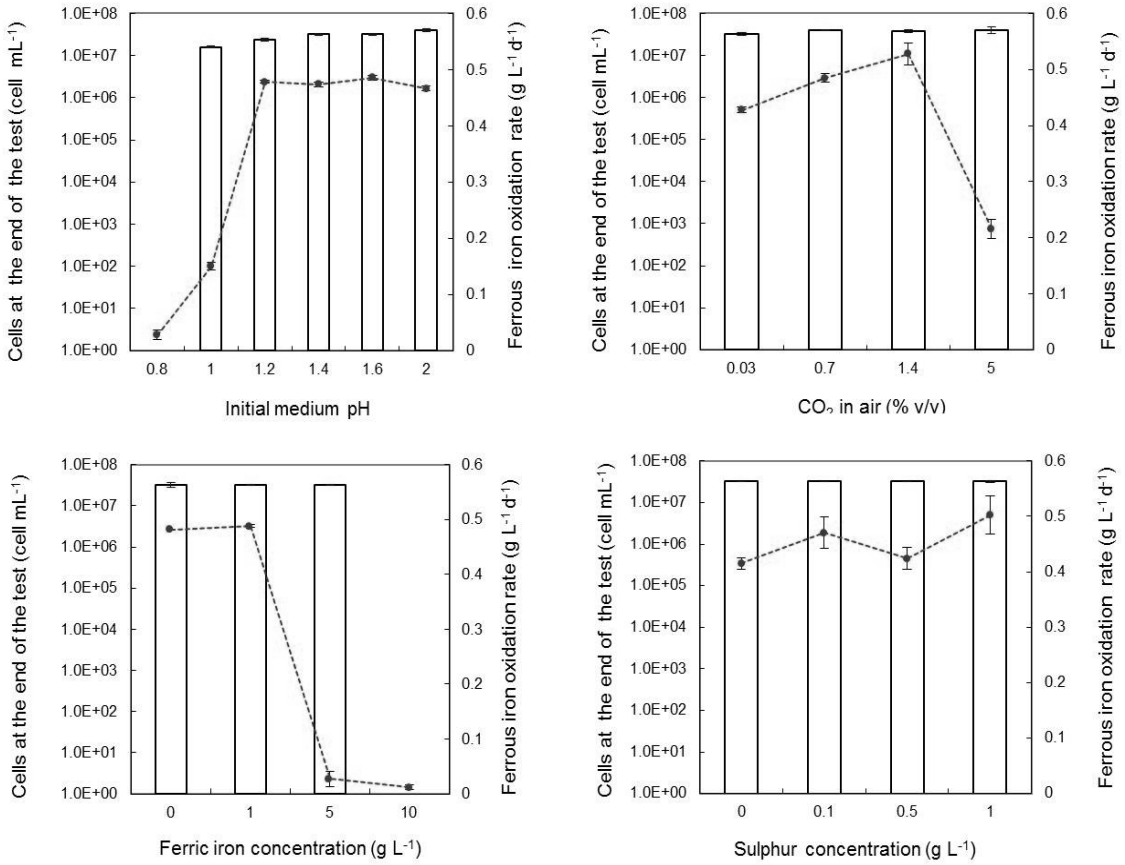

FIGURE 4.1 Influence of initial pH, carbon dioxide enrichment in air, ferric iron concentration, and sulphur concentration on the oxidation rate of 1 g L^{-1} ferrous iron (lines) and on the cell growth (bars). The experiments were carried out at 75°C using the mixed thermoacidophilic culture. Error bars of the duplicates are displayed in the plots. The bottles were inoculated with $3.2 \cdot 10^7$ cells mL^{-1}.

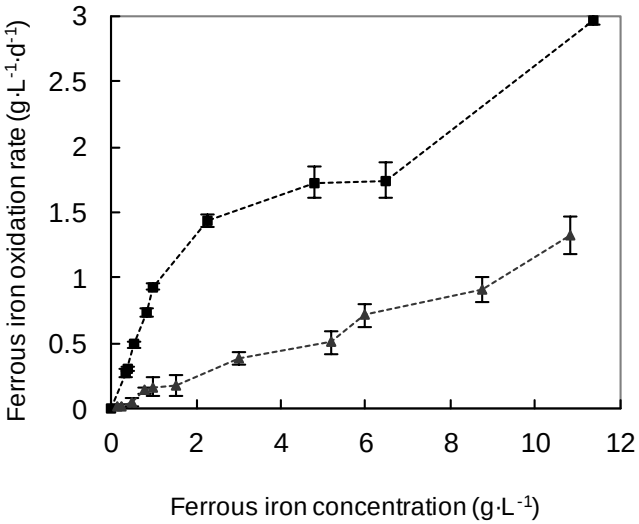

FIGURE 4.2 Biological ferrous iron oxidation rate at different initial ferrous iron concentrations. The biological ferrous iron oxidation rate was evaluated at two pH values: ■ pH = 1.3, ▲ pH = 0.9. Error bars of the duplicates are displayed in the plots.

The maximum specific growth rate and saturation constant were obtained by the reciprocal plot of the substrate versus the specific growth rate. The saturation constant was 0.18 g L^{-1} and the maximum specific growth rate was 0.066 h^{-1} at pH 1.3. The strong effect of the pH on the specific growth rate is shown in Figure 4.3. At ferrous iron concentrations of 1 g L^{-1} the overall (observed) growth yield was higher ($3 \cdot 10^7$ cells kg^{-1} ferrous iron) than at concentrations above 6 g L^{-1} ($1 \cdot 10^7$ cells kg^{-1} ferrous iron).

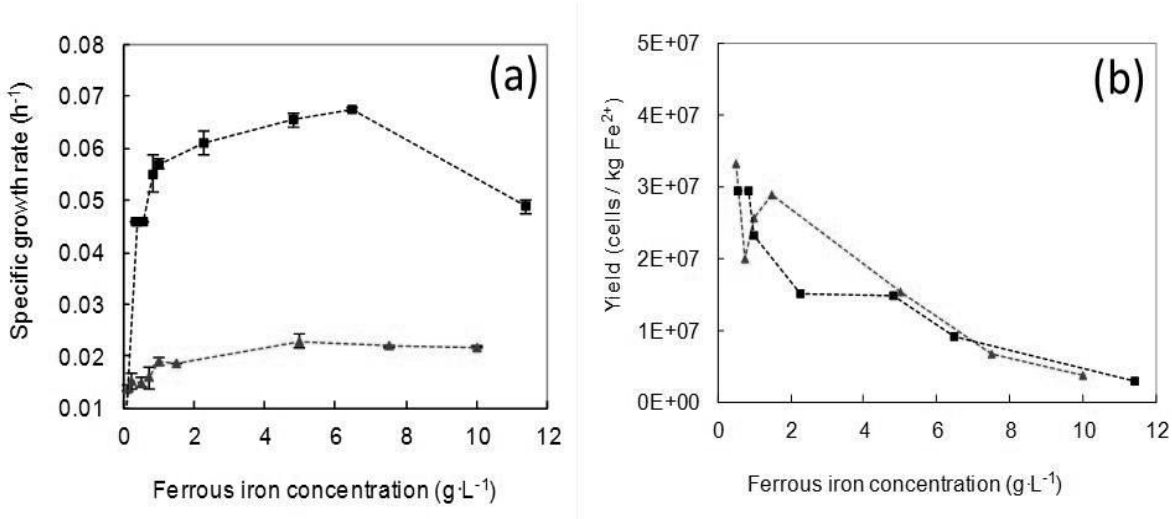

FIGURE 4.3 Specific growth rate (a) and yield of the mixed culture (b) calculated at different initial ferrous iron concentrations. The kinetic parameters were evaluated at two pH values: ■ pH = 1.3, ▲ pH = 0.9. Error bars of the duplicates are displayed in the plots.

4.3.4 Continuous bioreactor tests

The conditions selected for start-up of the continuous reactors were based on the results from batch experiments. In two reactors (CSTR-1 and CSTR-2), the influence of dilution rate and influent ferrous iron concentration on the ferrous iron oxidation rate was determined. CSTR-1 was fed with 3 g L^{-1} and CSTR-2 with 6 g L^{-1} ferrous iron. The start-up strategy of the bioreactors was to increase the dilution rate (D) up to the point where D approaches the maximum specific growth rate (μ_{max}). In both reactors, ferrous iron oxidation rates were determined at the different dilution rates.

The CSTR reactors were started at pH 2 and their adaptation to pH 1.1 was successfully achieved at a dilution rate of 0.01 h^{-1} in CSTR-1 and 0.02 h^{-1} in CSTR-2. The ferrous iron was almost completely (> 90%) oxidized to ferric iron. This was reflected by the high redox potential of 500-600 mV. During periods when ferrous iron oxidation was incomplete, redox values were lower at 400-500 mV (Fig. 4.4). Throughout the continuous experiments, the oxygen level in both reactors remained at 3.23 mg L^{-1}, which is 87 % of saturation at 75°C, showing that oxygen supply was not limiting growth.

In CSTR-1, increase of the dilution rate from 0.01 to 0.022 h^{-1} accelerated the ferrous iron oxidation rate from 0.4 to 1.4 g L^{-1} d^{-1}. Further increase of the dilution rate after 190 days to a maximum of 0.036 h^{-1} resulted in an increase of the effluent ferrous iron concentration and a corresponding lower redox potential (Fig. 4.4), indicating washout of the cells (Fig. 4.5). Subsequently, the reactor was again operated at lower dilution rates and stable iron oxidation was restored. The maximum specific growth rates were calculated using a Lineweaver-Burk plot. Specific growth rates of 0.022 h^{-1} and 0.037 h^{-1} were obtained at pH values of 1.1 and 1.2, respectively. The maximum specific growth rate at pH 1.3, as determined in batch culture, was 0.066 h^{-1}.

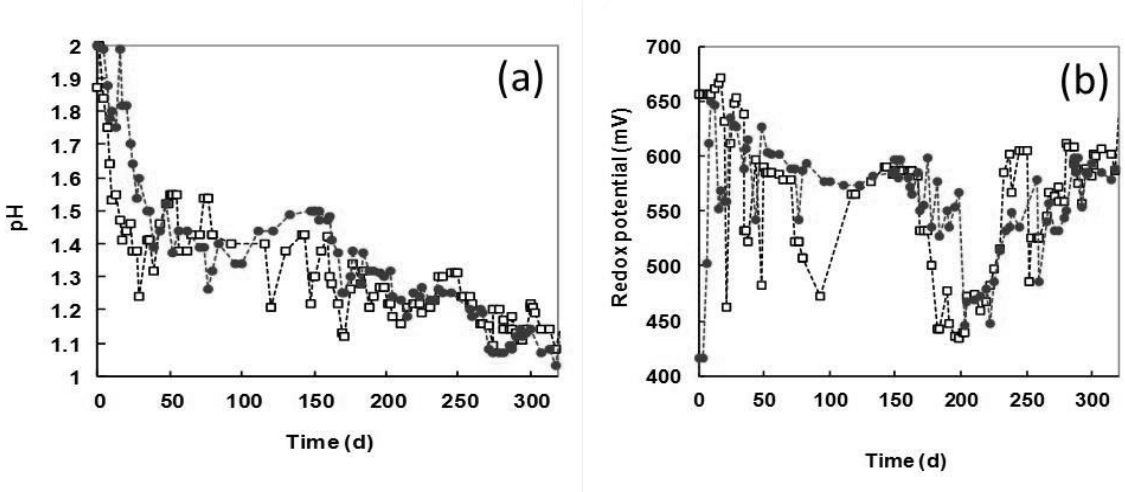

FIGURE 4.4 Redox potential observed during the adaptation to the lower pH in continuous reactors. Legend: □ CSTR-1, ● CSTR-2.

In CSTR-2, the increase of ferrous iron supply in the influent from 3 g L^{-1} to 6 g L^{-1} led to instability of the oxidation process (day 77 – day 203). The ferrous iron oxidation rate fluctuated between 0.5 and 2.5 g L^{-1} d^{-1} and during the period that the reactor was supplied with 6 g L^{-1}, the culture did not reach steady-state iron oxidation (Fig. 4.5). Once the concentration was halved to 3 g L^{-1}, the culture returned to steady state ferrous iron oxidation with a rate of 1.5 g L^{-1} d^{-1} at pH 1.1 at a dilution rate of 0.02 h^{-1}. The unsteady situation observed at 6 g L^{-1} ferrous iron in the influent suggests that elevated ferric iron concentrations may be inhibiting for the cells.

The high ferrous iron oxidation rate of 1.5 g L^{-1} d^{-1} was maintained in CSTR-2 during 80 days of stable operation, demonstrating the stability of the culture. Although high iron oxidation rates were obtained at the suboptimal pH of 1.1, the maximum specific growth rate was only one-third of the maximum value of 0.066 h^{-1}, achieved in batch tests.

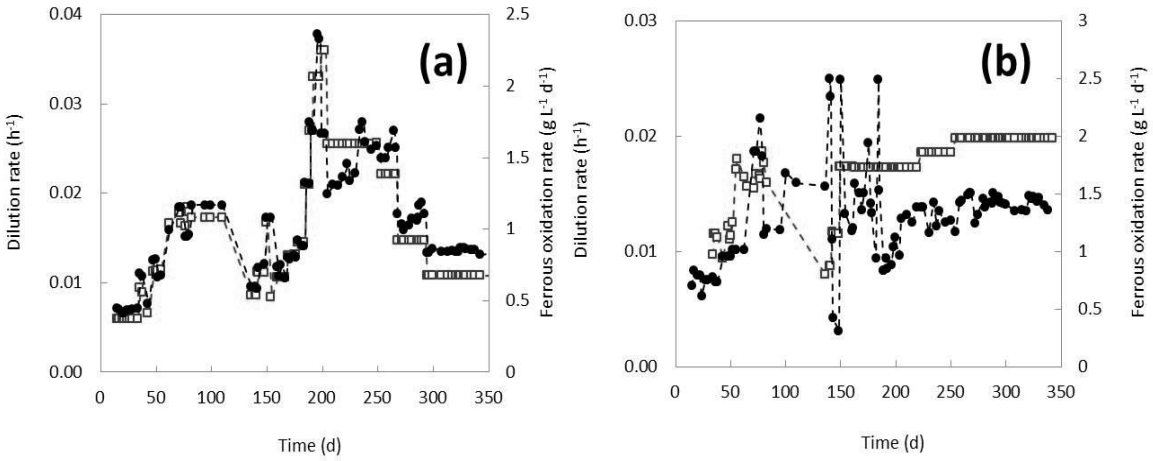

FIGURE 4.5 Ferrous iron oxidation rates at different specific growth rates in (a) CSTR-1 and (b) CSTR-2. Legend: ● ferrous iron oxidation rate, □ Dilution rate.

4.3.5 Morphology of the thermoacidophilic mixed culture

Based on cell morphology, the thermoacidophilic mixed culture can be classified as *Sulfolobales*-like. Figure 4.6(a) shows the lobed coccoid morphology. The size of the cells ranged from 0.5 and 1 μm. These results correspond to the reported morphology of the known *Sulfolobales*-genera *Methallosphaera*, S*ulfolobus*, and *Acidianus* [93].

In samples from batch tests, nano size precipitates were observed on the cell surface (Fig. 4.6(a)). This indicates that the cell activity or the cell surface mediates the formation of these precipitates. The nano precipitates were easily separated and settled as a yellow powder, identified as K-jarosite by XRD analysis (Fig. 4.7). Also in continuous bioreactor tests, the microorganisms induced jarosite precipitation. During these continuous bioreactors tests, also the production of exopolysaccharide (EPS) like substances was

observed (Fig. 4.8). The EPS, which had a typical mucous appearance, was observed between cells and seemed to provide attachment sites for precipitates. The cell surface composition was randomly determined by SEM-EDX at 26%wt.C, 25%wt.Fe, 4%wt.N, 9%wt.S and 35%wt. O.

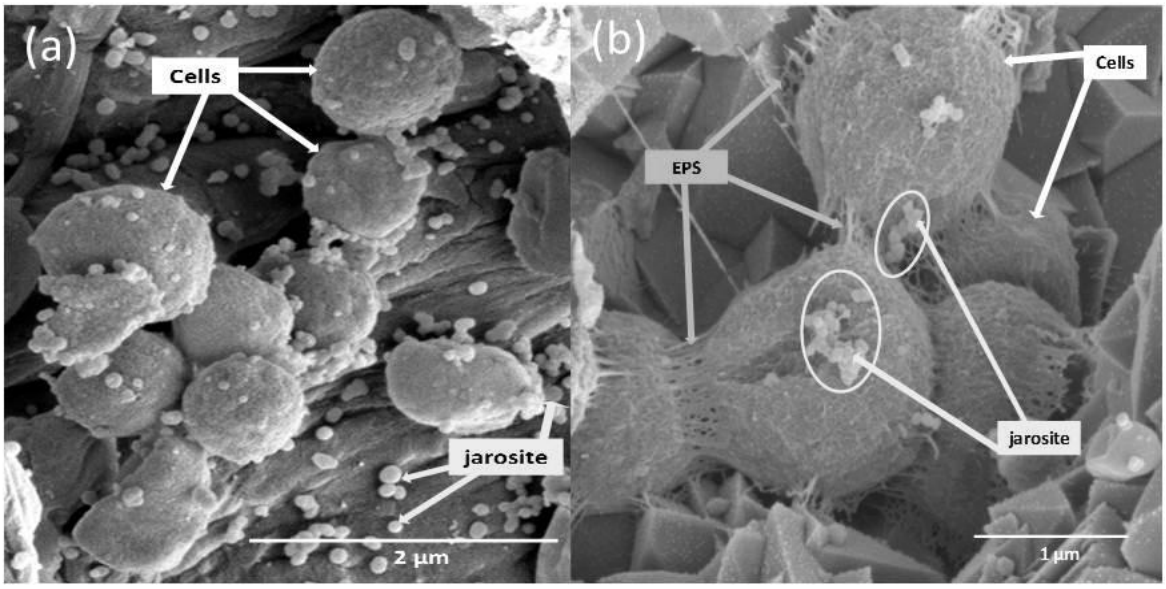

FIGURE 4.6(a) SEM photograph of the mixed culture growing in batch tests in ferrous iron at 75°C and pH of 1.5. Photograph with SE detection at 3 KV and magnification of 25,000 x. Figure 4.6(b) SEM photograph of the mixed culture growing in continuous reactors using ferrous iron at 72°C and pH of 1.2. EPS like material was observed between cells and providing attachment to precipitates. Photograph with SE detection at 3 KV and magnification of 35,000 x.

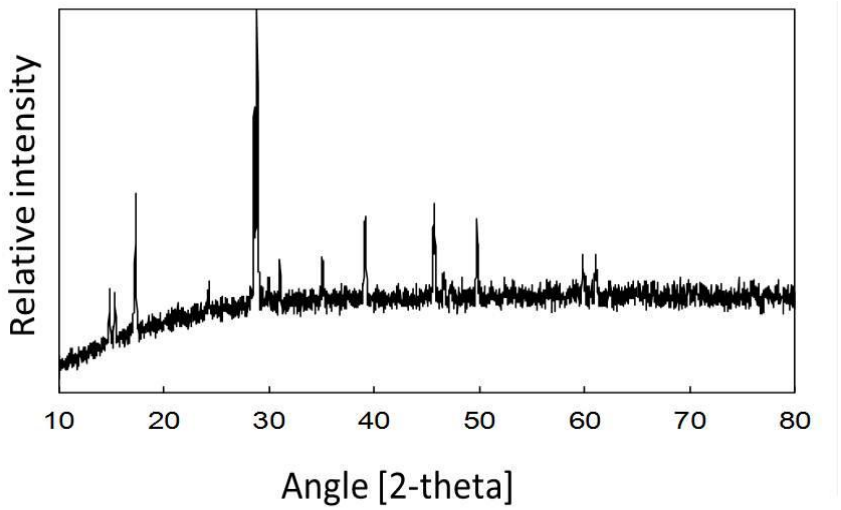

FIGURE 4.7 X ray diffraction identification of K-jarosite nano precipitates. Wide angles were measured in the angular range 5–50° (2θ), with a step size of 0.02° (2θ) and an acquisition time of 0.6 s per step.

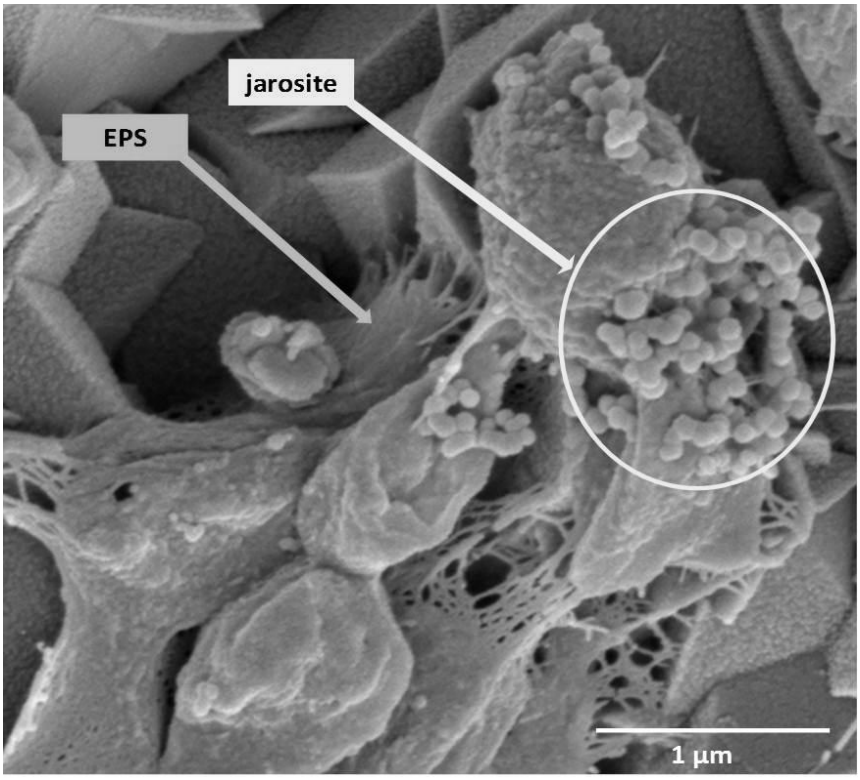

FIGURE 4.8 SEM photograph of the mixed culture growing in continuous reactors using ferrous iron at 72°C and pH of 1.2. EPS like material was observed between cells and providing attachment to precipitates. Photograph with SE detection at 3 KV and magnification of 35,000 x.

4.4 DISCUSSION

4.4.1 Selection of microorganisms and factors affecting the kinetics of iron oxidation by thermoacidophilic culture at 75°C and pH 1.1-1.3.

From batch tests, a mixed culture was selected for further experiments because of its high ferrous iron oxidation rate at 75°C in comparison with the pure cultures. Several factors were studied on the biological oxidation of low ferrous iron concentrations needed for the scorodite process of 1 g L^{-1}.

Supply of another substrate source or enrichment of carbon dioxide did not improve the cells growth but a high concentration of carbon dioxide resulted in a small increase of the iron oxidation rate. The results suggest that the cells may be sensitive to high carbon dioxide concentrations, which decreases the activity of the cells. To our best knowledge, carbon dioxide inhibition of thermoacidophilic microorganism has not been yet described. In contrast, for meso-acidophilic microorganisms carbon dioxide inhibition has been described, although there is no general consensus about the limiting or inhibitory levels [7, 35, 69, 169].

A decrease of pH below 0.8 led to inactive microorganisms. The drastic effect of the pH is a bottleneck for the application of these microorganisms at extremely low pH process conditions. This suggests that a pH decrease in thermoacidophilic cultures must be taken into consideration in the bioleaching of sulphide minerals.

The maximum specific growth rates obtained in the current research, of 0.066 h^{-1} at pH 1.3, are within the typical values reported in literature for thermoacidophilic microorganisms, even though we worked at lower, suboptimal pH conditions (Table 4.1).

4.4.2 Potential applications of the archaeal culture for biomineral formation

In the current study, we determined the kinetics of ferrous iron oxidation by a mixed thermoacidophilic culture in batch and continuous bioreactors at pH values and substrate concentrations below the optimum values for growth. In a continuous CSTR reactor, ferrous iron oxidation was obtained at pH of 1.1 and 75°C. The reactor had a steady ferrous iron oxidation rate of 1.5 g L^{-1} d^{-1} during 80 days at a dilution rate of 0.02 h^{-1}, demonstrating the stability of the process during long term operation.

The presence of polysaccharide-like material suggests that biofilm formation may be possible. This would facilitate biomass retention in suspended growth bioreactors. The formation of EPS by archaea is scarcely reported for thermophiles (above 60°C) [8] and also not for moderate thermophiles (45°C) [13, 171].

The apparent formation of EPS was stimulated during the continuous operations at a low pH value of 1.2 and not during the batch tests. This suggests that EPS could play a major role in shielding the cells from the extreme pH conditions in the bulk solution, by its attachment to surfaces as shown in detail in Fig. 4.8.

In this research, we observed the production of nano-jarosite precipitates at pH 1.1-1.3 during continuous ferrous oxidation by thermoacidophilic archaeon culture. Jarosite formation is favoured at a pH between 1.7 and 2.3 in the temperature range of 60-100°C [34]. Jarosites of biogenic origin are produced at pH values between 2 and 2.5 [15, 51, 77, 78, 165]. Despite the low pH, it seems that the stability domains of jarosite at these temperatures (70 - 75°C) shift towards a more acidic region. In this acidic region (0.1 M H_2SO_4), jarosite remains stable and it will dissolve above 0.5M H_2SO_4 [34]. XRD analysis suggested that the main precipitated formed is K-jarosite. This could be related to the addition of ammonium and potassium to the medium. However, the formation of ammonium-jarosite only takes place above 160 mM NH_4^+ [77, 165], whereas our medium only contained 1.03 mM NH_4^+, therefore we consider the formation of ammonium jarosites unlikely

K-jarosite only needs very low K concentrations to be produced (4 mM K^+) [77], while our medium contained 8.24 mM K^+. Based on the absence of ammonio-jarosite production, it is unlikely that the biomass nitrogen measures were overlapped by nitrogen

contained in the precipitates. More importantly, it also dismisses the possibility that the nitrogen source was stripped out from the medium.

The objective of this research was to study the growth of thermoacidophilic cultures at suboptimal pH and substrate conditions to be used in biomineral production. Biomass retention by using activated carbon as carrier material was tested, but this was not successful because the activated carbon disintegrated at the applied conditions. However, in a mesophilic high fluidized-bed reactor a tenfold increase in the iron oxidation rates was observed when jarosite was used as carrier material for biomass instead of activated carbon [101]. This suggests that jarosite may be used as carrier material in thermoacidophilic reactors to increase the ferrous iron oxidation rates.

The low pH of 1.1 strongly affected the growth rate of the microorganisms, but it did not affect the iron oxidation capacity. Thus, it may be possible to grow the culture at optimal pH conditions to increase cell density, and to use these cells for iron oxidation to mediate biomineral formation in continuous processes. In this study, we demonstrated that it is feasible to grow thermoacidophilic microorganisms in continuous bioreactors at pH values and substrate concentrations below what is considered to be optimum values for growth.

Chapter 5

Indirect biomineralization of bioscorodite crystals

Abstract

Scorodite ($FeAsO_4 \cdot 2H_2O$) is the most stable and therefore safe form of arsenic for long-term storage. This study describes how thermoacidophilic archaea induce scorodite formation at pH 1.2 and 75°C. Our results show the formation of ferric arsenic precipitates on the cell surface despite of pH 1 on solution. Precipitates partially covered the cell surface. These precipitates grew to scorodite crystals in solution. The observations of this study suggest that the iron arsenate precipitates on the cell surface are the precursor of the scorodite crystals observed in solution. Ferric iron precipitates are a direct result of the metabolic activity of the thermoacidophilic archaea. Bioscorodite crystals in solution acted as seed for secondary nucleation, which dominates the crystallization of scorodite.

This chapter is in preparation for submission:
Gonzalez-Contreras, P; Weijma, J, Buisman, C. J. N., Indirect biomineralization of bioscorodite and partial cell encrustation by thermoacidophilic archaeon. (*In preparation)*.

5.1 INTRODUCTION

Humans may be exposed to inorganic arsenic via air, drinking water, food and soil. The effects of arsenic exposure include a variety of skin cancer, internal cancers, cardiovascular, peripheral vascular disease, diabetes and adverse reproductive outcomes [92]. Although arsenic is toxic to humans, some organisms have evolved to tolerate this metalloid up to 20 g L^{-1} [39, 80, 114, 135, 158, 161]. Organisms can oxidize, reduce, methylate and demethylate arsenic.

Scorodite crystals are presently known as the safest medium for arsenic immobilization due to their low solubility, high stability and compactness [18, 106, 146]. Previously, we demonstrated the biogenic formation of scorodite by the thermoacidophilic iron oxidizing archaeon *Acidianus sulfidivorans* at pH 0.8 and 80°C (Chapter 3). Bioscorodite crystals resembled scorodite mineral as found in nature, suggesting that microorganisms may mediate scorodite formation in nature. Characteristic of biological scorodite formation is that the rate of ferrous iron oxidation dictates the scorodite crystallization rate. This results in low ferric iron concentrations on a microscale level, low supersaturation levels and therefore high degree of crystallinity (Chapter 3). Biologically mediated scorodite formation may have a strong environmental impact as it may be applied as an environmentally acceptable strategy for arsenic remediation and storage.

Iron oxidizing microorganisms are very active in the ferric hydroxide mineralization. These microorganisms can promote mineralization through oxidation and hydrolysis of cell-bound Fe(II), the binding of ferric iron species and colloids to negatively charged ligands, or the alteration of local pH and redox conditions due to their metabolic activity [103]. During biomineralization, occasionally the microorganisms are encrusted by the minerals. This has been mainly observed in neutrophilic iron oxidizing microorganisms. For example, at neutral pH, and under partially reduced conditions, chemolithoautotrophic Fe(II) oxidation by *Gallionella ferruginea* leads to high rates of iron mineralization [103]. To avoid complete biomineral encrustation, microorganisms have develop several strategies such as EPS production in combination with zones of low pH, produced as a result of the precipitation of iron oxides [28, 58, 81, 84, 98]. This mechanism has also been observed with biominerals that do not contain iron, such as Vaterite ($CaCO_3$) [149] and Uraninite (UO_2) [71]. The mineral encrustation process may lead to nutrient limitation and deficiency in substrate uptake by the microbes [81].

Theoretically, acidophilic iron oxidizing microbes do not need a mechanism to avoid encrustation because the acidic environment keeps ferric iron dissolved. In the current study, we aim to elucidate the role of the archaea in the scorodite formation.

5.2 MATERIALS AND METHODS

Bioscorodite crystals formation was achieved following the same procedure as in Chapter 3. This is keeping the scorodite supersaturation at a low level by slow biological oxidation of ferrous iron. Batch experiments were carried out at pH 1.2 and 75°C. Arsenic, iron, pH and redox potential were measured during the 38-day experiment in samples filtered over 0.2 μm membranes. In a second study, ferrous iron concentrations between 0.2 and 1 g Fe^{2+} L^{-1} were studied to determine if ferrous iron oxidation kinetic would influence bioscorodite precipitation.

5.2.1 Microorganism

Instead of using a pure culture of *Acidianus sulfidivorans*, we now used an enriched culture of iron-oxidizing thermoacidophilic Archaea. Originally, the mixed culture has a reported optimum growth temperature of 70°C and a pH optimum of 1.8 [68]. At pH growth conditions for scorodite, i.e. pH<1.3, with the mixed culture a higher ferrous iron oxidation rate of 0.5 g L^{-1} d^{-1} was obtained (Chapter 4) when compared with 0.04 g L^{-1} d^{-1} for *A. sulfidivorans* (Chapter 3).

5.2.2 Medium

Growth medium 150 DSM-18786 was prepared without ferrous iron source and arsenate. All chemicals used were analytical-reagent grade. Iron (II) sulphate heptahydrate ($FeSO_4 \cdot 7H_2O$) was used as the ferrous iron source and was dissolved in 0.25 mol L^{-1} sulphuric acid (H_2SO_4) before use. Arsenate was added as disodium hydrogen arsenate heptahydrate ($Na_2HAsO_4 \cdot 7H_2O$). All the solutions were adjusted to pH 1.0 with concentrated sulphuric acid. Arsenate and ferrous iron were added to the bottles once the temperature of the medium reached 75°C.

5.2.3 Iron speciation in aqueous phase

Iron species (Fe^{2+} and Fe^{3+}) in the aqueous phase were measured using Dr. Lange Cuvette test LCK 320 and a Xion 500 spectrophotometer (Hach-Lange, Germany).

5.2.4 Arsenic in aqueous phase

The arsenic was measured with a HPLC system coupled to a UV detector (Chapter 2). Accuracy of arsenic speciation measurements have an error of less than 1% according to statistical analysis.

5.2.5 Structure characterization of solids

Solids were taken after 10, 20 and 37 days of crystallization for structural characterization.

X -ray diffraction (XRD) was used to identify the nature of the solid materials. Wide angle X-ray scattering (WAXS) powder diffractograms were recorded on a Philips PC-APD diffractometer in the reflection geometry in the angular range 5–50°(2θ), with a step size of 0.02°(2θ) and an acquisition time of 0.6 s per step. The CuKα1 radiation from the anode, generated at 40 kV and 50 mA, was monochromatized using a 15 μm Ni foil (λ = 0.1542 nm). The diffractometer was equipped with a 1° divergence slit, a 0.2 mm receiving slit and a 1° scatter slit.

The structural H_2O content of the solid phases was determined with a thermogravimetric analyser (Perkin-Elmer TGA7 equipped with Pyris software). The thermal gravimetrical analysis was performed with about 10 mg of air-dried powdered material at a heating rate of 10°C min^{-1} from 50°C to 900°C under air/nitrogen atmosphere.

Fourier transform infrared (FT-IR) spectra of the solid samples were obtained on a Varian Scimitar 1000 FT-IR spectrometer equipped with a DTGS-detector. The measurement resolution was set at 4 cm^{-1} and the spectra were collected in the range of 4000–400 cm^{-1} for KBr disks and 4000-650 cm^{-1} for attenuated total reflectance (ATR) with 64 coadded scans. KBr sample disks were prepared from a mixture of 1 wt % of finely ground sample in KBr. The sample chamber was purged by N_2 gas for 10 min before scanning was started. ATR was performed on a PIKE MIRacle ATR equipped with a diamond w/ZnSe lens single reflection plate.

The morphology of the culture was investigated with scanning electron microscopy (SEM). Samples were prepared by mild centrifugation. The pellets were fixed in glutaraldehyde 2.5% and dehydrated with a grades series of ethanol-water mixtures (70 to 100%). Then the samples were dried by the critical-point method. Samples were glued on a copper sample holder using conductive carbon tape and silver tape and sputter coated with 20 nm Platinum (JFC 1200, JEOL, Japan). The surfaces were analysed with a FESEM (JEOL 6300 F, Tokyo, Japan) at room temperature, at a working distance of 15 mm and SE detection at 3.5 kV. All images were recorded digitally (Orion, 6 E.L.I. sprl, Belgium) at a scan rate of 100 seconds (full frame) at a size of 2528 x 2030, 8 bit. Noise reduction and resizing of the images was done with Adobe Photoshop CS. Besides, SEM energy dispersive X-ray spectroscopy (EDS) (INCA energy, Oxford Instruments Analytical, High Wycombe, England) was used to identify all the elements present in the samples.

5.3 RESULTS

In experiments without arsenic addition, we observed that the mixed culture formed spherical precipitates on the cell surface with a size between 50 and 100 nm (Fig. 5.1). These nano spherical precipitates varied little in size, with a morphology resembling the

crystal habit of the iron oxide ferrihydrite [33]. Structural analysis of the precipitates by XRD, FT-IR, and TGA (Fig. 5.4), revealed however that it was crystalline K-jarosite [$KFe^{3+}_3(OH)_6(SO_4)_2$]. In the experiments with arsenic addition, three stages of scorodite biomineralization were recognized in agreement with the observations after 10, 20 and 37 days of incubation.

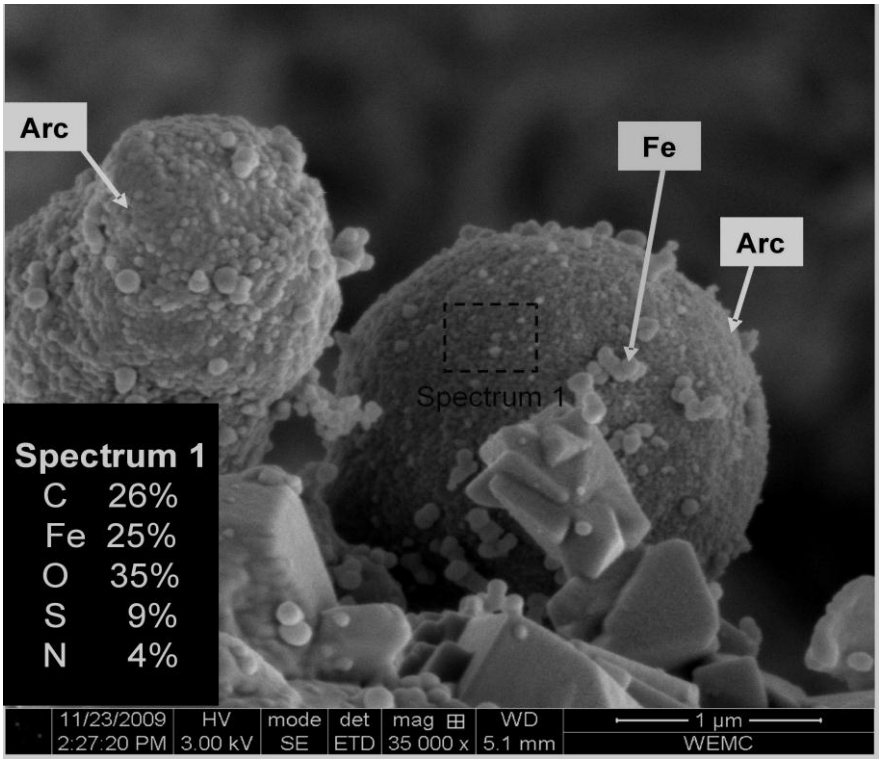

FIGURE 5.1 SEM picture and EDX analysis of the thermoacidophilic archaeon (Arc) and iron oxides nano - precipitates (Fe) in the surface of the cells.

5.3.1 Stage I: biologically mediated formation of scorodite precursors

After 10 days of incubation, 65% of the arsenic and 25% of the iron was removed from solution after filtration over a 0.2 µm filter (Fig. 5.2). A large fraction of the removed arsenic probably has adsorbed to the jarosite already present on the cell surface (inoculum). Precipitates were not visible to the naked eye. Round-shaped, iron- and arsenic-containing precipitates with a size of up to 1 µm were found by SEM-EDX analysis (Figs. 5.3A and 5.3B). An Fe/As molar ratio of 1.02-1.05 strongly suggests that these precipitates are a precursor of the larger scorodite crystals found in later stages. The precipitates appeared to be associated with archaeal cells as indicated by the fairly high carbon content of 5-14%wt. The SEM picture in Fig. 5.3A suggests that at least part of the cell was encrusted with the precipitates. Besides the scorodite precursors, SEM-EDX analysis also showed the presence of jarosite precipitates of the same type as previously found in incubations without arsenic.

5.3.2 Stage II: Growth of biologically formed scorodite mineral

In a sample taken after 20 days of incubation, arsenate depletion from solution had increased to 91% (Fig. 5.2). Angular precipitates with high arsenic and iron content were distinguished by SEM-EDX analysis (spectrum 6 in Fig. 5.3C). The Fe/As molar ratio of the precipitates was close to one, which is the Fe/As molar ratio of scorodite. The size of the precipitates was 1-10 μm, which is larger than the Fe/As precipitates from Stage I (maximum size: 1 μm). Light-green precipitates resembling the colour of scorodite first appeared to the naked eye after 17 days. Like in stage I, nano jarosite particles were still present in stage II. Some arsenic was associated with these particles, possibly due to adsorption (spectrum 8 in Fig. 5.3D).

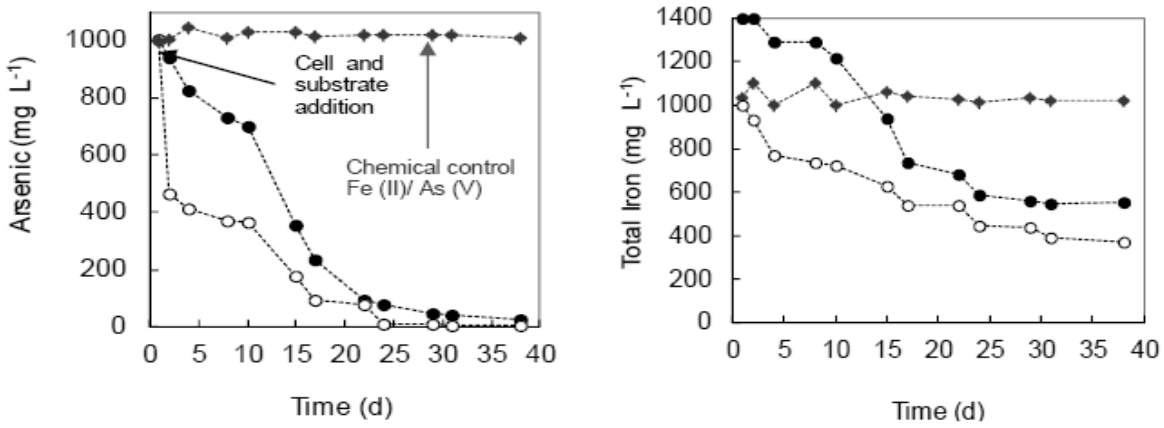

FIGURE 5.2 Kinetics of the biologically mediated scorodite formation in batch experiments and chemical controls. Experiments were started with cells, ferrous iron (Fe^{2+}) and arsenate (As^{5+}). Legend: (●, ○) Differences between duplicates bottled are due to different biological iron oxidation rates; ♦ chemical control (no cells).

5.3.3 Stage III: Ageing of biologically formed scorodite mineral

The last stage of fully crystallized biologically formed scorodite crystals, after 37 days of incubation, is shown in Figure 3E. The crystals now have a size ranging from 10 μm up to 100 μm. The characteristic morphology, orthorhombic with a dipyramidal habit (Figs. 5.3F and 5.3G), and colour of bioscorodite crystals resembles scorodite mineral found in natural samples. The crystallinity and structure of scorodite was confirmed by FT-IR, TGA and XRD analysis (Figs. 5.3A, 5.3B and 5.3C). Also at this stage, still some nano jarosite particles were present.

The differences between the three stages of biologically mediated scorodite formation described above were mainly due to growth and ageing. The FT-IR spectra of the precipitates at stage I contained a higher water fraction as compared with the samples taken in stage II and III (Fig. 5.4B). This suggests that ageing proceeds by desorption of water molecules, which leads to a more structurally ordered phase and favours crystallization of the lowest energy phases.

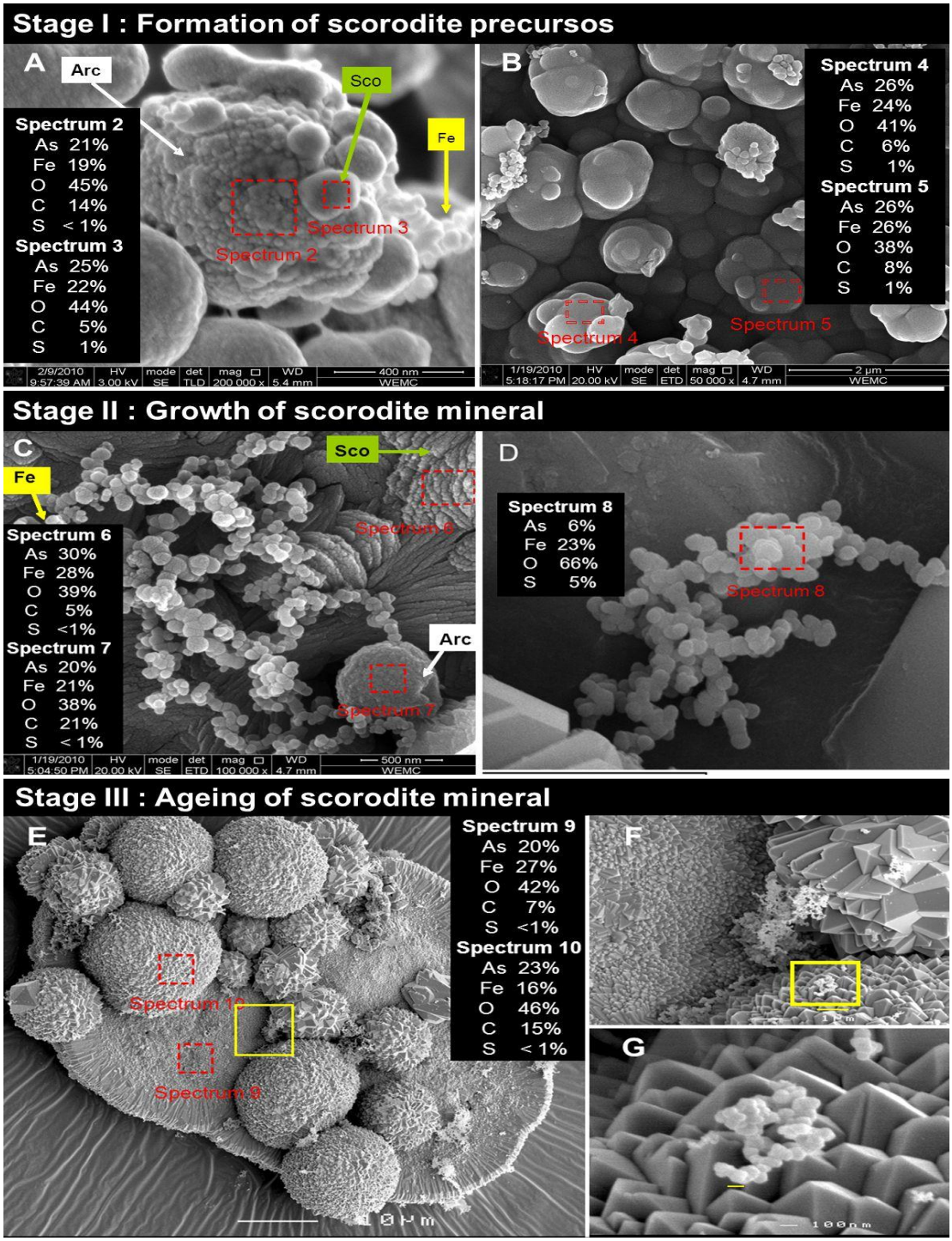

FIGURE 5.3 SEM picture and EDX analysis of stages of biologically mediated scorodite formation. Stage I: (A) SEM analysis of archaeon and scorodite precursor relationship; (B) scorodite precursor and jarosite relationship. Stage II: (C) growing scorodite and jarosite, (D) jarosite not attached to cells. Stage III: (E) General view of scorodite biomineral organization, (F) zoom of the area selected in E; (G) zoom of the area selected F is showing the nano-jarosite crystals deposited over scorodite crystals. Legend: Sco = scorodite precursor, Fe = jarosite nano-precipitates, Arc = archaeon.

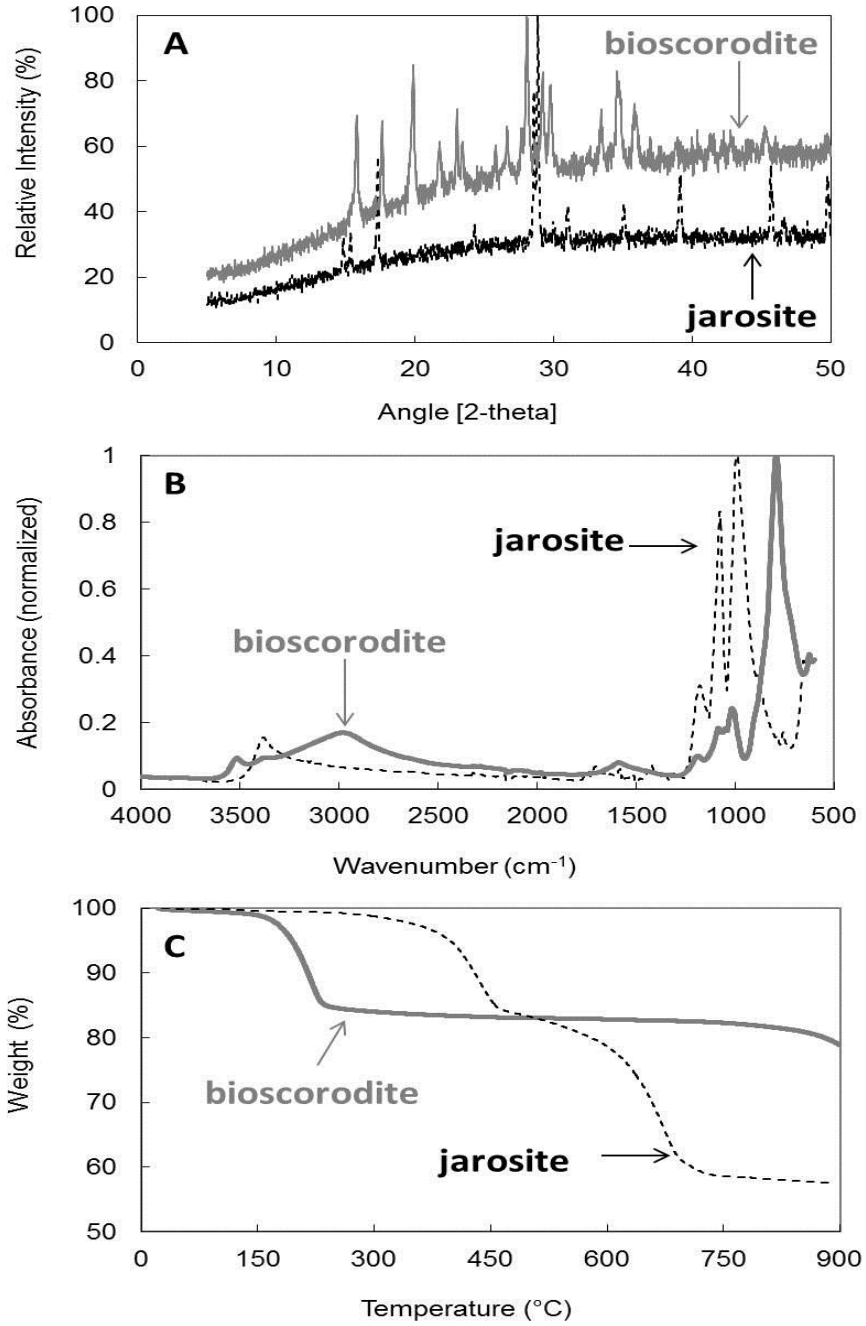

FIGURE 5.4 Structural characterization of bioscorodite crystals and K-jarosite nano precipitates. (A) X-ray diffraction data matching the XRD pattern. (B) Fourier transform infra-red spectra of precipitates identified arsenate bending bands at 819 cm^{-1}, strong O-H bonding at 2900-3080 cm^{-1} stretching corresponding to O-H bond between crystalline water groups and oxygen of the arsenate molecules, and weaker O-H bond between oxygen atoms in crystalline water at 3516 cm^{-1}, sulphate vibrations at 1180, 1780, 993 cm^{-1}, hydroxyl (OH) of the structure is identified in the vibration at 3338 cm^{-1}. (C) Thermo Gravimetric Analyser shows the structural water content between 170°C and 240°C, at 400°C hydroxyl (OH) is converted to H_2O, and near to 700°C sulphate is converted to sulphur oxide.

5.3.5 Biological scorodite formation at different ferrous iron concentrations

The influence of ferrous iron oxidation kinetics on the biogenic precipitation of scorodite was investigated. Ferrous iron concentrations between 0.2 and 1 g Fe^{2+} L^{-1} were tested. Arsenate was added to keep an Fe/As molar ratio of 1 in the experiments.

Bioscorodite formation was observed as a greenish precipitate (naked eye) at concentrations of 1g Fe^{2+} L^{-1}. At 0.7 g Fe^{2+} L^{-1} only few precipitates were observed, while at lower ferrous iron concentrations precipitates were not formed (Fig. 5.5).

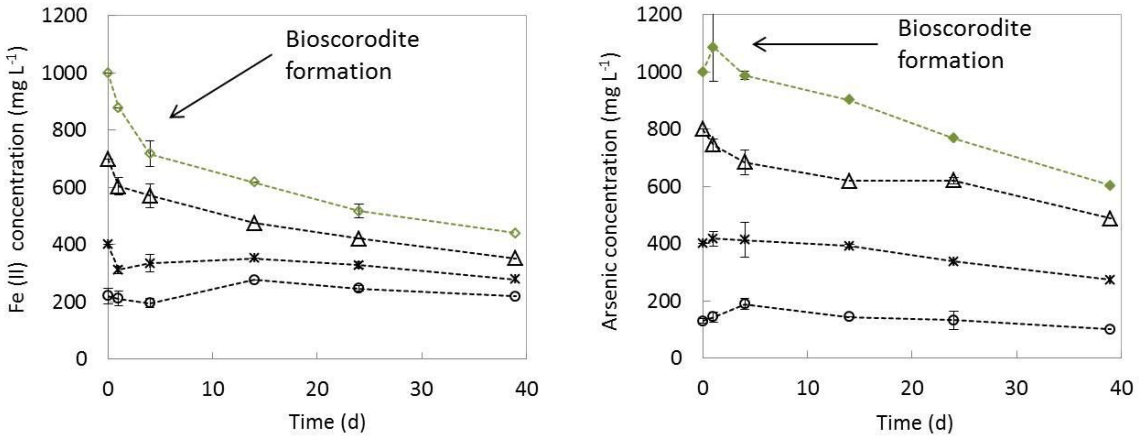

FIGURE 5.5. Bioscorodite formation at different ferrous iron concentrations.

Ion Activity Product of bioscorodite crystals was calculated for all the experiments. The saturation level for all the experiments was calculated on basis of the equilibrium IAP of bottles exhibiting bioscorodite formation. As expected, at lower iron and arsenic concentrations, the solution is undersaturated with respect to scorodite. As scorodite precipitation depends on the iron and arsenic concentrations in the bulk solution, the function of the microorganisms is mainly to oxidize iron at low pH values.

5.4 DISCUSSION

Thermoacidophilic microorganisms were partially covered by arsenic and iron containing precipitates. This suggests that the microorganisms mediated the formation of these precipitates. Based on those observations, the alteration of the saturation state and the subsequent formation of nuclei occur on the cell surface rather than in solution. However, bulk solution concentrations of ferrous iron seem also to regulate bioscorodite precipitation.

Generally, enzymatic oxidation of Fe(II) occurring at extremely low pH due to the activity of acidophiles does not promote ferric hydroxide precipitation because the Fe(III)

formed remains soluble [103]. In the current research, we observed bioscorodite formation on the surface of thermoacidophilic archaea despite of a bulk pH of 1.2.

A possible mechanism for the formation of bioscorodite crystals is proposed and discussed below (Fig. 5.6). As soon as biological iron oxidation takes place in the presence of arsenate (Step 1), precursors of bioscorodite crystals (iron arsenate precipitates) are formed on the cell surface (Step 2). The nucleation of ferric arsenate precursors is favoured on the cell surface because the energy barrier for critical nucleus formation (Sc, saturation on cell surface) is less than the energy needed for nucleation from solution without crystal seeds (Sb, saturation in bulk solution)(Step 3).

Bioscorodite precursors formed at the cell surface grow to form more stable crystals in the bulk solution (Step 4). These crystals are used as seeds for secondary nucleation of bioscorodite crystals in the bulk solution (Step 5). It was also observed that ferrous iron oxidation and bioscorodite formation depended on the initial ferrous iron concentration in the bulk solution. This means that secondary nucleation in the bulk solution dominates the precipitation (Step 6).

Bioscorodite formation seems to be regulated by the bulk saturation rather than by the nucleation on the cell surface. The main role of the microorganism is to oxidize ferrous iron, harvesting energy for growth under extreme conditions. Scorodite formation is more a side effect. Nucleation on the cell surface and its role in the crystallization onset of bioscorodite require further research.

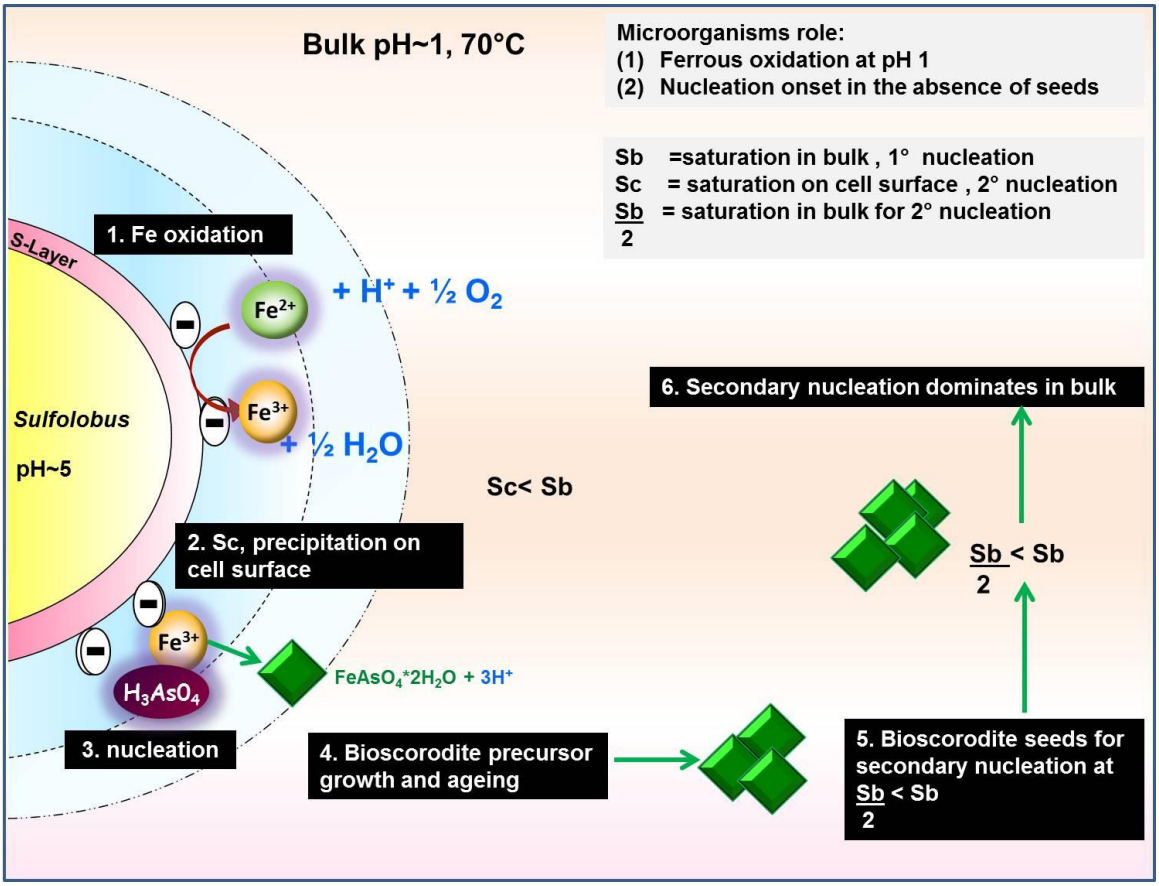

FIGURE 5.6 Indirect biomineralization of bioscorodite crystals by thermoacidophilic archaea. Steps legends: (1) Biological iron oxidation and ferric iron adsorption on negatively charges sites from S-layer in *Sulfolobus*, (2) arsenate and ferric iron nucleation into bioscorodite precursor because the supersaturation on the cell surface (Sc) is less that in the bulk (Sb), (3,4) bioscorodite precursor growth and ageing, (5) bioscorodite crystallized at Sc are used as seeds for secondary nucleation (sb/2), (6) secondary nucleation dominates in bulk conditions at Sb/2 < Sb. The blue zone represents the surrounding bulk solution.

Chapter 6

Low arsenic leaching from bioscorodite crystals during its long-term storage

Abstract

We evaluated arsenic leaching rates from bioscorodite crystals produced with the aid of thermoacidophilic microorganisms. The most stable bioscorodite was produced at pH 1.1, leaching 0.16 μg As L^{-1} after one year under standard TCLP test conditions. Bioscorodite production at pH 1.5 induced less stable precipitates due to high precipitation rates. At an Fe/As molar ratio above 1, jarosite precipitates were formed along with bioscorodite. Concomitant jarosite precipitation did not affect scorodite stability. Leaching of arsenic from bioscorodite crystals was influenced by precipitation kinetics, ageing time and structural water content of the crystals. A high precipitation rate decreased the stability of bioscorodite crystals. An increase of the ageing time from 10 to 22 days reduced the arsenic leaching concentrations from 0.5 to 0.02 mg L^{-1} after one year of storage under landfill conditions. An unexpected low amount of structural water was found in bioscorodite crystals, i.e. less than $2H_2O$ probably due to concealed secondary iron phases. With this study, process conditions (pH, an Fe/As ratio, precipitation rate and ageing time) were determined for the production of highly stable bioscorodite crystals for arsenic removal and disposal.

This chapter has been submitted as:
Gonzalez-Contreras, P; Weijma, J, Buisman, C. J. N., Low arsenic leaching from biogenic scorodite crystals produced for arsenic immobilization and disposal.

6.1 INTRODUCTION

Arsenic is a toxic element that has recognized strong impact in public health and in the environment. Arsenic cannot be reused and its consumption is limited to 10% of the worldwide production [100].

Arsenic stability of the final products resulting from an arsenic removal process should be as high as possible to ensure safe long term arsenic disposal. Leaching of arsenic waste is normally determined by the Toxicity Characteristic Leaching Procedure (TCLP) test (US EPA 2007, Method 1311) [53]. The TCLP test is considered the most aggressive leaching test to assess the toxicity of mineral processing wastes. The test simulates the worst case scenario of co-disposal of mineral processing waste and municipal waste in an unlined municipal waste landfill [53, 56, 88]. The maximum contaminant level (MCL) of the TCLP test for arsenic is 5 mg L^{-1}. Above this value, waste is considered to be hazardous for the purpose of disposal [53]. All the technologies considered as "best available technology" for arsenic removal efficiently remove arsenic from wastewater streams, with the final solid product successfully passing the TCLP test [89]. However, these technologies do not deal with the long term stability of the solid product.

Currently, scorodite is considered the safest material known for arsenic immobilization due to its low solubility, high stability, and compactness with 30 wt% of arsenic [18, 106, 146]. Scorodite ($FeAsO_4 \cdot 2H_2O$) is a secondary mineral related to weathering of arsenopyrite, pyrite, and enargite [29, 60, 110, 151, 158]. Conventionally, chemical scorodite crystals are produced in an autoclave at 150 - 200°C, the so-called hydrothermal scorodite [48, 162]. Scorodite is also produced at atmospheric conditions at 90°C with the aid of foreign or parent seed crystals [38, 59]. The stability of hydrothermal and atmospheric scorodite is assessed by the TCLP test. These crystals leach concentrations between 0.1 and 13 mg L^{-1} of arsenic in 20 h [17, 18, 27, 66, 67, 74, 82, 154]. The reported data for scorodite stability do not correlate with the temperature at which the crystallization took place, the structure or the nature of the crystals, i.e. amorphous or 'partially crystalline' materials.

Despite the good properties of scorodite as arsenic stabilizing product, a scorodite production process is not currently applied to remove arsenic from industrial wastewaters. The main reason is that at ambient temperatures, ferrihydrite/arsenic adsorption is more simple and less costly as compared to chemical scorodite precipitation [144, 159]. However, the sludge produced from the adsorption process displays high stability only if it contains Fe/As molar ratios higher than 3 and if it is disposed in a slightly acidic medium. Arsenic released from ferrihydrite is between 1 and 2 mg L^{-1} from Fe/As = 2.3 and below 0.5 mg L^{-1} with Fe/As = 9 in 20 h of leaching under TCLP test conditions [137, 144, 159]. There are several advantages of atmospheric (<100°C) scorodite precipitation compared to

ferrihydrite/arsenic adsorption, especially regarding the quality of the final product. Scorodite production requires 3 to 5 times less iron and therefore produces 3 to 5 times less waste material. The high stability and favourable settling and dewatering properties of scorodite can reduce the costs of sludge management and disposal.

Recently, biogenic scorodite or "bioscorodite" was produced with the aid of biological ferrous oxidizing thermoacidophilic microorganisms at 75°C and pH 1 in a sulphuric acid medium (Chapter 3). Biological iron oxidation controls arsenic precipitation by increasing the saturation of the solution (Chapter 3). Structural research of bioscorodite crystals demonstrated that its dipyramid octahedron morphology resembles the naturally occurring scorodite mineral better than the chemically produced hydrothermal or atmospheric scorodite (Chapter 3).

The objective of this research was to find the main parameters that affect the leaching behaviour of bioscorodite. For that purpose, we carried out long-term leaching tests with bioscorodite crystallized under various conditions.

6.2 EXPERIMENTAL SECTION

6.2.1 Bioscorodite samples

Bioscorodite crystals were produced in batch flasks as described in Chapter 3 at different pHs, Fe/As molar ratios, and crystal ageing times. The microorganisms used for bioscorodite production were described previously (Chapter 4). Sulphuric acid medium at 0.1 M without arsenic and iron was used to wash the solids by sedimentation at room temperature. Arsenic concentrations were not detected in the medium used for washing. The sedimentation was completed in 2 minutes due to the big flakes size obtained. Following the separation, solids were dried at 70°C during 24 h prior to their use in leaching tests. Separated solids were characterized by XRD, BET, TGA, FT-IR, and SEM prior to the leaching tests. Only samples C and E (Table 6.1) were not fully characterized due to the low amount of material obtained. It was decided to use the material from these two samples for arsenic leaching tests, with the characterization performed afterwards.

6.2.2 Jarosite transformation into scorodite phases

Thermoacidophilic microorganisms incubated in the absence of arsenic produced nano K-jarosites precipitates (Chapter 4). Arsenic adsorption onto jarosite was tested at pH 1 and 75°C in 0.1M sulphuric acid medium. To elucidate the role of jarosite nano-crystals in the bioscorodite formation process, we tested if scorodite can be formed by transformation of jarosite in the presence of arsenic. Jarosite nano-precipitates produced by the microorganisms in the absence of arsenic were filtered over a 0.2 μm membrane filter to remove cells. The jarosite (fraction < 0.2 μm) without microorganisms was exposed for 23

days to the same experimental conditions as applied for scorodite precipitation, i.e. in the presence of arsenic (1 g L^{-1}) at 75°C and pH 1.2 and at a concentration of 50 g jarosite L^{-1}.

6.2.3 Iron speciation in aqueous phase

Iron species in the aqueous phase were measured using Dr. Lange Cuvette test LCK 320 for ferrous iron (Fe^{2+}) and ferric iron (Fe^{3+}), and a Xion 500 spectrophotometer (Hach-Lange, Germany).

6.2.4 Arsenic speciation in aqueous phase

Arsenic speciation in aqueous phase was measured by anionic ion exclusion chromatography using sulphuric acid as mobile phase, followed by UV detection. The validation of this method is described in Chapter 2.

6.2.5 Evaluation of solids stability by the TCLP test

The TCLP test was performed in serum bottles agitated in a shaker at 20°C following the EPA procedure [53]. Acetate buffer at pH 4.95 was used as leaching medium. The solid to liquid ratio was fixed at 20, thus 2.5 grams of scorodite was mixed with 50 mL of solution. Bioscorodite crystals were produced in batch tests displaying a characteristic 'flake' shape with a size less than 1 cm. Therefore, size reduction of the samples for leaching tests was not required. The duration of the TCLP test was extended from 20 h to 1 year under the same leaching conditions. Volume lost through sampling was replaced with acetate buffer. In this way, after one year 10% of the original volume of the solution was replaced with new acetate solution. Data were compensated for the 10% of dilution produced by the re-filling of the bottles.

6.2.6 Precipitates structure characterization

X-ray diffraction (XRD) was used to identify the nature of the solid materials. Wide angle X-ray scattering (WAXS) powder diffractograms were recorded on a PANalytical ExpertPro System (Almelo, The Netherlands) in the angular range 5–50°(2θ), with a step size of 0.02°(2θ) and an acquisition time of 0.6 s per step. The CuKα1 radiation from the anode, generated at 40 kV and 50 mA, was monochromatized using a 15 μm Ni foil (λ = 0.1542 nm). The diffractometer was equipped with a 1° divergence slit, a 0.2 mm receiving slit, and a 1° scatter slit.

The structural H_2O content of the solid phases was determined with a thermogravimetric analyser (Perkin-Elmer TGA7 equipped with Pyris software). The thermogravimetric analysis was performed with about 10 mg of air-dried powdered material at a heating rate of 10°C min^{-1} from 20°C to 400°C under air. The furnace had a temperature precision ± 2°C and the balance precision was of 0.001%.

Fourier transform infrared (FT-IR) spectra of the solid samples were obtained on a Varian Scimitar 1000 FT-IR spectrometer equipped with a DTGS-detector. The measurement resolution was set at 4 cm^{-1}, and the spectra were collected in the range 4000–400 cm^{-1} for KBr-disks and 4000-650 cm^{-1} for attenuated total reflectance (ATR) with 64 coadded scans. KBr sample disks were prepared from a mixture of 1 %wt. of finely ground sample in KBr. The sample chamber was purged by N_2 gas for 10 minutes before scanning was started. ATR was performed on a PIKE MIRacle ATR equipped with a diamond w/ZnSe lens single reflection plate.

BET surface area analysis was performed with a Tristar 3000 porosity analyser (Micrometrics).

Crystal habit of the solids was investigated with scanning electron microscopy (SEM). Samples were glued on a copper sample holder using conductive carbon tape and silver tape and sputter coated with 20 nm platinum (JFC 1200, JEOL, Japan). The surface was analysed with a FESEM (JEOL 6300 F, Tokyo, Japan) at room temperature, a working distance of 15 mm and SE detection at 3.5 kV. All images were recorded digitally (Orion, 6 ELI. sprl., Belgium) at a scan rate of 100 s (full frame) at a size of 2528 x 2030, 8 bit. Noise reduction and resizing of the images was done with Adobe Photoshop CS.

6.2.7 Determination of Ion Activity Product of bioscorodite formation (described in Chapter 3)

6.3 RESULTS AND DISCUSSION

6.3.1 Structural characterization of solids

Bioscorodite samples were produced at different Fe/As molar ratios and different pH (Table 6.1). The nature of the solids was identified with XRD, FT-IR and TGA analysis. All the samples were identified as scorodite crystals displaying a light greenish colour except for samples G and H, which were composed of scorodite and jarosite displaying a yellowish-orange colour.

Morphology of solids

The crystal habit was investigated with Scanning Electron Microscopy (SEM). All precipitates consisted of well-defined dipyramid octahedron crystals, displaying smooth surfaces. A small fraction of jarosite nano-precipitates was deposited over bioscorodite crystals as indicated in Figure 6.1. The size of single crystal units (dipyramid octahedron) of bioscorodite was between 0.1 μm and 1 μm. The aggregates were formed by small pyramids located in a uniform lattice. In batch tests, these aggregates grew to a size of up to 100 μm.

TABLE 6.1 Precipitation parameters used to produce bioscorodite samples at 75°C

sample	pH	Fe/As	log IAP formation	precipitation arsenic rate (mg L^{-1} d^{-1})	Ageing time (days (±1))[a]	precipitated phase
A	0.8	1	-20.8	60	10	BSco[b]
B	1.2	1	-20.4	54	10	BSco
C	1.2	1	-19.7	48	10	BSco
D	1.5	1	-19.6	100	10	BSco
E	0.9	1	-20.9	30	22	BSco
F	1.2	1	-21.9	30	22	BSco
G	0.9	3	-19.7	18	22	BSco+Jar[c]
H	1.2	3	-20.1	25	22	BSco+Jar

[a] ageing time is defined here as total time of arsenic depletion substracted from induction time, [b]BSco= bioscorodite,[c]Jarosite

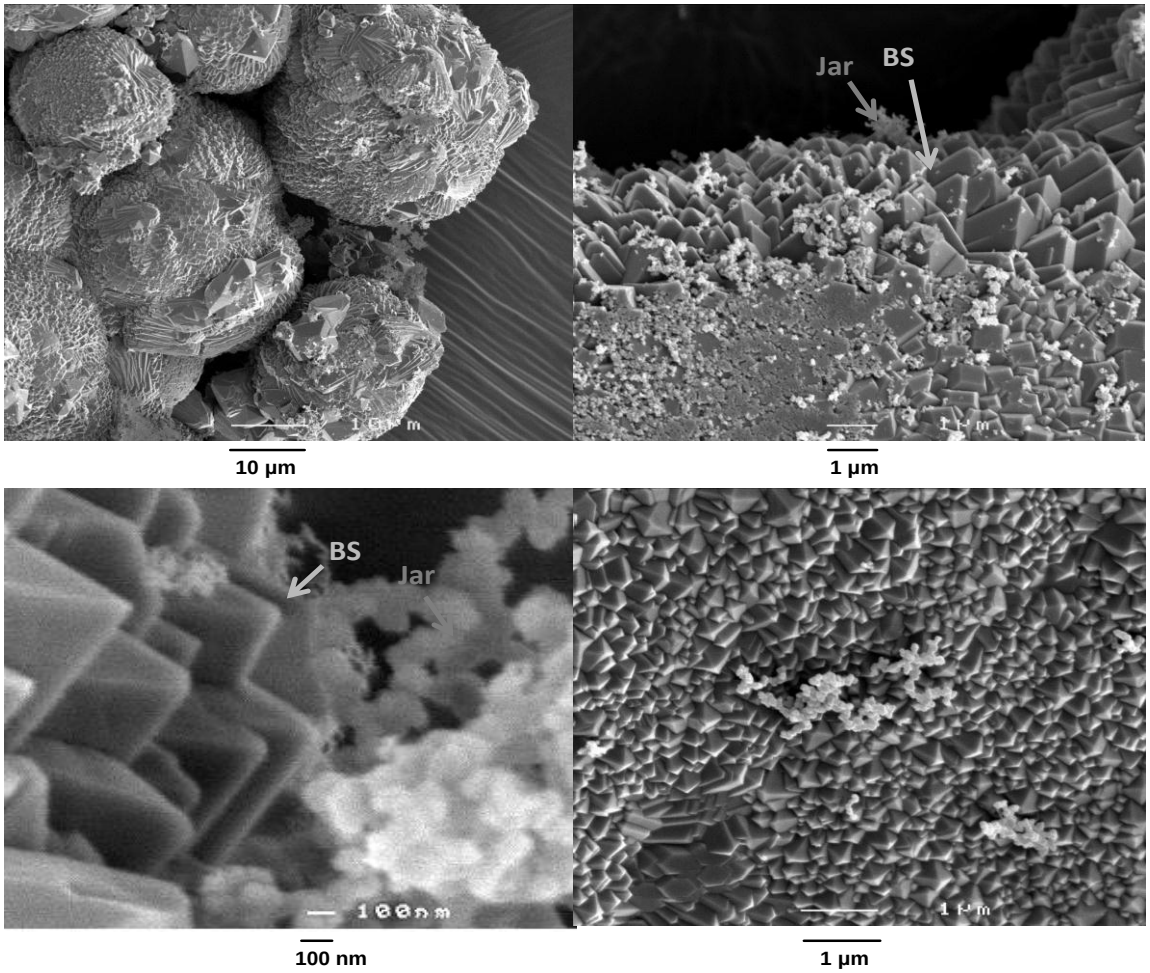

FIGURE 6.1 Selection of SEM photographs from bioscorodite crystals. Legend: Bioscorodite (BS); Jarosite (J).

Crystallinity of solids

The X-Ray Diffraction patterns displayed by bioscorodite crystals matched the patters of scorodite mineral (Fig. 6.2). Because XRD only shows the main solid phases, in samples G and H only jarosite was identified. As shown later, it was found that bioscorodite crystals were also present in these samples.

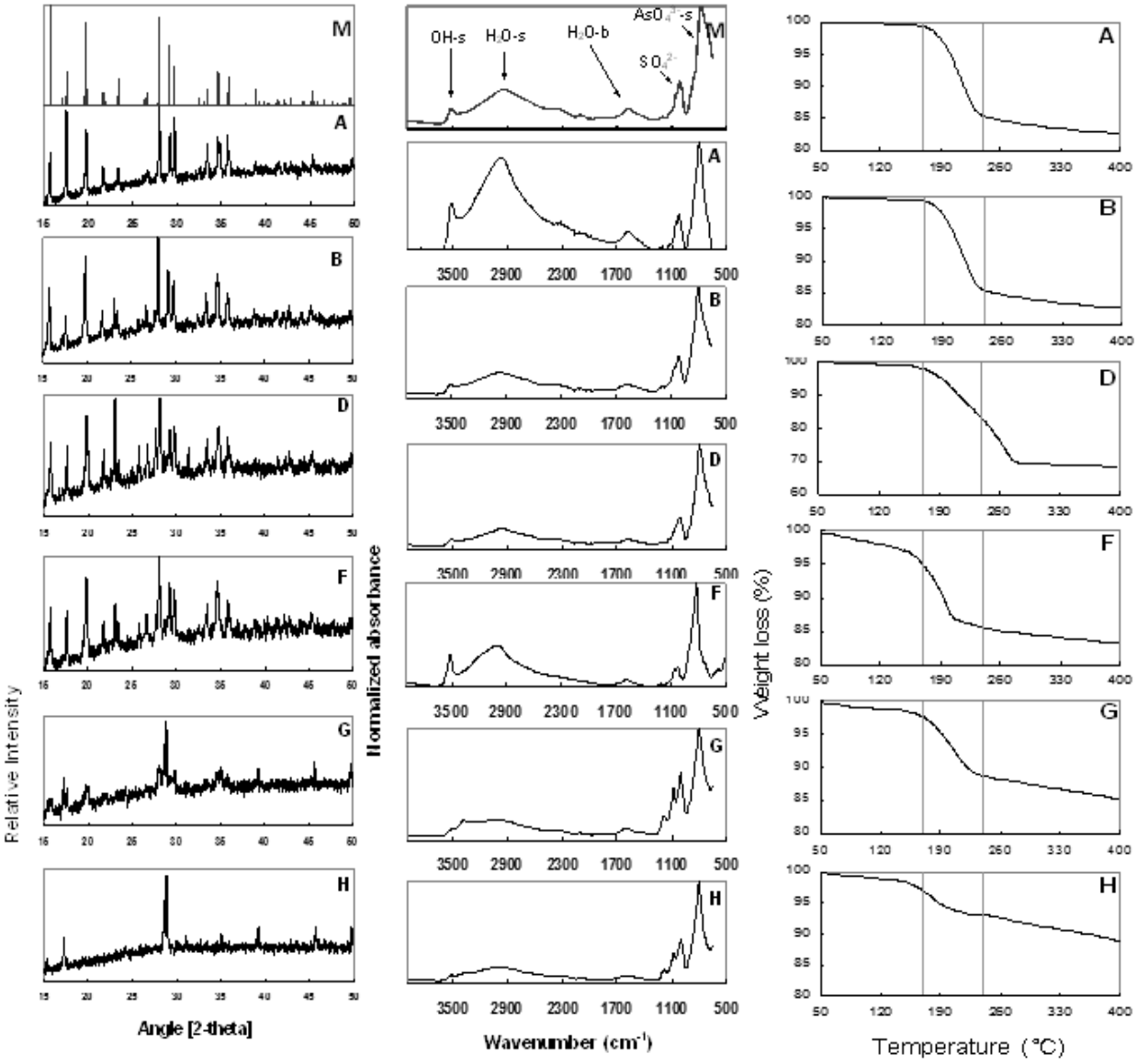

FIGURE 6.2 Results of structural characterization of bioscorodite precipitates. The theoretical spectra of mineral scorodite are labelled "M". All the samples were identified as scorodite except samples G and H which main phase was jarosite mixed with scorodite. FT-IR spectra have been normalized to unity for comparison (Table 6.2). The deflection points of scorodite in TGA analysis were measured between 170 and 270°C (Table 6.3). The legend of the samples is described in Table 6.1.

Sulphate incorporation into bioscorodite crystals

Scorodite produced by chemical synthesis in a sulphuric acid medium often display a relatively high sulphate peak in FT-IR spectra. This sulphate peak, half the size of the arsenate peak, is due to sulphate incorporation into the crystal structure [73]. The FT-IR analysis shown in Figure 6.2 reveals the characteristic peaks of arsenate (V1 AsO_4^{3-}) and water stretching bonding (H_2O str.) of scorodite, in addition to the three sulphate peaks which are characteristic for jarosite (V1, V2, and V3 SO_4^{2-}). In the samples containing only scorodite crystals, FT-IR spectra showed only one of the three sulphate vibrations (V1 SO_4^{2-}), with a low sulphate/arsenate ratio (samples A, B, D and F). In contrast, the appearance of three sulphate vibrations with a high sulphate/arsenate ratio indicated the presence of jarosite in samples G and H. The FT-IR analysis also shows that the biologically produced crystals contain less sulphate than the chemically produced scorodite. Probably the sulphate read on the FT-IR is from the washing of the precipitates with 0.1 M H_2SO_4. A detail of the vibrations for all the samples is shown in Table 6.2.

TABLE 6.2 FT-IR spectral assignment for bioscorodite crystals before leaching tests. FT-IR spectra assignment values of scorodite mineral, chemical crystallized scorodite and FasH phase were taken from literature [73]. The legend of the samples is described in Table 6.1.

IR	Scor	FasH	A	B	D	F	G	H
As-O-Fe str	720	740-751	-	-	-	-	-	-
V1 (AsO_4^{3-})	795	790-841	796.5	819.7	819.7	792.6	798.5	796.6
V3 (AsO_4^{3-})	900	860-898-963	-	-	-	900.7	898.8	900.7
V1 (SO_4^{2-})	-	-	1018.4	1024.2	1022.2	1016.4	1001.0	1001.0
V3 (SO_4^{2-})	-	-	-	1053.1	1051.2	-	1080.1	1080.1
V3 (SO_4^{2-})	-	-	-	-	-	1193.9	1184.3	1182.4
H_2O bend	1620	1620	1583.5	1589.3	1589.3	1585.4	1591.3	1591.3
H_2O str	2960	-	2989.6	2958.8	3003.1	2964.9	2999.3	3014.7
OH str	3516	3557-3498-3325	3516.2	3518.1	3520.0	3514.3	3514.3	3514.3

Structural water content

The structural water content of bioscorodite crystals was measured by TGA analysis in the characteristic inflection point of scorodite between 170 and 270°C (Fig. 6.2 Table 6.3). The theoretical water content in mineral scorodite is 15.6%wt., which is equivalent to $2H_2O$. In sample D, which was produced at pH 1.5, 25.8%wt. of structural water was measured. This is equal to 3.4 molecules of water molecules per molecule of scorodite, i.e. 1.4 times more than the theoretical amount of $2H_2O$. In contrast, samples A, F, G and H contained less than $2H_2O$. In the bioscorodite samples (excluding sample D), the structural water content was between 0.6 and 1.8 molecules H_2O per molecule scorodite.

TABLE 6.3 Structural water measured by TGA analysis between 170 and 270°C on bioscorodite samples before leaching tests (c). The legend of the samples is described in Table 6.1.

	A	B	D	F	G	H
(a) 120-250	14.22	14.76	19.22	12.80	10.38	6.05
(b) 170-250	13.74	14.34	18.10	9.63	9.11	4.03
(c) 170-270	14.24	14.94	25.84	9.98	9.57	4.68
(d) 170-400	16.14	16.59	31.61	11.58	12.28	8.11
Interstitial water (a-b)	0.48	0.42	1.13	3.17	1.27	2.02
Water loss after 270°C	1.9	1.7	5.8	1.6	2.7	3.4

The characteristic inflection points of jarosite occur at higher temperatures than those of scorodite i.e. at 400°C, where hydroxyl (OH) is converted to H_2O, and close to 700°C, where sulphate is converted to sulphur oxide (Chapter 5). As it is shown in Fig. 5.4, in jarosite precipitates the weight changes in relation to the temperature changes are not seen before 300°C. Therefore, the weight loss around 170°C in jarosite samples was not expected, indicating the presence of scorodite in samples G and H.

Other ferric arsenate sub-hydrate (FAsH) phases ($FeAsO_4 \cdot 0.75H_2O$) have been produced in autoclave precipitation at 150-230°C [73]. FAsH crystallizes in the triclinic system, in contrast to scorodite, which exists in the orthorhombic system. But also FAsH and scorodite display two different XRD patterns. In contrast to FAsH, bioscorodite crystals resemble mineral scorodite (XRD pattern, FT-IR) with an orthorhombic system that contains less structural water. The lower water content found in several bioscorodite samples may have a relation with a concealed iron phase. This secondary phase could be jarosite or ferrihydrite, the latter would be suggested from a small broadening in the base line of the XRDs. Whether a secondary iron phase was present in the bioscorodite crystals, this was not identified by the analysis performed hereby. To refer to the structural water content in the bioscorodite crystals and to a hypothetical iron secondary phase we will refer as apparent structural water content.

Surface area

BET analysis was only performed for a selected number of samples. The analysis indicated that bioscorodite samples have a relatively low surface area of 4(±2) $m^2\ g^{-1}$. These values are in agreement with surface area values reported for hydrothermal and atmospheric scorodite produced by chemical precipitation: 1.5 to 14 $m^2\ g^{-1}$ [27, 66, 136]. The values are clearly different from the much higher surface area of 40 $m^2\ g^{-1}$ reported for 'nanocrystalline' scorodite, produced chemically at 70°C [136].

6.3.2 Effect of pH, Fe/As molar ratio and crystallization rates on bioscorodite crystals properties

pH effect

The range of pH tested was based on previous studies in which we observed that bioscorodite precipitates are formed between pH 0.8 and 1.5 (Chapter 3). Sample D (pH 1.5) consisted of a light-greenish precipitate that XRD identified as scorodite but which contained 3.4 molecules of structural water instead of 2. The higher structural water content in sample D may be related to a more amorphous phase present in the sample, induced by the higher pH of 1.5. The rest of the samples were not affected by the pH.

The influence of Fe/As molar ratios

When an Fe/As molar ratio above 3 was used (i.e. in samples G and H), scorodite and jarosite were simultaneously formed, conferring a yellowish- orange colour to the precipitate. Previously, we observed that an Fe/As ratio above 3 delays scorodite crystallization and induces jarosite formation at pH 1 (Chapter 3). Also in the absence of arsenic, thermoacidophilic microorganisms produced jarosite (Chapter 4). It was found that jarosite has a high arsenic adsorption capacity of 20 g As^{5+} g^{-1} jarosite at pH 1 (data not shown). This coincided with data reported in literature of 21 g As^{5+} g^{-1} jarosite at the pH range of 1.5-2.5 [6]. Jarosite with adsorbed arsenic did not transform into scorodite. Jarosite is an unwanted product in the bioscorodite process because it can act as a temporary sink for arsenic and trace metals.

Reported values of the solubility product (log IAP) for jarosite are between -93.2 and -98.9 [108]. In contrast, bioscorodite crystals precipitated at a solubility product between -19.6 and -21.9 (log IAP). In the experiments using an Fe/As molar ratio above 3 (Samples G and H), scorodite precipitated until arsenic was completely depleted. Arsenic depletion was followed by jarosite precipitation from the remaining iron.

The calculated solubility product varied between -19.6 and -21.9 as log IAP (Table 1). Sample D had the highest solubility product; 20 times higher than sample E and 200 times higher than sample F. These values indicate that sample D precipitated the fastest and sample F the slowest.

6.3.3 Stability of bioscorodite crystals

Ageing of samples

The total time in which complete arsenic depletion is achieved, consists of induction time, nucleation time, and latent time. Ageing is a term that is used to cover all irreversible changes that take place in a precipitate after its formation [122]. Therefore we define ageing time as the total time minus the induction time. In other words, ageing is

considered to take place from the moment the first precipitates are observed in the solution until the end of the experiment when all arsenic is depleted. Samples A, B, C and D had an induction time of 5 days (±1) and an ageing time of 10 days. In contrast, samples E, F, G and H had an induction time of about 8 days (±1) and an ageing time of 22 days.

Arsenic leaching rates

The results of long-term arsenic leaching tests show that samples A, B, C and D leached between 1.5 and 2 mg L^{-1} of arsenic after one year (Fig. 6.3). These four samples have the same ageing time of 10 days. The most stable was sample A (pH 0.8), which after 350 days leached 1.5 mg L^{-1} of arsenic. In contrast, sample D (pH 1.5) leached 2 mg L^{-1} after only 50 days. The results suggest that the rapid crystal growth rate obtained at a pH of 1.5 leads to the formation of less stable precipitates. It is known that fast precipitation can lead to rapid crystal growth with all the faces growing so rapidly as to disappear [123].

Samples E, F, G and H have a longer ageing time of 22 days. Sample F was the most stable, displaying 0.16 µg L^{-1} of arsenic after one year of leaching. In contrast, sample E initially leached 0.1 mg L^{-1} of arsenic, increasing to 0.2 mg L^{-1} after 50 days and 1 mg L^{-1} after 250 days.

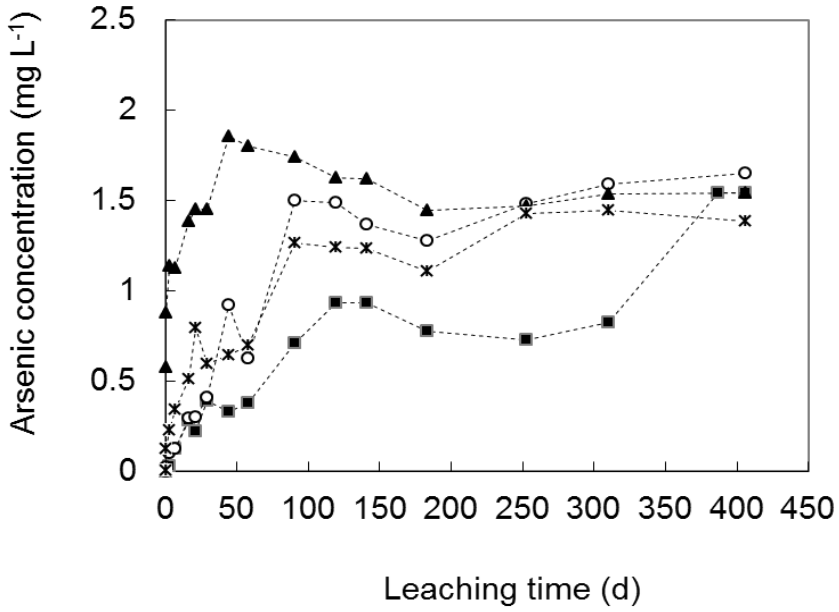

FIGURE 6.3 Arsenic leaching in long term of bioscorodite samples from Group I, produced at high arsenic precipitation rates. The legend of the samples, pH and Fe/As molar ratios used are described in Table 6.1. Legend: ■ = A, x = B, ○ = C, ▲= D.

The results indicate that bioscorodite produced at a pH of 0.9 (sample E) is less stable than the bioscorodite produced at pH 1.2 (sample F). After 50 days, samples G and H

leached 0.2 mg L^{-1} of arsenic. If arsenic was adsorbed to jarosite during the precipitation of scorodite, it should have been detected during the leaching of bioscorodite. However, low arsenic leaching rates were obtained in sample G and H. This means that an Fe/As ratio higher than 1 does not affect the arsenic leaching rates when jarosite is present in the samples.

A comparison of the different leaching rates of all the samples is presented in Figure 6.4. Only sample D displayed high arsenic concentrations after 24 h of leaching. The other samples released 0.2 mg As L^{-1} after 1 week. The differences between the different bioscorodite crystals only became apparent after leaching times of longer than 2 months. TCLP tests with duration of 20 h did not show any differences between the various bioscorodite phases (Fig. 6.4). Therefore, in the case of bioscorodite, the TLCP test is unsuitable to predict or estimate long-term leaching rates. For scorodite crystals, tests with a duration of more than 2 months should be performed to determine the final arsenic leaching value for safe, long-term disposal.

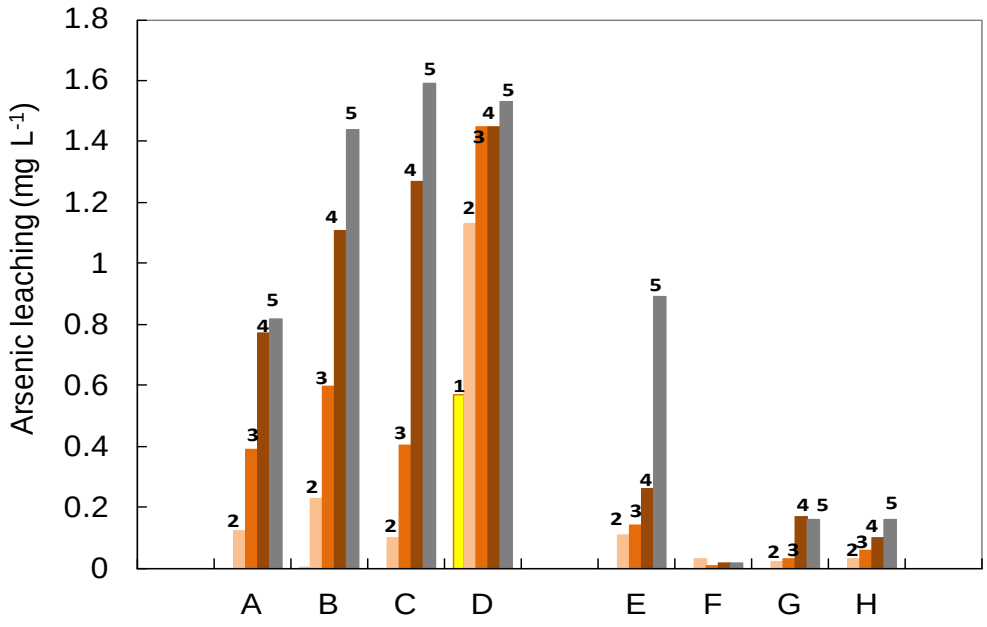

FIGURE 6.4 Sample comparison of different leaching times from 24 h until 1 year. Numbers in the bars indicate the time of sampling at the leaching test: (1) 24 h, (2) 1 week, (3) 1 month, (4) 6 months and (5) 1 year. It can be seen that only bioscorodite sample D displays high arsenic leaching concentrations tested by the TCLP test (1). The legend of the samples, pH and Fe/As molar ratios used are described in Table 6.1.

Effect of ageing on arsenic leaching rates

Besides the variation in ageing time as displayed in Table 6.1 (10 or 22 days of ageing), we also studied the effect of ageing time more specifically with samples E, F, G and H.

For this purpose, the crystallization process was stopped after 2, 12 and 22 days of ageing, which corresponds to a total incubation time of 10, 20 and 30 days. For all samples it was found that bioscorodite crystals with an ageing time of 2 or 12 days was less stable than bioscorodite crystals with an ageing time of 22 days. Figure 6.5 shows the fluctuations of arsenic leaching versus ageing time.

The amount of arsenic leached from the bioscorodite crystals was equivalent to or lower than the amount leached from hydrothermal scorodite. The main objective of our research was to evaluate the arsenic leaching from bioscorodite crystals and to establish parameters that affect the stability. Besides the low arsenic leaching rates obtained from bioscorodite crystals we also observed a remarkable relation between structural water content and stability of the crystals. Because of the significance of these observations they are discussed separately in the next section.

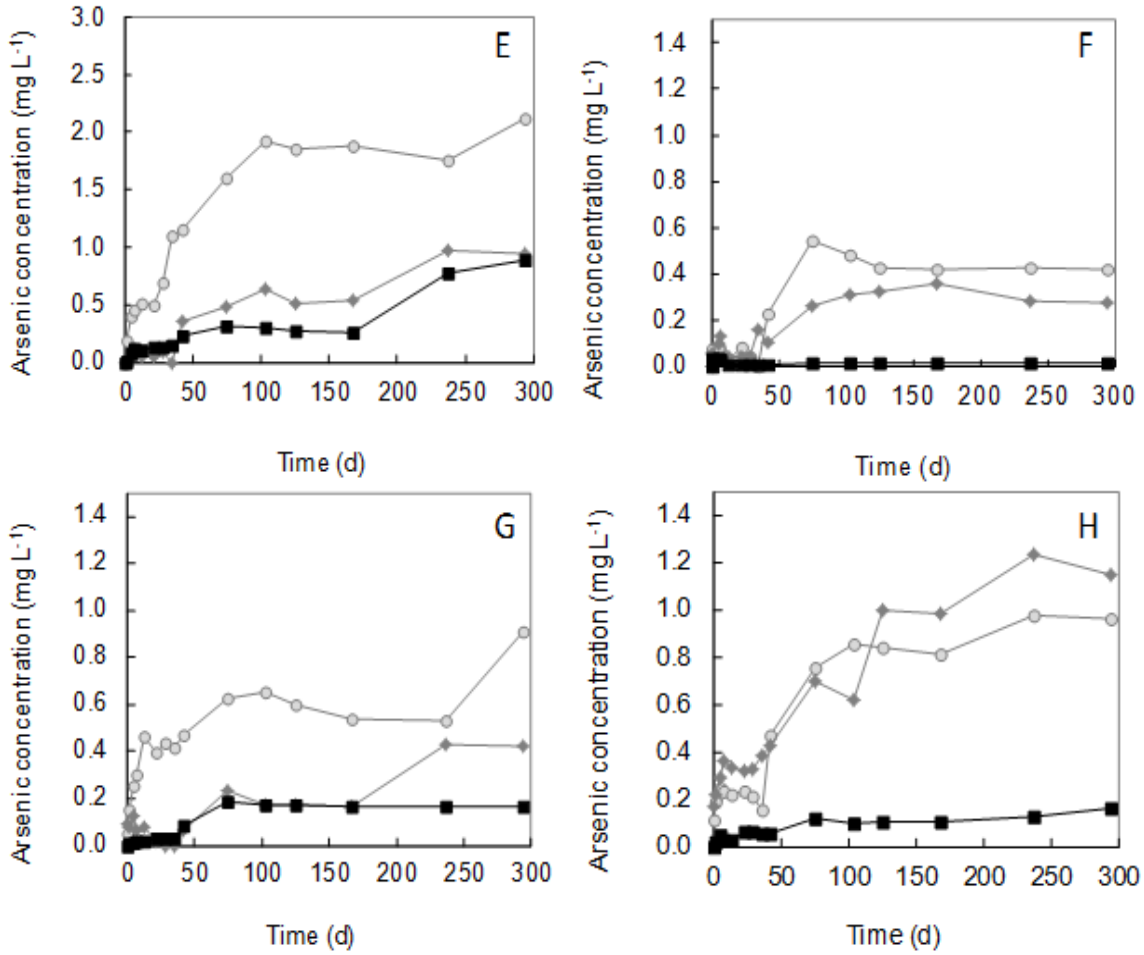

FIGURE 6.5 Long-term arsenic leaching testing of bioscorodite samples precipitated at 75°C and ageing during 22 days. Ageing time legend: ● day 2, ♦ day 16, ■ day 22 (Induction time of 8 ± 1 days).The legend of the samples is described in Table 6.1.

6.3.4 Effect of apparent structural water content on arsenic leaching rates

As it was discussed before, the apparent structural water would mean that the low structural water content measured in bioscorodite crystals was due to the presence of a secondary iron phase. This secondary iron phase could be ferrihydrite, which would also lose structural water but that by the methods hereby used could not be identified because the main phase was scorodite.

It was found that the IAP values (solubility product at saturation) are related to the structural water content of the crystals. Sample D was precipitated at the highest IAP value of $2.5 \cdot 10^{-20}$ (log IAP = -19.6) and contained the highest amount of structural water (Fig. 6.6a). In contrast, the calculated IAP of sample F was the lowest with $1.3 \cdot 10^{-22}$, containing less than $2H_2O$, just like samples G and H.

Surprisingly, the apparent structural water content of the crystals showed a clear correlation with their stability (Fig. 6.6b). Bioscorodite crystals containing 2 or more structural molecules of water displayed the lowest stability. In contrast, bioscorodite crystals containing between 0.8 and 1.5 molecules of water displayed high stability values. The structural water content in scorodite has been indicated as the stabilizing factor in the orthorhombic system of scorodite, specifically because the strong hydrogen bonding between the crystalline water groups and the oxygen of the arsenate molecules [73, 102]. In our results, the most stable bioscorodite (sample F) contained only 1.28 molecules of structural water. The relation between more stability and less apparent structural water content would also indicated that the presence of a secondary iron phase provide more stability to the bioscorodite crystals.

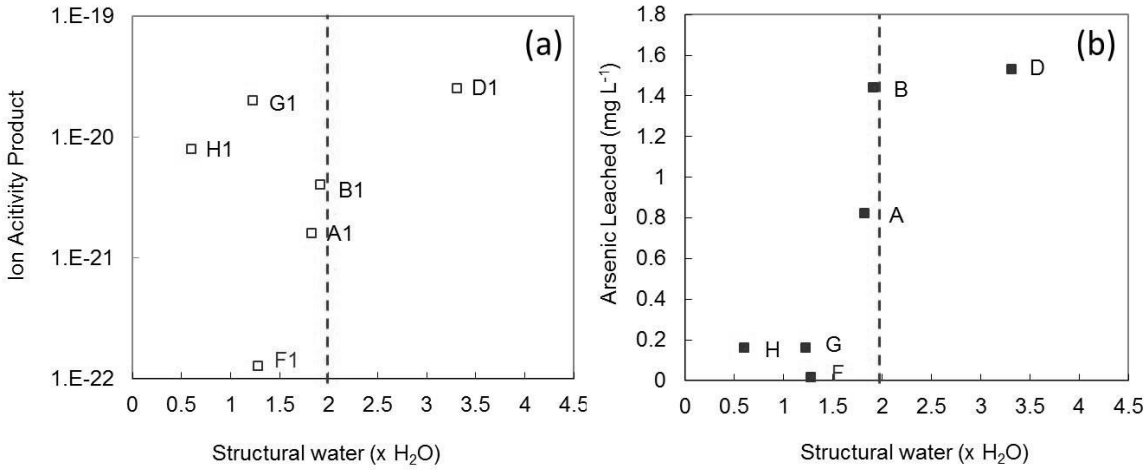

FIGURE 6.6 Influence of apparent structural water on bioscorodite properties. (a) Comparison between IAP vs. structural water of bioscorodite precipitates. (b) Comparison between long-term stability, expressed as arsenic leached, vs. the structural water in bioscorodite. The dashed line indicates the theoretical water of mineral scorodite of $2H_2O$ (15.6%). The legend of the samples is described in Table 6.1.

6.3.5 Environmental significance of the stability of bioscorodite crystals

Our results suggest that stable bioscorodite crystals can be produced when precipitation conditions are controlled by microorganisms. The most stable bioscorodite crystals in this research were produced at pH 1.2 with an Fe/As molar ratio of 1 and ageing of 22 days. These bioscorodite crystals were exposed to synthetic landfill conditions and after one year it leached only 16 μg L^{-1} of arsenic.

The iron oxidation capacity of the archaea controlled the precipitation of ferric iron, which simultaneously controlled the arsenic precipitation rate. Arsenic precipitation rates controlled the saturation level of bioscorodite. Slow precipitation, i.e. saturation controlled, lead to a better orientation of the crystals (crystalline), preventing aggregation (amorphous). If high microbial oxidation rates lead to fast supersaturation, it may lead to the formation of amorphous precipitates. Thermoacidophilic microorganisms used for bioscorodite crystallization have already been grown at sub-optimal conditions with respect to pH and substrate concentration (Chapter 4). If further reduction of the oxidation rate is required to prevent the formation of amorphous precipitates, other parameters that control microbial growth can be adjusted such as nutrient availability and oxygen supply.

Besides precipitation rate, also ageing time plays a crucial role in the stability of the crystals. It may be possible to use only ageing time to control the stability of rapidly precipitated solids. The biological scorodite precipitation process combines both: the arsenic precipitation rate is controlled by microorganisms and the ageing time can be controlled in continuously operated biological reactors. Stable arsenic crystals were produced with less structural water content probably due to concealed secondary iron phases such as ferrihydrite.

Scorodite processes are not yet part of the best available technologies for arsenic removal. The production of bioscorodite crystals may be an efficient solution for the treatment of diluted and highly concentrated wastewater. The next step towards application of this biological process is to scale up to a demonstration-size continuous bioreactor, producing scorodite suitable for safe long term disposal.

Chapter 7

Structural changes of bioscorodite crystals during long-term storage

Abstract

In a previous study we produced stable bioscorodite crystals suitable for arsenic disposal. In the current research, we evaluated the changes that the bioscorodite crystals undergo after one year exposure to landfill conditions and its dissolution mechanism. After one year, no structural changes were observed in bioscorodite crystals that had leached less than 0.2 mg As L^{-1}. In these samples, the structural water content varied between 0.5 and $1.5H_2O$, which is lower than the mineral scorodite ($FeAsO_4 \cdot 2H_2O$). The lower water content in bioscorodite crystals was explained by the presence of secondary iron phases. In contrast, in some of the samples that had leached more than 0.8 mg As L^{-1}, an increase of the structural water up to $4H_2O$ was observed. XRD analysis of these crystals showed a loss of crystallinity that appeared to have relation with the loss of the characteristic habit of scorodite in those crystals. Bioscorodite crystals dissolution followed a non-stoichiometric dissolution but secondary precipitates were not identified by the structural characterization of the crystals. This study demonstrates that small structural differences in bioscorodite crystals greatly affect their long-term stability under TCLP leaching conditions.

This chapter is in preparation for submission:
Gonzalez-Contreras, P; Weijma, J, Buisman, C. J. N., Structural changes of bioscorodite during long-term storage.

7.1 INTRODUCTION

Scorodite is considered the safest material for arsenic immobilization due to its low solubility [18, 106, 146]. However, scorodite dissolution is strongly controlled by the pH with a minimum dissolution at pH 4. This means that waters with a pH below 3 and above 5 will increase the solubility of scorodite [18]. The TCLP test provides the most aggressive conditions to test scorodite stability [53]. This test simulates the accelerated dissolution of minerals in the presence of organic acids produced by microorganisms [103]. The values obtained from the TCLP test are useful to compare the stability of different materials for arsenic disposal. If scorodite is chosen to immobilize arsenic, storage conditions must be such that it provides the highest possible stability during long-term disposal.

Recently, biogenic scorodite or "bioscorodite" crystals were produced with the aid of biological ferrous oxidizing thermoacidophilic microorganisms at 75°C and pH 1 in a sulphuric acid medium (Chapter 5). Biological iron oxidation controls scorodite precipitation by increasing the saturation level of the solution (Chapter 3). We furthermore found that the most stable bioscorodite crystals release arsenic concentrations ranging from 0.016 to 0.2 mg As L^{-1} under TCLP test conditions during one year (Chapter 6). These arsenic leaching values are extremely low compared to those reported between 0.1 and 13 mg L^{-1} [17, 18, 27, 66, 67, 74, 82, 154]. However, some of our samples leached more than 1 mg As L^{-1}, pointing to a lower crystal stability. It was hypothesized that this lower stability was due to a higher saturation level during crystallization and/or shorter ageing time after crystallization at pH 1 and 75°C.

Dissolution of chemically produced scorodite has been described as an incongruent process when tested at landfill conditions, i.e. TCLP test conditions. Re-precipitation of the dissolved iron occurs as 2-line ferrihydrite to which arsenic can subsequently adsorb [18]. Understanding the long-term release of arsenic from scorodite requires identification of the factors that control its dissolution.

The objective of this research is to study the structural changes that bioscorodite crystals undergo during long-term disposal. To this purpose, we used various techniques to compare the structural characteristics of scorodite samples before and after 1-year leaching. We also investigated the dissolution mechanisms under landfill conditions by measuring iron and arsenic dissolution during leaching.

7.2 EXPERIMENTAL SECTION

7.2.1 Long-term exposure of bioscorodite crystals under landfill conditions.

Six bioscorodite samples (A,B,D,F,G,H) were taken from a previous study (Chapter 6). These samples were produced at different pH, Fe/As molar ratios and crystal ageing times. An initial structural characterization of these samples was available (Chapter 6). Samples C and E from that previous study were not used here because the initial characterization was not available. Solids characterization and arsenic leaching rates following the TCLP test during a period of one year were reported in the same study (Chapter 6). The characterization methods used in the current study are described in detail in Chapter 6.

7.3 RESULTS AND DISCUSSION

7.3.1 Structural changes of bioscorodite crystals after long-term exposure under landfill conditions.

After one year of storage under landfill conditions, bioscorodite crystals were examined by SEM, XRD, FT-IR and TGA analysis. Bioscorodite samples were classified as very stable, leaching 0.016 to 0.2 mg L^{-1} arsenic (F, G and H) or less stable, leaching 0.8 to 1.5 mg L^{-1} arsenic (A, B and D).

TABLE 7.1 Precipitation parameters used to produce bioscorodite samples at 75°C and structural changes observed after one year of leaching under TCLP conditions.

I.D	pH	Fe/As	log IAP formation	Ageing days	Leaching Rates	Phase Prec.	Structural changes		
				(±1))[a]	(mg As L^{-1} $year^{-1}$)[b]		XRD[e]	H_2O[f]	Habit (SEM)[g]
A	0.8	1	-20.8	10	1	BSco[c]	Same	1.5-1.8↓	Yes
B	1.2	1	-20.4	10	1.5	BSco	Less	2.0-3.5↑	Yes
D	1.5	1	-19.6	10	1.5	BSco	Less	3.5-4↑	Yes
F	1.2	1	-21.9	22	0.016	BSco	Same	1-1.5↑	No
G	0.9	3	-19.7	22	0.2	BSco+ Jar[d]	Same	1.2	No
H	1.2	3	-20.1	22	0.2	BSco+ Jar	Same	0.4-0.6↓	No

[a] ageing time is defined here as total time of arsenic depletion subtracted from induction time, [b]Arsenic leaching rates observed after one year in TCLP tests conditions, [c]BSco= bioscorodite, [d]Jarosite, [e]crystallinity measured by XRD, [f]arrow indicates increase or decrease of apparent structural water content, i.e. structural water due to scorodite and concealed iron phases, [g]habit change due to dissolution resulting in loss of the dipyramid octahedron habit.

Morphological changes in crystals

SEM photos were taken from the very stable and less stable samples (Fig. 7.1). Bioscorodite crystals have their habit oriented into a fixed lattice, in which the octahedron dipyramids can be easily identified. It was found that during the leaching test, the less

stable samples undergo changes in their lattice (Fig. 7.1, samples A, B and D). The ordered fixed lattice was transformed into a flat surface of terraces, losing the characteristic dipyramidal habit of scorodite (Fig. 7.1, sample B1). The SEM photos suggest that dissolution started at the top of the octahedron pyramids of the less stable crystals, leading to a more rounded habit (Fig. 7.1, sample D). These rounded tops may indicate the most fragile position at which the dissolution process starts. The dissolution seems to proceed by a layer-stripping process. In contrast, the very stable crystals kept their dipyramidal habit and only small pits on some faces of the crystals were observed (Sample F, G and H).

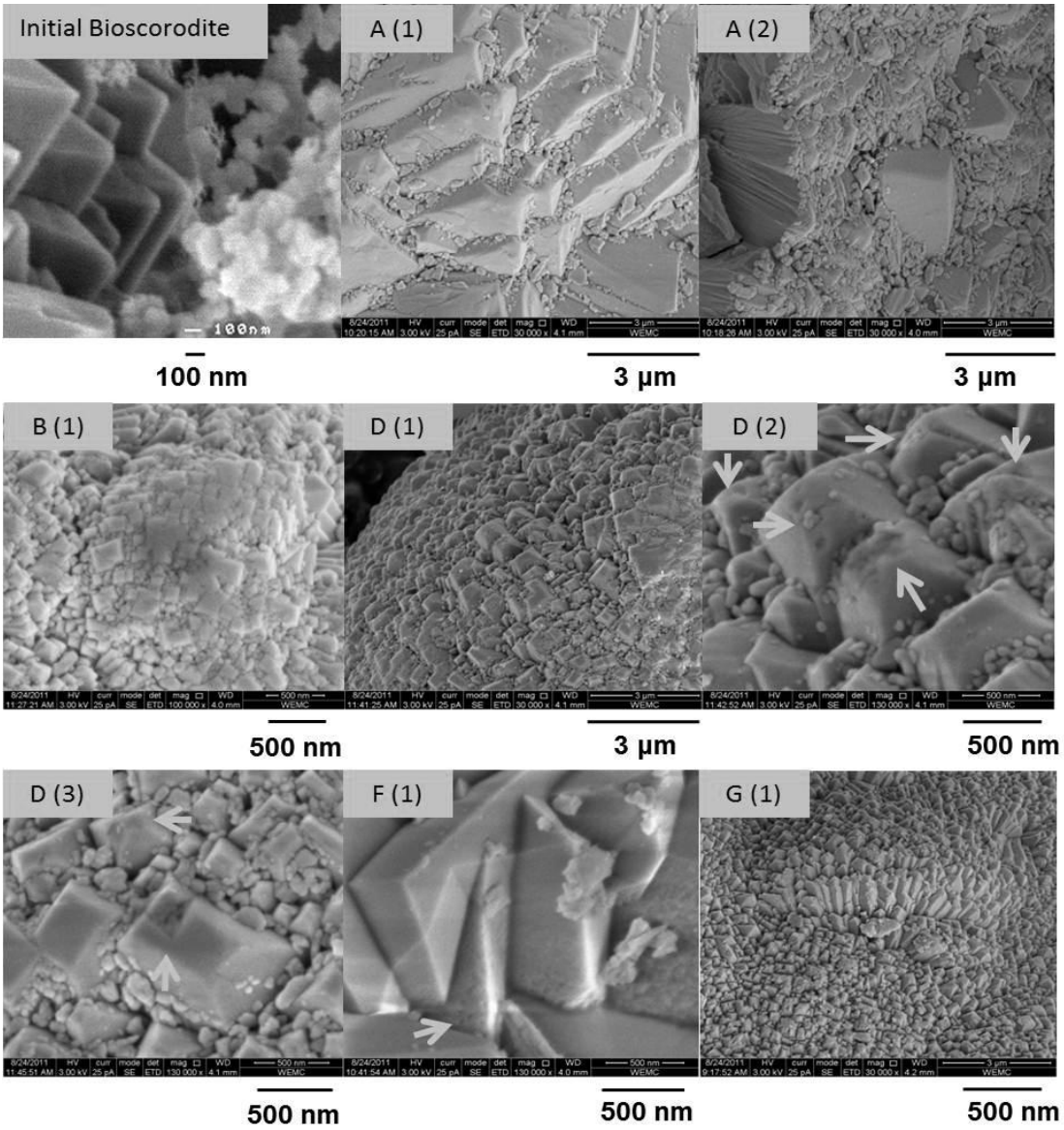

FIGURE 7.1 SEM photographs of bioscorodite samples after one year of leaching under landfill conditions. Arrows are indicating the dislocation of the dipyramid octahedron. The legend of the samples is described in Table 7.1.

Crystallinity changes in solids

XRD spectra of sample B before and after leaching showed a decrease in the intensity of diffraction peaks (Fig. 7.2). Such a broadening and decrease of intensity of the XRD peaks is known to indicate a loss of crystallinity (degree of structural order) [122] . The rest of the samples displayed an unchanged diffraction pattern after one year of leaching indicating that the crystallinity remained. Secondary phases were not detected in the XRD spectra.

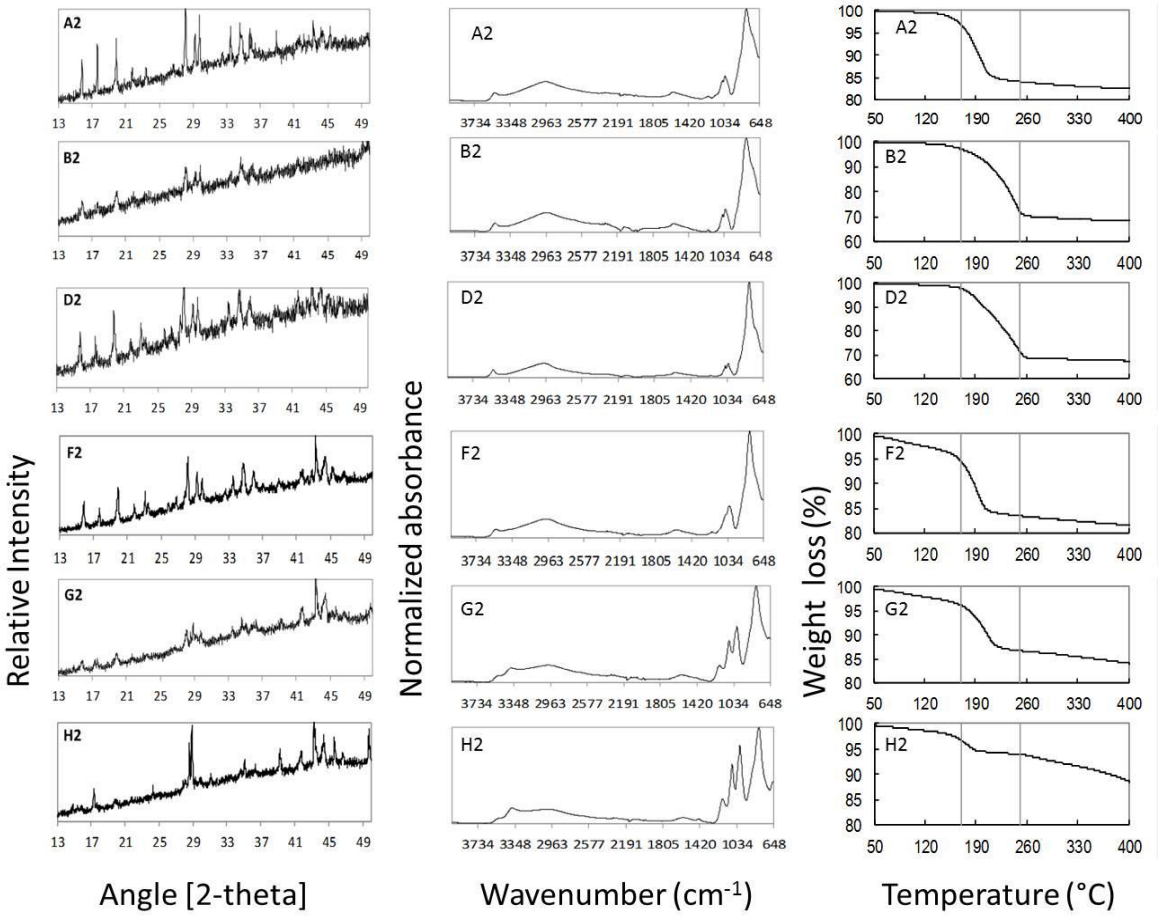

FIGURE 7.2 Characterization of bioscorodite samples after one year of dissolution under landfill conditions. FT-IR spectra have been normalized to unity for comparison (Appendix, Table A1). The deflection points of scorodite in TGA analysis were measured between 170 and 270°C (Appendix, Table A2). The legend of the samples, pH and Fe/As molar ratios used are described in Table 7.1.

Sulphate incorporation

Before and after leaching, bioscorodite crystals contained less than 1.3% of sulphate in their structure, based on weight loss at 700°C (Appendix, Table A2). Most of the sulphate contamination is more likely to be the result of washing of the precipitates with sulphuric

acid than of sulphate incorporation into the structure. Also the arsenate/sulphate peak ratio did not fluctuate as shown in the FT-IR analysis indicating that the sulphate content on the crystals was constant (Fig. 7.2).

Structural water content changes

Surprisingly, after one year of leaching the structural water content had changed in all the samples, except in sample G (Fig. 7.3). The weight loss of the samples at various temperature ranges is displayed in the Appendix (Table A2). The inflection point of bioscorodite, assessed by TGA analysis, was between 170 and 270°C. In samples B and D the structural water content increased from 2 to $4H_2O$. In sample A, the water content decreased from 1.8 to 1.5 H_2O. Samples F, G and H, on the other hand had a more stable but lower structural water content between 0.5 and $1.5H_2O$. The occurrence of bioscorodite crystals with structural water content below $2H_2O$ suggests the presence of (undetected) secondary iron phases such as ferrihydrite.

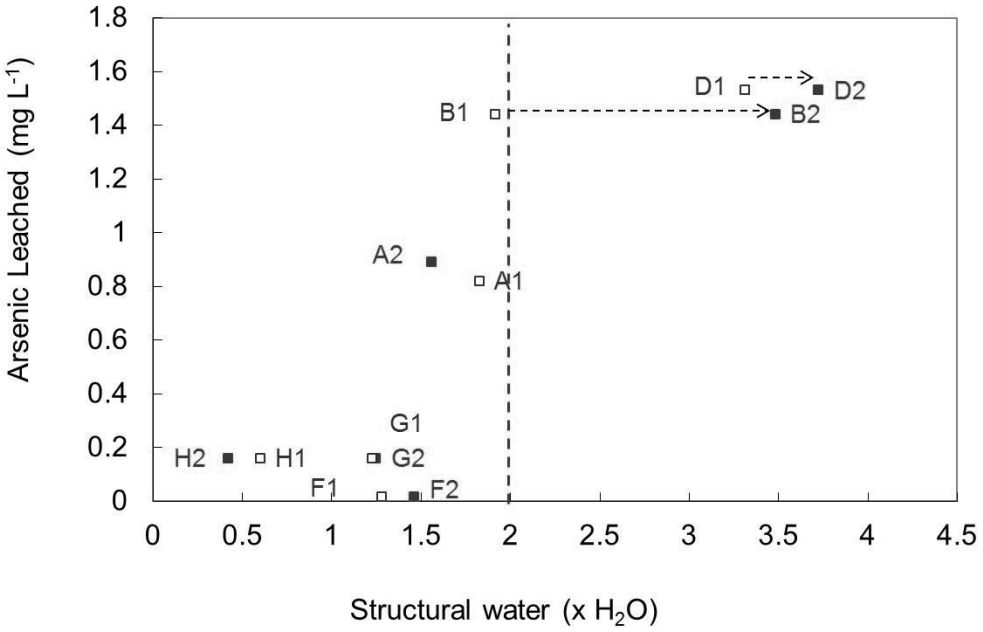

FIGURE 7.3 Comparison between long-term stability, expressed as arsenic leached, vs. the structural water contained in bioscorodite precipitates. The dashed line indicates the theoretical water of mineral scorodite of $2H_2O$ (15.6%). Arrows indicate the main increase of structural water of bioscorodite crystals after one year of leaching tests. The legend of the samples is described in Table 7.1. Subscript legend: (1) samples evaluated before leaching tests and (2) evaluated after leaching tests.

Sub-hydrate ferric arsenate phases have been precipitated in hydrothermal systems (170-225°C) [49, 73, 144, 157]. Some of those phases are very stable, leaching <0.3 mg L^{-1} in 40h [49]. Compared to scorodite, sub-hydrate ferric arsenate phases clearly differ in their XRD and FT-IR patterns [73]. The relation between the structural water content and leaching behaviour of bioscorodite precipitates requires further investigation. It is needed to determine which iron phases are concealed in the precipitates that probably are responsible for the lower structural water content observed in bioscorodite samples.

7.3.2 Bioscorodite crystals dissolution

In the leaching tests, the pH fluctuated between 4.9 and 5.4 and the redox potential (Eh) between 230 and 250 mV. During the first 20 days of leaching, the pH of the solution increased from 4.9 ± 0.05 to 5.2 ± 0.07 in all tests. After 20 days, pH values stabilized at 5.0 ± 0.04. The pH increase during the first 20 days may be due to congruent dissolution of scorodite as indicated in Equation 7.1:

$$FeAsO_4 \cdot 2H_2O + 3H^+ \leftrightharpoons Fe^{3+} + H_3AsO_4 + 2H_2O \qquad \text{(eq. 7.1)}$$

During the first 30 days of the test, the Fe/As molar ratios in solution were 3 - 5 (samples A,B,F) or even higher than 20 (D, G, H) (Fig. 7.4). This different behaviour of samples D, G and H probably relates to the presence of iron phases other than scorodite. Indeed, jarosite ($KFe_3(OH)_6(SO_4)_2$) was found in samples G and H during the structural characterization. Sample D was the least stable sample. This sample probably contained amorphous phases which leach faster than scorodite. The Fe/As molar ratios of 3 - 5 in samples A,B,F indicated that incongruent dissolution was taking place rather than congruent dissolution, as the latter would lead to an Fe(III)/As molar ratio in solution of one (Fig. 7.4).

After 20 days of leaching, the Fe(III)/As molar ratio in samples A and B decreased below 1 (0.16-0.78). After 100 days of leaching also the Fe(III)/As molar ratio in sample D decreased below 1. An Fe(III)/As molar ratio below 1 indicates that bioscorodite, like chemical scorodite [18], dissolves incongruently at pH 5, leading to the formation of secondary iron precipitates such as ferrihydrite (Equation 7.2):

$$FeAsO_4 \cdot 2H_2O + OH^- \rightleftharpoons \frac{1}{5}(Fe_5HO_8 \cdot 4H_2O)\downarrow + H_2AsO_4^- + \frac{3}{5}H_2O \qquad \text{(eq.7.2)}$$

However, secondary iron precipitates were not identified in any of the samples after one year of leaching. Moreover, the calculated solubility product values (log IAP) for ferrihydrite during bioscorodite dissolution ranged between -51 and -49. This indicates that the solution was undersatured with respect to ferrihydrite as the reported log IAP

values for ferrihydrite are between -40 and -38 [108]. Ferrihydrite undersaturation in all experiments can be explained by the fact that more than 50% of the ferric iron released from scorodite was reduced to ferrous iron (Fig. 7.4). Furthermore, the pH remained stable during the leaching experiments without the addition of base. Any small addition of base would lead to an increase of the saturation level with respect to ferrihydrite precipitation.

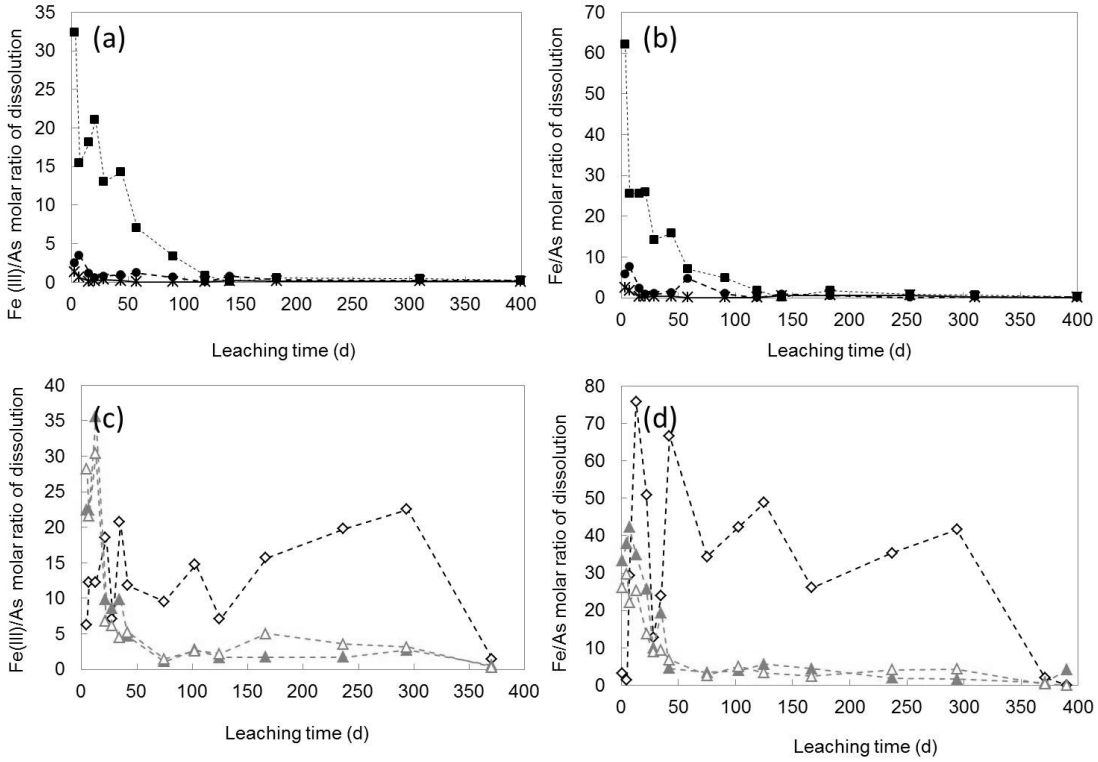

FIGURE 7.4 Dissolved Fe/As and Fe(III)/As molar ratios observed during one year of bioscorodite crystals dissolution under landfill conditions. (a-b) samples with 10 days of ageing and (c-d) samples with 22 days of ageing. The legend of the samples, pH and Fe/As molar ratios used are described in Table 7.1.Legend: * = A, ● = B, ■ = D, ◊ = F, ▲= G, ∆ = H.

In samples G and H, higher iron concentrations were attributed to the dissolution of jarosite present in these samples. Even after 300 days of leaching, the Fe(III)/As molar ratios of these samples did not decrease below 5. This indicates that jarosite present in the samples was dissolving continuously during the experiment. The arsenic leaching from samples G and H was below 0.2 mg As L^{-1} (Fig. 7.3). These results suggest that the presence of jarosite does not affect the stability of scorodite crystals.

In the most stable sample (sample F), the Fe(III)/As molar ratio fluctuated between 10 and 15 during 300 days of leaching. As jarosite precipitates were not detected in this sample, the consistently high Fe(III)/As molar ratio indicates that secondary iron mineral

phases were not formed, as this would lead to a decrease of the Fe(III)/As molar ratio. These results suggest that iron is released faster than arsenic.

7.3.3 Environmental significance of bioscorodite crystals dissolution

If precipitated under controlled conditions, bioscorodite crystals are very stable during long-term storage (arsenic leaching below 0.2 mg L^{-1}). This long-term stability makes bioscorodite crystals suitable to be used as an arsenic immobilizing material. The parameters that control the stability of bioscorodite crystals were determined in a previous study (Chapter 6). Arsenic leaching concentrations from bioscorodite crystals were influenced by the saturation level during crystallization and/or ageing time after crystallization.

Stable bioscorodite crystals did not undergo structural changes during long-term storage. In contrast, bioscorodite crystals which were classified as less stable (arsenic leaching above 0.8 mg L^{-1}), undergo structural transformations. The changes observed in the less stable bioscorodite crystals were: removal of material from the top of their dipyramidal habit that led to less intensity in XRD patterns (less crystallinity).

The structural water contained in the crystals was previously related to the stability of the bioscorodite crystals (Chapter 6). In the current study, we found that, structural water content in unstable samples changed during the leaching test. In the least stable samples structural water content was higher than $2H_2O$ and some samples even contained $4H_2O$ after the leaching. On the other hand, the structural water content stabilizes between 0.4 and $1.5H_2O$ in samples that leached less than 0.2 mg L^{-1} As. Structural water content below the theoretical known of scorodite ($2H_2O$), seems to dominate in bioscorodite crystals structure resulting in low arsenic leaching rates. The lower structural water content as discussed above may be due to concealed secondary iron phases such as ferrihydrite.

Bioscorodite crystals undergo a non-stoichiometric dissolution without concomitant ferrihydrite precipitation, even after 300 days of leaching. In case ferrihydrite precipitation would have occurred, arsenic released from scorodite can adsorb to it. Arsenic adsorption to ferrihydrite may conceal the actual arsenic concentrations in a landfill medium, as arsenic adsorbed to ferrihydrite will eventually be released back into the solution. Especially when solid material is analysed in short leaching tests (e.g. 20 h), this may lead to an underestimation of arsenic leaching concentrations.

APPENDIX 7.1

TABLE A1 FT-IR spectral assignment for bioscorodite crystals before and after leaching tests. FT-IR spectra assignment values of scorodite mineral, chemical crystallized scorodite and FasH phase were taken from literature[73]. The legend of the samples is described in Table 7.1.

			Spectral assignment of bioscorodite samples <u>before</u> leaching test					
IR	**Scor**	**FasH**	**A1**	**B1**	**D1**	**F1**	**G1**	**H1**
As-O-Fe str	720	740-751	-	-	-	-	-	-
V1 (AsO_4^{3-})	795	790-841	796.5	819.7	819.7	792.6	798.5	796.6
V3 (AsO_4^{3-})	900	860-898-963	-	-	-	900.7	898.8	900.7
V1 (SO_4^{2-})	-	-	1018.4	1024.2	1022.2	1016.4	1001.0	1001.0
V3 (SO_4^{2-})	-	-	-	1053.1	1051.2	-	1080.1	1080.1
V3 (SO_4^{2-})	-	-	-	-	-	1193.9	1184.3	1182.4
H_2O bend	1620	1620	1583.5	1589.3	1589.3	1585.4	1591.3	1591.3
H_2O str	2960	-	2989.6	2958.8	3003.1	2964.9	2999.3	3014.7
OH str	3516	3557-3498-3325	3516.2	3518.1	3520.0	3514.3	3514.3	3514.3
			Spectral assignment of bioscorodite samples <u>after</u> leaching test (1 year)					
IR	**Scor**	**FasH**	**A2**	**B2**	**D2**	**F2**	**G2**	**H2**
As-O-Fe str	720	740-751	-	-	-	-	-	-
V1 (AsO_4^{3-})	795	790-841	790.8	792.7	796.6	796.6	798.5	802.3
V3 (AsO_4^{3-})	900	860-898-963	893.0	896.8	902.6	898.8	898.8	-
V1 (SO_4^{2-})	-	-	1018.4	1016.4	1016.4	1016.4	1001.0	1001.0
V3 (SO_4^{2-})	-	-	1051.2	1051.2	1049.2	1051.2	1082.0	1082.0
V3 (SO_4^{2-})	-	-	1205.5	1205.5	1199.7	1201.6	1182.3	1180.4
H_2O bend	1620	1620	1587.4	1579.7	1585.4	1585.4	1585.4	1593.2
H_2O str	2960	-	2972.3	2968.4	2968.4	2981.9	2983.8	3010.8
OH str	3516	3557-3498-3325	3512.3	3516.2	3516.2	3520.0	3373.4-3508.5	3379.2-3506.5

TABLE A2 Weight loss (%) of bioscorodite crystals assessed by TGA. Before (1) and after (2) leaching. The legend of the samples is described in Table 7.1.

	A1	A2	B1	B2	D1	D2
(a) 120-250°C	14.2	15.4	14.7	26.5	19.2	27.6
(b) 170-250°C	13.7	12.9	14.3	24.3	18.1	26.1
(c) 170-270°C[(1)]	14.2	13.2	15.0	27.2	25.8	29.1
(d) 170-500°C	16.1	14.8	16.6	29.2	31.6	30.4
(e) 170-800°C	-	15.3	-	30.0	-	30.5
(f) 120-1000°C	-	23.3	-	35.9	-	34.0
Interstitial water (a-b)	0.5	2.5	0.4	2.1	1.1	2.4
% SO4 (e-d)	-	0.5	-	0.8	-	0.1

	F1	F2	G1	G2	H1	H2
(a) 120-250°C	12.8	14.0	10.4	11.2	6.0	4.6
(b) 170-250°C	9.6	11.1	9.1	9.4	4.0	2.7
(c) 170-270°C[(1)]	10.0	11.4	9.6	9.7	4.7	3.3
(d) 170-500°C	11.6	13.6	12.2	13.8	8.1	13.2
(e) 170-800°C	-	15.0	-	20.7	-	30.0
(f) 120-1000°C	-	21.5	-	23.8	-	34.2
Interstitial water (a-b)	3.2	2.9	1.3	1.8	2.0	2
% SO4 (e-d)	-	1.3	-	7	-	17

1) Structural water

Chapter 8

Continuous bioscorodite crystallization in CSTR systems

Abstract

In CSTRs, ferrous iron was biologically oxidized followed by crystallization of scorodite ($FeAsO_4 \cdot 2H_2O$) at pH 1.2 and 72°C. The CSTRs were fed with 2.8 g L^{-1} arsenate and 2.4 g L^{-1} ferrous and operated at a HRT of 40h, without seed addition or crystal recirculation. Both oxidation and crystallization were stable for periods up to 200 days. The arsenic removal efficiency was higher than 99% at feed Fe/As molar ratios between 1 and 2, resulting in effluents with 29 ± 18 mg As L^{-1}. Arsenic removal decreased to 40% at feed Fe/As molar ratios between 2 and 5. Microorganisms were not affected by arsenic concentrations up to 2.8 g As^{5+} L^{-1}. The bioscorodite solid yield was 3.2 g/g arsenic removed. Bioscorodite crystals precipitated as aggregates, causing scaling on the glass wall of the reactor. The precipitates appeared amorphous but XRD confirmed that these were crystalline scorodite. Arsenic leaching of bioscorodite crystals was 0.4 mg L^{-1} after 100 days under TCLP conditions, but when jarosite had been co-precipitated leaching was higher at 0.8 g L^{-1}. The robustness of the continuous process, the high removal efficiency and the very low arsenic leaching rates from bioscorodite sludge make the process very suitable for arsenic removal and disposal.

This chapter (except arsenite oxidation section) has been submitted as:
Gonzalez-Contreras, P; Weijma, J, Buisman, C. J. N., Continuous bioscorodite crystallization in CSTRs for arsenic removal and disposal.

8.1 INTRODUCTION

As arsenic is present in over 320 minerals [85], its presence in metallurgical operations cannot be avoided. Worldwide, there are over 150 locations recognized as significant arsenic contamination sites as a result of ore deposit and mining [87]. Since 2000, worldwide arsenic production has increased from 40 to 60 thousand metric tons. In contrast, the consumption has decreased from 25 to 5 thousand metric tons since 2004 [100]. At many production sites, arsenic trioxide is accumulated and stored until a suitable technology for its disposal is developed.

Arsenic is traditionally removed from industrial wastewaters from mineral processing and metallurgical operations by lime neutralization with co-precipitation of arsenic with ferric iron [144, 159]. Arsenical ferrihydrite precipitation requires a high iron consumption with respect to arsenic, i.e. Fe/As > 4 and thus large amounts of waste material are produced [143, 159]. Solid-liquid separation of arsenical ferrihydrite is extremely inefficient. This gelatinous material contains no more than 6%wt arsenic, with a maximum solid content of 20-25%wt [143]. The disposal and storage of these compounds is not entirely safe as they easily undergo physical and chemical changes with time, resulting in arsenic releases into the environment [143, 157].

Although scorodite production is not recognized as part of the best available technologies for arsenic removal, scorodite is considered the safest material for arsenic immobilization due to its low solubility, high stability, and compactness with 30%wt. of arsenic [18, 106, 146]. Since scorodite precipitation at atmospheric conditions and 90°C (using stepwise neutralization and foreign seeds) was demonstrated [38, 59], it has gained potential over the high-pressure autoclaving technology.

In recent publications, the production of biogenic scorodite or “bioscorodite” crystals in batch systems at pH 1.2 and 80°C was described (Chapter 3 and 5). In this process, biological oxidation controls the saturation level inducing bioscorodite formation. The structural properties of bioscorodite crystals are very similar to those of the mineral scorodite as found in nature.

Bioscorodite crystallization process has several advantages. For example, biological iron oxidation and crystallization take place simultaneously in a single reactor. Besides, neutralization steps are not needed because bioscorodite crystallization occurs at a constant pH (1-1.2) and at a relatively low temperature of 70°C. Bioscorodite crystals are the sole solid product because seeds in the biocrystallization are not needed. Furthermore, iron requirement is fixed to Fe/As = 1, therefore sludge production is low and less iron chemical addition is needed. Finally, the high stability, favourable settling and dewatering properties of bioscorodite crystals can reduce the costs of sludge management and disposal.

The objective of this research is to evaluate a continuous bioscorodite crystallization reactor for arsenic removal from metallurgical streams.

8.2 MATERIAL AND METHODS

8.2.1 Microorganism and medium

A mixed culture of *Sulfolobales* was used, which was originally collected from a hot, sulphur-rich coal dump [68]. Iron oxidation kinetics of the mixed culture at the suboptimal growth conditions suitable for bioscorodite crystallization were previously studied (Chapter 4). The growth medium for the thermoacidophiles contained: 1 g L^{-1} $(NH_4)_2SO_4$, 0.1 g L^{-1} KCl, 0.5 g L^{-1} $MgSO_4 \cdot 7H_2O$, and 0.5 g L^{-1} K_2HPO_4 as described by Plumb et al. (2002). Ferrous iron stock solutions were prepared by dissolving iron (II) sulphate heptahydrate ($FeSO_4 \cdot 7H_2O$) at several concentrations in 0.1 mol L^{-1} sulphuric acid. The arsenic solutions were prepared from disodium hydrogen arsenate heptahydrate ($Na_2HAsO_4 \cdot 7H_2O$) (Fluka, Switzerland). Sodium arsenite standard solution Tritipur (0.05 mol L^{-1} ± 0.1% $NaAsO_2$) (Merck, Germany).

8.2.2 Biocrystallization reactors

Two aerated Continuous Stirred Tank Reactors (CSTR) with 1 L of working volume were used. The temperature was controlled at 72 ± 2°C with a heating bath at 75°C (Julabo, Germany). The air flow to the reactors was controlled by mass flow controllers (Brooks, type 5850 TR) at a rate of 0.3 volume of air per volume of medium per minute using a stainless diffuser. The effluent air was dehumidified with condensers connected to a cooling bath (Julabo, Germany) and the condensate was returned to the CSTR. No evaporation was observed. Mixing was achieved by a double two-blade propeller operated at 300 rpm connected to a mechanical stirrer (Sigma Aldrich, Netherlands). The reactor was operated without liquid or solid recirculation.

Redox potential and pH were measured with glass electrodes QR480X - Pt billed - S8 and QP181X - S8, respectively (Prosense, The Netherlands). Slope calibration of pH electrode was made with pH 1 and pH 4 buffers. Dissolved oxygen was measured using an oxygen dipping probe DP-PSt3 (Presens, Germany) connected to a Fibox-3, Fiber optic oxygen transmitter (Presens, Germany). The oxygen sensor was calibrated at 0% with nitrogen and at 100% with water-saturated air. Cells were counted in a Bürker-Türk chamber (Brand, Germany).

8.2.3 Operation of CSTRs

Two reactor systems were used: CSTR-1 and CSTR-2. Previously reported results from CSTR-1 operation are used as biological control (blank) in the absence of arsenic (Chapter 4). In this previous work, CSTR-1 was operated at a Hydraulic Retention Time (HRT) of

40 h without recirculation of biomass, obtaining a ferrous iron oxidation rate of 1.5 g L^{-1} d^{-1} at pH 1.1 and 72 ± 2°C

In the current work, the arsenate concentration in CSTR-1 was gradually increased in time from 0.5 to 2.4 g As L^{-1} to adapt the microorganisms to high arsenic concentrations. Scorodite seeds were not added to the bioreactor, but some jarosite was present in the inoculum. In a previous study it was demonstrated that arsenate adsorbs to jarosite at pH 1.0, but this does not lead to the transformation into scorodite (Chapter 6). The inoculum for CSTR-2 contained no jarosite or scorodite. Arsenic and iron concentrations of 2.8 g L^{-1} As^{5+} and 2.4 g L^{-1} Fe^{2+} were supplied to the reactor at pH 1.2 and 72 ± 2°C. CSTR-2 was inoculated with 10% v/v biomass from a ferrous iron oxidizing CSTR reactor. This biomass was not adapted to high arsenic concentrations. The inoculum contained soluble ferric and ferrous iron concentrations in the order of 10 g Fe L^{-1}.

8.2.4 Determination of the Ion Activity Product of bioscorodite crystals (Chapter 3)

Calculation of the Ion Activity Product (IAP) of bioscorodite crystals is based on its congruent dissolution:

$$FeAsO_4 \cdot 2H_2O\ (scorodite) \rightleftharpoons Fe^{3+} + AsO_4^{3-} + 2H_2O \qquad \text{(eq. 8.1)}$$

The supersaturation in aqueous solutions is expressed by the IAP of the lattice ions in solution, divided by the solubility product of the salt, K_a (IAP at saturation). The IAP of scorodite is defined as the product of the activities of ferric and arsenate in solution (equation 8.2).

$$IAP_{SCORODITE} = (\alpha Fe^{3+})(\alpha AsO_4^{3-}) \qquad \text{(eq. 8.2)}$$

The IAP values reported for scorodite mineral, scorodite produced by chemical synthesis and values calculated for bioscorodite crystals were previously compared (Chapter 3, 6 and 7).

8.2.5 Determination of linear crystal growth

In the bioscorodite process, the addition of seeds is not needed. Therefore, the linear growth rate depends on the crystals appearing in suspension. The change of mass (crystal growth rate) is related to the arsenic precipitation (removal) from solution. Combination of the overall crystal growth equation and the equations that describe the total mass and surface area of crystals leads to the following equation for crystal growth rate (G):

$$G = \frac{L \cdot M \cdot V}{3 \cdot W}\left(-\frac{d[As^{5+}]}{dt}\right) (\text{m s}^{-1}) \qquad \text{(eq. 8.3)}$$

where L is the size of the crystals (m), M is the molecular weight of scorodite (g mol^{-1}), V is the reactor volume (m^3), and W is the mass weight of the crystals (kg). The derivation of the equations is showed in detail in Appendix 8.2.

8.2.6 Analysis

Iron species in the aqueous phase were measured using Dr. Lange Cuvette test LCK 320 for ferrous iron (Fe^{2+}) and ferric iron (Fe^{3+}) and a Xion 500 spectrophotometer (Hach-Lange, Germany).

Arsenic speciation was measured by anionic ion exclusion chromatography using sulphuric acid as mobile phase, followed by UV detection. The validation of this method is described in Chapter 2.

Protein measurements were performed using the Total Protein Kit, Micro Lowry, Onishi & Barr Modification (Sigma Aldrich, Germany). Before protein quantification samples were centrifuged at 12000 rpm during 15 min and the obtained pellet was dissolved in acidified milliQ water at pH 2. To 1 mL of sample, 3 mL of 3M NaOH was added and boiled during 5 min in closed tubes. After cooling-down, 1.15 mL of 4M H_2SO_4 was added. Samples were centrifuged at 12000 rpm during 15 min and the protein concentration was measured following the protein protocol.

8.2.7 Structural Characterization of Precipitates

Precipitates for structural characterization were separated from the liquid phase by their sedimentation. The separated solids were washed with 0.1M sulphuric acid prior to their use in leaching tests. The bioscorodite separation method used in our research resembles the disposal of the material without any pre-treatment. The samples were dried at 70°C before structural analysis.

X-ray diffraction (XRD) was used to identify the nature of the solid materials. Wide angle X ray scattering (WAXS) powder diffractograms were recorded on a PANalytical Expert Pro System (Almelo, The Netherlands) in the angular range 5–50° (2θ), with a step size of 0.02° (2θ) and an acquisition time of 0.6 s per step. The CuKα1 radiation from the anode, generated at 40 kV and 50 mA, was monochromatized using a 15 μm Ni foil (λ = 0.1542 nm). The diffractometer was equipped with a 1° divergence slit, a 0.2 mm receiving slit, and a 1° scatter slit.

The structural H_2O content of the solid phases was determined with a thermogravimetric analyser (Perkin-Elmer TGA7 equipped with Pyris software). The thermogravimetric analysis was performed with about 10 mg of air-dried powdered material at a heating rate

of 10°C min^{-1} from 20°C to 900°C under air/nitrogen atmosphere. The furnace had a temperature precision of ± 2°C and the balance precision was 0.001%.

Fourier transform infrared (FT-IR) spectra of the solid samples were obtained on a Varian Scimitar 1000 FT-IR spectrometer equipped with a DTGS-detector. The measurement resolution was set at 4 cm^{-1}, and the spectra were collected in the range 4000-600 cm^{-1} for attenuated total reflectance (ATR) with 64 coadded scans. The sample chamber was purged by N_2 gas for 10 min before scanning was started. ATR was performed on a PIKE MIRacle ATR equipped with a diamond w/ZnSe lens single reflection plate. The vibrations assigned to scorodite and to bioscorodite crystals are shown in detail in the Supplementary Information (Appendix 8.1).

Crystal habit of the solids was investigated with scanning electron microscopy (SEM). Samples were glued on a copper sample holder using conductive carbon tape and silver tape and sputter coated with 20 nm platinum (JFC 1200, JEOL, Japan). The surfaces were analysed with a FESEM (JEOL 6300 F, Tokyo, Japan) at room temperature, a working distance of 15 mm and SE detection at 3.5 kV. All images were recorded digitally (Orion, 6 ELI. sprl., Belgium) at a scan rate of 100 s (full frame) at a size of 2528 x 2030, 8 bit. Noise reduction and resizing of the images was done with Adobe Photoshop CS.

Free water of bioscorodite sludge was determined. First, the samples were settled or filtered and the remained sludge was dried at 70°C. The free water on sludge is calculated from the difference in weight before and after the drying step.

8.2.8 Arsenic solid stability analysis by the Toxicity Characteristic Leaching Procedure (TCLP)

The TCLP test was performed in serum bottles, stirred in a shaker at 20°C following the EPA procedure [53]. Acetate buffer at pH 4.95 was used as leaching medium. The solid to liquid ratio was fixed at 20%w/w. Bioscorodite aggregates from CTSR-1 and from CSTR-2 with a size below 1 cm were tested. A second sample of bioscorodite aggregates was taken from CSTR-2. Aggregates were crushed to test the maximum arsenic leaching rate from the precipitates. The duration of the TCLP test was extended from 20 h to 100 days under the same leaching conditions. For this test a mixing rate of 100 rpm instead of 30 rpm (suggested by the TCLP test) was provided.

8.3 RESULTS AND DISCUSSION

8.3.1 Bioscorodite CSTRs efficiency

Biological ferrous iron oxidation

Two continuous bioreactors were operated for bioscorodite production: CSTR-1 (biomass slowly adapted to arsenic) and CSTR-2 (biomass not adapted to arsenic).

Thermoacidophilic microorganisms oxidized ferrous iron at pH 1.2 in both reactors (Fig. 8.1). In CSTR-1 a ferrous iron oxidation rate of 1.5 g Fe^{2+} L^{-1} d^{-1} was obtained (Fig. 8.2a). This value coincided with the maximum expected rate based on the blank without arsenic (Chapter 4). CSTR-2, which was operated with a slightly lower ferrous iron loading rate compared to CSTR-1, achieved complete ferrous oxidation at a rate of 1 g Fe^{2+} L^{-1} d^{-1} (Fig. 8.2b).

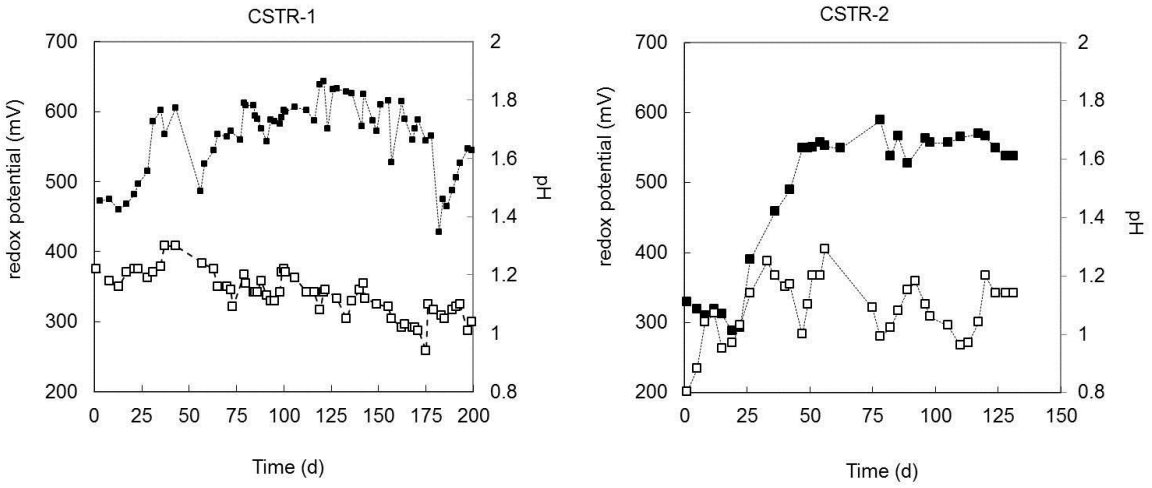

FIGURE 8.1 Fluctuation of pH (□) and redox potential (■) in bioscorodite CSTR systems at 72°C.

Biological ferrous iron conversion was not affected by the various arsenate concentrations used in the systems (0.5 to 2.8 g As^{5+} L^{-1}). The cell count was in the order of 1 to $4 \cdot 10^6$ cells mL^{-1}, which is similar to the cell count in previous runs (Chapter 4). The low cell count coincided with the low protein value of 2 mg protein L^{-1} (measured in CSTR-2). Based on the measured protein concentration, an average specific ferrous iron oxidation rate of 0.5 g Fe^{2+} mg^{-1} protein d^{-1} was calculated (Fig. 8.2b). Specific ferrous iron oxidation values are not commonly reported. Some values reported by other authors are 0.293 g Fe^{2+} mg^{-1} protein d^{-1} for *Sulfolobus metallicus* [41] and 0.7 g Fe^{2+} mg^{-1} protein d^{-1} for mesophilic iron oxidizers [24].

Oxygen Transfer Rates (OTR)

The oxygen solubility of 3.75 mgO_2 L^{-1} was measured at 75°C in 0.1 M sulphuric acid. OTR values were calculated for both reactors based on the ferrous iron biological conversion capacity. OTR values obtained ranged between 6 and $7.8 \cdot 10^{-5}$ mol O_2 m^{-3} s^{-1}. The volumetric mass transfer coefficient (k_La) was calculated using the model for liquid phase [160] and the calculated OTR. Dissolved oxygen concentrations measured in the liquid phase fluctuated between 2.5 and 2.6 mg O_2 L^{-1}. The calculated k_La for CSTR-1 and

CSTR-2 were 6.6 and 5.4 h^{-1}, respectively. In the blank reactor without arsenic, the calculated k_La was slightly higher at 8.2 h^{-1}. This suggests that there was a limitation regarding the volumetric mass transfer rate. It is known that in thermophilic bioleaching systems, a solids concentration higher than 12%w/v will limit the oxygen and carbon dioxide availability or influence the transfer coefficient [138]. Required values of k_La for ferrous iron oxidation are in the order of 30 h^{-1} [2, 19]. Depending on the mineral to bioleach, k_La values can decrease to 5 h^{-1}, for example for pyrite or enargite [2, 19].

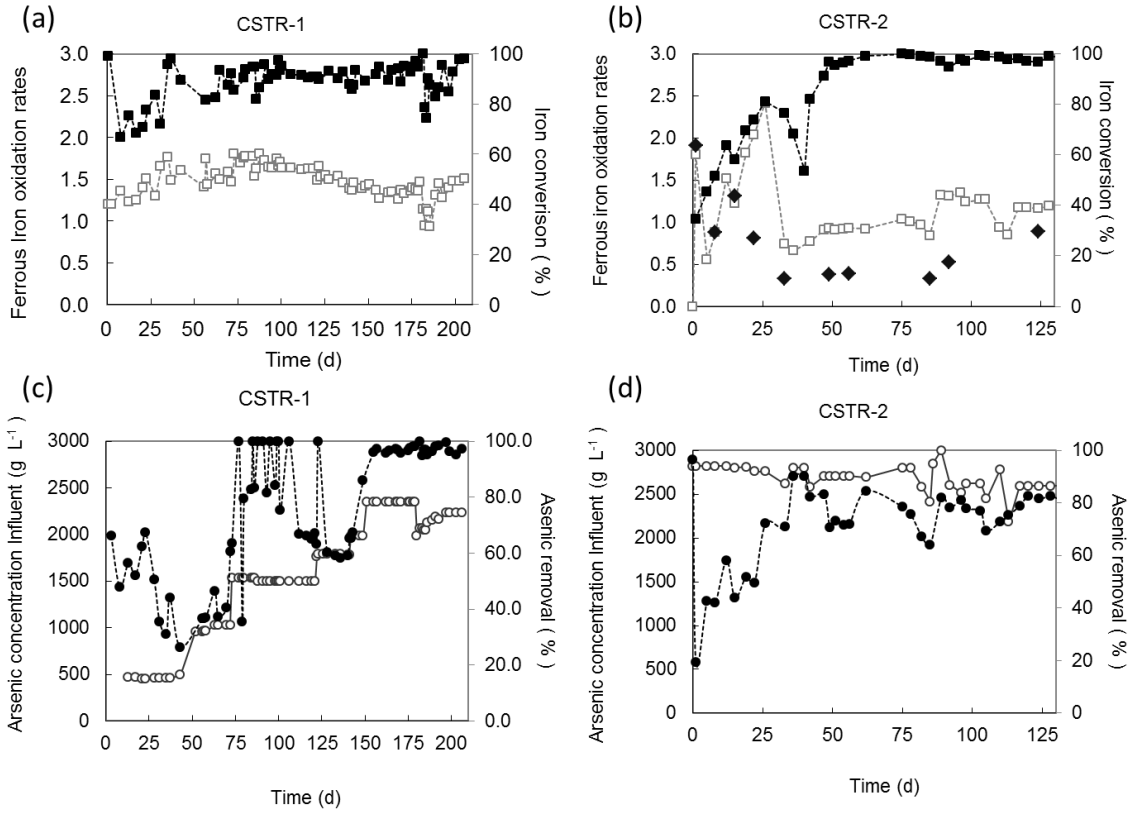

FIGURE 8.2 Biological ferrous iron oxidation of thermoacidophilic microorganisms during bioscorodite production at pH 1.2 and 72°C in the presence of arsenic concentrations from 0.5 to 2.8 g As^{5+} L^{-1}. Legend: □ ferrous iron oxidation rate (g Fe^{2+} L^{-1} d^{-1}), ■ Ferrous iron conversion (% oxidized), ♦ specific ferrous iron oxidation rate (g Fe^{2+} mg^{-1} protein d^{-1}), ○ arsenate concentrations supplied to the bioreactors (g As^{5+} L^{-1}), ● arsenic removal from solution (% precipitated).

Arsenic precipitation

Arsenic removal efficiencies of 99.6% and 80% were achieved in CSTR-1 and CSTR-2, respectively (Fig. 8.2c, d). In CSTR-1, the high arsenic removal efficiency led to an effluent arsenic concentration of 29 ± 18 mg L^{-1} As^{5+}. Arsenic removal efficiency in CSTR-2 was not the maximum, the reactor was stopped at 125 days. Arsenate

precipitation was negatively affected at Fe/As molar supply ratios higher than 2. The fluctuation of Fe/As molar ratios in the influent and effluent of the reactor are shown in Figure 8.3. When the Fe/As molar ratio in the influent of CSTR-1 fluctuated between 2 and 5, only 40% of arsenic removal efficiency was achieved. In contrast, when the Fe/As molar ratios fluctuated between 2 and 1.4, an arsenic removal efficiency of 99% was achieved.

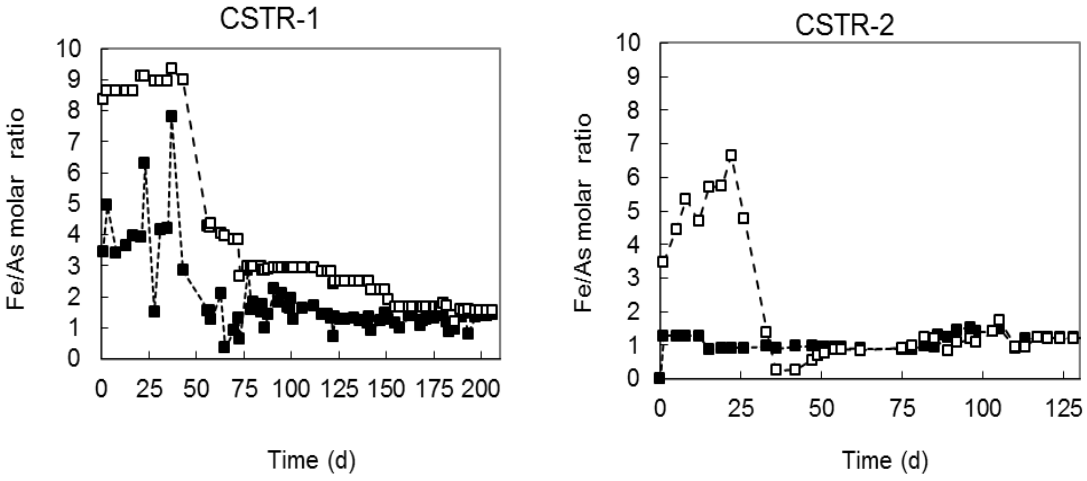

FIGURE 8.3 Fluctuation of Fe/As molar ratios in bioscorodite CSTR systems. Legend: ■ Fe/As Influent, □ Fe/As precipitated from solution in effluent.

Simultaneous biological ferrous iron and arsenite oxidation

In a parallel study, arsenite oxidation at pH 1.2 and 72°C was evaluated in CSTRs. In a previous batch experiment, arsenite was oxidized to As^{5+} at a maximum rate of 0.016 g As^{3+} L^{-1} d^{-1}, simultaneously with the oxidation of ferrous iron at pH 1.2 and 72°C (data not shown).

A fraction of the total arsenic in the stream supplied to the CSTR was replaced with arsenite. In a first test, 10% of total arsenic was replaced with arsenite (0.24 g As^{3+} L^{-1}). In a second test 30% was replaced (0.75 g As^{3+} L^{-1}). In the first test (10% As^{3+}), ferrous oxidation rates initially decreased from 1.5 to 0.45 g L^{-1} d^{-1} and then gradually increased to 0.9 g L^{-1} d^{-1} after 47 days (Fig. 8.4). In the second test (30% As^{3+}), ferrous oxidation rates initially decreased from 0.9 to 0.45 g L^{-1} d^{-1} and then gradually increased to 1.2 g L^{-1} d^{-1} after 100 days. From these results it can be concluded that the ferrous iron oxidation capacity of the microorganisms is negatively affected by arsenite. Despite of arsenite inhibition, low arsenite oxidation rates (0.1-0.2 g As^{3+} L^{-1} d^{-1}) were measured at pH 1.2 and 72°C.

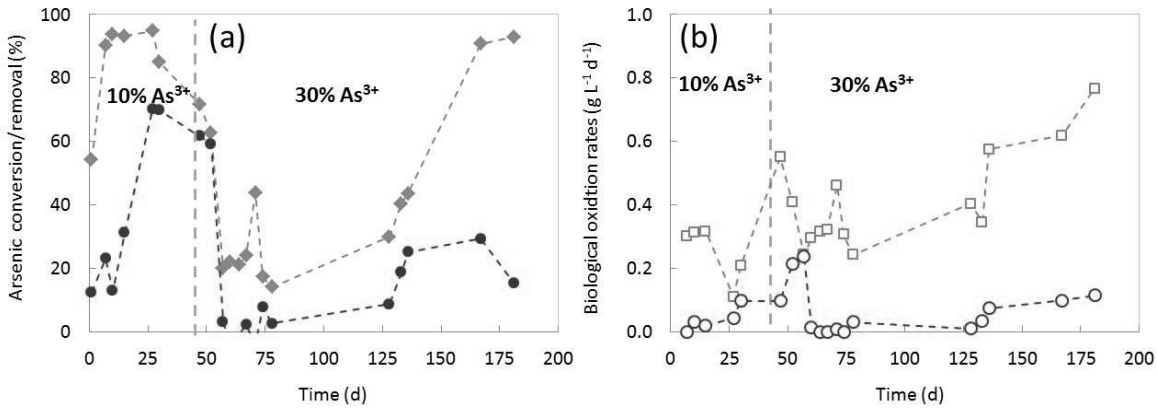

FIGURE 8.4 Arsenite adaptation and oxidation of thermoacidophilc microorganisms in a CSTR for bioscorodite crystallization. Legend: ♦ arsenic precipitated (%), ● arsenite oxidation (%), □ ferrous iron oxidation rates (g L^{-1} d^{-1}), ○ arsenite oxidation rates (g L^{-1} d^{-1}).

These results suggest that thermoacidophilic archaea can oxidize, at low rates, arsenite to arsenate at pH 1.2 and 72°C. It was also observed that at low concentrations (0.24 g L^{-1}) arsenite can affect negatively the microorganisms affecting their capacity to oxidize ferrous iron. Despite of the inhibiting effect of arsenite, it seems that the cell can slowly adapt to arsenite.

8.3.2 Bioscorodite precipitation and product selection

Product selection

Previously, it was shown that in the absence of arsenic in the same system, jarosite will precipitate (Chapter 4). Bioscorodite crystals will precipitate first (log IAP between -22 and -20), followed by jarosite using the remaining ferric iron (log IAP between -99 and -93). In CSTR-1, jarosite and bioscorodite crystals were simultaneously precipitated. During the first 75 days of operation, mainly jarosite was precipitated because the Fe/As molar ratios were higher than 2 (Fig. 8.5c). After 75 days, bioscorodite dominated the precipitates with Fe/As molar ratios between 1 and 2. In CSTR-2, the sole product was bioscorodite crystals (Fig. 8.5d).

Precipitate samples were not taken during the continuous operation of the reactors. In the reactor effluent very little arsenic was measured (either dissolved or solid), indicating that arsenic was accumulated in the reactor as precipitates. Thus, the crystals remained in the systems until the end of the run. The amount of bioscorodite and jarosite found in the reactors matched the arsenic and iron mass balances. In CSTR-1, the final product contained 56% of bioscorodite crystals and the rest was jarosite. In contrast, the product in CSTR-2 was only bioscorodite.

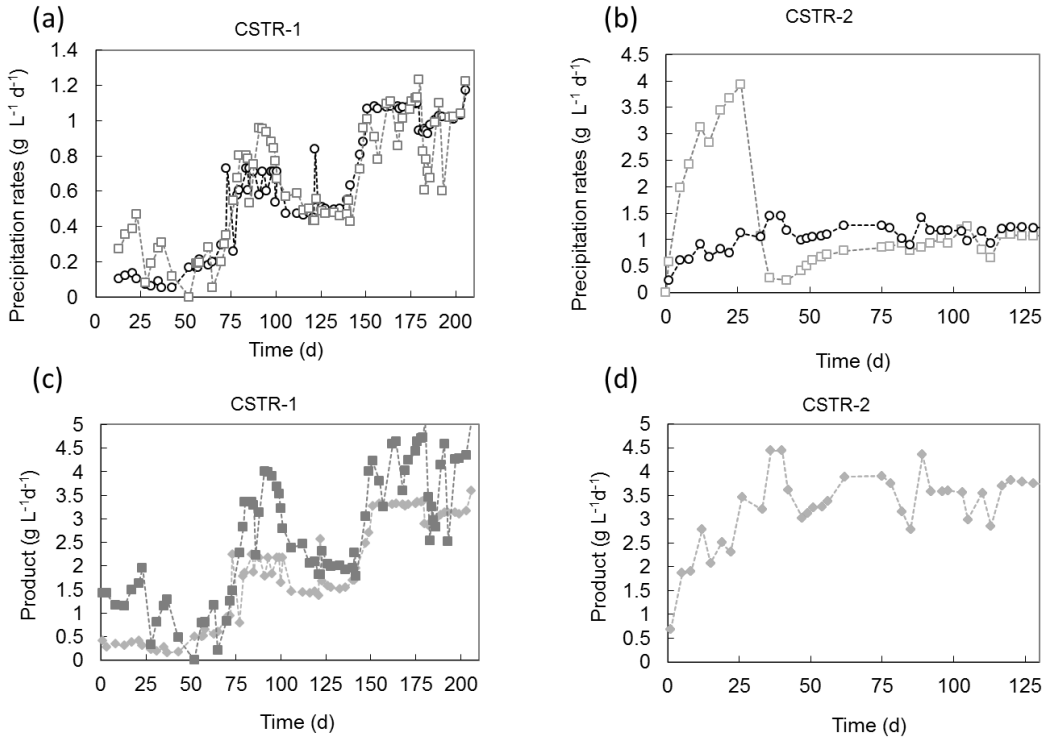

FIGURE 8.5 Arsenic and iron precipitation rates during bioscorodite production at pH 1.2 and 72°C. Legend: □ Iron precipitation rates (g Fe L^{-1} d^{-1}), ○ Arsenic precipitation rates (g As^{5+} L^{-1} d^{-1}). Bioscorodite and Jarosite production are calculated based on iron and arsenic mass balance: ■ precipitates containing iron (jarosite plus bioscorodite) (g Fe L^{-1} d^{-1}), ♦ precipitates containing arsenic (bioscorodite) (g As^{5+} L^{-1} d^{-1}).

Bioscorodite productivity/sludge yield

Bioscorodite overall volumetric productivity (Q_P) was calculated for both bioreactors. At the end of the operation, CSTR-1 had a Qp of 3.2 g bioscorodite L^{-1} d^{-1} and CSTR-2 a Qp of 3.6 g bioscorodite L^{-1} d^{-1}. The bioscorodite yield in CSTR-1 was 3.2 g/g arsenic removed and in CSTR-2 was 3.1 g/g arsenic removed.

Bioscorodite crystallization kinetics

The calculated IAP values for both reactors correspond to the values reported for bioscorodite crystals in batch tests (Chapter 3). When 99% of arsenic removal efficiency was achieved in CSTR-1, the IAP values decreased from -21 to -23. In CSTR-2, the IAP values fluctuated around -21 ± 0.5 with no further changes (Fig. 8.6). Overall linear crystal growth rates were calculated for the bioscorodite crystals assuming an average size of 100 μm (L) from the first flakes observed in suspension (before these aggregated on the walls). The mass (W) of bioscorodite was calculated based on arsenic precipitation. In CSTR-1 and CSTR-2 the crystals grew with rates of 16 μm d^{-1} and 20 μm d^{-1}, respectively.

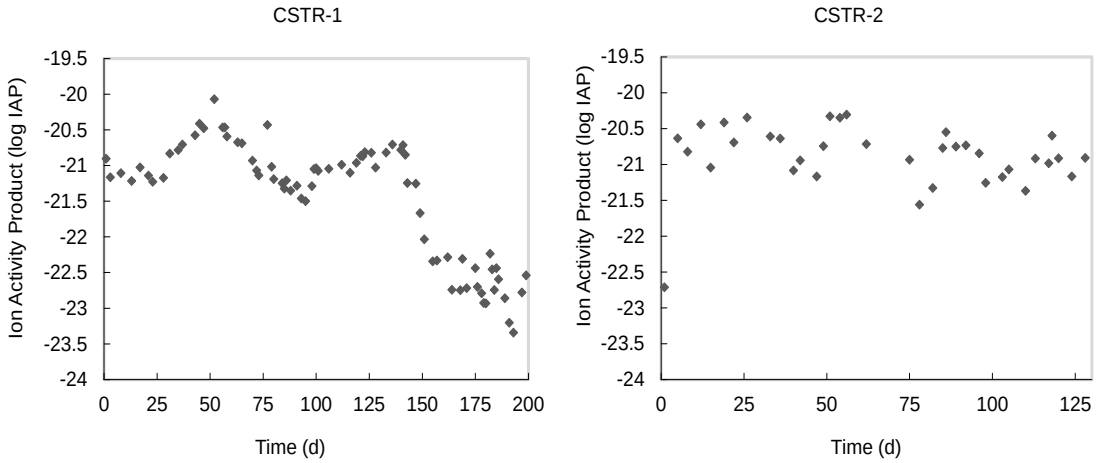

FIGURE 8.6 Ion Activity Product for bioscorodite in CSTR systems at 72°C.

8.3.3 Characterization of bioscorodite precipitates

Morphology

In both reactors scaling was observed. In CSTR-1, four types of precipitates were identified: (1) small bioscorodite particles in suspension (less of 1% of the total amount solids), (2) bioscorodite aggregates deposited in the bottom of the reactor, (3) bioscorodite deposited over jarosite covered walls and (4) jarosite attached to the glass walls. In CSTR-2 precipitates were bioscorodite agglomerates deposited at the bottom of the reactor. In CSTR-2 the scaling was only temporal because the bioscorodite flakes fell back into suspension.

SEM photos revealed that the crystals were aggregates without symmetrical properties (Fig. 8.7a, b and c). Bioscorodite produced in CSTRs has an amorphous-appearing habit (showing no faces), but which actually were crystalline as assessed through XRD. This is a difference with bioscorodite produced in batch tests which resembled the habit of scorodite mineral, i.e. dypiramidal octahedron (Chapter 3). The growth of bioscorodite crystals in layers indicates that crystalline bridges occurred between crystals rather than just aggregation of crystals. In both reactors, contact nucleation on the walls predominated. Bioscorodite produced in CSTRs is a high dense material that precipitates in flakes. As a result, it displays fast settling rates making it impossible to keep solids in suspensions.

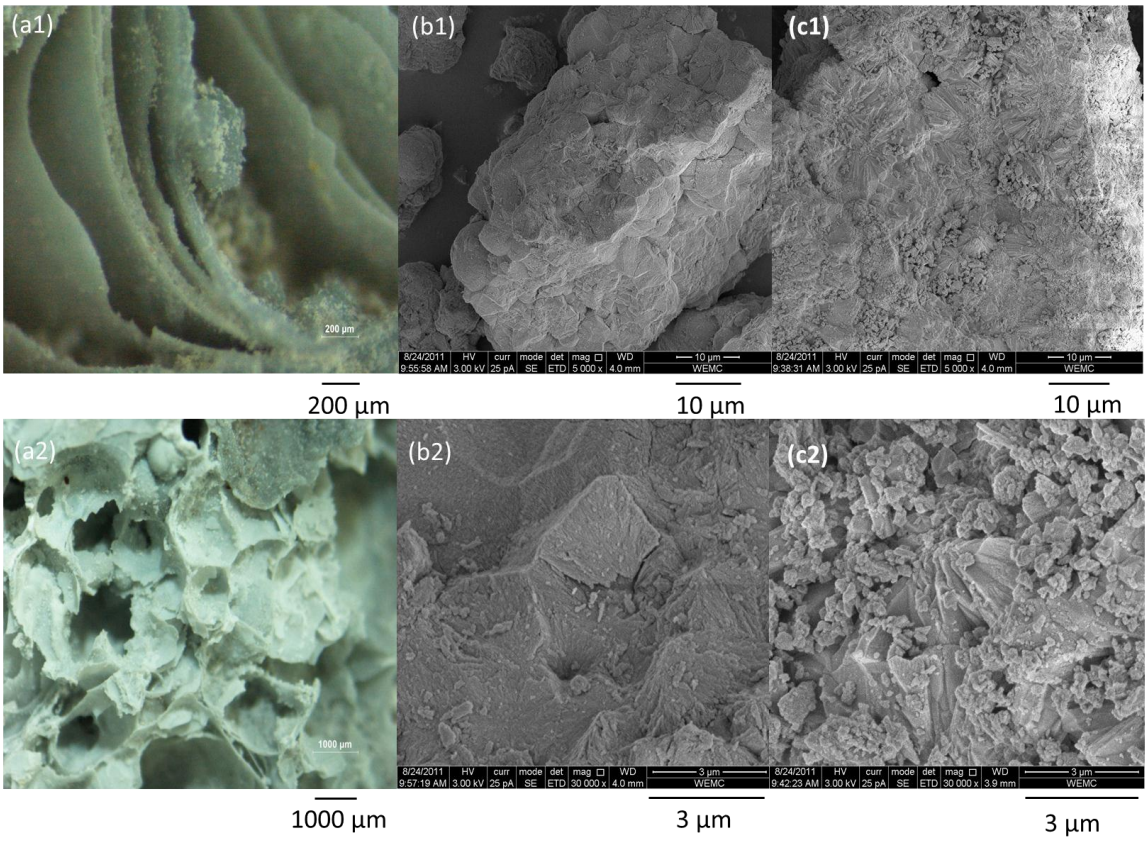

FIGURE 8.7 Bioscorodite agglomerates obtained in CSTRs. Optical photographs: (a1) and (a2). SEM photographs at magnifications of 5,000 x (b1 and c1) and 30,000 x (b2 and c2).

Structural characterization of bioscorodite crystals

All the samples were identified by XRD as crystalline bioscorodite. The crystals contained structural water between 1.7 and $2H_2O$. The lower structural water content was probably due to concealed ferrihydrite phases in the samples. Low ferrihydrite content in the samples would not be identified in XRD analysis but it would decay to other phases at lower temperatures than at which scorodite loses its structural water. The FT-IR spectrum of sample (a) shows sulphate contamination based on the 3 peaks assigned to sulphate. This contamination was due to the washing with 0.1 M sulphuric acid. In sample (a), sulphate transformation to sulphur dioxide near 680°C was confirmed by TGA analysis (Fig. 8.8a).

The FT-IR spectrum of samples (b), (c) and (e) displayed a phosphate peak at 1010 cm^{-1} rather than the three peaks of sulphate (Fig. 8.8). Phosphate contamination has been found in scorodite and parascorodite by FT-IR analysis [134]. In that study stretching vibrations at 1022 and 1050 cm^{-1} were assigned to phosphate. In these samples, the absence of sulphate contamination was confirmed by TGA analysis.

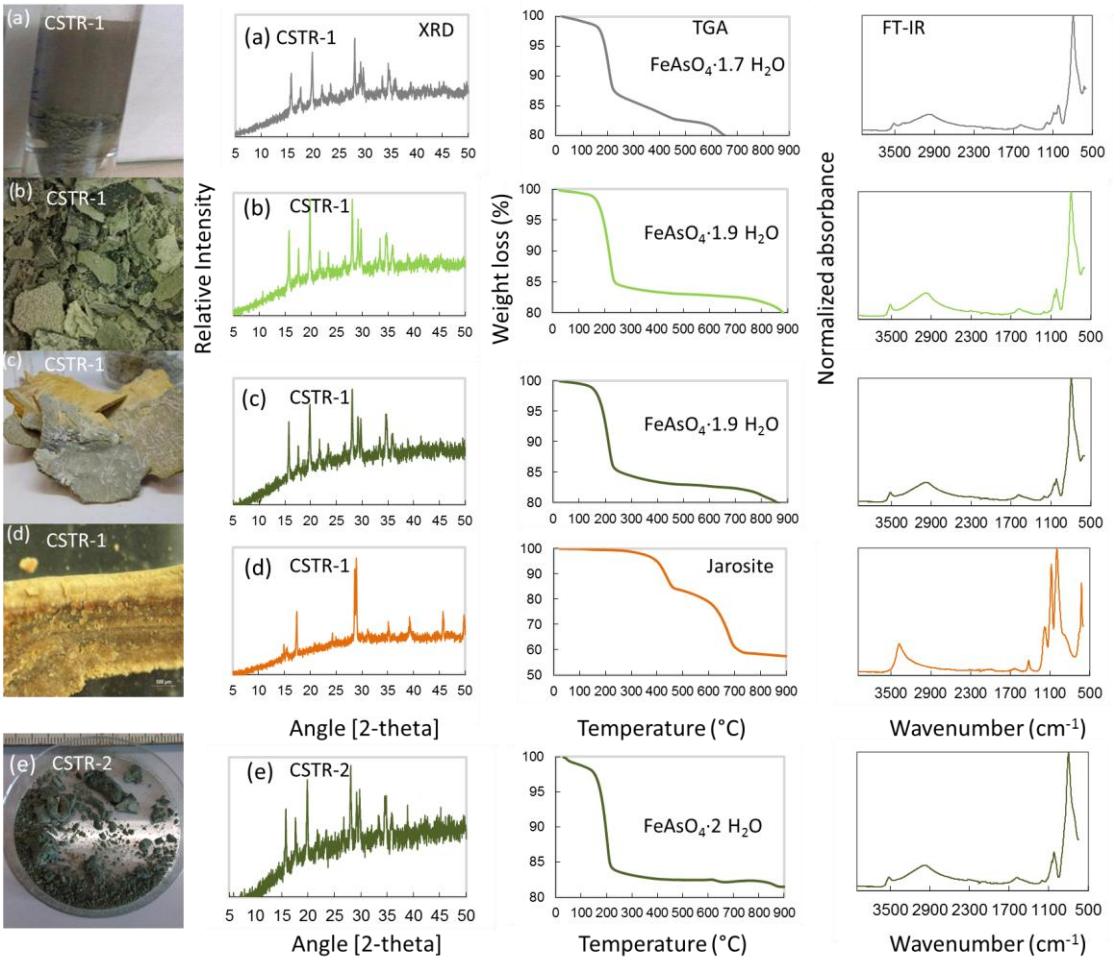

FIGURE 8.8 Bioscorodite phases obtained in CSTRs: (a) powder bioscorodite in suspension (liquid), (b) bioscorodite deposited in the bottom of the reactor (light green), (c) bioscorodite deposited over jarosite wall (olive green), (d) jarosite deposited in glass wall (yellowish-orange) and (e) bioscorodite from CSTR-2 (olive green). Structural water determined by TGA was calculated between 150 and 250°C.

Free water content of the bioscorodite sludge

Bioscorodite sludge free water content was determined through filtration and sedimentation, obtaining values of 4.7%wt and 6.2%wt water, respectively. The low content of free water in the precipitates shows the very good dewatering properties of bioscorodite precipitates.

Bioscorodite stability measured as arsenic leaching rates

Bioscorodite produced in CSTRs displays an aggregate morphology forming layers on the reactor wall. This morphology does not enable to measure either the distribution size or the settling rates of the precipitates. The TCLP test was conducted with three samples: one from CSTR-1 and two from CSTR-2: one aggregate and one crushed sample. After

five days, arsenic leaching rates rapidly increased for all the tests to about 0.6 mg L^{-1}. After two months, the arsenic concentration stabilized between 0.4 and 0.6 mg L^{-1} (Fig. 8.9). The crushed sample from CSTR-2 behaved very similar to the other samples. After 100 days of leaching, bioscorodite precipitates from CSTR-1 had a two-fold higher arsenic leaching rate than bioscorodite from CSTR-2, i.e. 0.8 mg As L^{-1}. This may be related to the presence of jarosite in precipitates of CSTR-1. The arsenic leaching from bioscorodite samples was below the limit of 5 mg L^{-1} in 20 h, which is proposed as the maximum permissible arsenic concentration from solid material under TCLP test conditions [53]. After 100 days, arsenic leaching values indicated that equilibrium had not yet been achieved in the samples.

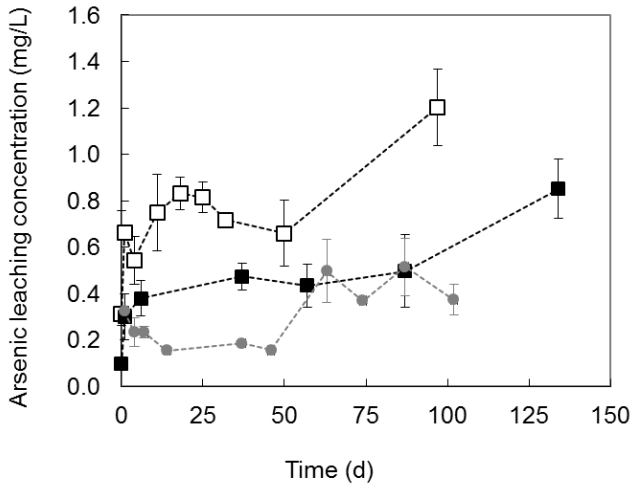

FIGURE 8.9 Arsenic leaching values from the stability tests data under TCLP test conditions. Legend samples: □ bioscorodite from CSTR-1 (random size sample), ■ bioscorodite from CSTR-2 (random size sample), ● bioscorodite from CSTR-2 (crushed sample).

8.3.4 Implications for Bioscorodite technology for arsenic removal and safe disposal

Bioscorodite formation in CSTRs was shown to be a reliable stable process in which seeding or recycling of crystals is not required. In this study, arsenic concentrations between 0.5 and 2.8 g As^{5+} L^{-1} were used, which is within the range typically found in metallurgical streams. The concomitant precipitation of arsenic with ferric iron in the bioscorodite process avoids arsenic inhibition of the microorganisms. By adjustment of the Fe/As molar ratio and recycling of diluted arsenic streams, concentrated arsenic streams or arsenic trioxide powder may also be treated by this new process and converted to bioscorodite for suitable disposal.

The absence of seeds or parent crystals in bioscorodite crystallization at 72°C is a major advantage when compared to chemical synthesis of scorodite at the same temperatures,

which require seed material. Being the only product, bioscorodite can be easily disposed without further post treatment. In contrast to the atmospheric chemical synthesis of scorodite at 95°C, gypsum seeds are needed to achieve 90% of arsenic removal efficiency. In addition, only one third of the final sludge of this process is scorodite, which has to be separated to decrease the volume waste [38, 59]. Other authors have replaced gypsum by hydrothermal scorodite seeds [27]. In that study, arsenic was efficiently removed up to 70% from diluted streams (1 g As^{5+} L^{-1}). However, arsenic efficiency depended on the seed recycling. No seeds recycling resulted in no removal of arsenic. From the data presented by the authors in that study, it was calculated that only 5.5%wt of the final sludge was new atmospheric scorodite, which is very difficult to distinguish from the hydrothermal scorodite seeds.

Other advantages of the bioscorodite process are the constant pH and temperature, the use of air instead of oxygen to support the biological oxidation, and the diluted sulphuric acid medium of 0.08M. Apart from these advantages, bioscorodite crystallization has a precipitation rate three times lower than chemical synthesis (at the same arsenic concentrations). The bioscorodite process removed 1 g As L^{-1} d^{-1}, producing 3 g scorodite L^{-1} d^{-1}. The rate of the bioscorodite process can be improved by the retention of biomass, which may enable operation with higher volumetric loading rates of iron and arsenic. The scaling of precipitates in the reactor was also inconvenient because it is difficult to collect solids from the reactor and it interferes with the mixing. Further studies are focused on the use of more advanced bioreactors which may improve the quality of the sludge for easy disposal, and increase the volumetric arsenic loading rates that can be treated.

8.4 CONCLUSIONS

The studied process of bioscorodite formation in continuous reactors has an arsenic removal efficiently of 99%, resulting in an effluent with 29 ± 18 mg As L^{-1} at pH 1.2 and 72°C. The bioscorodite precipitates were crystalline scorodite displaying arsenic leaching rates of 0.4 g As L^{-1} after 100 days of storage. Bioscorodite sludge is suitable for arsenic disposal and storage. The described process of continuous bioscorodite production shows the potential for the use of bioscorodite as arsenic immobilizing material.

APPENDIX 8.1

TABLE A1 FT-IR vibrations assigned to scorodite and bioscorodite samples. FT-IR spectra assignment values of scorodite mineral, chemical crystallized scorodite and FasH phase were taken from literature [73]. Legend of samples: CSTR-1 (a) powder bioscorodite in suspension (liquid), (b) bioscorodite crystals deposited in the bottom of the reactor (light green), (c) bioscorodite deposited over jarosite wall (olive green), (d) jarosite deposited in glass wall and CSTR-2 (e) bioscorodite.

IR	Scor	FasH	(a)	(b)	(c)	(e)	Jarosite (d)
As-O-Fe str	720	740-751	-	-	-	-	624.9
V1 (AsO_4^{3-})	795	790-841	792.7	798.5	796.5	792.4	-
V3 (AsO_4^{3-})	900	860-898-963	-	-	-	-	-
V1 (SO_4^{2-})	-	-	1016.4	1018.4	1018.4	1020.3	999.1
V3 (SO_4^{2-})	-	-	-	-	-	-	1080.1
V3 (SO_4^{2-})	-	-	-	-	-	-	1180.4
H_2O bend	1620	1620	1587.4	1585.4	1585.4	1585.4	1423.4
H_2O str	2960	-	2976.1	2976.1	2978	2970.3	-
OH str	3516	3557-3498-3325	3516.2	3518	3518	3516.2	3379.2

APPENDIX 8.2

Determination of linear crystal growth

Crystal growth kinetics is based on the diffusion-reaction [122]. These theories suggest that there are two steps in the mass deposition (crystal growth). First a diffusion process, whereby solute molecules are transported from the bulk of the fluid phase to the solid surface. This diffusion step is followed by a first-order reaction when the solute molecules arrange themselves into the crystal lattice. The two steps can be associated in an overall crystal growth coefficient K_G (eq. A1).

$$\frac{1}{K_G} = \frac{1}{k_d} + \frac{1}{k_r} \qquad \text{eq.A1}$$

For extremely rapid reactions, i.e. large k_r, $K_G \sim k_d$, and the crystallization process is controlled by diffusional operation. If the value of k_d is large then $K_G \sim k_r$, and the process is controlled by the surface integration.

Mass deposition rate is defined as [122]:

$$R_G = \frac{1}{A} \cdot \frac{\partial m}{\partial t} = K_G \cdot \left(c - c^*\right)^g \quad \text{eq.A2}$$

Mass deposition rate equation is related to linear growth rate through

$$R_G = \frac{1}{A} \cdot \frac{\partial m}{\partial t} = \frac{3\alpha}{\beta} \cdot \rho_s \cdot G = \frac{3\alpha}{\beta} \cdot \rho_s \cdot \frac{\partial L}{\partial t} = \frac{6\alpha}{\beta} \cdot \rho_s \cdot \upsilon \quad \text{eq.A3}$$

Reorienting the eq.A3 we obtain G (m s^{-1})

$$G = \frac{\partial L}{\partial t} = \frac{\beta}{3\alpha \cdot A \cdot \rho s} \frac{\partial m}{\partial t} \quad \text{eq.A4}$$

For the case of bioscorodite crystals the change of mass (crystal growth) is related to the arsenic precipitation from solution:

$$\frac{\partial m_{(BS)}}{\partial t} = M_{(BS)} \cdot V \left(\frac{-\partial \left[As^{5+}\right]}{\partial t} \right) \quad \text{eq.A5}$$

Combining the total mass (eq.A6) and surface area (eq.A7) of crystals we obtain eq.A8:

$$W = n \cdot \rho_s \cdot \alpha \cdot L^3 \quad \text{eq.A6}$$

$$A = n \cdot \beta \cdot L^2 \quad \text{eq.A7}$$

$$\frac{\beta}{\alpha \cdot A} = \frac{L \cdot \rho_s}{W} \quad \text{eq.A8}$$

$$G = \frac{L \cdot M \cdot V}{3 \cdot W} \left(\frac{-\partial \left[As^{5+}\right]}{\partial t} \right) \text{ (m } s^{-1}\text{)} \quad \text{eq.A9}$$

For octahedra $6\alpha/\beta = 0.816$,

$$R_G = 0.408 \cdot \rho_s \cdot G \quad \text{(kg } m^{-2}\ s^{-1}\text{)} \quad \text{eq.A10}$$

ρ_s = scorodite density 3280 kg m^{-3}
$M_{(BS)}$ = 230 grams mol^{-1} scorodite
L = characteristic size crystals (m)
n = number of crystals
V= volume of reaction (m^3)
W= mass weight crystals (kg)
α, β volume and surface shape factors

Chapter 9

Continuous bioscorodite crystallization in an airlift reactor

Abstract

Bioscorodite ($FeAsO_4 \cdot 2H_2O$) was crystallized in an airlift reactor fed with 2.4 g L^{-1} arsenate and 2.4 g L^{-1} ferrous iron, and operated at pH 1.2 and 72°C. Arsenic removal was limited by the biological ferrous iron oxidation. In continuous operation, the iron oxidation efficiency initially was 30% and increased to 80% in few days when the dissolved oxygen concentration was increased. The bioscorodite yield was 3 g/g arsenic removed. The first precipitates were identified as scorodite having a dipyramidal octahedron habit with an Fe/As molar ratio of 1.55. The stability test (TCLP) classified the crystals as suitable for storage with a leached arsenic concentration of 0.5 mg L^{-1} after 60 days. The morphology and size (160 μm) of the crystals guarantees their free-flowing nature avoiding scaling. The biggest and most stable crystals can be harvested by sedimentation, to select the material best suited for final disposal.

This chapter has been accepted as:
Gonzalez-Contreras, P; Weijma, J, Buisman, C. J. N., Arsenic removal in an airlift reactor for continuous bioscorodite production. *Crystal Growth & Design* **2012,** *12*, 2699-2706.

9.1 INTRODUCTION

Arsenic release is widely known from groundwater contamination in Bangladesh [90]. Besides this naturally occurring contamination, also anthropogenic sources can lead to a significant release of arsenic. For example, in 2005 during the Hurricane Katrina, 1470 metric tons of arsenic were released [45, 52]. These were contained in 12 million m^3 of wood debris. Despite the fact that in some countries the use of arsenic for wood preservation is restricted, five thousand metric tons of arsenic are still consumed annually for this purpose [100]. During the last decade, arsenic production has increased from about 50 to 60 thousand metric tons per year due to mineral processing [100]. Arsenic waste from mineral processing and coal washing is disposed of in tailings. In the last century, more than 100 significant upstream tailing dam failures have been documented [116]. The risk of arsenic contamination from metallurgical effluents, tailing failures and other anthropogenic sources should be minimized to limit harmful effects on water sources. To achieve this, there is a need for low cost, effective and simple technologies that guarantee arsenic immobilization.

Arsenic is traditionally removed from industrial wastewaters from mineral processing and metallurgical operations by lime neutralization with co-precipitation of arsenic with ferric iron [144, 159]. Arsenical ferrihydrite precipitation requires a high iron consumption with respect to arsenic, i.e. Fe/As > 4 and thus large amounts of waste material are produced [143, 159]. More recent technologies focus on arsenic immobilization into scorodite crystals. Scorodite ($FeAsO_4 \cdot 2H_2O$) is a natural mineral that contains 30%wt arsenic and an Fe/As molar ratio of 1 [42, 104, 106, 128, 145]. Because of its low arsenic solubility, mineral scorodite is the preferred arsenic mineral for disposal in tailing dams or in dry stack facilities. Originally, scorodite precipitation systems required the use of autoclaving technology, i.e. high pressure and high temperatures [37, 48]. Subsequently, the feasibility of atmospheric scorodite precipitation (<100°C) in the sulphate system was demonstrated by control of the saturation level [38, 154, 155].

Biogenic scorodite (bioscorodite) crystallization in batch and continuous systems was previously demonstrated (Chapter 3 and 8). In this process, biological oxidation reactions control arsenic precipitation by increasing the saturation level of scorodite in the solution. Thus bioscorodite can be precipitated in one single step at pH 1.2 and 72°C. In a CSTR, 99% of arsenic removal efficiency was achieved from streams with 2.8 g L^{-1} As^{5+} (Chapter 8). The produced bioscorodite crystals were very stable, displaying arsenic leaching rates of 0.4 mg L^{-1} after 100 days of storage under landfill conditions (TCLP test). Continuous crystallization of bioscorodite in CSTR systems leads to agglomeration of precipitates and formation of scaling on the reactor wall. The scaling of bioscorodite precipitates impedes the free-flowing nature of the crystals, hampering the removal of sludge for disposal.

To solve the scaling problem, we propose to use an airlift reactor for continuous bioscorodite production. Airlift reactors have several advantages compared to the traditional CSTR [150] such as: (1) mixing is induced by aeration (no impeller) , (2) shear rates are significantly lower, thereby facilitating the growth of biofilms, (3) the solids retention time can be separated from the hydraulic retention time, (4) lower investment and operational cost compared to CSTR systems and (5) the air used for mixing also supplies the oxygen and carbon dioxide required for biological oxidation and growth. These advantages make an airlift reactor a suitable candidate for a biomineral production process.

The objective of this research was to implement an airlift reactor for continuous bioscorodite crystallization and arsenic removal. By the use of an airlift reactor, we aim to avoid flakes formation and surface scaling of bioscorodite precipitates, thereby facilitating sludge harvesting for final disposal.

9.2 MATERIAL AND METHODS

9.2.1 Microorganisms

A mixed culture of *Sulfolobales* was used to inoculate the reactor. The iron oxidation kinetics of this culture was previously studied at suboptimal growth conditions suitable for bioscorodite crystallization (Chapter 4).

9.2.2 Airlift reactor system and start up

An airlift reactor with 9 L of working volume was used. The temperature was controlled at 72 ± 2°C with a heating bath at 90°C (Julabo F25, Germany). The air flow to the reactors was controlled by mass flow controllers (Brooks Thermal Mass Flow meter, type 5850 TR, 0-60 L h^{-1} air). For specific tests, pure oxygen was added to the air flow by a separate mass flow controller. The air flow was recycled at 300 L h^{-1}, providing a superficial air velocity in the riser of 45 cm s^{-1}. Water vapour in the bleed air was condensed with a cooling bath (Julabo F25, Germany) and the condensate was returned to the reactor. The reactor was operated without recirculation of liquid or solids.

The reactor was inoculated with 10%v/v of thermoacidophilic microorganisms growing in the absence of arsenic at pH 1.2 and 72°C. The airlift reactor was operated in three consecutive stages: (I) batch mode during 35 days, (II) then it was switched to continuous operation during 37 days at a hydraulic retention time of 38h (days 36-72 of operation) and (III) during 25 days under continuous operation the ferrous iron oxidation was optimized (days 73-98 of operation). No scorodite or external seeds were added to the bioreactor.

The concentration of iron and arsenic supplied to the reactor was based on the results of a previous study, producing bioscorodite using a continuous CSTR system (Chapter 8). Influent composition varied in the different stages: (I) 1.8 g Fe^{2+} L^{-1} and 2.4 g As^{5+} L^{-1} giving and an Fe/As molar ratio of 1 and in (II) iron concentrations were increased to 2.4 g Fe^{2+} L^{-1} and arsenic concentration were kept at 2.4 g As^{5+} L^{-1} giving an Fe/As molar ratio of 1.3. During stage III, iron concentrations were increased to 6 g Fe^{2+} L^{-1}. Ferrous iron stock solutions were prepared by dissolving iron (II) sulphate heptahydrate ($FeSO_4 \cdot 7H_2O$) at several concentrations in 0.1 mol L^{-1} sulphuric acid. The arsenic solutions were prepared from disodium hydrogen arsenate heptahydrate ($Na_2HAsO_4 \cdot 7H_2O$) (Fluka, Switzerland).

We compared the biological ferrous oxidation and arsenic removal efficiency with the biological ferrous oxidation efficiency in the absence of arsenic (Chapter 4) and with the bioscorodite production in CSTRs (Chapter 8).

Redox potential and pH were measured with glass electrodes QR480X - Pt billed - S8 and QP181X - S8 (Prosense, The Netherlands), respectively. Slope calibration of the pH electrode was done with pH 1 and pH 4 buffers. Dissolved oxygen was measured using an oxygen dipping probe DP-PSt3 (Presens, Germay) connected to a Fibox-3, Fiber optic oxygen transmitter (Presens, Germany). The oxygen sensor was calibrated at 0% with nitrogen and at 100% with water-saturated air. Cells activity was followed by their capacity to oxidize ferrous iron at pH 1.

9.2.3 Calculation of the Ion Activity Product of bioscorodite

Calculation of the Ion Activity Product (IAP) of bioscorodite crystals was based on its congruent dissolution. The IAP values reported for scorodite mineral, scorodite produced by chemical synthesis and bioscorodite crystals were previously compared (Chapter 3).

9.2.4 Determination of linear crystal growth rates

In the bioscorodite process, the addition of seeds is not needed. Therefore, the linear crystal growth rate of bioscorodite describes the growth process of solids materials appearing in solution. The change of mass (crystal growth) is related to the arsenic precipitation from solution. The equations to determine crystal growth rates were previously described in Chapter 8.

9.2.5 Iron speciation in aqueous phase

Iron species in the aqueous phase were measured using Dr. Lange Cuvette test LCK 320 for ferrous iron (Fe^{2+}) and ferric iron (Fe^{3+}), and a Xion 500 spectrophotometer (Hach-Lange, Germany).

9.2.6 Arsenic speciation in aqueous phase

Arsenate (As^{5+}) was only add to the experiments but in any case both species (As^{3+} and As^{5+}) were controlled in all arsenic measurements.Arsenic speciation in aqueous phase was measured by anionic ion exclusion chromatography using sulphuric acid as mobile phase, followed by UV detection. The validation of this method is described in Chapter 2.

9.2.7 Arsenic solid stability analysis by the Toxicity Characteristic Leaching Procedure (TCLP)

An enhanced TCLP test was performed in serum bottles, stirred in a shaker at 20°C following the EPA procedure [53]. Acetate buffer at pH 4.95 was used as leaching medium. The solid to liquid ratio was fixed at 20%w/w. Size reduction of the samples was not required. The duration of the TCLP test was extended from 20 h to 60 days under the same leaching conditions. A mixing rate of 100 rpm instead of 30 rpm (suggested by the TCLP test) was provided.

9.2.8 Structural characterization of precipitates

Four bioscorodite samples were selected for structural characterization. Sample S1 was collected after 10 days of batch operation when the first crystals were observed and only XRD analysis was performed on it. Sample S2 was collected at the end of batch operation, after 35 days. During continuous operation (Stage II), samples S3 and S4 were collected after 41 and 72 days of operation, respectively. During the optimization of ferrous iron oxidation (stage III), solid samples were not collected. Solid samples were separated from the liquid phase by sedimentation. Samples S2, S3 and S4 were analyzed by all the methods described in the following text. The separated solids were washed with 0.1M sulphuric acid prior characterization and to their use in leaching tests. The samples were dried at 70°C before structural characterization.

X-ray diffraction (XRD) was used to identify the nature of the solid materials. Wide angle X-ray scattering (WAXS) powder diffractograms were recorded on a PANalytical ExpertPro System (Almelo, The Netherlands) in the angular range 5–50°(2θ), with a step size of 0.02°(2θ) and an acquisition time of 0.6 s per step. The CuKα1 radiation from the anode, generated at 40 kV and 50 mA, was monochromatized using a 15 μm Ni foil (λ = 0.1542 nm). The diffractometer was equipped with a 1° divergence slit, a 0.2 mm receiving slit, and a 1° scatter slit.

The structural H_2O content of the solid phases was determined with a thermogravimetric analyser (Perkin-Elmer TGA7 equipped with Pyris software). The thermogravimetric analysis was performed with about 10 mg of air-dried powdered material at a heating rate of 10°C min^{-1} from 20°C to 900°C under air. The furnace had a temperature precision of ± 2°C and the balance precision was of 0.001%.

Fourier transform infrared (FT-IR) spectra of the solid samples were obtained on a Varian Scimitar 1000 FT-IR spectrometer equipped with a DTGS-detector. The measurement resolution was set at 4 cm^{-1}, and the spectra were collected in the range 4000–400 cm^{-1} for KBr-disks and 4000-650 cm^{-1} for attenuated total reflectance (ATR) with 64 coadded scans. KBr sample disks were prepared from a mixture of 1%wt of finely ground sample in KBr. The sample chamber was purged by N_2 gas for 10 minutes before scanning was started. ATR was performed on a PIKE MIRacle ATR equipped with a diamond w/ZnSe lens single reflection plate. The vibrations assigned to bioscorodite crystals are displayed in Chapter 6.

Crystal morphology was investigated with scanning electron microscopy (SEM). The samples were fit on SEM sample holders by carbon adhesive tape (EMS Washington USA) and subsequently coated with about 10 nm Carbon (K950X, Quorum Technologies, UK). Samples were morphologically analysed at 2 kV, 50 pA, WD 5 mm at room temperature, in a field emission scanning electron microscope (Magellan 400, FEI, Eindhoven, The Netherlands). Images were digitally recorded, optimized and resized with Adobe Photoshop CS. EDX analyses were accomplished in the same field emission scanning electron microscope by an X-Max/Aztec X-ray analyser (Oxford Instruments Analytical, High Wycombe, England) at an acceleration voltage of 15 kV, 200pA, WD 5mm.

9.3 RESULTS AND DISCUSSION

9.3.1 Ferrous iron oxidation and arsenic removal efficiency during batch and continuous mode operation of an airlift reactor

During batch operation of the airlift reactor at pH 1.2 and 72 ± 2°C a 90% of biological ferrous iron oxidation was achieved (Fig. 9.1), resulting in an increase in the redox potential. Precipitation of arsenic and ferric iron occurred simultaneously. During batch operation, 80% of arsenic removal was found.

In continuous mode after 35 days of batch operation, ferrous iron oxidation rates of 0.4 ± 0.1 g L^{-1} d^{-1} were obtained, which correspond to 30% of the maximum expected biological oxidation rate, based on previous results (Chapter 8). During continuous operation the redox potential varied between 350 and 400 mV, confirming that ferrous iron oxidation was occurring at low rate. The pH in the reactor fluctuated between 1.1 and 1.2. During continuous operation, only 30% of the supplied ferrous iron was oxidized. Consequently, only 30% of iron was precipitated and 40% of arsenic removal was achieved. Thus arsenic precipitation rates of 0.40 ± 0.08 g L^{-1} d^{-1}, which increased to 0.51 g L^{-1} d^{-1} at the end of the operation, and iron precipitation rates of 0.38 ± 0.04 g L^{-1} d^{-1} were obtained (Fig. 9.2).

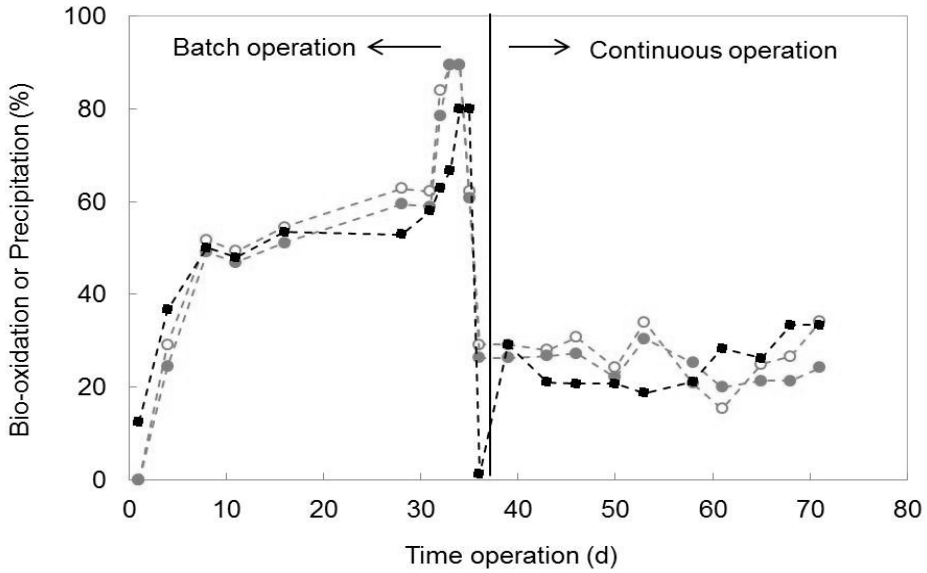

FIGURE 9.1 Biological ferrous iron conversion, iron and arsenic precipitation obtained in airlift reactor at pH 1.2 and 72°C during batch and continuous operation. Continuous mode operation started at 35 days. Legend: ● ferrous iron conversion (%), ○ iron precipitation (%), ■ arsenic precipitation (%).

In the influent, the Fe(II)/As(V) molar ratio was controlled at 1.1, while based on the precipitation rates of ferric iron and arsenic a fluctuation of Fe(III)/As(V) molar ratios between 0.8 to 1.77 was observed during the continuous mode operation.

These results suggest that during continuous operation of the airlift reactor, biological ferrous iron oxidation was the limiting factor for arsenic precipitation and as a consequence for the precipitation of bioscorodite.

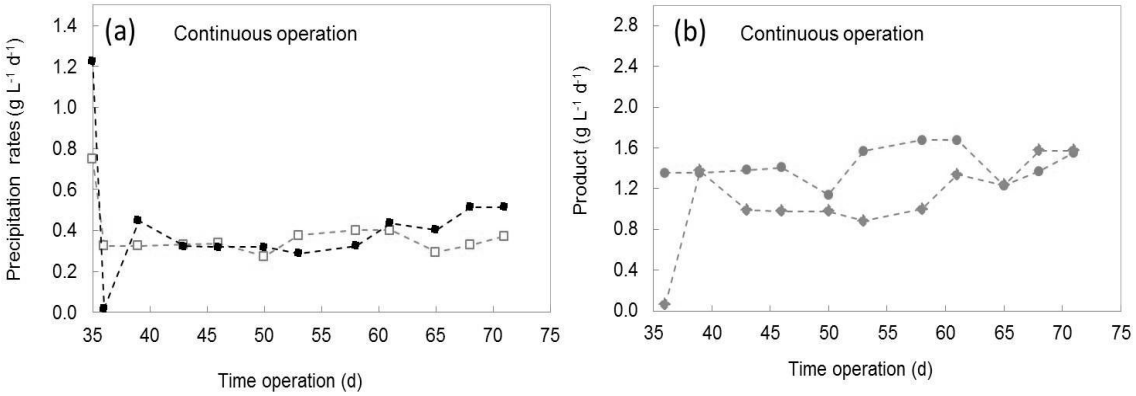

FIGURE 9.2 (a) Iron and arsenic precipitation rates obtained in a continuous airlift reactor at pH 1.2 and 72°C. (b) Bioscorodite produced calculated based on iron and arsenic precipitation rates. Legend: ■ arsenic precipitation rates, □ iron precipitation rates, ● ferric iron precipitates, ♦ bioscorodite.

9.3.2 Enhancement of biological ferrous oxidation in airlift reactor

As mentioned above, biological iron oxidation was the rate limiting step for bioscorodite crystallization in the airlift reactor. The iron oxidizers used in the bioscorodite process are thermoacidophilic microorganisms. These microorganisms are autotrophic archaea that use energy (ferrous oxidation) at a low efficiency. It has been estimated that some acidophiles require 120 mol of Fe(II) to generate 1 mol of glucose [103]. This implies that these microorganisms need to oxidize large amounts of ferrous iron in order to sustain growth. In the bioscorodite process, these microorganisms are cultivated under suboptimal growth conditions such as low pH and low substrate concentrations (Chapter 4). Despite these suboptimal growth conditions, in a previous CSTR research study the microorganisms oxidized ferrous iron at pH 1.2 with a 100% of efficiency at a rate of 1 g Fe^{2+} L^{-1} d^{-1} (Chapter 8).

In order to improve the growth of thermoacidophiles in the airlift reactor, ferrous iron concentration was increased from 2.4 (stage II) to 6 g L^{-1} and dissolved oxygen concentration was increased from 3 to 4.4 mg O_2 L^{-1} by the addition of pure oxygen to the supplied air. After 7 days, the ferrous iron conversion increased to 50% and after 15 days to 70% (Fig. 9.3). The equivalent ferrous iron oxidation rate at this stage of operation was 2.8 g Fe^{2+} L^{-1} d^{-1} at HRT of 38 h. The optimization and enhancement of ferrous iron oxidation result in an increase of the redox potential from 320 mV (influent) to 500 mV.

Despite the increased ferrous iron concentration, iron precipitation was only 20% during this test, mainly because arsenic was not supplied during this period. The increase of ferrous oxidation under the new operational conditions shows that thermoacidophiles were under sub optimal growth conditions.

Oxygen Transfer Rates (OTR)

OTR values were calculated based on the ferrous iron biological conversion capacity. OTR values obtained ranged between 8 and $10 \cdot 10^{-5}$ mol O_2 m^{-3} s^{-1}. The volumetric mass transfer coefficient (k_La) was calculated using the model for liquid phase [160] and the calculated OTR. Dissolved oxygen concentrations measured in the liquid phase fluctuated between 3.85 and 3.88 mg O_2 L^{-1}. The calculated k_La was between 20 and 23 h^{-1}. The obtained k_La values during the airlift operation coincide with the reported values of k_La for ferrous iron oxidation in the order of 30 h^{-1} [2, 19].

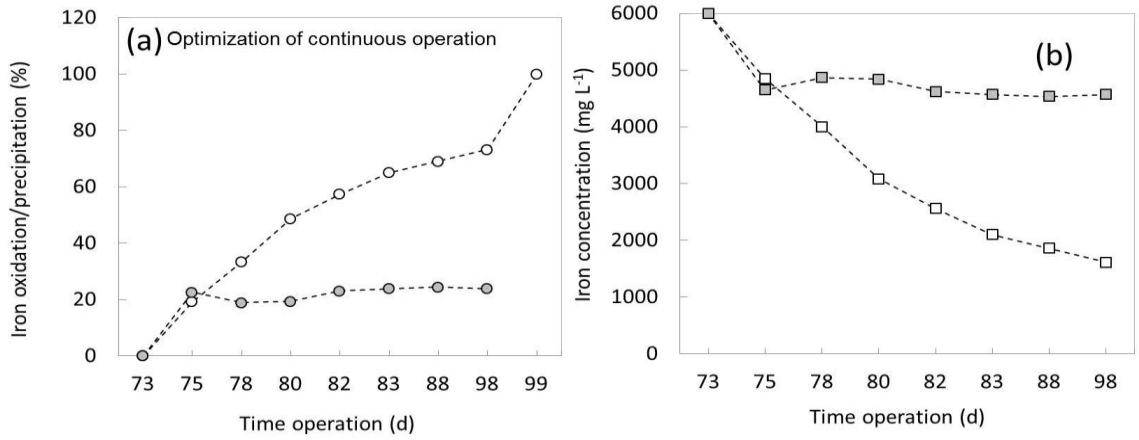

FIGURE 9.3 Improvement of ferrous iron oxidation rates in the absence of arsenic in an airlift reactor at pH 1.2 and 72°C operated at HRT of 38h. Influent concentration was 6000 mg Fe^{2+} L^{-1}. (a) Biological ferrous iron conversion and iron precipitation. (b) Ferrous and total iron concentrations in the effluent. Legend: ○ ferrous iron conversion, ● total iron precipitated, ■ total iron in effluent, □ ferrous iron in effluent.

9.3.3 Bioscorodite crystals precipitation

The first precipitates were observed after 10 days of batch operation. The weighed mass of bioscorodite produced in the reactor at the end of the batch operation period (230 g) corresponded well with the expected mass based on arsenic and ferric iron precipitation rates (220 g). This indicates that nearly all the ferric iron was used for bioscorodite precipitation.

After 10 days of batch operation solid were observed and quantified at 2 g L^{-1}. At the end of the batch mode, solid concentration has increased to 10 g L^{-1} due to bioscorodite precipitation (Fig. 9.4). During continuous operation, the solids concentration increased from 6 to 12 g L^{-1} due to mineral production in 25 days.

The average volumetric bioscorodite production rate during continuous operation of the airlift was 1.3 g bioscorodite L^{-1} d^{-1}. This is one-third below the production rate obtained in CSTR systems (Chapter 8). The bioscorodite yield was 3.0 g per g arsenic removed. This value corresponds with the yield obtained in CSTR systems (3.1-3.2) (Chapter 8).

The calculated IAP values for bioscorodite decreased from -20 during batch operation to -22 during continuous operation. These values correspond to the IAP values reported for previous experiments (Chapter 3 and 6).

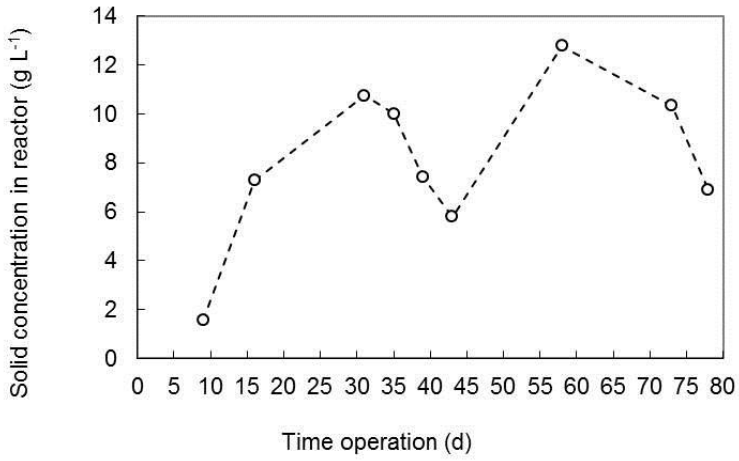

FIGURE 9.4 Fluctuation of solid concentration in a bioscorodite airlift reactor at pH 1.2 and 72°C. Continuous mode operation started after 35 days.

9.3.4 Characterization of bioscorodite crystals

Free water content of sludge

The free water content of the precipitates was measured in 10 filtered samples and in 10 settled samples taken from the reactor during continuous operation. The filtered samples contained 2.5 ± 0.5% of free water, the settled samples contained 2.2 ± 0.6% of free water. The low free water content of the precipitates shows the very good dewatering properties of bioscorodite crystals.

Size distribution of precipitates

Stokes' diameter of bioscorodite crystals precipitates was calculated based on their settling rates. Settling rates between 20 and 140 m h^{-1} were measured (Fig. 9.5). The calculated density of the crystals was 3322 kg m^{-3}, which is in agreement to the reported density of scorodite (3100-3200 kg m^{-3}) [166]. The size distribution frequency (Fig. 9.6) indicates that bioscorodite crystals grew from an average size of 30 μm during batch operation to 160 μm at the end of the continuous operation phase. During the first days of continuous operation of the airlift reactor, at 41 days of operation, two crystal size populations were observed (50 and 100 μm) (sample S3 in Fig. 9.6). After prolonged operation of the airlift reactor (72 days), increase in the crystals size led to a monosized population of larger crystals (175 μm). Probably the growth of the crystals in time was due to the dissolution of small crystals (ripening).

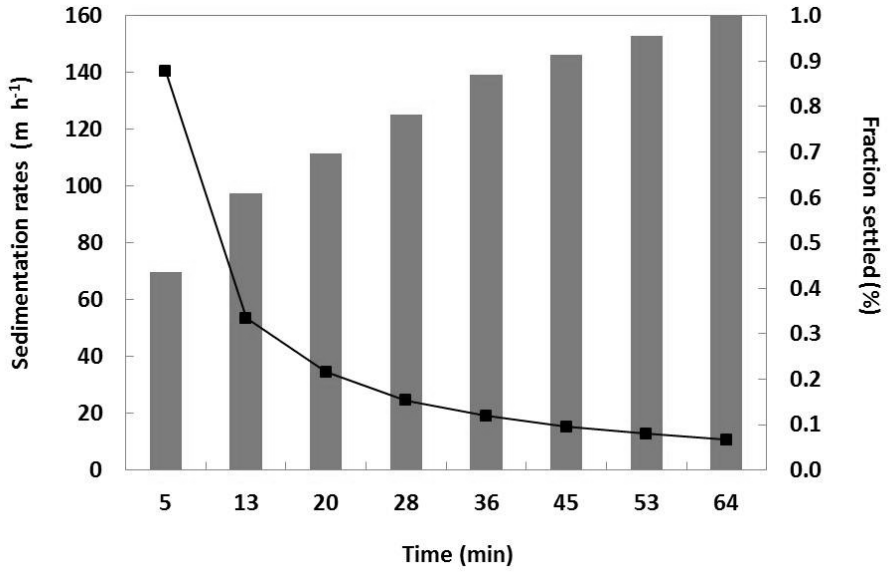

FIGURE 9.5 Sedimentation rates of bioscorodite crystals produced in airlift reactors at pH 1.2 and 72°C. Legend: bars indicate the accumulative settled fraction of crystals and the line indicates the sedimentation rates.

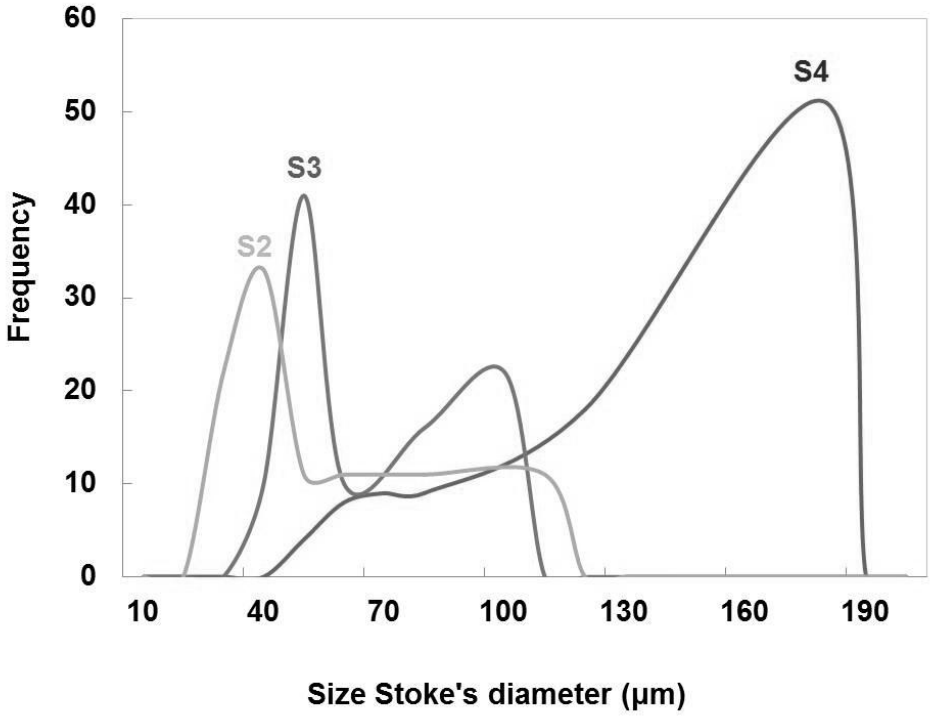

FIGURE 9.6 Size distribution frequency of bioscorodite crystals produced in an airlift reactor at pH 1.2 and 72°C. Stokes' diameter was calculated based on sedimentation analysis. Legend: (S2) 30d of batch, (S3) 41d and (S4) 72d in continuous operation.

Crystal growth rates

The occurrence of different crystal sizes implies that the crystals grow at different rates. In the airlift reactor for bioscorodite production, the crystal growth rates increased from 10 μm d^{-1} at the start to 32 μm d^{-1} at the end of the operation. In CSTR systems, bioscorodite agglomerates grew with rates between 16 and 20 μm d^{-1} (Chapter 8).

Structural characterization of bioscorodite crystals

As mentioned before, the first precipitates were observed in solution after 10 days of batch operation. These precipitates (sample S1) were identified as crystalline scorodite by XRD analysis. Samples S2 (end of batch operation after 30 days) and S4 (72 days of operation) were also identified as crystalline scorodite (Fig. 9.7).

Bioscorodite crystals contained exactly $2H_2O$ of structural water (Fig. 9.7). Sulphate incorporation in the structure was not observed. FT-IR analysis revealed peaks at 1015 and 1030 cm^{-1}, which were probably related to phosphate contamination (Fig. 9.8). Phosphate contamination in scorodite and parascorodite minerals has been documented before with FT-IR vibrations at 1010 and 1040 cm^{-1} [134].

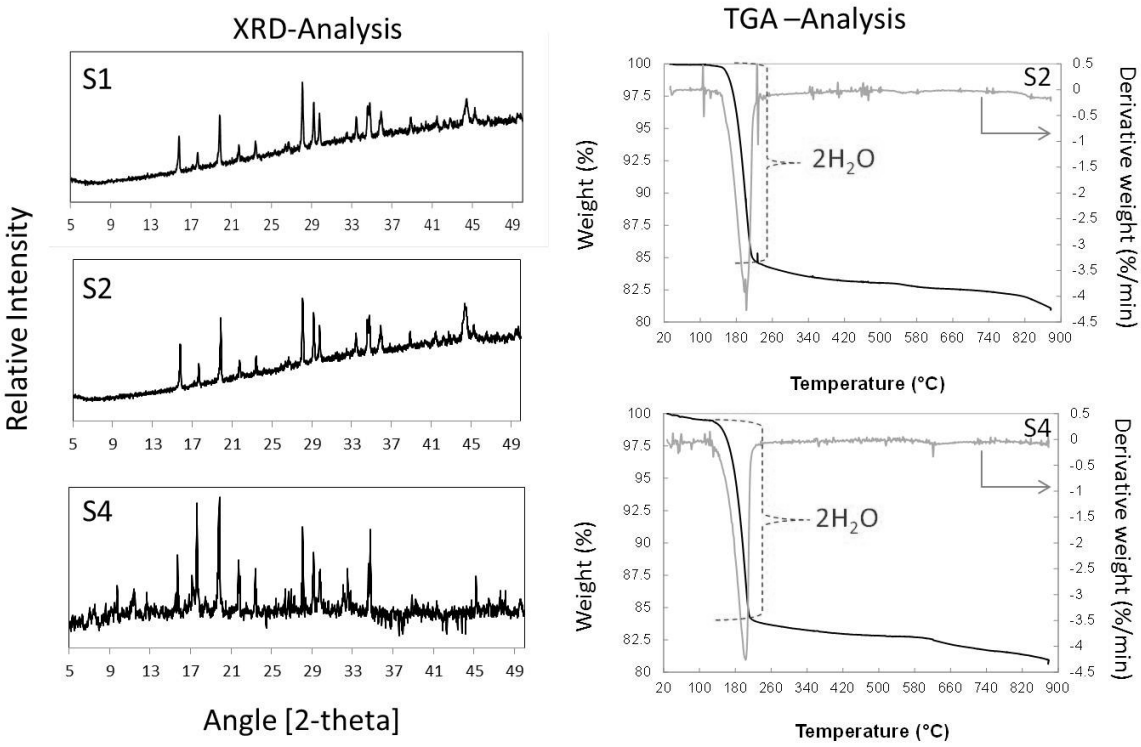

FIGURE 9.7 Structural characterization by XRD and TGA analysis of bioscorodite crystals produced in airlift reactor at pH 1.2 and 72°C. Legend: (S1) 7d of batch, (S2) 30d of batch (S4) 72d in continuous operation. XRD of S3 is not displayed in the Figure but it has the same XRD pattern that S4.

Morphology of bioscorodite crystals

In contrast to bioscorodite production in a CSTR reactor, surface scale with precipitates was not observed in the airlift reactor. In a separate control experiment, the air flow through the reactor was decreased to achieve an air superficial velocity of 15 cm s^{-1}. At this lower air flow (one-third of the normal flow), formation of bioscorodite scaling on the reactor glass wall did occur.

The morphology of three bioscorodite samples (S2, S3 and S4) was studied by SEM photos and EDX analysis. Figure 9.9 shows details of (a) the size distribution, (b) bioscorodite aggregates and (c) the crystal habit of bioscorodite. The SEM observations confirmed that during continuous airlift operation, the size of bioscorodite crystals increased. Bioscorodite crystals produced in batch and continuous operation, displayed a dypiramidal octahedron habit.

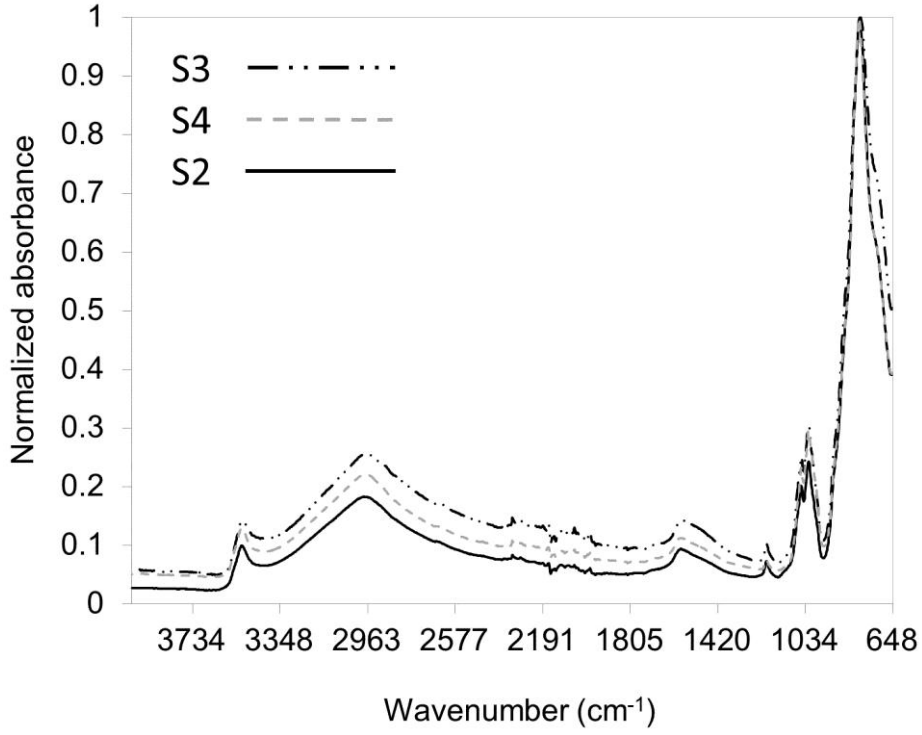

FIGURE 9.8 Fourier Transform Infrared (FT-IR) spectra of bioscorodite samples produced in an airlift reactor at pH 1.2 and 72°C. Legend: (S2) 30d of batch, (S3) 41d in continuous operation and (S4) 72d in continuous operation.

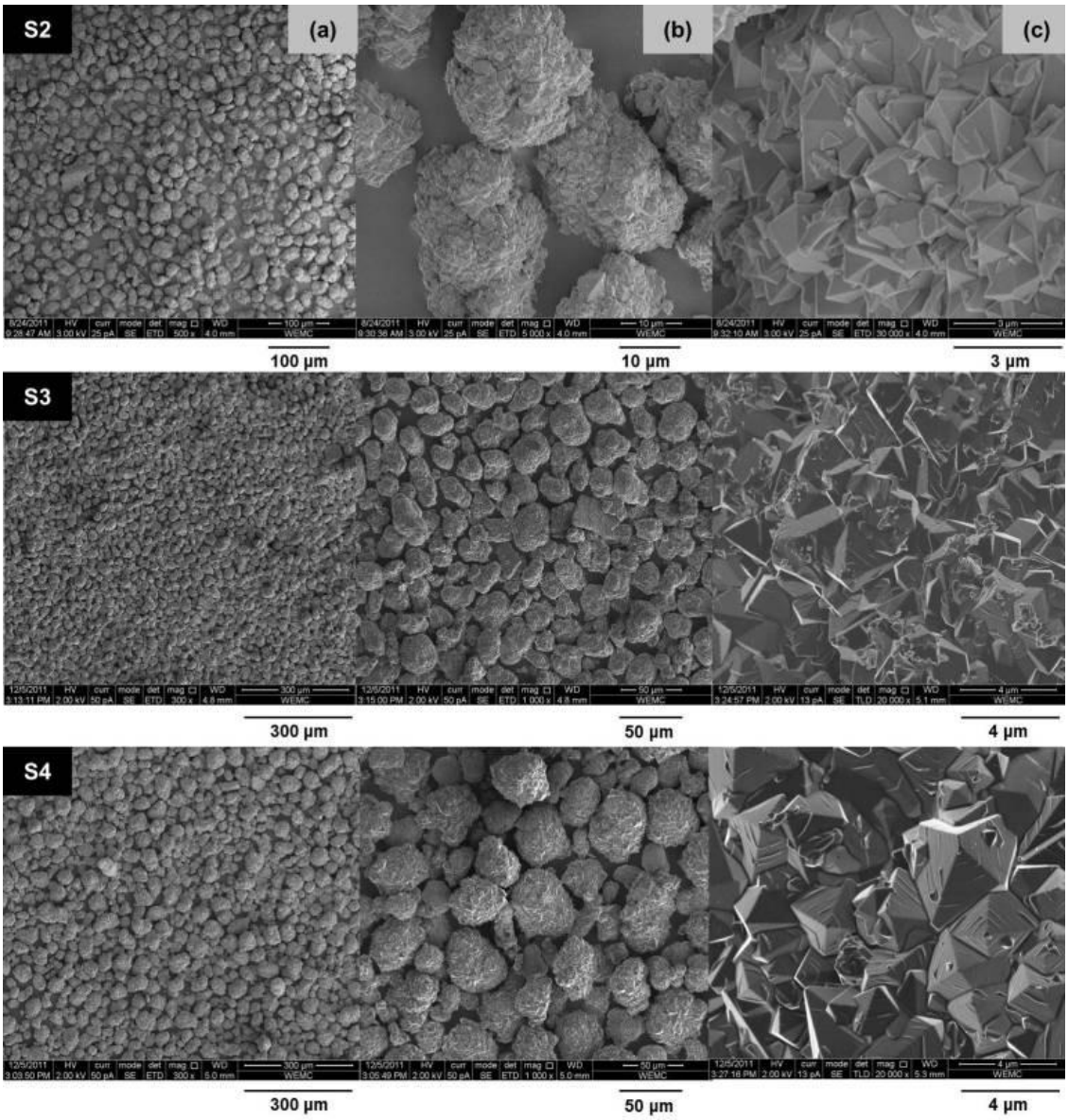

FIGURE 9.9 SEM pictures and of bioscorodite crystals produced in airlift reactor at pH 1.2 and 72°C. SEM pictures give a detail of (a) the distribution size, (b) aggregates and (c) habit of bioscorodite crystals. Legend: (S2) 30d of batch, (S3) 41d in continuous operation and (S4) 72d in continuous operation.

Crystals produced during batch operation, had a smooth surface. In contrast, on the surface of crystals produced during continuous operation, screw dislocations appeared (Fig. 9.10). These screw dislocations cause steps on the surface of bioscorodite crystals, providing a surface for secondary nucleation. Indeed, growth of secondary small crystals on the surface of bigger crystals was observed (Fig. 9.10). The screw dislocations may be formed by internal crystal stress but also by collisions with other particles.

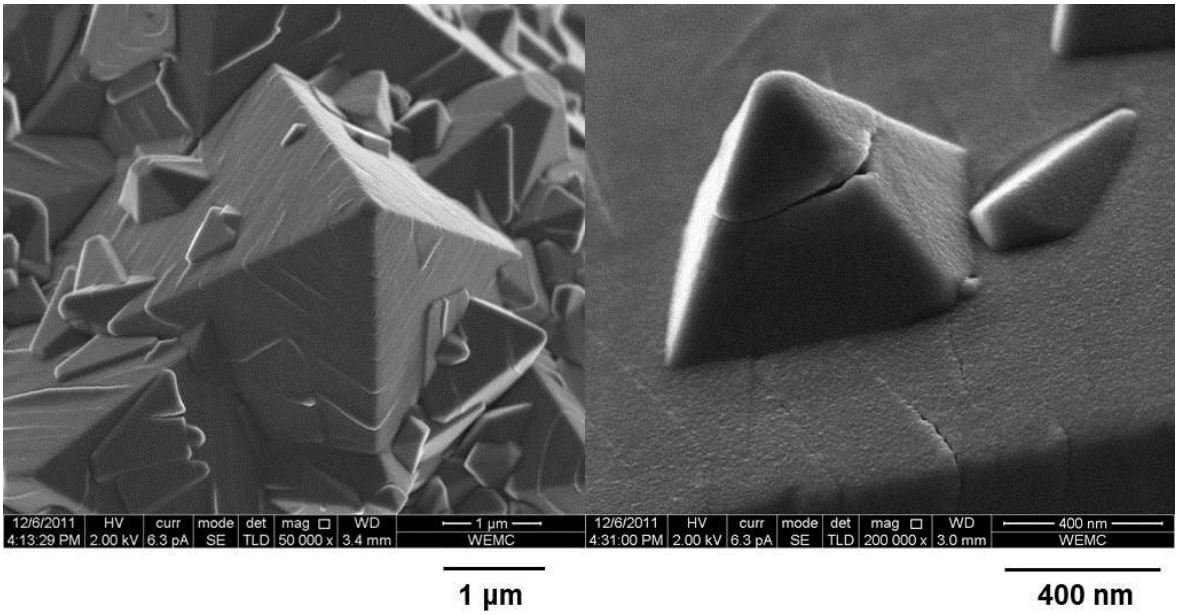

FIGURE 9.10 SEM pictures and of bioscorodite crystals produced in airlift reactor at pH 1.2 and 72°C. These SEM pictures show a detail of the dislocations observed during the continuous operation.

In bioscorodite crystals, Fe/As molar ratios of 1.55 ± 0.08 were measured by SEM-EDX at different times of operation (Fig. 9.11). These Fe/As molar ratios were higher than the expected stoichiometric value of 1. The SEM-EDX analysis also revealed a small fraction (1.4 ± 0.03%wt) of phosphorus, confirming the previous results of FT-IR analysis. The higher than stoichiometric iron content in the bioscorodite crystals suggests that a phase containing mainly iron oxides was present.

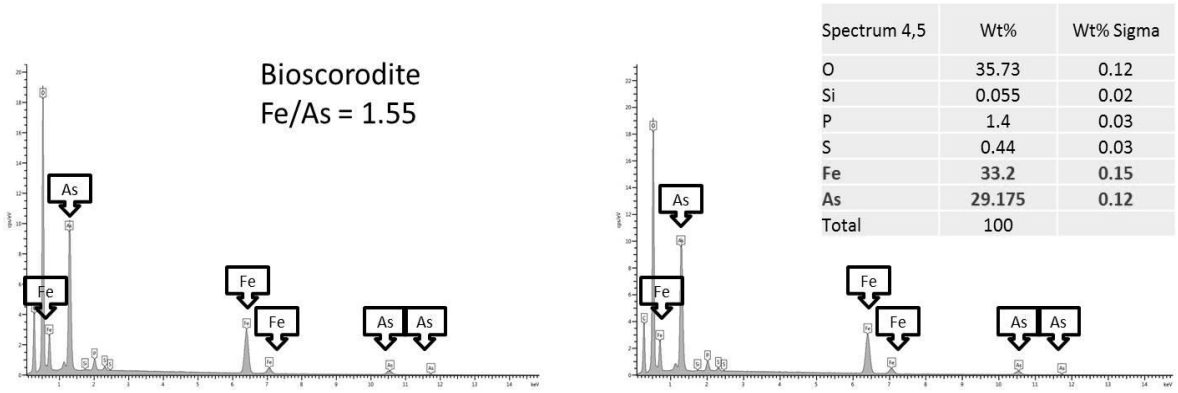

Spectrum 4,5	Wt%	Wt% Sigma
O	35.73	0.12
Si	0.055	0.02
P	1.4	0.03
S	0.44	0.03
Fe	33.2	0.15
As	29.175	0.12
Total	100	

FIGURE 9.11 SEM-EDX analysis of bioscorodite samples produced in an airlift reactor at pH 1.2 and 72°C. Legend: spectrum 4 (S3) 41d in continuous operation and spectrum 5 (S4) 72d in continuous operation.

Dissolution of bioscorodite crystals

Dissolution of bioscorodite crystals was tested under TCLP conditions. In bioscorodite crystals produced during batch operation, arsenic leaching concentrations of 3 mg As L^{-1} were measured after 60 days. In contrast, bioscorodite crystals produced during continuous operation leached 1.9 mg As L^{-1} after 60 d (Fig. 9.12a). To assess if the continuous produced bioscorodite contained less stable phases, the TCLP test of sample S4 was repeated while replacing the leaching solution with fresh acetate medium after 7 and 15 days. After two replacements, the arsenic leaching decreased from 2.5 mg L^{-1} to 0.5 mg L^{-1} and remained at this concentration after 65 days of storage (Fig. 9.12b).

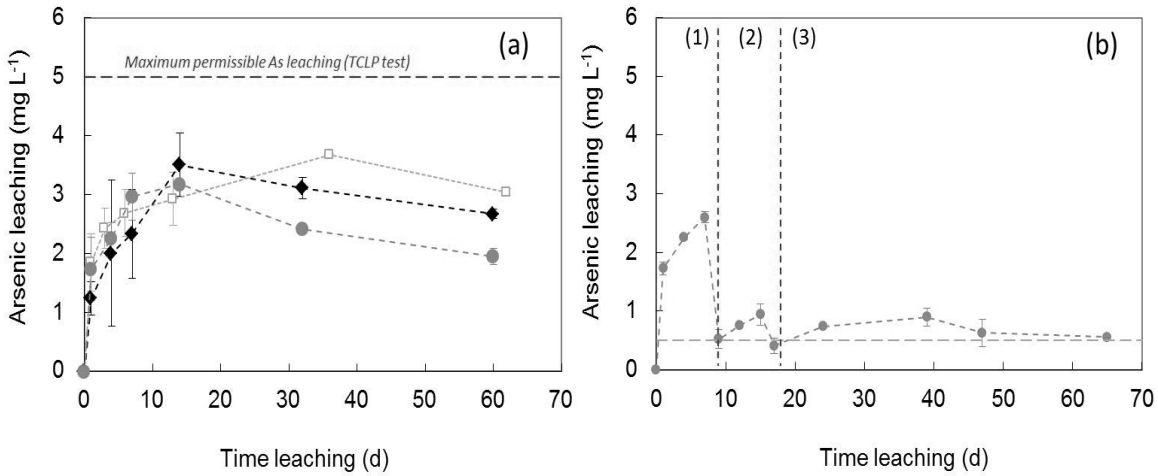

FIGURE 9.12 Arsenic leaching rates observed in bioscorodite crystals produced in airlift reactor at pH 1.2 and 72°C. (a) Bioscorodite crystals evaluated under the TCLP test conditions without pre-treatment. (b) Bioscorodite crystals (S4) evaluated under the TCLP test conditions replacing the leaching solution with fresh acetate medium after (1) 7 days and (2) 15 days. Legend: □ S2 - 30 days in batch operation, ♦ S3 - 41 days in continuous operation and ● S4 - 72 days in continuous operation.

It was expected that the bioscorodite crystals with dislocations on the surface (produced during continuous operation of the airlift reactor) were the least stable. Against our expectations, the bioscorodite crystals with a smooth surface (produced during batch operation) were less stable than the crystals with dislocations. The arsenic leaching concentration was inversely correlated to the crystal size and ageing time of the crystals in the bioreactor (Fig. 9.13). Thus, sample S4 with an average crystal size of 160 μm, obtained after 58 days of ageing (20 days batch operation and 38 days under continuous operation) was the most stable. The relation between crystal size/ageing and bioscorodite dissolution implies that the most stable crystals can be selectively removed from the bioreactor based on their size. The high airflow mix in the bioscorodite airlift reactor avoided surface scaling of the crystals and guaranteed the free-flowing nature of the crystals.

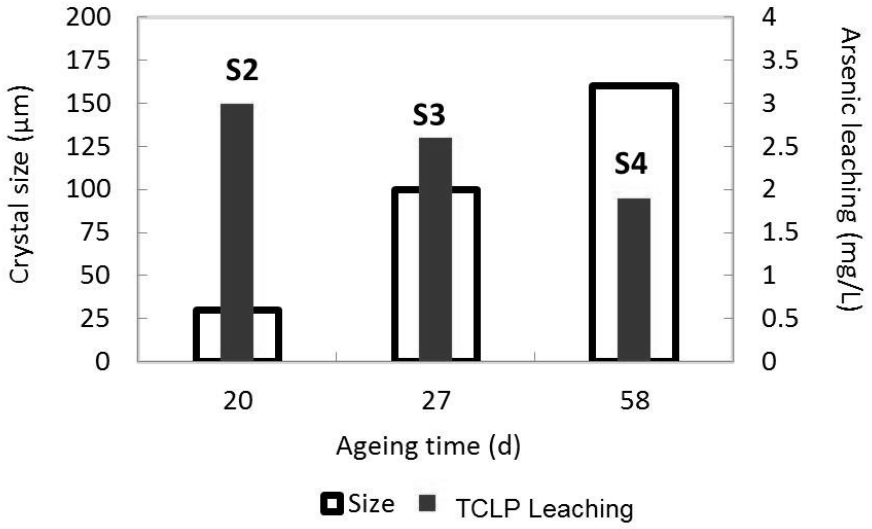

FIGURE 9.13 Arsenic leaching concentrations related to ageing and size of bioscorodite crystals produced in an airlift reactor at pH 1.2 and 72°C. Legend: Legend: (S2) 30d in batch operation, (S3) 41d in continuous operation and (S4) 72d in continuous operation.

9.3.5 Airlift reactor as technology for arsenic removal

Bioscorodite crystals production in an airlift reactor is suitable for arsenic removal and bioscorodite disposal. The high mixing rates in an airlift reactor avoids the scaling of precipitates on the reactor walls. This facilitates the handling and selective disposal of bioscorodite sludge. Concomitant arsenic and ferric iron precipitation was observed, leading to the crystallization of bioscorodite crystals. The retention of these crystals in the airlift reactor allowed for further crystal growth and ageing, thereby lowering the arsenic leaching potential of these crystals under landfill conditions. The stability of the crystals produced in the airlift reactor was slightly less than the stability of crystals produced in CSTR-systems. Probably this is due to the occurrence of dislocations on the surface of bioscorodite crystals produced in the airlift reactor. The low arsenic leaching concentration makes the airlift reactor crystals very suitable to be used as arsenic immobilizing material. Since large airlift reactors have been demonstrated as bioreactors, it seems that the bioscorodite process can be relatively simple scaled up.

9.4 CONCLUSIONS

Bioscorodite crystal was continuously produced in an airlift reactor avoiding the scaling of walls. The crystals can be selectively disposed based on their crystal size and ageing. The low arsenic dissolution makes the airlift reactor crystals very suitable to be used as arsenic immobilizing material.

Chapter 10

Storage of bioscorodite crystals

Abstract

Scorodite is considered a good material for arsenic immobilization. Bioscorodite crystals previously produced in airlift reactors at pH 1.2 and 72°C were compared to mineral scorodite from a natural source. The results show that the structure of bioscorodite crystals is very similar to mineral scorodite. The bioscorodite habit resembles the octahedron (1-9μm) habit of scorodite, forming aggregates with a size up to 150 μm. The mineral scorodite and bioscorodite crystals had an iron content with Fe/As molar ratios of 1.37 and 1.55, respectively. This is higher than the expected theoretical Fe/As molar ratio of 1 in scorodite. Arsenic leaching rates of the bioscorodite crystals depended on the leaching medium used. In a previous study in acetate medium at pH 5, bioscorodite crystals leached 2.4 mg As L^{-1}. In the current study, in diluted sulphuric/nitric acid (pH 4) bioscorodite crystals leached 0.6 mg As L^{-1} after 60 days. When acetate medium was refreshed, the arsenic leaching rate decreased to 0.5 mg L^{-1}. The assessment of the stability data suggests that bioscorodite crystals should be stored at pH 4, preferably under aerobic conditions and in the absence of organic waste.

This chapter is in preparation for submission:
Gonzalez-Contreras, P; Weijma, J, Buisman, C. J. N., On the storage of bioscorodite crystals for arsenic immobilization.

10.1 INTRODUCTION

Crystalline ferric arsenate, known as scorodite ($FeAsO_4 \cdot 2H_2O$), is a naturally occurring secondary mineral related to weathering of arsenopyrite, pyrite, and enargite [29, 60, 110, 151, 158]. Scorodite formation and dissolution is very important in controlling the mobility of arsenic in acid mine drainage, hot springs, and other surface and near-surface waters [42, 143]. These crystals are considered a good material for arsenic immobilization because they have a low solubility, high arsenic content (25-30%wt), high stability and compactness [18, 106, 146]. These properties make scorodite a suitable and stable material for arsenic immobilization and safe storage [42, 105, 106, 128, 145].

The synthesis of scorodite crystals is considered the next step for arsenic removal and immobilization from metallurgical wastewaters or for the final stabilization of arsenic trioxide [144, 157, 159]. Synthetic scorodite crystals have been formed using different approaches such as high pressure precipitation in autoclaves (150°C) [37, 48, 59, 143] or atmospheric precipitation (95°C) by stepwise neutralization and seed addition [26, 38, 65, 154, 155]. Bioscorodite crystals were also produced by control of the saturation level with the aid of thermoacidophilic microorganisms at 72°C and pH 1.2 in the absence of seeds (Chapter 6). Depending on the method used to produce scorodite crystals, formation of other phases of ferric arsenate has been reported. For example, when the temperature rises above 170°C, during hydrothermal crystallization of scorodite, ferric arsenate sub-hydrate [73, 94] and basic ferric arsenate sulphate bases are produced [49, 73, 74, 119]. During atmospheric scorodite precipitation, several short-lived hydrated precursor phases (poorly ferric arsenate) are formed [96, 106, 112]. These different ferric arsenate phases can have different solubility product values and arsenic leaching rates different from those of scorodite crystals. The potential of scorodite crystals as arsenic storage material becomes difficult to assess when the results are influenced by those less stable phases.

The objective of this research is to compare bioscorodite crystals to mineral scorodite and to assess its potential as arsenic storage material. The results are also compared to the reported data of chemically produced scorodite crystals.

10.2 Experimental Section

10.2.1 Scorodite mineral

A scorodite mineral specimen was obtained from a mineral supplier (Mineralrock, Italy). The specimen was originally taken from Hermerdon Bal Mine, Devon, England. Samples were physically separated avoiding contamination with other minerals as much as possible (Fig. 10.1). The specimen was crushed in order to carry out the structural analysis.

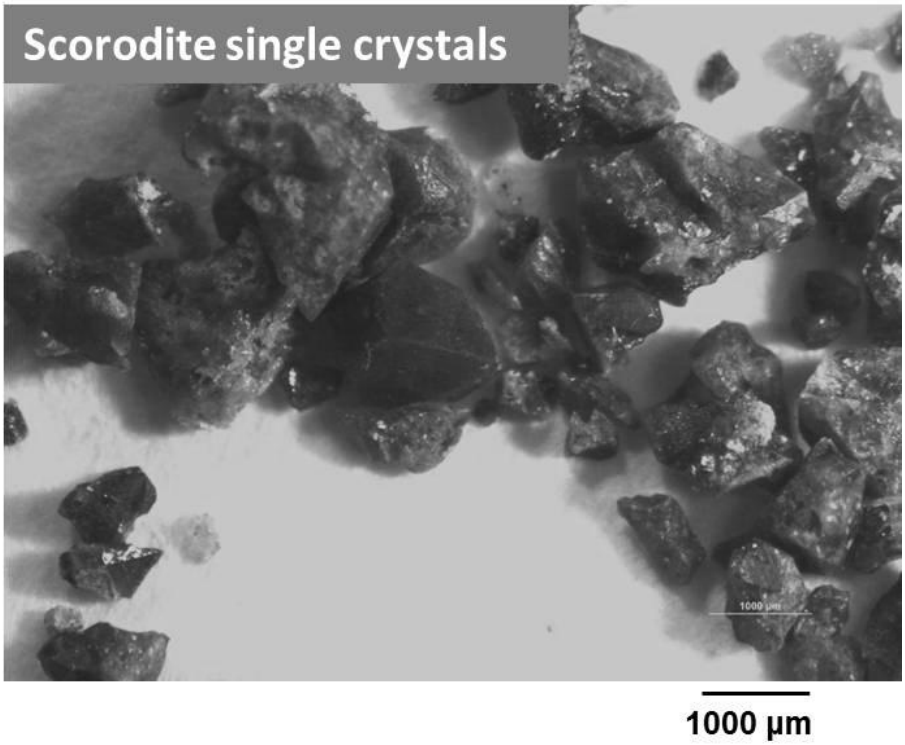

FIGURE 10.1 Mineral scorodite crystals physically separated from quartz massive.

10.2.2 Biogenic scorodite samples (bioscorodite)

Bioscorodite crystals were produced in an airlift reactor at pH 1.2 and 72°C (Chapter 9). Solid samples were separated from the liquid phase by sedimentation. Sulphuric acid medium at 0.1 M without arsenic and iron was used to wash the solids at room temperature, followed by sedimentation. Sedimentation only required 2 minutes due to the high settling velocity of the material. No arsenic was detected in the medium used for washing. Immediately after separation, solids were dried at 70°C during 24 h.

10.2.3 Evaluation of solids stability by the TCLP and SPLP Test

The TCLP test was performed in serum bottles agitated in a shaker at 20°C following the EPA procedure [53]. Acetate buffer at pH 4.95 was used as leaching medium. The solid to liquid ratio was fixed at 20, thus 2.5 grams of scorodite was mixed with 50 mL of solution. Size reduction of the bioscorodite samples was not required. The duration of the TCLP test was extended from 20 h to 60 days under the same leaching conditions.

The Synthetic Precipitation Leaching Procedure (SPLP) was performed in similar conditions to the TCLP test differing only in the leaching medium. The leaching medium in the SPLP tests simulates acid rain at pH 4 (sulphuric acid/nitric acid 60/40%wt) [54].

10.2.4 Precipitates structure characterization

X-ray diffraction (XRD) was used to identify the nature of the solid materials. Wide angle X-ray scattering (WAXS) powder diffractograms were recorded on a PANalytical ExpertPro System (Almelo, The Netherlands) in the angular range 5–50°(2θ), with a step size of 0.02°(2θ) and an acquisition time of 0.6 s per step. The CuKα1 radiation from the anode, generated at 40 kV and 50 mA, was monochromatized using a 15 μm Ni foil (λ = 0.1542 nm). The diffractometer was equipped with a 1° divergence slit, a 0.2 mm receiving slit, and a 1° scatter slit.

The structural water content of the solid phases was determined with a thermogravimetric analyser (Perkin-Elmer TGA7 equipped with Pyris software). The thermogravimetric analysis was performed with 10 mg of air-dried powdered material at a heating rate of 10°C min^{-1} from 20°C to 400°C under air. The furnace had a temperature precision ± 2°C and the balance precision was 0.001%.

Fourier transform infrared (FT-IR) spectra of the solid samples were obtained on a Varian Scimitar 1000 FT-IR spectrometer equipped with a DTGS-detector. The measurement resolution was set at 4 cm^{-1}, and the spectra were collected in the range 4000–400 cm^{-1} for KBr-disks and 4000-650 cm^{-1} for attenuated total reflectance (ATR) with 64 coadded scans. KBr sample disks were prepared from a mixture of 1%wt of finely ground sample in KBr. The sample chamber was purged by N_2 gas for 10 minutes before scanning was started. ATR was performed on a PIKE MIRacle ATR equipped with a diamond w/ZnSe lens single reflection plate.

Crystal morphology was investigated with scanning electron microscopy (SEM). The samples were fit on a SEM sample holder by carbon adhesive tabs (EMS Washington USA) and subsequently coated with about 10 nm Carbon (K950X, Quorum Technologies, UK). Samples were morphologically analysed at 2 kV, 50 pA, WD 5 mm at room temperature, in a field emission scanning electron microscope (Magellan 400, FEI, Eindhoven, the Netherlands). Images were digitally recorded, optimized and resized with Adobe Photoshop CS. EDX analyses were accomplished in the same field emission scanning electron microscope by an X-Max/AZtec X-ray analyser (Oxford Instruments Analytical, High Wycombe, England) at an acceleration voltage of 15 kV, 200pA, WD 5mm.

10.3 RESULTS AND DISCUSSION

10.3.1 Morphology of scorodite mineral, bioscorodite crystals and chemically synthesized scorodite

The scorodite mineral specimen displayed an intense green colour. Bioscorodite crystals displayed a pale-green colour. The dipyramidal octahedron habit was identified in both

samples differing only in size (Fig. 10.2). While in the scorodite specimen the crystal unit size was between 500 and 1000 μm, in the bioscorodite crystals was between 1 and 9 μm. Bioscorodite occurred in aggregates with a size between 50 and 150 μm (Chapter 9) and the characteristic dipyramidal octahedron habit of scorodite was observed. In chemically synthesized scorodite (at 90°C and 150°C), the characteristic habit was only observed at a size of 500 nm, forming aggregates with a size of 5 μm [18, 75, 111]. Chemically synthesized crystals at 95°C have been successfully grown up to 10 μm as single octahedrons, i.e. these crystals do not aggregate to form bigger precipitates [65, 67, 153]. However, those crystals required the use of 30 to 50 g As L^{-1} and chemical oxidants in order to achieve a size between 6 and 10 μm. In comparison with the data presented in literature, it seems that bioscorodite crystals produce the biggest agglomerates displaying a defined octahedron habit with a size of 150 μm.

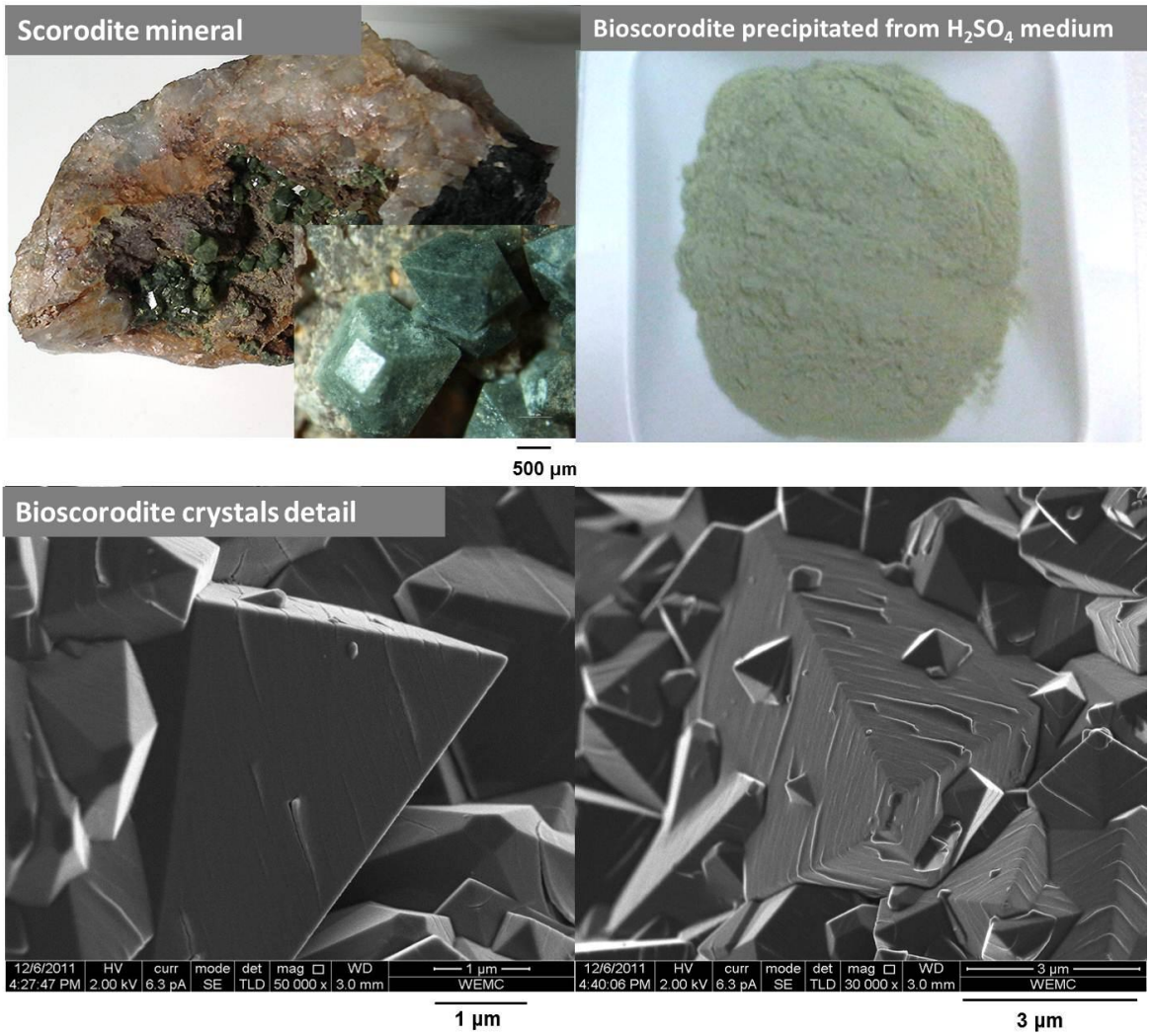

FIGURE 10.2 Pictures and SEM photos showing details of the colour and habit of scorodite mineral and bioscorodite crystals.

10.3.2 Arsenic content in the crystals

SEM-EDX analysis of mineral scorodite specimen shows that it contained 31.4%wt. As, 32%wt.Fe and 0.05%wt.P, giving an Fe/As molar ratio of 1.38 (Fig. 10.3). This Fe/As molar ratio is higher than the theoretical expected value of 1 (32.4%wt.As and 24.2%wt.Fe) [166]. Bioscorodite crystals contained 29%wt.As, 34%wt.Fe, 1.4%wt.P and 0.3%wt.S, giving an Fe/As molar ratio of 1.55. Other synthetic scorodite crystals contain between 29 and 31%wt. of arsenic [65, 67, 73, 75, 153]. Therefore, arsenic content in all these scorodite crystals resembles the mineral scorodite. It is clear that bioscorodite crystals contain more iron than other artificially synthesized scorodite crystals.

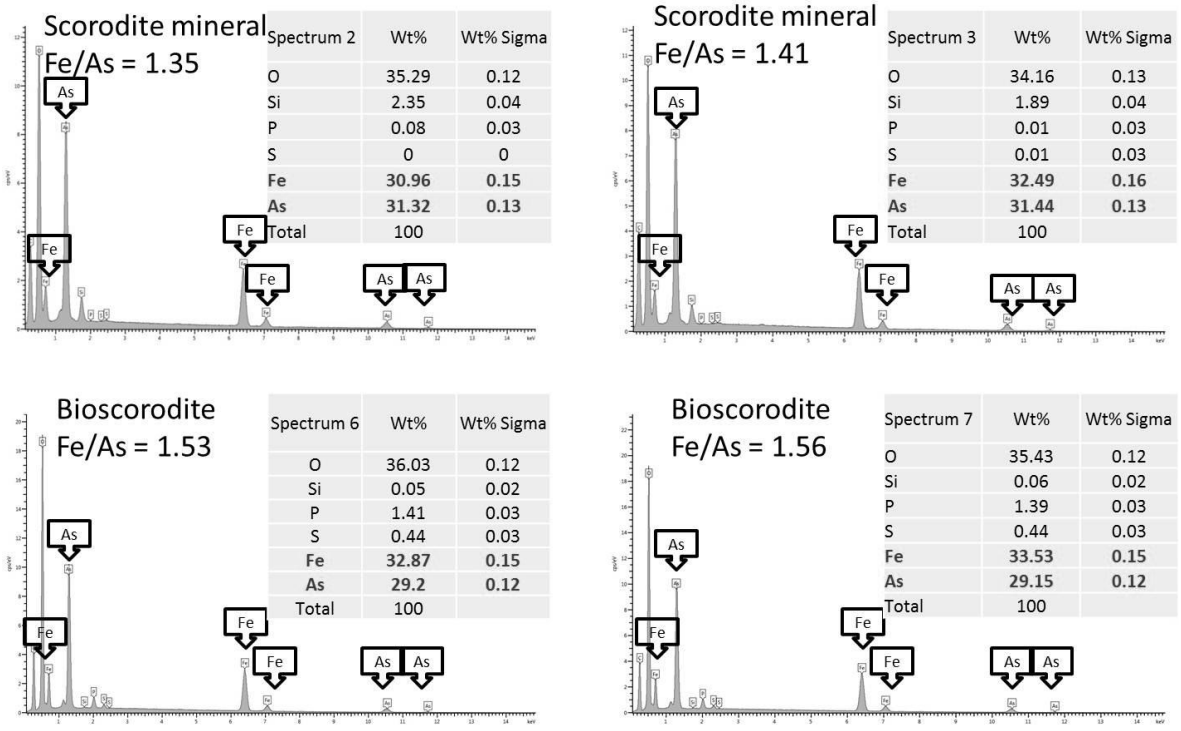

FIGURE 10.3 SEM-EDX analysis of scorodite mineral samples and bioscorodite crystals.

10.3.3 Structural characterization

Structural water content

In the mineral scorodite and in bioscorodite crystals a structural water content of exactly $2H_2O$ was measured (Fig. 10.4). The same amount is often reported for chemically synthesized scorodite [18, 48, 112, 113]. Unstable phases (amorphous) of ferric arsenate have been reported to contain a structural water content higher than $2H_2O$ [37, 96, 106, 112].

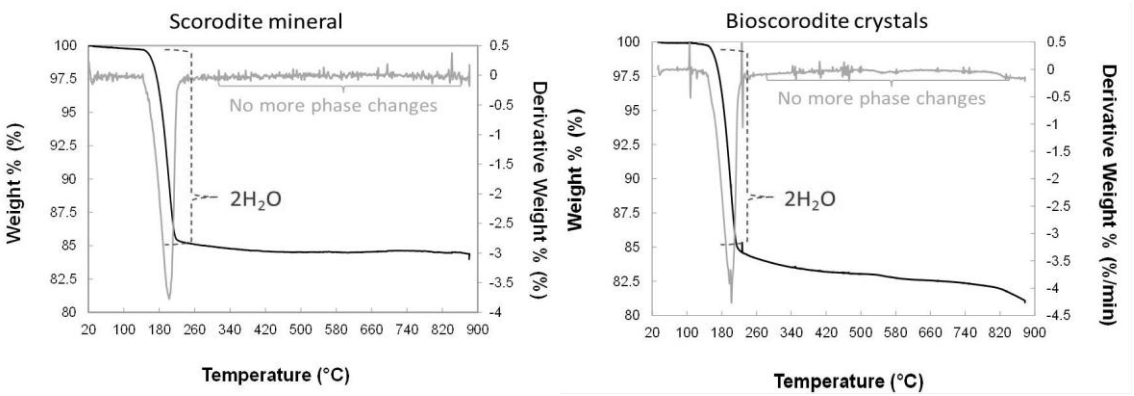

FIGURE 10.4 Structural water content of mineral scorodite and bioscorodite crystals measured by TGA analysis.

Crystallinity and contamination

XRD patterns of mineral scorodite and bioscorodite crystals were compared (Fig. 10.5). In both samples only scorodite was identified. The FT-IR spectra revealed that bioscorodite crystals only differ from mineral scorodite in the vibrations observed at 1010 and 1040 cm^{-1}. Probably these two vibrations are due to phosphate contamination, which corresponds with the phosphorus found by SEM-EDX analysis. In the mineral scorodite analysed in the current study also phosphorous was observed by SEM-EDX but phosphate bands in the FT-IR spectra were not observed (Fig. 10.5). However, FT-IR bands at 1022 and 1053 cm^{-1} assigned as phosphate contamination were previously reported in mineral scorodite and parascorodite [134].

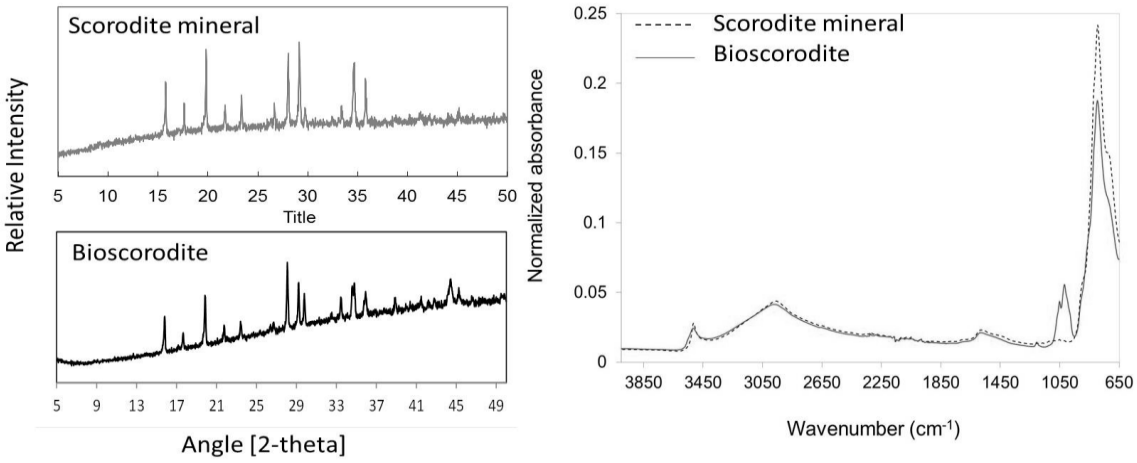

FIGURE 10.5 Structural characterization of mineral scorodite and bioscorodite crystals by XRD and FT-IR analysis.

Sulphate contamination was not identified in the FT-IR spectra of the bioscorodite samples. In contrast, in chemically synthesized scorodite sulphate contamination have been identified [49, 73, 74, 119].

Bioscorodite sludge properties

Previous characterization of bioscorodite sludge showed that it contains only 2.2% of free water (Chapter 9). The good dewatering properties of bioscorodite crystals confirm that the sludge can be easily processed. The sedimentation rates of bioscorodite crystals are in the order of 50 to 140 m h^{-1} (Chapter 9), allowing separation in normal settlers.

Stability evaluated through arsenic leaching rates

Bioscorodite crystals stability was previously evaluated using the TCLP test (Chapter 9). This test simulates the leaching of solids by organic acid medium in municipal solid waste (acetic acid, pH 5). After 60 days of leaching, bioscorodite crystals leached 2.4 mg As L^{-1}. In the same study, it was observed that replacement of the leaching medium (twice) resulted in a decrease of leached arsenic concentrations to 0.5 mg L^{-1} after 65 days (Chapter 9). These results indicate that the first arsenic released to the leaching medium comes from less stables phases.

In the current study, bioscorodite crystals were tested under SPLP test conditions. This test simulates an acid rain leaching medium (sulphuric and nitric acid mixtures, pH 4). Bioscorodite crystals under SPLP conditions leached only 0.6 mg As L^{-1} after 40 days (Fig. 10.6). The higher concentration obtained in the TCLP test was expected, because organic acids are known to accelerate the dissolution of minerals [103].

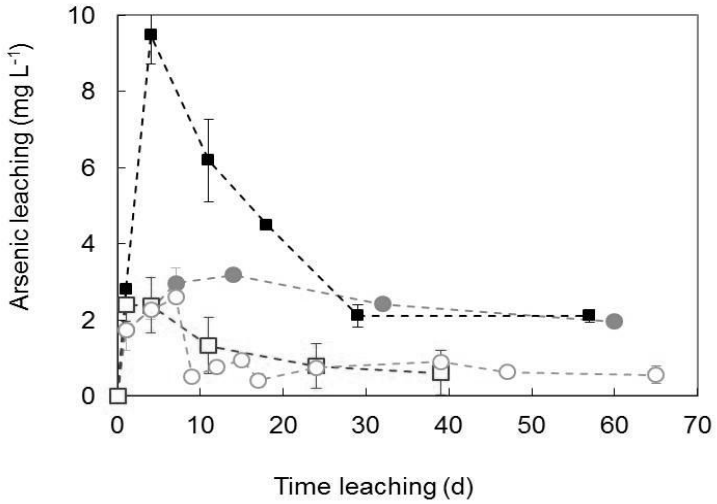

FIGURE 10.6 Arsenic leaching concentrations versus time for mineral scorodite and bioscorodite crystals. Legend: ■ crushed scorodite mineral under TCLP conditions (current study), ● bioscorodite crystals under TCLP conditions (Chapter 9), ○ bioscorodite crystals under TCLP conditions with two replacements of medium (Chapter 9), □ bioscorodite crystals under SPLP test (current study).

Krause and Ettel (1988) determined solubility of mineral scorodite at a pH range between 1 and 4, to assess congruent dissolution using mainly sulphuric and nitric acid [105]. Those tests at pH 4 are similar to the SPLP test conditions. Tests with organic acids have not been reported with mineral scorodite. In the current study, mineral scorodite was leached under TCLP test conditions, thus with organic acids. The crushed mineral displayed high arsenic leaching rates during the first days. After 10 days, arsenic concentrations of 10 mg As L^{-1} were measured, which decreased to 2 mg As L^{-1} after 60 days. Most likely, this decrease is the result of arsenic adsorption by secondary iron phases released either by crushing of the sample or by the incongruent dissolution of scorodite.

As discussed in the introduction, the various processes to crystallize scorodite do not always produce the most preferable materials. A comparison of arsenic leaching concentrations for mineral scorodite, bioscorodite (72°C) and chemically synthesized scorodite (95°C - 150°C) reveals a variation between 0.5 mg As L^{-1} and 13.6 mg As L^{-1} (Table 10.1). The data in Table 10.1 also show that scorodite dissolution is strongly controlled by the pH, with a minimum dissolution at pH 4 as also reported by many other authors [17, 18, 67, 105, 136]. Besides pH, also redox conditions are known to affect the solubility of iron arsenates: reduced redox conditions increase the solubility due to iron reduction [147]. Iron can be reduced by sulphate-reducing bacteria, but this reaction occurs only in the presence of organic matter.

The above discussion raises the question which test should be used to evaluate scorodite stability. The SPLP test has been indicated as suitable to simulate mine tailings [55]. In contrast, the TCLP test is considered the most aggressive leaching test to assess the toxicity of mineral processing wastes [53, 56, 88]. Selection of a suitable test should be based on the type of the landfill in which the material will be stored. For bioscorodite and scorodite, the TCLP test is considered a good procedure to evaluate the maximum arsenic leaching rates because it assesses the disposition of stable materials. Correct interpretation of the TCLP test results can indicate the presence of less stable phases in bioscorodite and scorodite crystals.

10.3.4 How to store bioscorodite crystals at mining sites and related environments

As mentioned before, the conditions at which scorodite is most stable are oxidized conditions and a pH around 4. The contact with organic acids has to be avoided as these accelerate the dissolution of minerals. Also contact with organic matter should be avoided as this stimulates the growth of sulphate reducing bacteria which can reduce ferric iron at anaerobic conditions. These specific conditions suggest that scorodite has to be stored separated from other metallurgical wastes. For example, if scorodite is stored together with sulphide mineral waste, this can lead to high arsenic leaching. Sulphide mineral

waste is stored at exactly the opposite conditions to those required for a stable storage of scorodite, i.e. neutral pH and reduced redox conditions. These conditions could lead to the growth of sulphate reducing bacteria, which will immobilize dissolved metals as metal sulphides in the presence of organic matter [116]. In the case of sulphide mineral waste, the above mentioned conditions prevent the growth of acidophilic microorganisms, which oxidize iron and sulphur and produce acid mine drainage. Other processes such as coating or encapsulation with phosphate are also used to dispose mine waste. In the case of scorodite, coating with phosphate cannot be used, as phosphate enhances the mobility of arsenic [116].

Based on the TCLP test data reported in literature (Table 10.1), between 0.7 and to 95 kg arsenic is released per ton of scorodite stored per year. Arsenic release of bioscorodite crystals at SPLP test storage conditions (pH 4 without organic acids) was determined at 4.3 kg arsenic per ton bioscorodite per year. The comparison between bioscorodite, mineral scorodite and chemically synthesized scorodite crystals shows the potential of scorodite crystals to immobilize arsenic. The efforts of several researchers to develop or improve technologies to crystallize scorodite are expected to make scorodite crystals the most logic option for safe arsenic storage.

10.4 CONCLUSION

Bioscorodite crystal resembles the scorodite mineral as found in nature. This material is suitable to be used for safe arsenic disposition. Arsenic leaching rates of the bioscorodite crystals depend on the pH and leaching medium and are at the lower range of values reported for mineral scorodite and chemically synthesized scorodite crystals. The use of scorodite is expected to be adopted as a safe material for the future storage of arsenic.

TABLE 10.1 A comparison of arsenic leaching rates reported for mineral scorodite, bioscorodite (72°C) and chemically synthesized scorodite (95°C - 150°C).

Nature of crystals	Size crystals	Arsenic leaching TCLP test(*) pH 5, 20h	Arsenic leaching at other test conditions
Mineral			
scorodite [105]	-	-	0.32 mg/L pH 2.43, 14 d (H_2SO_4)
	-	-	1.49 mg/L pH 2.05, 14 d (H_2SO_4)
Crushed scorodite, (This study)	< 1 mm	2 mg/L 60 d	-
Biogenic crystals			
Bioscorodite 75°C (batch bottles) (Chapter 6 and 7)	10 µm	0.016 mg/L 363 d	-
Bioscorodite 72°C (CSTR systems) Chapter 8	Flakes	0.5 mg/L 100 d	-
Bioscorodite 72°C (continuous airlift reactor) Chapter 9	150 µm	0.5 mg/L 60 d (2 times medium was replaced)(Ch.9) 2 mg/L 60 d (Ch. 9)	0.6 mg/L pH 4, 60 d (SPLP) (This study)
Chemical synthesized crystals (70-95°C)			
Nanocrystalline scorodite 70°C [136]	50 nm	0.58 mg/L, 13 d	20.8 mg/L pH 1, 13 d 0.56 mg/L pH 2, 13 d 5.38 mg/L pH 7, 13 d
Amorphous ferric arsenate 70°C [136]	50-100 nm	60 mg/L, 13 d	90 mg/L pH 2, 13 d 30 mg/L pH 3, 13 d 50 mg/L pH 4, 13 d
Scorodite 95°C [27]	1.6 µm	13.6 mg/L, 18 h	-
	5.3 µm	0.1 mg/L, 18 h	
Scorodite 95°C [66]	16 µm	0.37 mg/L, 6 h	-
Scorodite 95°C [154]	10 µm	0.8 mg/L*	-
Scorodite 95°C [67]	17 µm	0.18 mg/L, 35 d	0.4 mg/L pH 3, 35 d 3.1 mg/L pH 7, 35 d 351 mg/L pH 9, 35 d
Scorodite 95°C [82]	-	0.3 mg/L, 4 h	0.45 mg/L pH 6, 4 h
Chemical synthesized crystals (150-175°C)			
Scorodite 150°C [27]	1.5 µm	13 mg/L, 8 h	-
	2.5 µm	5 mg/L, 8 h	
Scorodite 160°C [18]	-	0.35 mg/L, 460 d	0.61 mg/L pH 6, 460 d 5.89 mg/L pH 7, 460 d
Scorodite 160°C [17]	0.3 µm	0.35 mg/L, 460 d	5.89 mg/L pH7, 460 d 386 mg/L pH 9, 460 d
Scorodite 160°C [154]	5 µm	4.8 mg/L*	-
Scorodite 160°C [105]	2.5 µm	-	0.2 mg/L pH 5.57, 14 d (H_2SO_4) 0.19 mg/L pH 3.45, 14 d (H_2SO_4) 0.33 mg/L pH 2.85, 14 d (H_2SO_4)
Scorodite 175°C [74]	-	0.1 mg/L*	-

Chapter 11

General discussion

11.1 INTRODUCTION

As long as modern society relies on the extraction of minerals for the supply of metals, the volume of processed mineral is increasing. Some studies confirm that we have already reached "peak metal", meaning that humankind has extracted more metal to date than is left to mine [50]. Arsenic, a metalloid, has an exceptional history. Arsenic is a toxic element for humans and was widely used in the 20th century in electronics, wood preservation and agricultural applications. Currently, the use of arsenic is banned for most applications, leading to the accumulation of arsenic waste mainly in the form of arsenic trioxide [100].

Arsenic trioxide is a by-product from ore extraction for the production of precious and base metals such as copper and gold [90, 100]. Arsenic removal from metallurgical streams is achieved by precipitation with iron, mainly as arsenical ferrihydrite. Although arsenical ferrihydrite precipitation occurs at ambient temperature, it requires a high iron supply (Fe/As > 5) and addition of neutralizing agents [143, 144, 159]. Therefore, arsenical ferrihydrite generates a large amount of sludge containing less than 1%wt arsenic and a free water content between 30 and 65%wt **(Chapter 1)**.

More recent technologies focus on arsenic immobilization into scorodite crystals. Scorodite ($FeAsO_4 \cdot 2H_2O$) is a naturally occurring mineral that contains 30%wt arsenic and an Fe/As molar ratio of 1 [42, 105, 106, 128, 145]. Because of its low arsenic solubility, mineral scorodite is considered the most stable arsenate mineral. Originally, scorodite precipitation methods require the use of autoclaving technology, i.e. high pressure and high temperatures [37, 48]. Subsequently, the feasibility of atmospheric scorodite precipitation (<100°C) was demonstrated by control of the saturation level [38, 154, 155]. To control the saturation level of scorodite at 85°C, a stepwise neutralization procedure is carried out in several steps. Also a decrease of the initial supersaturation level is required, which is achieved by the addition of seed material, either parent or foreign. A delicate balance between seed addition/recycle and neutralization steps is required to precipitate scorodite crystals at atmospheric conditions. The development of atmospheric scorodite precipitation has been hampered mainly because of these requirements **(Chapter 1)**.

The aim of the work described in this thesis is to develop a controlled process for biological crystallization of scorodite from metallurgical streams. This is achieved by balancing biological oxidation and crystallization reactions in one single process step.

11.2 BIOSCORODITE CRYSTALLIZATION FOR ARSENIC REMOVAL

11.2.1 Proof of principle: Bioscorodite crystallization

In the theoretical concept of bioscorodite crystallization **(Chapter 1)**, biological oxidation of ferrous iron and arsenite is required at acidic conditions. To test bioscorodite crystallization, acidophilic iron oxidizing microorganisms were selected. The proof of principle tests of bioscorodite crystallization were carried out in mesophilic batch experiments **(Chapter 3)**. In these experiments, the addition of gypsum seeds decreased the saturation level of bioscorodite. *Thiobacillus ferrooxidans* oxidized ferrous iron at pH 1.4 and 30°C in the presence of arsenate. However, bioscorodite formation was not observed. Additional tests with varying seed concentrations and pH values (pH < 1.4) were performed, but bioscorodite formation was not observed. From these experiments it was concluded that despite control of the saturation level, bioscorodite formation is highly dependent on temperature.

Experiments at thermophilic conditions were conducted using *Acidianus sulfidivorans* (pH 0.3-3), an extreme acidophilic archaeon. Ferrous iron was biologically oxidized at pH 0.8 and 80°C using atmospheric oxygen as the final electron acceptor. Bioscorodite saturation was controlled by biological oxidation and as a result crystal growth was favoured over primary nucleation, resulting in the formation of bioscorodite crystals in the presence of 1 g As^{5+} L^{-1} **(Chapter 3)**. The crystallization onset of bioscorodite at 80°C does not require the use of seed crystals. In contrast, chemical scorodite crystallization at 80 to 95°C does require the addition and recycle of seeds **(Chapter 1)**. The use of gypsum seeds in bioscorodite crystallization did not accelerate the kinetics of precipitation at 80°C. Instead, it was demonstrated that gypsum may induce amorphous phase formation **(Chapter 3)**. In chemical controls (no microorganisms addition), ferric iron addition lead to the formation of a yellow precipitate, which was identified as poorly crystalline ferric arsenate.

The proof of principle of bioscorodite crystallization was delivered using thermoacidophilic microorganisms at pH 0.8 and 80°C. The nucleation process of bioscorodite occurs in the absence of seeds, which would classify bioscorodite as a product of primary nucleation. However, also “concealed nucleation seeds” could have been present in the experiments in the form of impurities. Also microorganisms or the glass wall could have provided a surface for nucleation, leading to secondary nucleation of bioscorodite. The nucleation of bioscorodite will be further discussed in section 11.2.3.

11.2.2 Thermoacidophilic archaea are robust microorganisms

Thermoacidophilic microorganisms carry out oxidation reactions at pH below 3 and temperatures between 60 and 85°C. Therefore, in bioscorodite crystallization,

microorganisms need to oxidize iron at suboptimal growth pH conditions in the presence of arsenic.

Some thermoacidophilic microorganisms can oxidize ferrous iron at very low pH values and in the presence of 1 g $As^{5+}L^{-1}$ **(Chapter 3)**. However, thermoacidophiles growing at suboptimal growth conditions oxidize ferrous iron at very low rates of 0.04 g $Fe^{2+}L^{-1}d^{-1}$. Bioscorodite crystallization needs thermoacidophilic microorganisms that oxidize ferrous iron at a pH below 1.3 at relatively high rates, but also in the presence of high arsenic concentrations (>0.5 g As L^{-1}).

A mixed thermoacidophilic culture was used to increase the chance of selecting microorganisms adapted to the conditions required for bioscorodite formation **(Chapter 4)**. Iron oxidation kinetics of these microorganisms was studied in batch bottles and CSTRs **(Chapter 4)**.

At low ferrous iron concentrations (1 g Fe^{2+} L^{-1}), the thermoacidophilic culture shifts from an exponential to a linear growth behaviour. At pH values below 0.8 microorganisms were inactive. The minimum pH for highly active microorganisms is 1 **(Chapter 4)** and the maximum to avoid amorphous precipitation is 1.3 **(Chapter 3)**. Therefore, the pH range for bioscorodite precipitation was established between 1 and 1.3.

In CSTRs at 72°C and pH 1.3, a maximum growth rate of $0.066h^{-1}$ was obtained, which decreased to $0.022h^{-1}$ at pH 1.1. Biological ferrous oxidation rates of 1.5 g L^{-1} d^{-1} were achieved in CSTRs operated during 80 days at a HRT of 40h. This demonstrates that a continuous cultivation of thermoacidophilic microorganisms is feasible under the extreme conditions required for bioscorodite formation.

The effect of arsenic on thermoacidophilic microorganisms was tested in CSTRs. Arsenate (As^{5+}) was added to the CSTRs to produce bioscorodite. Thermoacidophilic microorganisms oxidize iron in the presence of arsenate concentrations up to 2.8 g As^{5+} L^{-1} at pH 1.2 and 72°C **(Chapter 8)**. Ferrous iron oxidation rates of 1.5 g L^{-1} d^{-1} were obtained in the presence of arsenate, which are the same as those obtained in the absence of arsenic **(Chapter 4)**. It can thus be concluded that the presence of arsenate concentrations up to 2.8 g As^{5+} L^{-1} does not inhibit ferrous iron oxidation.

Arsenite (As^{3+}) can also be present in some metallurgical streams. The effect of arsenite addition on biological ferrous iron oxidation was studied in CSTRs operated as bioscorodite crystallization reactors **(Chapter 8).** A fraction of the total arsenic in the stream was replaced with arsenite. In a first test, 10% of the total arsenic was replaced with arsenite (0.24 g $As^{3+}L^{-1}$). In a second test 30% was replaced (0.75 g $As^{3+}L^{-1}$). In the first test (10% As^{3+}), ferrous oxidation rates initially decreased from 1.5 to 0.45 g L^{-1} d^{-1} and then gradually increased to 0.9 g L^{-1} d^{-1} after 47 days. In the second test (30% As^{3+}), ferrous oxidation rates initially decreased from 0.9 to 0.45 g L^{-1} d^{-1} and then gradually increased to 1.2 g L^{-1} d^{-1} after 100 days. From these results it can be concluded that the

ferrous iron oxidation capacity of the microorganisms is negatively affected by arsenite. Despite of arsenite inhibition, low arsenite oxidation rates (0.1-0.2 g As^{3+} L^{-1} d^{-1}) were measured at pH 1.2 and 72°C. Arsenite oxidation at thermophilic conditions was not expected, as arsenite oxidation is only known for mesophilic organisms [115, 135]. The ability of thermoacidophilic microorganisms to cope with high arsenate concentrations and their adaptation to arsenite is a topic that deserves further research.

Thermoacidophilic microorganisms were also grown in an airlift reactor at pH 1.2 and 72°C **(Chapter 9)**. During batch mode operation in the airlift reactor, a high ferrous iron conversion rate to ferric iron was obtained in the presence of 2.4 g As L^{-1}. As soon as the reactor was switched to continuous mode (HRT of 38h), the ferrous conversion rate dropped to 30% of the earlier observed maximum. To enhance the biological ferrous oxidation rate, which was the limiting step in the airlift reactor operation, two adjustments were made. First the ferrous iron concentration in the feed supply was increased from 2.4 to 6 g Fe^{2+} L^{-1}, providing enough substrate for growth. Secondly, the dissolved oxygen concentration was increased from 3 to 4.4 mg O_2 L^{-1} by the addition of pure oxygen to the air circulation flow. As a result of these measures, after 7 days the ferrous conversion rate increased to 50% and after 15 days it increased to 70%, i.e. an iron oxidation rate of 2.8 g Fe^{2+} L^{-1} d^{-1} **(Chapter 9)**. These results show that also in a continuous airlift reactor, high iron conversion rates can be achieved.

Themoacidophilic microorganisms are generally autotrophic archaea that oxidize ferrous iron or sulphur to harvest energy with a very low efficiency. It was estimated that acidophiles require 120 mol of Fe^{2+} to generate 1 mol of glucose [103]. This implies that these microorganisms need to oxidize a large amount of ferrous iron in order to sustain growth. It seems that in the airlift reactor, the conditions were such that the microorganisms need more substrate in order to sustain growth.

11.2.3 What is the role of the microorganisms in the bioscorodite crystallization?

During bioscorodite crystallization in batch tests it was observed that thermoacidophilic microorganisms were partially covered by precipitates containing arsenic and iron **(Chapter 5)**. This suggests an indirect biomineralization of bioscorodite on the cell surface, which may act as seed for secondary nucleation. A possible mechanism for the formation of bioscorodite crystals is proposed and discussed below.

As soon as biological iron oxidation takes place in the presence of arsenate, precursors of bioscorodite crystals (iron arsenate precipitates) are formed on the cell surface. The nucleation of ferric arsenate precursors is favoured on the cell surface because here the required saturation level is lower than in the bulk solution. Bioscorodite precursors formed at the cell surface grow to form more stable crystals in the bulk solution. These crystals are used as seeds for secondary nucleation of bioscorodite crystals in the bulk solution. In

batch tests, it was also observed that ferrous iron oxidation and bioscorodite formation depend on the initial ferrous iron concentration in the bulk solution **(Chapter 5)**. In continuous bioscorodite crystallization in CSTRs **(Chapter 8)** and in an airlift reactor **(Chapter 9)**, the limiting step for bioscorodite crystallization was the biological oxidation of ferrous iron.

Bioscorodite formation seems to be regulated by the bulk saturation rather than by the nucleation on the cell surface. The main role of the microorganisms is to oxidize ferrous iron under extreme conditions. Nucleation on the cell surface and its role in the crystallization onset of bioscorodite crystals require further research.

11.3 BIOSCORODITE CRYSTALS CHARACTERIZATION AND STABILITY PROPERTIES

11.3.1 Bioscorodite crystals characterization

Bioscorodite precipitates were identified as crystalline materials displaying a pale-greenish colour. As Fe/As molar ratios higher than 3 were used, concomitant bioscorodite and jarosite precipitation was observed. In that case, the precipitates displayed an orange-yellowish colour **(Chapter 6)**. Bioscorodite precipitated in batch bottles exhibited a characteristic flake morphology. Bioscorodite flakes up to 1 cm were observed, which consisted of small round aggregates. The characteristic dipyramidal octahedron habit of scorodite was identified in bioscorodite crystals **(Chapter 6)**. The continuous crystallization of bioscorodite resulted in a slightly different morphology. Bioscorodite aggregates produced in CSTRs were identified as scorodite by XRD analysis, but they displayed an amorphous appearing morphology **(Chapter 8)**. Layers of precipitates were observed on the reactor walls (scaling). The precipitated layers were overlapping, suggesting that crystalline bridges occurred between the crystals. Mixing in the CSTRs was not strong enough to keep solids in suspensions, probably due the high density and large size of the bioscorodite precipitates. In contrast to the CSTRs, bioscorodite crystals produced in the airlift reactor exhibit a free-flowing nature **(Chapter 9)**. Bioscorodite crystal scaling was not observed in the airlift reactor. The precipitates displayed a round morphology in which the dypiramidal octahedron habit of the crystal was easily identified. During the continuous operation of the airlift reactor, screw dislocations were observed on the surface of the crystals. These dislocations could have been formed due to collisions with other particles as a result of the high mixing intensity in the reactor **(Chapter 10)**.

The size of the crystals produced in batch bottles was between 0.1 and 1 μm **(Chapter 3, 6).** The size of bioscorodite crystals produced in CSTRs could not be measured due to the scaling of precipitates. During the continuous operation of the airlift reactor, the crystal size increased from 50 to 160 μm. The density of bioscorodite crystals was 3322 kg m^{-3},

which in combination with the crystal size gave high sedimentation rates between 50 and 140 m h^{-1} **(Chapter 9)**.

Bioscorodite crystals produced in batch tests contained 31.5%wt As and 28.1%wt Fe (Fe/As molar ratio of 1.1) **(Chapter 3)**. These values are close to the arsenic (32.4%) and iron (24.2%) content in mineral scorodite (an Fe/As molar ratio of 1) [44, 166]. Bioscorodite crystals produced in the airlift reactor contained slightly less arsenic (29.2%) and slightly more iron (33.2%) **(Chapter 9)**, giving an Fe/As molar ratio of 1.5. Natural specimens of mineral scorodite were also analysed for arsenic and iron content. In these natural specimens, an Fe/As molar ratio between 1.35 and 1.41 was found **(Chapter 10)**.

Phosphate contamination was identified by FT-IR analysis in several bioscorodite samples **(Chapter 8, 9)**. The phosphate content was quantified by SEM-EDX analysis of the crystals, showing 1.4%wt P and 0.4%wt S **(Chapter 9)**. The presence of phosphate was not expected as it is not normally found as a contaminant in scorodite crystals. Chemically produced scorodite in sulphuric acid medium is often contaminated with sulphate. However, in literature phosphate has also been found in mineral scorodite and parascorodite [134]. For comparison purposes, a specimen of mineral scorodite was also analysed by SEM-EDX analysis. The mineral scorodite contained between 0.01%wt and 0.08%wt P and between 0% and 0.01% S **(Chapter 10)**.

Bioscorodite crystals produced in initial batch tests had a structural water content of $2H_2O$ **(Chapter 3)**. Precipitates produced in follow-up batch tests contained less water than the theoretical amount of $2H_2O$ **(Chapter 6)**. In precipitates containing only bioscorodite crystals (i.e. no jarosite contamination), a structural water content as low as $1H_2O$ was measured. In precipitates containing both bioscorodite and jarosite, the structural water content was as low as $0.4H_2O$. Bioscorodite crystals produced in CSTRs contained between 1.7 and $2H_2O$ of structural water content **(Chapter 8)**. Bioscorodite crystals produced in the airlift reactor contained exactly $2H_2O$ **(Chapter 9)**, which matched the water content measured in the natural specimens of scorodite mineral **(Chapter 10)**.

The question rises why some of the bioscorodite crystals contained less structural water than the theoretical value of $2H_2O$. A possible explanation could be the presence of iron phases such as ferrihydrite. At low fractions, ferrihydrite will not appear in the precipitates XRD analysis. Any ferrihydrite present may transform to another phase at temperatures below 120°C, which could change the total structural water content observed by TGA analysis of the samples. However, when iron was in excess with respect to arsenic (Fe/As>3), jarosite formation was observed and not ferrihydrite. The lower structural water content observed in bioscorodite crystals is still an unresolved subject that deserves further research.

11.3.2 Arsenic stability properties of bioscorodite crystals

The most stable bioscorodite produced in this research leached only 0.16 μg As L^{-1} during one year of storage under TCLP test conditions. These crystals were produced at pH 1.1 and 75°C in batch bottles experiments **(Chapter 6)**. Bioscorodite crystals produced in CSTRs and the airlift reactor leached between 0.4 and 0.8 mg As L^{-1} during at least 60 days of leaching under TCLP test conditions **(Chapter 8, 9)**.

The long-term leaching studies performed under TCLP test conditions provided the insight that at least 50 days are needed to achieve a steady arsenic leaching concentration from bioscorodite. This implies that leaching tests carried out during only 20h (standard TCLP test duration) can lead to erroneous conclusions about the stability of bioscorodite crystals.

Several factors that affect the stability of bioscorodite crystals were identified: ageing, concomitant jarosite precipitation, and the structural water content of the crystal. These factors are discussed in more detail below.

Ageing increases the stability of the bioscorodite crystals; a longer ageing time (retention time of crystals in the reactor) decreases the arsenic leaching rates. This was observed in batch tests where an increase of ageing time from 10 to 22 days reduced arsenic leaching concentrations from 0.5 to 0.02 mg As L^{-1} **(Chapter 6)**. The effect of ageing was also observed in bioscorodite crystals produced in a continuous airlift reactor. When the retention time of crystals in the reactor was increased from 30 to 72 days, arsenic leaching concentrations of the crystals decreased from 3.5 to 1.9 mg As L^{-1} **(Chapter 9)**. An explanation for this phenomenon is that ageing leads to larger crystals and to a transformation of more amorphous precursors to more stable crystals.

Concomitant precipitation of jarosite with bioscorodite crystals was observed when Fe/As molar ratios higher than 3 were used **(Chapter 6, 8)**. In bioscorodite produced from batch tests, the presence of jarosite did not increase arsenic leaching from the precipitates **(Chapter 6)**. The presence of jarosite may actually lead to a decrease of arsenic leaching rates as arsenic released from bioscorodite crystals can be adsorbed to jarosite precipitates. In CSTR experiments however, the presence of jarosite increased the arsenic leaching rates from 0.4 to 0.8 mg As L^{-1} **(Chapter 8)**. An explanation for this observation requires further investigation.

The stability of bioscorodite crystals was related to the structural water content of the crystals **(Chapter 6 and 7)**. Two groups of bioscorodite crystals were identified based on their structural water content: one group that contains less than $2H_2O$ and another that contains more than $2H_2O$. Bioscorodite crystals containing less than $2H_2O$ (i.e. between 1 and $1.5H_2O$) were the most stable crystals with arsenic leaching concentrations below 0.2 mg As L^{-1} after one year of storage under TCLP test conditions. In contrast, bioscorodite crystals containing more than $2H_2O$, were less stable with arsenic leaching concentrations

above 1 mg As L^{-1} after one year of storage under TCLP test conditions. Precipitation rates seem to play a role in the formation of crystals with less or more than $2H_2O$ of structural water **(Chapter 6)**. When precipitation rates were high, e.g. as a result of high ferrous oxidation rates or high pH values, the precipitates contained more than $2H_2O$, resulting in less stable crystals. In contrast, when precipitation rates were low, produced bioscorodite crystals contained less than $2H_2O$, resulting in more stable crystals.

Bioscorodite crystals were also analysed after long-term (1 year) leaching tests **(Chapter 7)**. Some bioscorodite crystals with high leaching rates transformed to a less crystalline phase, as indicated by XRD analysis. Close observation of the crystals showed that the starting point of dissolution occurred at the top of the octahedrons. The most surprising observations were again regarding the water content. Some of the very unstable crystals increased their water content up to even $4H_2O$.

The relation between structural water content and stability was surprising, especially the structural water content below $2H_2O$ in bioscorodite crystals. Further research is needed to determine if the low structural water can be explained by the presence of other iron phases in the bioscorodite samples.

In addition to TCLP test conditions, also other test conditions were applied to determine bioscorodite stability. To mimic the conditions found in tailings at metallurgical sites, additional leaching tests were performed at SPLP test conditions. This test simulates the leaching of minerals at pH 4 (H_2SO_4/HNO_3) in the absence of organic acids. At SPLP test conditions, bioscorodite crystals only leached 0.6 mg As L^{-1} **(Chapter 10)**. The leaching behaviour under TCLP and SPLP test conditions suggests that bioscorodite crystals should be stored at pH 4, preferably under aerobic conditions and in the absence of organic waste.

11.3.3 Bioscorodite crystals as biofilm support

The right conditions for bioscorodite formation are suboptimal for the growth of thermoacidophilic microorganisms. This suggests the idea that biomass retention may be needed to maintain a sufficiently active biomass population in the crystallization bioreactors. During CSTR experiments, the production of an exopolysaccharide-like substance was observed **(Chapter 4).** This EPS-like substance may have been used by the cells for attachment to the minerals. Bioscorodite layers on the CSTR reactor wall **(Chapter 8)** may have supported biofilm formation, providing protection to shear stress and biomass washout. In the airlift reactor experiments, bioscorodite crystals were in suspension due to the high mixing rates **(Chapter 9)** and no bioscorodite layers were observed. The high mixing intensity in the airlift reactor may have impeded the attachment of cells to the bioscorodite crystals, resulting in biomass washout at low growth rates. This washout of cells may be an explanation to the lower iron oxidation rates observed during the start-up phase of the airlift reactor (continuous operation).

11.4 REACTOR TECHNOLOGY SELECTION: ARSENOTEQ™ PROCESS

In this thesis, two reactor configurations were tested for bioscorodite production: CSTRs **(Chapter 8)** and an airlift reactor **(Chapter 9)**. The arsenic removal efficiency obtained in CSTRs was as high as 99%, resulting in effluents with 29 mg As L^{-1} at pH 1.2 and 72°C. The bioscorodite sludge was very suitable for arsenic disposal due to its low arsenic leaching concentrations of 0.4 mg L^{-1} after 100 days of storage under TCLP test conditions. However, scaling of the bioscorodite precipitates on the glass wall impeded the harvesting of solids from the reactor.

Bioscorodite crystals production in an airlift reactor is suitable for arsenic removal and bioscorodite disposal at pH 1.2 and 72°C **(Chapter 9)**. The high mixing intensity in the airlift reactor avoided the scaling of precipitates on the reactor wall, facilitating the harvesting of bioscorodite sludge for disposal. Bioscorodite crystals can be retained in the airlift reactor allowing growth and crystal ageing. As a consequence the arsenic leaching rates are minimized (see 11.3.2). Once bioscorodite crystals have grown large enough, they can be harvested from the airlift reactor based on their sedimentation rates. Since airlift bioreactors are already widely applied [150], it seems likely that the bioscorodite process can be implemented at full-scale in a relatively simple manner. The bioscorodite process is patented by Paques B.V (Balk, The Netherlands) as the ARSENOTEQ™ process. In the following sections, the ARSENOTEQ™ process is compared to traditional scorodite crystallization and to arsenical ferrihydrite precipitation.

11.4.1 Chemicals addition for pH control/neutralization

The bioscorodite process takes place at pH 1.2 and 72°C and neutralization steps are not required **(this thesis)**. In contrast, chemically produced scorodite needs at least two neutralization steps to control the saturation level at 85°C. Arsenical ferrihydrite precipitation is also based on neutralization reactions in order to increase the pH from 4 to 7 **(Chapter 1)**.

11.4.2 Oxygen consumption

Based on the results presented in **Chapter 9**, the oxygen requirement for bioscorodite production in an airlift reactor is 0.1 kg oxygen per kg ferrous iron produced. This oxygen demand is relatively low when compared to bioleaching processing, in which the same microbial population consumes between 1.8 and 2.6 kg oxygen per kg sulphide mineral oxidized [138]. For the thermoacidophilic bioleaching process, the dissolved oxygen concentration should be kept between 1.5 and 4.1 mg O_2 L^{-1} [138]. For the bioscorodite process, the minimum required dissolved oxygen concentration has not been established. In the airlift reactor experiments, the dissolved oxygen concentration was kept at 4.4 mg

O_2 L^{-1} (138% sat.) by the addition of pure oxygen, to make sure that oxygen limitation did not occur **(Chapter 9)**. Whether or not pure oxygen supply (i.e. oxygen enriched air) is required for full-scale application of the process still needs to be evaluated.

11.4.3 Iron consumption and sludge disposal costs

One of the advantages of the bioscorodite process is the low iron requirement per amount of arsenic removed. A molar Fe/As consumption of 1.5 is required for bioscorodite **(Chapter 9)**. In contrast, arsenical ferrihydrite precipitation needs at least an Fe/As supply of 5, and even higher values (Fe/As > 10) are often used **(Chapter 1)**. The low iron requirement of the bioscorodite process also translates to a low sludge production.

Because seed addition is not required in the bioscorodite process, only bioscorodite crystals are produced. The use of foreign seeds can affect the cost of sludge disposal. If a sludge mix of scorodite and gypsum is disposed of without further separation steps, the sludge volume will be 5 times higher than the volume when scorodite is produced without gypsum seeds [155].

The transport of sludge to a disposal site is typically the most costly feature of disposal. Therefore, on-site disposal is the preferred option to reduce the transport costs. The produced sludge from mining influenced waters (78%) is mainly disposed of in metallurgical processing tailing ponds (35%) and in sludge settling ponds (43%) [79].

The produced sludge should have a free water content as low as possible, thereby lowering the costs of dewatering steps. Because bioscorodite crystals contain only 2% of free water after sedimentation, dewatering of bioscorodite sludge is not required. Apart of volume and dewatering, also the risk of arsenic leaching from the sludge can influence the cost of disposal. If arsenic containing sludge is classified as non-hazardous by TCLP test (< 5 mg As L^{-1}), the cost of disposal is mainly associated to transport and disposal in existing tailings at metallurgical sites. If, on the other hand, the sludge is classified as hazardous waste (TCLP test > 5 mg As L^{-1}), the disposal cost may increase by a factor of five [79].

11.4.4 Bioscorodite crystals selection for disposal

Bioscorodite crystals produced in the airlift reactor have crystal sizes up to 160 μm and sedimentation rates up to 150 m h^{-1} **(Chapter 9)**. As previously discussed, arsenic stability is related to crystal ageing: a longer crystal retention time in the reactor increases crystal stability. It was also observed that the crystal size increases with longer retention times. Airlift reactors such as the CIRCOX® reactor have an internal settling device at the top that avoids crystal washout from the reactor. If the airlift reactor is operated as a sedimentation column for short time intervals, bioscorodite sedimentation can take place. The higher settling velocity of larger crystals according to Stokes' law enables selective

harvesting of the largest crystals. Selection of the largest crystals will thus guarantee that the oldest and most stable crystals are harvested for disposal.

The ARSENOTEQ™ process is a compact system with only one reactor in which biological oxidation and crystallization reactions are simultaneously taking place. Bioscorodite sludge can be disposed of directly after harvesting due to its low free water content and good stability properties. Fig. 11.1 shows a schematic presentation of the bioscorodite process for arsenic removal and immobilization, using an airlift reactor. The arsenite oxidation pre-treatment displayed on the left side of the figure is required only when the stream contains arsenite (As^{3+}), which has to be oxidized in order to prevent microorganism inhibition. Schematic presentations of the arsenical ferrihydrite process and the atmospheric scorodite process were given in the introduction (Fig. 1.3 and 1.4).

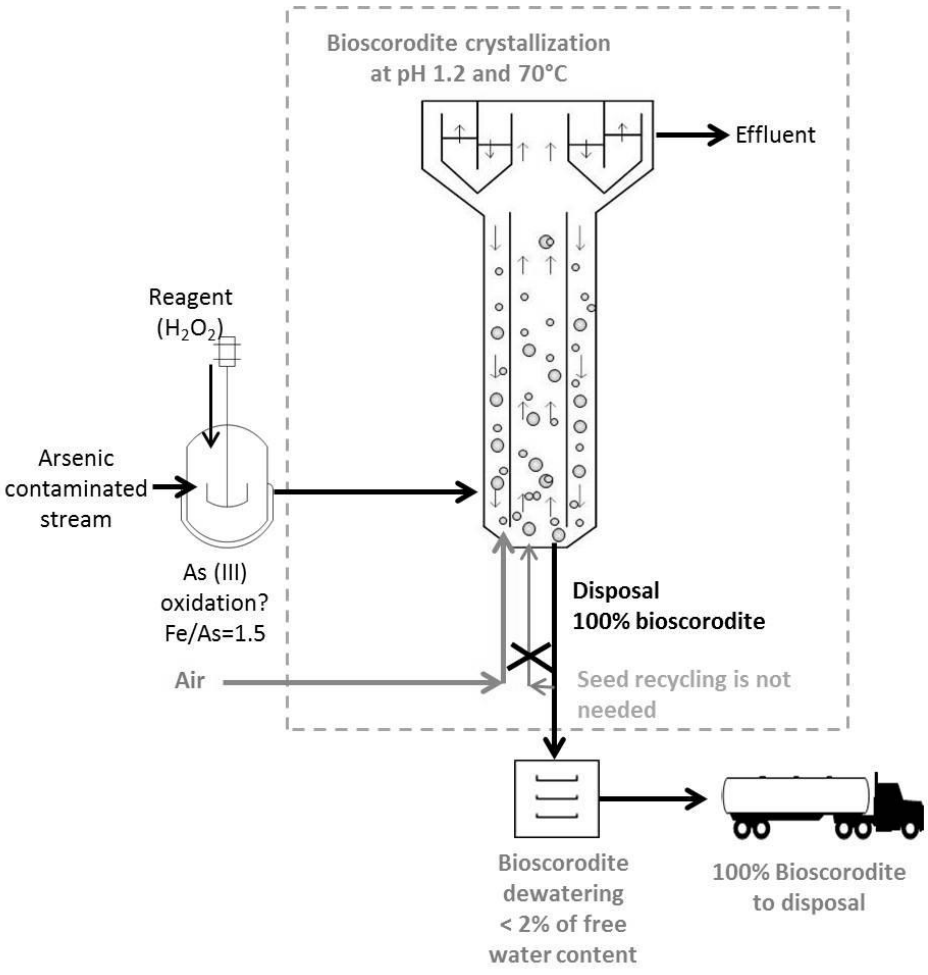

FIGURE 11.1 Schematic presentation of the bioscorodite process for arsenic removal and immobilization, using an airlift reactor at pH 1.2 and 72°C.

11.5 COST COMPARISON

A rough prospective cost evaluation was carried out, comparing the bioscorodite process with the existing chemical scorodite precipitation process at 85°C and the arsenical ferrihydrite process at 30°C. This cost comparison includes only the operation cost and capital cost are not included. The aim of the cost comparison is to identify the economic advantages and disadvantages of the bioscorodite technology.

Previous comparison studies of arsenic removal processes suggest that arsenical ferrihydrite precipitation is more suitable than scorodite precipitation due to the low cost of the former (lower process temperature of 30°C) [144, 159]. This statement is based under the assumption that both precipitates have the same stability. However, arsenical ferrihydrite has the same stability of scorodite only when it is precipitated at Fe/As molar ratios higher than 5. For the economical comparison we assumed an Fe/As ratio of 5 for arsenical ferrihydrite precipitation and a similar stability for all arsenic precipitates formed.

Table 11.1 shows the values used for the cost comparison of the three technologies: bioscorodite precipitation at 72°C (described in this thesis), chemical scorodite precipitation at 85°C, and arsenical ferrihydrite precipitation at 30°C. The operational parameters and assumptions considered for the cost comparison are:

(a) A metallurgical stream containing 10 g As L^{-1} at a flow of 10 m^3 h^{-1} is used in the comparison.
(b) The bioscorodite process uses only one reactor at 70°C
(c) Scorodite precipitation at 85°C requires at least two neutralization steps.
(d) Arsenical ferrihydrite precipitation uses only one reactor.
(e) HRT of the systems are taken from literature.
(f) Fe/As molar ratio requirements of bioscorodite and scorodite is 1.5.
(g) Fe/As molar ratio requirements of arsenical ferrihydrite is 5 (to achieve stable precipitates).
(h) The bioscorodite process does not need neutralization steps. Lime consumption is only required for pH control (0.01 kg lime/kg sludge).
(i) Neutralization steps in chemically produced scorodite and arsenical ferrihydrite are required in order to control the saturation level (0.1 kg lime/kg sludge).
(j) Pure oxygen is used as final electron acceptor for biological iron oxidation.
(k) Bioscorodite sludge does not need dewatering steps.
(l) Chemically produced scorodite/gypsum sludge requires dewatering steps.
(m) All the produced sludge is non-hazardous (TCLP test below 5 mg As L^{-1}).
(n) Safe sludge disposition costs include transport costs.
(o) 10% of heat losses are taken into account through the reactor walls.

TABLE 11.1 Operational cost comparison between bioscorodite precipitation at 70°C, atmospheric chemical scorodite precipitation at 85°C and ferric arsenate precipitation at 30°C. Calculations are based on streams containing 10 g As L^{-1} with a flow of 10 m^3 h^{-1}.

Process description	Values assumed	unit	Bioscorodite (Chapter 9)	Scorodite (Chapter 1)	Ferric arsenate sludge (Chapter 1)
System steps			1	2	1
Hydraulic retention time (HRT)		h	38	12	12
Volume system/reactor		m^3	380	120	120
Temperature operation		°C	70	85	30
pH		unit	1.2	1 to 4	2 to 7
Fe/As requirement		molar ratio	1.5	1.5	5
Arsenic loading rate		g As/L/d	6	20	20
Ferrous iron loading rate		g Fe/L/d	9	30	100
Oxygen consumption	0.1 kg O_2/kg Fe	g O_2/L/d	0.9	3	3
Arsenic content in sludge		%wt. As	30	30	2
Produced sludge		g/L/d	21	67	1000
Arsenic removed		kt As/ year	0.8	0.8	0.8
Energetic requirement	**Values assumed [72]**	**cost**	**Bioscorodite**	**Scorodite**	**Ferric arsenate sludge**
Aeration to transfer one kg of oxygen	2250 kJ/kg O_2	€/d	23	15	24
Heating one kg of water by one °C (10% heating losses)	4.18 kJ/°C/kg	€/d	127	363	36
Power needed for mixing one m^3	8 kJ/m^3	€/d	0.03	0.03	0.03
Pumping one m^3 per height loss	18 kJ/m^3/m	€/d	0.08	0.08	0.08
Electrical cost per energetic requirement	1.8E-05 Euro/kJ				
Oxidation cost	€ 0.15/kg O_2	€/d	54	54	180
Iron supply as scrap iron	€ 0.22/kg Fe	€/d	792	792	2640
Reactive cost (nutrients)	€ 0.2/kg reactive	€/d	86	0	0
Safe sludge disposal (As below TCLP value)	€ 49/m^3	€/d	119	170	3920
Neutralization step (0.1 kg lime/kg sludge)	€ 30/ton lime	€/d	2	24	360
Dewatering sludge	€ 150/ton sludge	€/d	0	1026	3790
Total excluding dewatering costs		M€/year	0.4	0.5	2.6
		M€/kt As	**0.5**	**0.6**	**3.0**
Total including dewatering costs		M€/year	0.4	0.9	4
		M€/kt As	**0.5**	**1.0**	**4.6**

The cost comparison of the three technologies shown in Table 11.1 and Fig. 11.2 indicates that despite the high energetic requirements for heating in the bioscorodite process (70°C), the total costs of the arsenic ferrihydrite process are 90% higher than those of the bioscorodite process. The difference in costs between bioscorodite and arsenical ferrihydrite are mainly associated to iron supply cost and sludge dewatering and disposal (Fig.11.2). The total costs of the arsenical ferrihydrite process was estimated at 4.6 M€ per kiloton of arsenic removed, including dewatering. This is 9 times more than the costs for the bioscorodite process, which was estimated at 0.5 M€/kt arsenic. If the associated costs for sludge dewatering are subtracted from the total costs, the arsenical ferrihydrite process is still 4 times more costly than the bioscorodite process. One of the assumptions made was that the arsenical ferrihydrite process produces a stable sludge that is classified as non-hazardous. If the produced arsenical ferrihydrite sludge is not stable and classified as hazardous, the cost of disposal may increase up to five times, leading to a total costs increase of 50%.

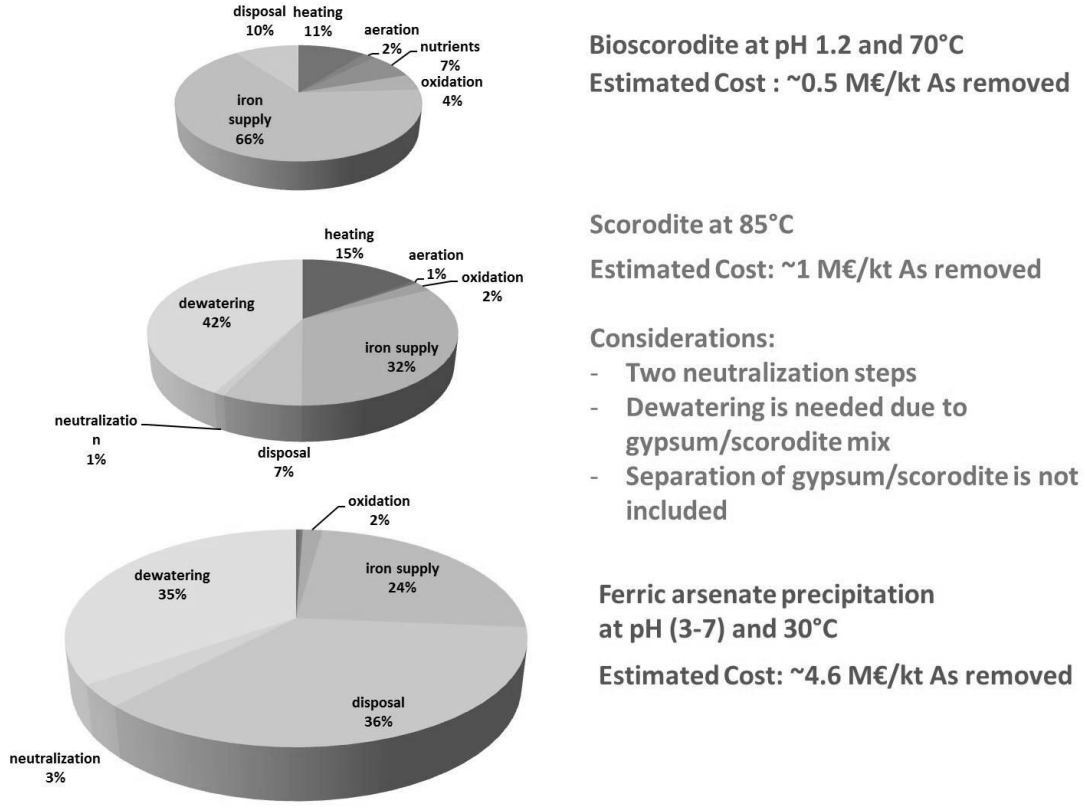

FIGURE 11.2 Comparative cost evaluation between bioscorodite precipitation at 70°C, scorodite precipitation at 85°C and arsenical ferrihydrite precipitation at 30°C. Estimated costs are in Million Euros per kilotons of arsenic removed. Only the most influential factors are displayed in the pie charts.

Although the costs related to heating in the bioscorodite process are higher than ferric arsenate precipitation, this does not make the technology prohibitively expensive when the total costs of the process are compared.

When bioscorodite precipitation is compared to chemical scorodite precipitation at 85°C without sludge dewatering, the costs for chemical scorodite precipitation are slightly higher at 0.6 M€/kt arsenic. However, if sludge dewatering is considered, the total costs of chemical scorodite precipitation increases to 1 M€/kt arsenic. It has to be mentioned that the costs related to post-treatment separation of the scorodite/gypsum mix are not included.

It is known from literature that in the chemical precipitation technologies, arsenic loading rates can be increased by operating these systems at lower hydraulic retention times (e.g. 12h). Arsenic loading rates in the bioscorodite process can be increased by either feeding concentrated streams or by increasing the reactor volume. Airlift reactors can be easily scaled up to 1000 m^3 and even 2000 m^3 CIRCOX® airlift reactors have been built by Paques B.V (Balk, The Netherlands) [150].

11.3 ALTERNATIVE APPLICATIONS

The main application for the bioscorodite process demonstrated in this thesis is regarding metallurgical streams with an arsenic content between 1 and 3 g As L^{-1}. However, the maximum potential application of bioscorodite can be up to 20 g L^{-1}, based on biological iron oxidation rates.

Apart from the treatment of metallurgical streams, arsenic trioxide (As_2O_3) may also be converted into bioscorodite. However, as in arsenic trioxide arsenite (As^{3+}) is present, a pre-oxidation step for arsenite would be needed.

Bioscorodite crystallization can also be applied as a post-treatment or polishing step for bioleaching reactors. Bioleaching tank reactors are already used at commercial scale producing effluent that contains arsenic. Also thermophilic bioleaching of chalcopyrite is already applied **(Chapter 1).** The effluent produced in those processes contains, besides other contaminants, arsenic that has been oxidized by the bacteria (in mesophilic bioleaching). Therefore, these effluents are also an excellent opportunity for application of the bioscorodite process for arsenic removal.

Another application can be found in treatment of the sludge that is currently produced in chemical processes to remove arsenic from groundwater. The techniques currently used for the stabilization of this sludge are very questionable. For example, the use of sludge that contains arsenic is mixed with livestock waste in Bangladesh and India, releasing gaseous arsine into the atmosphere as a result of microbial processes [156]. In urban areas

of Bangladesh and India, arsenic sludge is incorporated into construction materials including cement blocks and cement bases for latrines [156]. Examples of the bad handling of arsenic can be found in Amin (2010). She reports her observations as follows: "*two households threw the spent filter material at the backside of their house on the land*" and "*two households have disposed of the spent materials on the cow manure stockpile near their house and covered those with cow manure*" [5]. Problems with the handling and disposal of these filter materials should be solved to prevent reintroduction of arsenic into the water sources or the food cycle. Treatment of these filters using the Bioscorodite process could produce safe arsenic crystals for disposal and iron recycle to the filter manufacturer.

11.4 CONCLUDING REMARKS

Bioscorodite crystallization can be applied to remove arsenic from metallurgical streams by immobilizing it in bioscorodite crystals suitable for disposal. The bioscorodite process is carried out at pH 1.2 and 72°C in a single airlift bioreactor, which supports biological iron oxidation, bioscorodite crystallization and selective harvesting of the crystals.

The potential of the bioscorodite crystallization process is driven by its advantages over other technologies: (1) less iron consumption, (2) less sludge production, (3) no requirement of neutralization steps and (4) the production of stable bioscorodite crystals ready to be disposed of. These advantages are reflected in the cost comparison with other arsenic removal technologies, positioning the bioscorodite process as the most economical alternative. The results described in this Ph.D. thesis demonstrate the feasibility of bioscorodite crystallization and indicate this process as a logical option for effective and safe disposal of arsenic.

Further research is required to investigate the potential of arsenite oxidation by thermoacidophilic microorganisms, which could expand the range of application of the bioscorodite process. Another area that deserves further research is the role of the microorganisms in the onset of nucleation, for which the mechanism is still partially unknown. Also further research is required to clarify the production of bioscorodite crystals with a lower structural water content than the theoretical amount of $2H_2O$. Finally, optimization of the operation of a bioscorodite airlift reactor is required. The main optimization areas are oxygen transfer and determining the retention time of crystals in the reactor in order to harvest the largest and thus most stable bioscorodite crystals.

Chapter 12

Reference list

[1] HSC Chemistry, **2007**, Outotec Research: Finland p. Chemical Reaction and Equilibrium Software with Extensive Thermochemical Database and Flowsheet Simulation
[2] Acevedo, F., The use of reactors in biomining processes. *Electronic Journal of Biotechnology*, **2000**. 3(3): p. 184-194.
[3] Akter, K.F., et al., Arsenic speciation and toxicity in biological systems, in *Reviews of Environmental Contamination and Toxicology* **2006**. p. 97-149.
[4] Ali, I. and C.K. Jain, Advances in arsenic speciation techniques. *International Journal of Environmental Analytical Chemistry*, **2004**. 84(12): p. 947-964.
[5] Amin, N., Developing an environmentally appropriate, socially acceptable and gender-sensitive technology for safe-water supply to households in arsenic affected areas in rural Bangladesh, **2010**, Wageningen University: Wageningen.
[6] Asta, M.P., et al., Arsenic removal by goethite and jarosite in acidic conditions and its environmental implications. *Journal of Hazardous Materials*, **2009**. 171(1-3): p. 965-972.
[7] Astudillo, C. and F. Acevedo, Effect of CO_2 air enrichment in the biooxidation of a refractory gold concentrate by *Sulfolobus metallicus* adapted to high pulp densities. *Hydrometallurgy*, **2009**. 97(1-2): p. 94-97.
[8] Auernik, K.S., et al., The genome sequence of the metal-mobilizing, extremely thermoacidophilic archaeon *Metallosphaera sedula* provides insights into bioleaching-associated metabolism. *Applied and Environmental Microbiology*, **2008**. 74(3): p. 682-692.
[9] B'Hymer, C. and J.A. Caruso, Arsenic and its speciation analysis using high-performance liquid chromatography and inductively coupled plasma mass spectrometry. *Journal of Chromatography A*, **2004**. 1045(1-2): p. 1-13.
[10] Baes, C.F. and R.E. Mesmer, The thermodynamics of cation hydrolysis. *American Journal of Science*, **1981**. 281: p. 935-962.
[11] Bazylinski, D. and R. Frankel, *Biologically Controlled Mineralization of Magnetic Iron Minerals by Magnetotactic Bacteria*, in *Environmental Microbe-Metal Interactions*, D. Lovley, Editor **2000**, ASM Press: Washington. p. 109-144.
[12] Bazylinski, D.A. and R.B. Frankel, Biologically Controlled Mineralization in Prokaryotes. *Reviews in Mineralogy and Geochemistry*, **2003**. 54(1): p. 217-247.
[13] Becker, T., et al., In situ imaging of *Sulfobacillus thermosulfidooxidans* on pyrite under conditions of variable pH using tapping mode atomic force microscopy. *Process Biochemistry*, **2011**. 46(4): p. 966-976.
[14] Bertoldo, C., C. Dock, and G. Antranikian, Thermoacidophilic microorganisms and their novel biocatalysts. *Engineering in Life Sciences*, **2004**. 4(6): p. 521-532.
[15] Bigham, J.M., et al., Characterization of jarosites produced by chemical synthesis over a temperature gradient from 2 to 40°C. *International Journal of Mineral Processing*, **2010**. 94(3-4): p. 121-128.
[16] Bissen, M. and F.H. Frimmel, Arsenic - A review. Part I: Occurrence, toxicity, speciation, mobility. *Acta Hydrochimica et Hydrobiologica*, **2003**. 31(1): p. 9-18.
[17] Bluteau, M.C., L. Becze, and G.P. Demopoulos, The dissolution of scorodite in gypsum-saturated waters: Evidence of Ca-Fe-AsO_4 mineral formation and its impact on arsenic retention. *Hydrometallurgy*, **2009**. 97(3-4): p. 221-227.

[18] Bluteau, M.C. and G.P. Demopoulos, The incongruent dissolution of scorodite - Solubility, kinetics and mechanism. *Hydrometallurgy*, **2007**. 87(3-4): p. 163-177.
[19] Boon, M. and J.J. Heijnen, Gas-liquid mass transfer phenomena in bio-oxidation experiments of sulphide minerals: A critical review of literature data. *Hydrometallurgy*, **1998**. 48(2): p. 187-204.
[20] Bosecker, K., Bioleaching: Metal solubilization by microorganisms. *FEMS Microbiology Reviews*, **1997**. 20(3-4): p. 591-604.
[21] Brierley, J.A., Thermophilic iron-oxidizing bacteria found in copper leaching dumps. *Applied and Environmental Microbiology*, **1978**. 36(3): p. 523-525.
[22] Brierley, J.A., A perspective on developments in biohydrometallurgy. *Hydrometallurgy*, **2008**. 94(1-4): p. 2-7.
[23] Brooks, W., Arsenic. Ch., in *Minerals Yearbook, annual* **2011**, U.S. Geological Survey.
[24] Bryan, C.G. and D.B. Johnson, Dissimilatory ferrous iron oxidation at a low pH: A novel trait identified in the bacterial subclass *Rubrobacteridae*. *FEMS Microbiology Letters*, **2008**. 288(2): p. 149-155.
[25] Butcher, D.J., Environmental applications of arsenic speciation using atomic spectrometry detection. *Applied Spectroscopy Reviews*, **2007**. 42(1): p. 1-22.
[26] Caetano, M.L., C.L. Caldeira, and V.S.T. Ciminelli. *Precipitation of enriched arsenic residues from diluted industrial solutions.* in *HydroProcess 2006 International Workshop on Process Hydrometallurgy* **2006**. Iquique, Chili.
[27] Caetano, M.L., et al., Batch and continuous precipitation of scorodite from dilute industrial solutions. *Hydrometallurgy*, **2009**. 95(1-2): p. 44-52.
[28] Chan, C.S., et al., Microbial Polysaccharides Template Assembly of Nanocrystal Fibers. *Science*, **2004**. 303(5664): p. 1656-1658.
[29] Cidu, R., et al., Acid drainage from sulfides hosting gold mineralization (Furtei, Sardinia). *Environmental Geology*, **1997**. 30(3-4): p. 231-237.
[30] Clesceri, L.S., A.E. Greenberg, and A.E. Eaton, *Inductively Coupled Plasma (ICP) Method 3120-B*, in *Standard methods for the examination of water and wastewater* **1998**, APHA Press: Washington. p. 38-43.
[31] Clesceri, L.S., A.E. Greenberg, and A.E. Eaton, *Iron measured by Phenanthroline Method 3500-Fe-B*, in *Standard methods for the examination of water and wastewater* **1998**, APHA Press: Washington. p. 76-78.
[32] Collinet, M.N. and D. Morin, Characterization of arsenopyrite oxidizing *Thiobacillus*. tolerance to arsenite, arsenate, ferrous and ferric iron. *Antonie van Leeuwenhoek, International Journal of General and Molecular Microbiology*, **1990**. 57(4): p. 237-244.
[33] Cornell, R.M. and U. Schwertmann, *The Iron Oxides* **2003**, New York: Wiley-VCH.
[34] Das, G.K., et al., Jarosites: A review. *Mineral Processing and Extractive Metallurgy Review*, **1996**. 16(3): p. 185-210.
[35] De Kock, S.H., P. Barnard, and C.A. Du Plessis, Oxygen and carbon dioxide kinetic challenges for thermophilic mineral bioleaching processes. *Biochemical Society Transactions*, **2004**. 32(2): p. 273-275.
[36] Demopoulos, G.P., Aqueous precipitation and crystallization for the production of particulate solids with desired properties. *Hydrometallurgy*, **2009**. 96(3): p. 199-214.

[37] Demopoulos, G.P., D.J. Droppert, and G. Van Weert, Precipitation of crystalline scorodite ($FeAsO_4 \cdot 2H_2O$) from chloride solutions. *Hydrometallurgy*, **1995**. 38(3): p. 245-261.
[38] Demopoulos, G.P., et al. *The atmospheric Scorodite Process*. in *Copper 2003*. **2003**. Chili: Canadian Institute of Mining, Metallurgy and Petroleum
[39] Dinkla, I.J.T., et al., *Acidianus brierleyi* is the dominant thermoacidophile in a bioleaching community processing chalcopyrite containing concentrates at 70°C. *Advanced Materials and Research*, **2009**. 71-73: p. 67-70.
[40] Domic, E., *A Review of the Development and Current Status of Copper Bioleaching Operations in Chile: 25 Years of Successful Commercial Implementation*, in *Biominig*, D.E. Ralings and B.D. Johnson, Editors. **2006**, Springer. p. 81-95.
[41] Dopson, M., J.E. Sundkvist, and E.B. Lindstrom, Toxicity of metal extraction and flotation chemicals to *Sulfolobus metallicus* and chalcopyrite bioleaching. *Hydrometallurgy*, **2006**. 81(3-4): p. 205-213.
[42] Dove, P.M. and J.D. Rimstidt, The solubility and stability of scorodite, $FeAsO_4 \cdot 2H_2O$. *American Mineralogist*, **1985**. 70(7-8): p. 838-844.
[43] Dove, P.M. and J.D. Rimstidt, Solubility and stability of scorodite, $FeAsO_4 \cdot 2H_2O$: reply. *American Mineralogist*, **1987**. 72(7-8): p. 845-848.
[44] Downs, R.T. *The RRUFF project: an integrated study of the chemistry, crystallography, Raman and Infrared Spectroscopy of minerals. Data base ID R050465*. **2006**; Available from: http://rruff.info.
[45] Dubey, B., H.M. Solo-Gabriele, and T.G. Townsend, Quantities of arsenic-treated wood in demolition debris generated by Hurricane Katrina. *Environmental Science and Technology*, **2007**. 41(5): p. 1533-1536.
[46] Duquesne, K., et al., Immobilization of Arsenite and Ferric Iron by *Acidithiobacillus ferrooxidans* and Its Relevance to Acid Mine Drainage. *Applied and Environmental Microbiology*, **2003**. 69(10): p. 6165-6173.
[47] Duquesne, K., et al., Arsenite oxidation by a chemoautotrophic moderately acidophilic *Thiomonas sp.*: From the strain isolation to the gene study. *Environmental Microbiology*, **2008**. 10(1): p. 228-237.
[48] Dutrizac, J.E. and J.L. Jambor, The synthesis of crystalline scorodite, $FeAsO_4 \cdot 2H_2O$. *Hydrometallurgy*, **1988**. 19(3): p. 377-384.
[49] Dutrizac, J.E. and J.L. Jambor, Characterization of the iron arsenate-sulphate compounds precipitated at elevated temperatures. *Hydrometallurgy*, **2007**. 86(3-4): p. 147-163.
[50] Ed., Beyond mining. **2011**. 4(10): p. 653-653.
[51] Egal, M., et al., Kinetic control on the formation of tooeleite, schwertmannite and jarosite by *Acidithiobacillus ferrooxidans* strains in an As(III)-rich acid mine water. *Chemical Geology*, **2009**. 265(3-4): p. 432-441.
[52] Engelhaupt, E., Arsenic in Katrina's wood debris. *Environmental Science & Technology*, **2007**. 41(5): p. 1504.
[53] EPA, U.S., Method 1311. Toxicity Characteristic Leaching Procedure. Test Methods for Evaluating Solid Wastes Physical/Chemical Methods, D. United States Environmental Protection Agency: Washinton, Editor **1994**.
[54] EPA, U.S., Method 1312. Synthetic Precipitation Leaching Procedure. , D. United States Environmental Protection Agency: Washinton, Editor **1994**.

[55] EPA, U.S., Applicability of the Toxicity Characteristic Leaching Procedure to Mineral Processing Waste, D. United States Environmental Protection Agency: Washinton, Editor **1995**.

[56] EPA., U.S., EPA-HQ-RCRA-2006-0097. Criteria for the Safe and Environmentally Protective Use of Granular Mine Tailings Known as "Chat", D. Federal Register. United States Environmental Protection Agency: Washinton, Editor **2007**. p. 39331-39953.

[57] Etzel, K., et al., Etching of {111} and {210} synthetic pyrite surfaces by two archaeal strains, *Metallosphaera sedula* and *Sulfolobus metallicus. Hydrometallurgy*, **2008**. 94(1-4): p. 116-120.

[58] Ferris, F.G., Biogeochemical properties of bacteriogenic iron oxides. *Geomicrobiology Journal*, **2005**. 22(3-4): p. 79-85.

[59] Filippou, D. and G.P. Demopoulos, Arsenic immobilization by controlled scorodite precipitation. *JOM*, **1997**. 49(12): p. 52-58.

[60] Flemming, R.L., et al., Identification of scorodite in fine-grained, high-sulfide, arsenopyrite mine-waste using micro x-ray diffraction ($_{u}$XRD). *Canadian Mineralogist*, **2005**. 43(4): p. 1243-1254.

[61] Fowler, B.A., et al., *Arsenic*, in *Handbook on the toxicology of metals*, L. Friberg, C.F. Nordberg, and V.B. Vouk, Editors. **2007**, Elsevier: Amsterdam. p. 367-406.

[62] Francesconi, K.A. and D. Kuehnelt, Determination of arsenic species: A critical review of methods and applications, 2000-2003. *Analyst*, **2004**. 129(5): p. 373-395.

[63] Frankel, R.B. and D.A. Bazylinski, Biologically Induced Mineralization by Bacteria. *Reviews in Mineralogy and Geochemistry*, **2003**. 54(1): p. 95-114.

[64] Fuchs, T., et al., *Metallosphaera prunae, sp. nov.*, a novel metal-mobilizing, thermoacidophilic Archaeum, isolated from a uranium mine in Germany. *Systematic and Applied Microbiology*, **1996**. 18(4): p. 560-566.

[65] Fujita, T., et al., Novel atmospheric scorodite synthesis by oxidation of ferrous sulfate solution. Part I. *Hydrometallurgy*, **2008**. 90(2-4): p. 92-102.

[66] Fujita, T., et al., Effect of pH on atmospheric scorodite synthesis by oxidation of ferrous ions: Physical properties and stability of the scorodite. *Hydrometallurgy*, **2009**. 96(3): p. 189-198.

[67] Fujita, T., et al., Immobilization of arsenic from novel synthesized scorodite-analysis on solubility and stability. *Materials Transactions*, **2009**. 50(2): p. 321-331.

[68] Gericke, M. and A. Pinches, Bioleaching of copper sulphide concentrate using extreme thermophilic bacteria. *Minerals Engineering*, **1999**. 12(8): p. 893-904.

[69] Gericke, M., A. Pinches, and J.V. Van Rooyen, Bioleaching of a chalcopyrite concentrate using an extremely thermophilic culture. *International Journal of Mineral Processing*, **2001**. 62(1-4): p. 243-255.

[70] Gihring, T.M. and J.F. Banfield, Arsenite oxidation and arsenate respiration by a new *Thermus* isolate. *FEMS Microbiology Letters*, **2001**. 204(2): p. 335-340.

[71] Ginder-Vogel, M., B. Stewart, and S. Fendorf, Kinetic and mechanistic constraints on the oxidation of biogenic uraninite by ferrihydrite. *Environmental Science and Technology*, **2010**. 44(1): p. 163-169.

[72] Ginestet, P., *Comparative evaluation of sludge reduction routes* **2007**, London: IWA Publishing.

[73] Gomez, M.A., et al., Vibrational spectroscopy study of hydrothermally produced scorodite ($FeAsO_4 \cdot 2H_2O$), ferric arsenate sub-hydrate (FAsH; $FeAsO_4 \cdot 0.75H_2O$) and basic ferric arsenate sulfate (BFAS; $Fe[(AsO_4)1\text{-}x(SO_4)x(OH)x] \cdot wH_2O$). *Journal of Raman Spectroscopy*, **2010**. 41(2): p. 212-221.

[74] Gomez, M.A., et al. *Autoclave precipitation and characterization of Fe(III)-AsO_4-SO_4 phases*. in *Hydrometallurgy 2008: Proceedings of the 6th International Symposium*. **2008**.

[75] Gomez, M.A., et al., The effect of copper on the precipitation of scorodite ($FeAsO_4 \cdot 2H_2O$) under hydrothermal conditions: Evidence for a hydrated copper containing ferric arsenate sulfate-short lived intermediate. *Journal of Colloid and Interface Science*, **2011**.

[76] Gong, Z., et al., Arsenic speciation analysis. *Talanta*, **2002**. 58(1): p. 77-96.

[77] Gramp, J.P., et al., Monovalent cation concentrations determine the types of Fe(III) hydroxysulfate precipitates formed in bioleach solutions. *Hydrometallurgy*, **2008**. 94(1-4): p. 29-33.

[78] Gramp, J.P., et al., Biogenic synthesis and reduction of Fe(III)-hydroxysulfates. *Geomicrobiology Journal*, **2009**. 26(4): p. 275-280.

[79] Gusek, J.J. and L.A. Figueroa, *Mitigation of Metal Mining Influenced Water* **2009**: Society for Mining Metallurgy.

[80] Hallberg, K.B., H.M. Sehlin, and E.B. Lindstrom, Toxicity of arsenic during high temperature bioleaching of gold-bearing arsenical pyrite. *Applied Microbiology and Biotechnology*, **1996**. 45(1-2): p. 212-216.

[81] Hallberg, R. and F.G. Ferris, Biomineralization by Gallionella. *Geomicrobiology Journal*, **2004**. 21(5): p. 325-330.

[82] Harvey, M.C., et al., Scorodite dissolution kinetics: Implications for arsenic release. *Environmental Science and Technology*, **2006**. 40(21): p. 6709-6714.

[83] Hatzinikolaou, D.G., et al., Comparative growth studies of the extreme thermophile *Sulfolobus acidocaldarius* in submerged and solidified substrate cultures. *World Journal of Microbiology and Biotechnology*, **2001**. 17(3): p. 229-234.

[84] Hegler, F., et al., Does a low-pH microenvironment around phototrophic FeII-oxidizing bacteria prevent cell encrustation by FeIII minerals? *FEMS Microbiology Ecology*, **2010**. 74(3): p. 592-600.

[85] Henke, K., *Arsenic in Natural Environments* in *Arsenic: Environmental Chemistry, Health Threats and Waste Treatment*, K. Henke, Editor **2009**, John Willey & Sons, Ltd: Chichester, UK. p. 69-235.

[86] Henke, K. and A. Hutchison, *Arsenic Chemistry* in *Arsenic: Environmental Chemistry, Health Threats and Waste Treatment*, K. Henke, Editor **2009**, John Willey & Sons, Ltd: Chichester, UK. p. 9-59.

[87] Henke, K.R., *Locations of Significant Arsenic Concentration*, in *Arsenic: Environmental Chemistry, Health Threats and Waste Treatment*, K. Henke, Editor **2009**, John Willey & Sons, Ltd: Chichester, UK. p. 495-524.

[88] Henke, K.R., *Regulation of Arsenic: A Brief Survey and Bibliography*, in *Arsenic: Environmental Chemistry, Health Threats and Waste Treatment*, K. Henke, Editor **2009**, John Willey & Sons, Ltd: Chichester, UK. p. 545-556.

[89] Henke, K.R., *Waste Treatment and Remediation Technologies for Arsenic*, in *Arsenic: Environmental Chemistry, Health Threats and Waste Treatment*, K. Henke, Editor **2009**, John Willey & Sons, Ltd: Chichester, UK. p. 351-415.

[90] Henke, K.R. and D.A. Atwood, *Arsenic in Human History and Modern Societies*, in *Arsenic: Environmental Chemistry, Health Threats and Waste Treatment*, K. Henke, Editor **2009**, John Willey & Sons, Ltd: Chichester, UK. p. 277-297.

[91] Hol, A., et al., Processing of arsenopyritic gold concentrates by partial bio-oxidation followed by bioreduction. *Environmental Science and Technology*, **2011**. 45(15): p. 6316-6321.

[92] Hopenhayn, C., Arsenic in Drinking Water: Impact on Human Health. *Elements*, **2006**. 2: p. 103-107.

[93] Huber, H. and K.O. Stetter, Hyperthermophiles and their possible potential in biotechnology. *Journal of Biotechnology*, **1998**. 64(1): p. 39-52.

[94] Jakeman, R.J.B., et al., A new ferric orthoarsenate hydrate: Structure and magnetic ordering of $FeAsO_4 \cdot {}^{3}/_{4}H_2O$. *Inorganic Chemistry*, **1991**. 30(13): p. 2806-2811.

[95] Janssen, A.J.H., et al., Application of bacteria involved in the biological sulfur cycle for paper mill effluent purification. *Science of the Total Environment*, **2009**. 407(4): p. 1333-1343.

[96] Jia, Y., et al., Observation of surface precipitation of arsenate on ferrihydrite. *Environmental Science and Technology*, **2006**. 40(10): p. 3248-3253.

[97] Jia, Y., et al., Infrared spectroscopic and X-ray diffraction characterization of the nature of adsorbed arsenate on ferrihydrite. *Geochimica et Cosmochimica Acta*, **2007**. 71(7): p. 1643-1654.

[98] Kappler, A. and D.K. Newman, Formation of Fe(III)-minerals by Fe(II)-oxidizing photoautotrophic bacteria. *Geochimica et Cosmochimica Acta*, **2004**. 68(6): p. 1217-1226.

[99] Karavaiko, G.I., G.A. Dubinina, and T.F. Kondrateva, Lithotrophic microorganisms of the oxidative cycles of sulfur and iron. *Microbiology*, **2006**. 75(5): p. 512-545.

[100] Kelly, T.D. and G.R. Matos, Historical statistics for mineral and material commodities in the United States, Data Series 140, in *Arsenic statistics* **2010**, U.S. Geological Survey.

[101] Kinnunen, P.H.M. and J.A. Puhakka, High-Rate Ferric Sulfate Generation by a *Leptospirillium ferriphilum*-Dominated Biofilm and the Role of Jarosite in Biomass Retainment in a Fluidized-Bed Reactor. *Biotechnology and Bioengineering*, **2004**. 85(7): p. 697-705.

[102] Kitahama, K., R. Kiriyama, and Y. Baba, Refinement of the Crystal Structure of Scorodite. *Acta Cryst.*, **1975**. B31: p. 322-324.

[103] Konhauser, K., *Introduction to geomicrobiology* **2007**, Malden, MA [etc.]: Blackwell.

[104] Krause, E. and V.A. Ettel, Solubility and stability of scorodite, $FeAsO_4.2H_2O$: New data and further discussion. *American Mineralogist*, **1988**. 73: p. 850-854.

[105] Krause, E. and V.A. Ettel, Solubility and stability of scorodite, $FeAsO_4 \cdot 2H_2O$: New data and further discussion. *American Mineralogist*, **1988**. 73: p. 850-854.

[106] Krause, E. and V.A. Ettel, Solubilities and stabilities of ferric arsenate compounds. *Hydrometallurgy*, **1989**. 22(3): p. 311-337.

[107] Kumaresan, M. and P. Riyazuddin, Overview of speciation chemistry of arsenic. *Current Science*, **2001**. 80(7): p. 837-846.
[108] Langmuir, D., *Aqueous environmental geochemistry* **1997**, New Jersey: Prentice-Hall. 600.
[109] Langmuir, D., J. Mahoney, and J. Rowson, Solubility products of amorphous ferric arsenate and crystalline scorodite ($FeAsO_4 \cdot 2H_2O$) and their application to arsenic behavior in buried mine tailings. *Geochimica et Cosmochimica Acta*, **2006**. 70(12): p. 2942-2956.
[110] Lattanzi, P., et al., Enargite oxidation: A review. *Earth-Science Reviews*, **2008**. 86(1-4): p. 62-88.
[111] Le Berre, J.F., et al., Hydrothermal synthesis and stability evaluation of iron (III)-aluminum (III) arsenate solid solutions. *Metallurgical and Materials Transactions B: Process Metallurgy and Materials Processing Science*, **2007**. 38(2): p. 159-166.
[112] Le Berre, J.F., R. Gauvin, and G.P. Demopoulos, Characterization of poorly-crystalline ferric arsenate precipitated from equimolar Fe(III)-As(V) solutions in the pH range 2 to 8. *Metallurgical and Materials Transactions B: Process Metallurgy and Materials Processing Science*, **2007**. 38(5): p. 751-762.
[113] Le Berre, J.F., R. Gauvin, and G.P. Demopoulos, A study of the crystallization kinetics of scorodite via the transformation of poorly crystalline ferric arsenate in weakly acidic solution. *Colloids and Surfaces A: Physicochemical and Engineering Aspects*, **2008**. 315(1-3): p. 117-129.
[114] Lindstrom, E.B., A. Sandstrom, and J.E. Sundkvist, A sequential two-step process using moderately and extremely thermophilic cultures for biooxidation of refractory gold concentrates. *Hydrometallurgy*, **2003**. 71(1-2): p. 21-30.
[115] Lloyd, J.R. and R.S. Oremland, Microbial Transformations of Arsenic in the Environment: From Soda Lakes to Aquifers. *Elements*, **2006**. 2: p. 85-90.
[116] Lottermoser, B., *Mine Wastes: Characterization, Treatment and Environmental Impacts* **2010**, Berlin, Heidelberg: Springer-Verlag Berlin Heidelberg.
[117] Lowenstam, H.A., Minerals formed by organisms. *Science*, **1981**. 211(4487): p. 1126-1131.
[118] Mikkelsen, D., et al., Visualisation of pyrite leaching by selected thermophilic archaea: Nature of microorganism-ore interactions during bioleaching. *Hydrometallurgy*, **2007**. 88(1-4): p. 143-153.
[119] Monhemius, A.J. and P.M. Swash, Removing and stabilizing As from Copper Refining Circuits by Hydrothermal Processing. *JOM* **1999**. September: p. 30-33.
[120] Morin, P., et al., Separation of arsenic anions by capillary zone electrophoresis with UV detection. *Fresenius Journal of Analytical Chemistry*, **1992**. 342(4-5): p. 357-362.
[121] Mukherjee, A., A.E. Fryar, and B.M. O'Shea, *Major Occurrences of Elevated Arsenic in Groundwater and Other Natural Waters*, in *Arsenic: Environmental Chemistry, Health Threats and Waste Treatment*, K. Henke, Editor **2009**, John Willey & Sons, Ltd: Chichester, UK. p. 303-339.
[122] Mullin, J.W., *Crystallization* **2001**, Oxford [u.a.]: Butterworth-Heinemann.
[123] Myerson, A.S., *Handbook of Industrial Crystallization* **2002**: Butterworth Heinenmann 313.

[124] Myneni, S.C.B., et al., Experimental and theoretical vibrational spectroscopic evaluation of arsenate coordination in aqueous solutions, solids, and at mineral-water interfaces. *Geochimica et Cosmochimica Acta*, **1998**. 62(19-20): p. 3285-3300.
[125] Nemati, M. and S.T.L. Harrison, Comparative study on thermophilic and mesophilic biooxidation of ferrous iron. *Minerals Engineering*, **2000**. 13(1): p. 19-24.
[126] Nemati, M., J. Lowenadler, and S.T.L. Harrison, Particle size effects in bioleaching of pyrite by acidophilic thermophile *Sulfolobus metallicus* (BC). *Applied Microbiology and Biotechnology*, **2000**. 53(2): p. 173-179.
[127] Nordstrom, D.K., Worldwide occurrences of arsenic in ground water. *Science*, **2002**. 296(5576).
[128] Nordstrom, D.K. and G.A. Parks, Solubility and stability of scorodite, $FeAsO_4 \cdot 2H_2O$: discussion. *American Mineralogist*, **1987**. 72(7-8): p. 849-851.
[129] Norris, P.R., *Acidophile diversity in mineral sulfide oxidation*, in *Biominig*, D.E. Ralings and B.D. Johnson, Editors. **2006**, Springer. p. 201-216.
[130] Norris, P.R., N.P. Burton, and N.A.M. Foulis, Acidophiles in bioreactor mineral processing. *Extremophiles*, **2000**. 4(2): p. 71-76.
[131] O'Day, P., Chemistry and Minerology of Arsenic. *Elements*, **2006**. 2: p. 77-83.
[132] Olesik, J.W., Elemental analysis using ICP-OES and ICP/MS. *Analytical Chemistry*, **1991**. 63(1): p. 12A-21A.
[133] Olson, G.J., J.A. Brierley, and C.L. Brierley, Bioleaching review part B: Progress in bioleaching: Applications of microbial processes by the minerals industries. *Applied Microbiology and Biotechnology*, **2003**. 63(3): p. 249-257.
[134] Ondrus, P., et al., Parascorodite, $FeAsO_4 \cdot 2H_2O$-a new mineral from Kank near Kutna Hora, Czech Republic. *American Mineralogist*, **1999**. 84(9): p. 1439-1444.
[135] Oremland, R.S. and J.F. Stolz, The ecology of arsenic. *Science*, **2003**. 300(5621): p. 939-944.
[136] Paktunc, D. and K. Bruggeman, Solubility of nanocrystalline scorodite and amorphous ferric arsenate: Implications for stabilization of arsenic in mine wastes. *Applied Geochemistry*, **2010**. 25(5): p. 674-683.
[137] Paktunc, D., J. Dutrizac, and V. Gertsman, Synthesis and phase transformations involving scorodite, ferric arsenate and arsenical ferrihydrite: Implications for arsenic mobility. *Geochimica et Cosmochimica Acta*, **2008**. 72(11): p. 2649-2672.
[138] Plessis, C.A.D., J.D. Batty, and D.W. Dew, *Comercial Applications of Thermophile Bioleaching*, in *Biominig*, D.E. Ralings and B.D. Johnson, Editors. **2006**, Springer. p. 57-80.
[139] Plumb, J.J., et al., Enrichment and characterisation of thermophilic acidophiles for the bioleaching of mineral sulphides. *Minerals Engineering*, **2002**. 15(11): p. 787-794.
[140] Plumb, J.J., et al., *Acidianus sulfidivorans sp. nov.*, an extremely acidophilic, thermophilic archaeon isolated from a solfatara on Lihir Island, Papua New Guinea, and emendation of the genus description. *International Journal of Systematic and Evolutionary Microbiology*, **2007**. 57(7): p. 1418-1423.
[141] Povarennykh, A.S., The use of infrared spectra for the determination of minerals. *American Mineralogist*, **1978**. 63: p. 956-959.

[142] Ralings, D.E., *Relevance of cell physiology and genetic adaptability of biomining microorganisms to industrial processes*, in *Biominig*, D.E. Ralings and B.D. Johnson, Editors. **2006**, Springer. p. 177-198.
[143] Riveros, P.A. and J.E. Dutrizac, A Review of Arsenic Practices. *European Metallurgical Conference*, **2001**. 2: p. 373-394.
[144] Riveros, P.A., J.E. Dutrizac, and P. Spencer, Arsenic disposal practices in the metallurgical industry. *Canadian Metallurgical Quarterly*, **2001**. 40(4): p. 395-420.
[145] Robins, R.G., The solubility of metal arsenates. *Metallurgical Transactions B*, **1981**. 12(1): p. 103-109.
[146] Robins, R.G., Solubility and stability of scorodite, $FeAsO_4 \cdot 2H_2O$: discussion. *American Mineralogist*, **1987**. 72(7-8): p. 842-844.
[147] Rochette, E.A., G.C. Li, and S.E. Fendorf, Stability of arsenate minerals in soil under biotically generated reducing conditions. *Soil Science Society of America Journal*, **1998**. 62(6): p. 1530-1537.
[148] Roddick-Lanzilotta, A.J., A.J. McQuillan, and D. Craw, Infrared spectroscopic characterisation of arsenate (V) ion adsorption from mine waters, Macraes mine, New Zealand. *Applied Geochemistry*, **2002**. 17(4): p. 445-454.
[149] Rodriguez-Navarro, C., et al., Bacterially mediated mineralization of vaterite. *Geochimica et Cosmochimica Acta*, **2007**. 71(5): p. 1197-1213.
[150] Ruitenberg, R., C.E. Schultz, and C.J.N. Buisman, Bio-oxidation of minerals in air-lift loop bioreactors. *International Journal of Mineral Processing*, **2001**. 62(1-4): p. 271-278.
[151] Salzsauler, K.A., N.V. Sidenko, and B.L. Sherriff, Arsenic mobility in alteration products of sulfide-rich, arsenopyrite-bearing mine wastes, Snow Lake, Manitoba, Canada. *Applied Geochemistry*, **2005**. 20(12): p. 2303-2314.
[152] Sehlin, H.M. and E.B. Lindstrom, Oxidation and reduction of arsenic by Sulfolobus acidocaldarius strain BC. *FEMS Microbiology Letters*, **1992**. 93(1): p. 87-92.
[153] Shinoda, K., et al., Coprecipitation of large scorodite particles from aqueous Fe(II) and As(V) solution by oxygen injection. *Materials Transactions*, **2009**. 50(5): p. 1196-1201.
[154] Singhania, S., et al., Temperature and seeding effects on the precipitation of scorodite from sulfate solutions under atmospheric-pressure conditions. *Metallurgical and Materials Transactions B: Process Metallurgy and Materials Processing Science*, **2005**. 36(3): p. 327-333.
[155] Singhania, S., et al., Acidity, valency and third-ion effects on the precipitation of scorodite from mixed sulfate solutions under atmospheric-pressure conditions. *Metallurgical and Materials Transactions B: Process Metallurgy and Materials Processing Science*, **2006**. 37(2): p. 189-197.
[156] Sullivan, C., et al., Disposal of water treatment wastes containing arsenic - A review. *Science of the Total Environment*, **2010**. 408(8): p. 1770-1778.
[157] Swash, P. and A. Monhemius. *The Scorodite Process: A Technology for the Disposal of Arsenic in the 21st Century*. in *Effluent Treatment in the Mining Industry. University of Concepcion*. **1998**. Chile.

[158] Takatsugi, K., K. Sasaki, and T. Hirajima, Mechanism of the enhancement of bioleaching of copper from enargite by thermophilic iron-oxidizing archaea with the concomitant precipitation of arsenic. *Hydrometallurgy*, **2011**.

[159] Twidwell, L.G. and J.W. McCloskey, Removing Arsenic from Aqueous Solution and Long-term Product Storage. *JOM Journal of the Minerals Metals and Materials Society*, **2011**. 63(8): p. 94-100.

[160] van't Riet, K. and J. Tramper, *Basic Bioreactor Design* **1991**, New York: Marcel Dekker Inc. 465.

[161] Van Aswegen, P.C., J. van Niekerk, and W. Olivier, *The BIOX process for the Treatment of Refractory Gold Concentrates*, in *Biominig*, D.E. Ralings and B.D. Johnson, Editors. **2006**, Springer. p. 1-33.

[162] Van Weert, G. and D.J. Droppert, Aqueous processing of arsenic trioxide to crystalline scorodite. *JOM Journal of the Minerals Metals and Materials Society*, **1994**. 46(6): p. 36-38.

[163] Vaughan, D.J., Arsenic. *Elements*, **2006**. 2: p. 71-75.

[164] Vink, B.W., Stability relations of antimony and arsenic compounds in the light of revised and extended Eh-pH diagrams. *Chemical Geology*, **1996**. 130(1-2): p. 21-30.

[165] Wang, H., et al., Synthesis and properties of ammoniojarosites prepared with iron-oxidizing acidophilic microorganisms at 22-65°C. *Geochimica et Cosmochimica Acta*, **2007**. 71(1): p. 155-164.

[166] Webmineral. *Mineralogy Database. XRD patron Scorodite*. **2008 08-31-08**; Available from: http://webmineral.com

[167] Weiner, S. and P.M. Dove, An Overview of Biomineralization Processes and the Problem of the Vital Effect. *Reviews in Mineralogy and Geochemistry*, **2003**. 54(1): p. 1-29.

[168] WHO, Guidelines for Drinking-Water Quality. Volume 1-Recommendations. First addendum to third addition.www.who.int/water_sanitation_health/dwq/gdwq0506.pdf, **2006**.

[169] Witne, J.Y. and C.V. Phillips, Bioleaching of Ok Tedi copper concentrate in oxygen- and carbon dioxide-enriched air. *Minerals Engineering*, **2001**. 14(1): p. 25-48.

[170] Yu, L.L., T.A. Butler, and G.C. Turk, Effect of valence state on ICP-OES value assignment of SRM 3103a arsenic spectrometric solution. *Analytical Chemistry*, **2006**. 78(5): p. 1651-1656.

[171] Zeng, W., et al., Detection and analysis of attached microorganisms on the mineral surface during bioleaching of pure chalcopyrite with moderate thermophiles. *Hydrometallurgy*, **2011**. 106(1-2): p. 46-50.

[172] Zhu, Y. and B.J. Merkel, The Dissolution and Solubility of Scorodite, $FeAsO_4 \cdot 2H_2O$. Evaluation and Simulation with PHREEQC2. *Wiss.Mitt. Inst. für Geologie, TU Bergakedemie Freiberg, Germany*, **2001**. 18.

SUMMARY

Arsenic, a toxic element for humans, was widely used in the 20th century in electronics, wood preservation and agricultural applications. Currently, the use of arsenic is banned for most applications, leading to the accumulation of arsenic waste mainly as arsenic trioxide. The most stable end-product for arsenic immobilization is produced through its precipitation in scorodite crystals **(Chapter 1)**.

The aim of the work described in this thesis was to develop a controlled process for biological crystallization of scorodite from metallurgical streams. This is achieved by balancing biological oxidation and crystallization reactions in a single step.

The bioscorodite process is patented by Paques B.V (Balk, The Netherlands) as the ARSENOTEQ^{TM} process. In this thesis, the proof of principle, reactor selection and operational conditions of bioscorodite crystallization were studied.

The proof of principle of bioscorodite crystallization was provided using iron oxidizing thermoacidophilic microorganisms at pH 0.8 and 80°C in batch experiments **(Chapter 3)**. In these experiments, bioscorodite saturation was controlled by biological oxidation. As a result, crystal growth was favoured over primary nucleation, resulting in the formation of bioscorodite crystals in the presence of 1 g As^{5+} L^{-1}. The nucleation process of bioscorodite occurred in the absence of seeds.

A method to measure concentrations of inorganic arsenic species (As^{3+} and As^{5+}) by HPLC and UV detection was developed in **Chapter 2**.

Iron oxidation kinetics of thermoacidophilic microorganisms was studied in batch and in CSTR reactors **(Chapter 4)**. The iron oxidation capacity was affected by pH values below 1. However, at pH above 1 these microorganisms showed high iron oxidation rates. The iron oxidation capacity of the thermoacidophilic microorganisms was not affected by arsenate (As^{5+}) addition up to 2.8 g As L^{-1}. Addition of arsenite (As^{3+}) on the other hand, decreased the iron oxidation capacity **(Chapter 8)**. Surprisingly, despite arsenite inhibition, arsenite oxidation was measured at very low rates in a CSTR reactor operated at pH 1.2 and 72°C. Thermoacidophilic microorganisms were also grown in an airlift reactor achieving high iron conversion rates at pH 1.2 and 72°C **(Chapter 9)**. However, when growing in an airlift reactor, thermoacidophilic microorganisms needed additional substrate ($Fe(II)SO_4$) in order to sustain growth.

During batch experiments, formation of ferric arsenate precursor precipitates was observed on the surface of thermoacidophilic microorganisms **(Chapter 5)**. At neutrophilic conditions, the formation of precipitates on the cell surface expected and this can lead to cell encrustation by iron oxides. At acidic conditions, iron oxides precipitation was however not expected. The formation of precipitates on the cell surface suggests that the cell surface may play a role in bioscorodite formation. Nonetheless, the indirect biomineralization of scorodite seems to be regulated by saturation of the bulk rather than

by nucleation on the cell surface **(Chapter 5)**. The main role of the microorganisms in the process is therefore to oxidize ferrous iron under extreme pH conditions and in the presence of high arsenate/arsenite concentrations.

In **Chapter 6,** the long-term arsenic leaching behaviour of bioscorodite crystals was studied under TCLP test conditions. Arsenic concentrations as low as 0.016 mg As L^{-1} were measured in the tests after one year of leaching. The main parameters that affected the arsenic leaching concentrations of the bioscorodite crystals were: ageing time, precipitation rate and the structural water content. Once the leaching tests ended, a structural characterization of the remaining bioscorodite crystals was performed **(Chapter 7)**. These results confirmed the relation between the structural water content and the arsenic leaching from bioscorodite crystals previously observed in Chapter 6.

The operational conditions of bioscorodite production were softened to pH 1.2 and 72°C in CSTR and airlift reactors, achieving 99% of arsenic removal efficiency **(Chapter 8)**. Scaling of the bioscorodite precipitates on the glass wall impeded easy harvesting of solids from the CSTRs. The bioscorodite sludge was very suitable for arsenic disposal due to its low arsenic leaching concentrations of 0.4 mg As L^{-1} after 100 days under TCLP leaching test conditions.

In order to avoid scaling, an airlift reactor was tested for bioscorodite production at pH 1.2 and 72°C **(Chapter 9)**. The produced bioscorodite crystals resemble very well the scorodite mineral with respect to their arsenic content and the structural water content. The most stable crystals could be easily harvested by sedimentation from the bioreactor due to their relatively large size of up to 160 μm. Results from arsenic leaching tests with bioscorodite crystals classify the material as non-hazardous. The material displays very low arsenic leaching concentrations between 0.016 and 0.5 mg L^{-1}, measured after at least 50 days of leaching under TCLP test conditions. This makes the bioscorodite sludge very suitable for long-term arsenic disposal. Long-term leaching tests revealed that the bioscorodite stability can be optimized by selecting the right operational variables such as the ageing time in the bioreactor.

Bioscorodite crystals were compared to specimens of mineral scorodite **(Chapter 10)**. The morphology (crystal habit) and structural composition of bioscorodite crystals resemble the mineral scorodite. The stability properties of bioscorodite reported in this thesis show the potential of bio-scorodite crystals to immobilize arsenic. The assessment of stability data suggests that bioscorodite crystals should be stored at pH~4, preferably under aerobic conditions but in the absence of organic matter.

The ARSENOTEQ™ process is a compact system with only one reactor in which biological oxidation and crystallization reactions are simultaneously taking place. Due to its good stability properties, bioscorodite sludge can be disposed of directly after harvesting from the airlift reactor. The operational cost of the bioscorodite process are

90% less than the conventional arsenic ferrihydrite process (30°C) despite of the high energetic requirement for heating at 70°C **(Chapter 11)**. Operational costs of the bioscorodite process are lower than the operational costs of chemical scorodite precipitation at 85°C. This is mainly because neutralization steps, seeds addition, chemical oxidation, sludge post treatment and sludge dewatering are not required.

The potential application of the bioscorodite process for arsenic removal and immobilization is favoured due to (1) low iron consumption, (2) low sludge production, (3) no requirement for neutralization steps and (4) the production of stable bioscorodite, to be disposed of without further post-treatment of the solids.

Application of the bioscorodite process was demonstrated for metallurgical streams with an arsenic content from 1 to 3 g As L^{-1}. Based on measured biological iron oxidation rates, it was estimated that the process if feasible for the treatment of streams with arsenic concentrations up to 20 g As L^{-1}.

Apart from the treatment of metallurgical streams, this biological process may also have opportunities in the stabilization of arsenic trioxide by its conversion to scorodite for safe disposal. Other applications may be found in the stabilization of ferric arsenate sludge originating from the chemical processes to remove arsenic from groundwater. Treatment of those materials using the bioscorodite process could produce safe arsenic crystals for disposal and offers a potential for iron recycling. An overview and the main results of this thesis is presented in the diagram below.

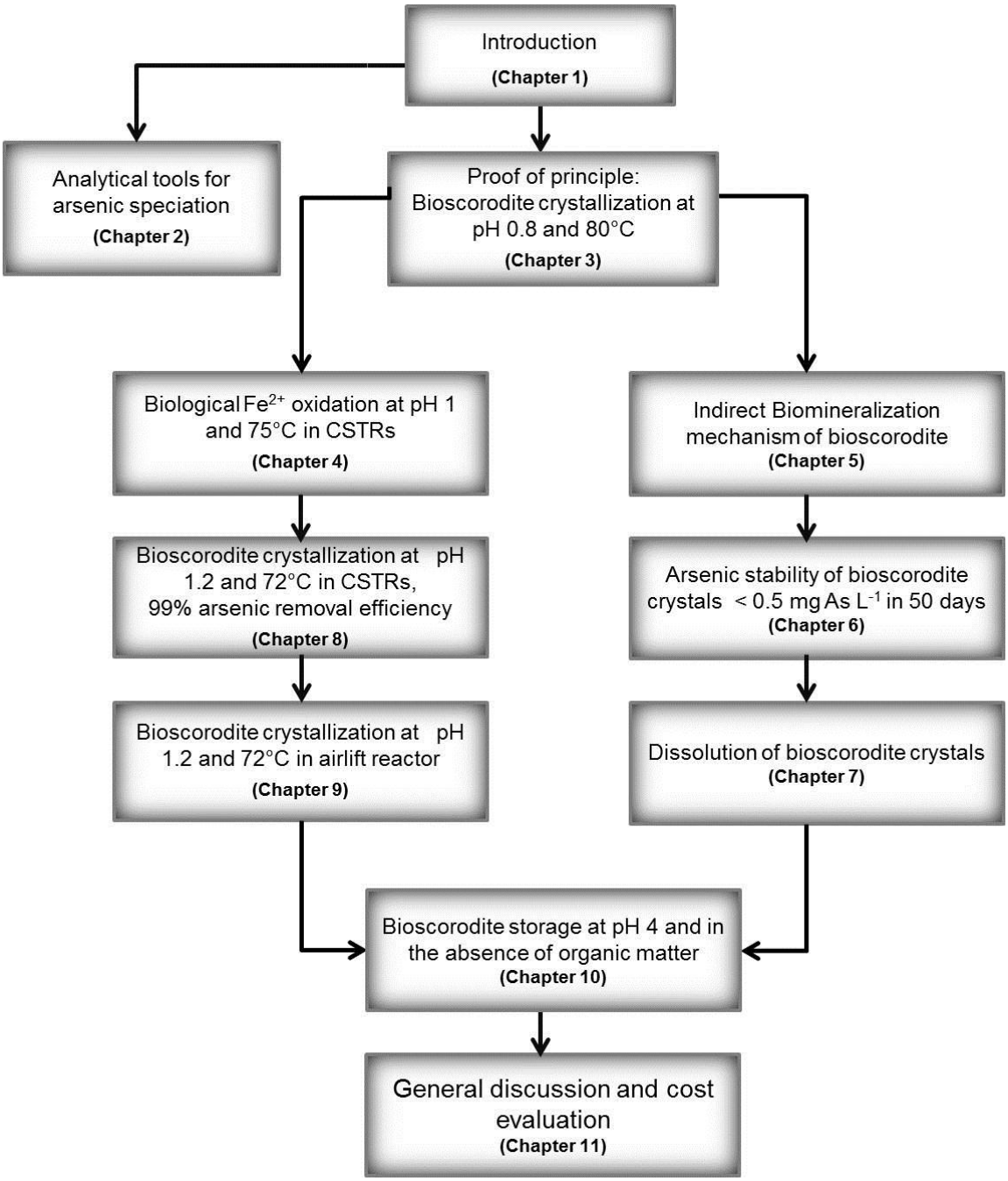

DIAGRAM. Overview and main outcome of this thesis.

SAMENVATTING

Arseen, een voor de mens giftig element, is in de 20e eeuw op grote schaal gebruikt in elektronica, voor de verduurzaming van hout en voor agrarische toepassingen. Tegenwoordig is het gebruik van arseen voor de meeste toepassingen verboden. Dit leidt tot een toename van de hoeveelheid arseenhoudend afval, waarbij het arseen voornamelijk voorkomt in de vorm van arseentrioxide. Het meest stabiele eindproduct, geschikt voor de immobilisatie van arseen, kan worden gevormd door precipitatie van dit element in de vorm van scorodiet kristallen (**hoofdstuk 1**).

Het in dit proefschrift beschreven werk is gericht op de ontwikkeling van een nieuw proces voor de biologische kristallisatie van scorodiet uit waterstromen afkomstig van de metallurgische industrie. De basis van dit nieuwe proces bestaat uit het evenwichtig controleren van biologische oxidatie- en kristallisatie reacties in een enkele stap.
Het bioscorodiet proces is gepatenteerd door Paques BV (Balk, Nederland) als het ARSENOTEQ™ proces. In dit proefschrift wordt het 'proof of principle' voor bioscorodiet kristallisatie geleverd. Daarnaast zijn verschillende reactortypen en operationele condities voor toepassing van het proces onderzocht.

Het 'proof of principle' van bioscorodiet kristallisatie is geleverd door middel van batch experimenten met ijzer-oxiderende thermoacidofiele micro-organismen bij een pH van 0,8 en een temperatuur van 80°C **(hoofdstuk 3)**. Bij deze experimenten werd de mate van bioscorodiet verzadiging gestuurd door middel van biologische oxidatie. Als gevolg hiervan vond met name kristalgroei plaats, en geen of weinig primaire nucleatie. Dit resulteerde in de vorming van bioscorodiet kristallen bij een arsenaat (As^{5+}) concentratie van 1 g L^{-1}. De nucleatie van het bioscorodiet vond plaats zonder de aanwezigheid van kiem materiaal. De ontwikkeling van een methode voor het meten van concentraties anorganisch arseen (As^{3+} en As^{5+}) met HPLC en UV detectie is beschreven in **hoofstuk 2**.

De kinetiek van ijzer oxidatie door thermoacidofiele micro-organismen is verder bestudeerd in zowel batch- als CSTR reactoren **(hoofdstuk 4)**. De ijzer oxidatie capaciteit van thermoacidofiele micro-organismen werd geremd bij pH-waarden lager dan 1. Bij pH waarden hoger dan 1 werd echter een hoge ijzer oxidatie snelheid gemeten. Deze snelheid werd niet beïnvloed door toevoeging van arsenaat (2,8 g L^{-1}). Door toevoeging van arseniet (As^{3+}) verminderde de ijzer oxidatiecapaciteit **(hoofdstuk 8)**. Ondanks deze remming werd toch oxidatie van arseniet aangetoond, zij het met een zeer lage snelheid. Deze arseniet oxidatie vond plaats bij pH 1,2 en 72°C in een CSTR reactor.

IJzer oxidatie door thermoacidofiele micro-organismen werd ook bestudeerd in een airlift reactor, waarbij eveneens hoge ijzer omzettingssnelheden werden bereikt bij pH 1,2 en 72°C **(hoofdstuk 9)**. Echter, wanneer de thermoacidofiele micro-organismen werden

toegepast in een airlift reactor, was extra substraat (ijzer(II)sulfaat) nodig om groei te ondersteunen.

Tijdens batch proeven zijn precursors van ijzerarsenaat precipitatie waargenomen op het celoppervlak van thermoacidofiele micro-organismen **(hoofdstuk 5)**. Het is bekend dat onder neutrofiele condities een ijzeroxide neerslag kan worden gevormd op het celoppervlak. Dit kan leiden tot inkapseling van de cel. Onder zure condities werd deze neerslag van ijzeroxiden echter niet verwacht. De vorming van een neerslag op het celoppervlak wijst erop dat het celoppervlak een rol speelt bij de vorming van bioscorodiet. Toch lijkt de indirecte biomineralisatie van scorodiet te worden geregeld door verzadiging van de bulk en niet door kiemvorming op het celoppervlak. De belangrijkste rol van de micro-organismen in het proces is dan ook om ijzer te oxideren onder extreme pH-omstandigheden in aanwezigheid van hoge arsenaat / arseniet concentraties.

In **Hoofdstuk 6** wordt de uitloging van arseen uit bioscorodiet kristallen beschreven voor lange termijn opslaag onder TCLP test condities (Toxicity Characteristic Leaching Procedure, een methode voor het bepalen van de mobiliteit). Na een jaar werd een minimale arseen concentraties gemeten van slechts 0,016 mg As L^{-1}. De belangrijkste parameters die de uitloging van arseen uit bioscorodiet kristallen bepalen zijn: verblijftijd in de reactor, precipitatiesnelheid en het structureel watergehalte. Na afloop van de uitloogproeven werd een structurele karakterisering van de bioscorodiet kristallen uitgevoerd (**hoofdstuk 7**). De resultaten bevestigden de relatie tussen het structureel watergehalte en de uitloging van arseen uit bioscorodiet kristallen, zoals eerder beschreven in hoofdstuk 6.

De extreme operationele omstandigheden voor bioscorodiet productie werden wat afgezwakt naar pH 1,2 en 72°C voor verdere studie in CSTR reactoren. Hierbij werd 99% efficiëntie voor arseenverwijdering bereikt **(hoofdstuk 8)**. Scaling van bioscorodiet op de glazen reactorwand belemmerde echter de afvoer van vaste stof uit de reactoren. Het bioscorodiet slib bleek desondanks zeer geschikt voor de opslag van arseen. Na 100 dagen uitloging onder TCLP test condities werd een concentratie van slechts 0,4 mg L^{-1} As gemeten.

Om scaling te voorkomen werd bij verdere experimenten gebruik gemaakt van een airlift reactor bij pH 1,2 en een temperatuur van 72°C **(hoofdstuk 9)**. De gevormde bioscorodiet kristallen kwamen zeer sterk overeen met mineraal scorodiet wat betreft het arseen gehalte en het gehalte aan structureel water. De meest stabiele kristallen konden gemakkelijk worden geoogst door middel van sedimentatie vanwege de grotere afmeting van deze kristallen tot ca. 160 μm. Op basis van de resultaten van uitloogproeven met bioscorodiet kristallen kan het materiaal worden geclassificeerd als ongevaarlijk. Het materiaal heeft een zeer lage arseen mobiliteit met concentraties tussen 0,016 en 0,5 mg L^{-1}, gemeten na

ten minste 50 dagen uitloging onder TCLP test condities. Dit maakt het bioscorodiet slib zeer geschikt voor de lange termijn opslag van arseen. Bij lange termijn uitlogingstesten bleek dat de stabiliteit van bioscorodiet kan worden geoptimaliseerd door het kiezen van de juiste operationele variabelen, zoals de verblijftijd in de bioreactor.

Bioscorodiet kristallen werden verder op verschillende wijzen vergeleken met specimen van mineraal scorodiet **(hoofdstuk 10)**. De morfologie en structurele samenstelling van bioscorodiet kristallen lijkt sterk op dat van mineraal scorodiet. De stabiliteitseigenschappen van het bioscorodiet beschreven in dit proefschrift tonen het potentieel van het materiaal om arseen te immobiliseren. De beoordeling van de stabiliteitseigenschappen suggereren dat bioscorodiet kristallen het best kunnen worden opgeslagen bij pH van ongeveer 4, bij voorkeur onder aërobe omstandigheden en in de afwezigheid van organische stof.

Het ARSENOTEQ™ proces is een compact proces bestaande uit slechts één reactor waarin de biologische oxidatie en kristallisatie reacties gelijktijdig plaatsvinden. Door de goede stabiliteitseigenschappen kan bioscorodiet slib worden opgeslagen direct na verwijdering van het materiaal uit de airlift reactor. De operationele kosten van het proces zijn ca. 90% lager dan het conventionele arseen ferrihydriet proces (wat plaatsvindt bij 30°C), ondanks de hogere energiebehoefte voor verwarming tot 70°C **(hoofdstuk 11)**. De operationele kosten zijn tevens lager dan die van het chemische proces voor scorodiet vorming bij 85°C. Dit komt voornamelijk omdat neutralisatie stappen, toevoeging van kiemmateriaal, chemische oxidatie, nabehandeling van het slib en slibontwatering bij het bioscorodiet proces niet benodigd zijn.

De potentiele toepassing van het bioscorodiet proces voor de verwijdering en immobilisatie van arseen wordt bevorderd door (1) een laag ijzer verbruik, (2) lage slibproductie, (3) geen vereiste voor neutralisatie stappen en (4) de productie van stabiel bioscorodiet, geschikt voor directe opslag zonder de noodzaak van een nabehandeling van het materiaal.

De toepasbaarheid van het bioscorodiet proces werd in dit proefschrift aangetoond voor metallurgische stromen met een arseengehalte van 1 tot 3 g As L^{-1}. Op basis van gemeten biologische ijzer oxidatie snelheden, wordt geschat dat het proces toepasbaar is voor de behandeling van waterstromen met arseen concentraties tot 20 g As L^{-1}.

Naast de behandeling van metallurgische stromen, biedt dit biologische proces ook mogelijkheden voor de stabilisatie van arseentrioxide door de omzetting hiervan naar scorodiet. Andere toepassingen kunnen worden gevonden in de stabilisatie van ijzer arsenaat houdend slib, afkomstig van de chemische processen die worden gebruikt voor de verwijdering van arseen uit grondwater. De behandeling van dit slib met het bioscorodiet proces zou kunnen leiden tot de vorming van arseen kristallen, geschikt voor veilige

opslag. Het biedt bovendien potentieel voor ijzer recycling. Een overzicht van de inhoud van dit proefschrift en de voornaamste resultaten is gepresenteerd in onderstaand schema.

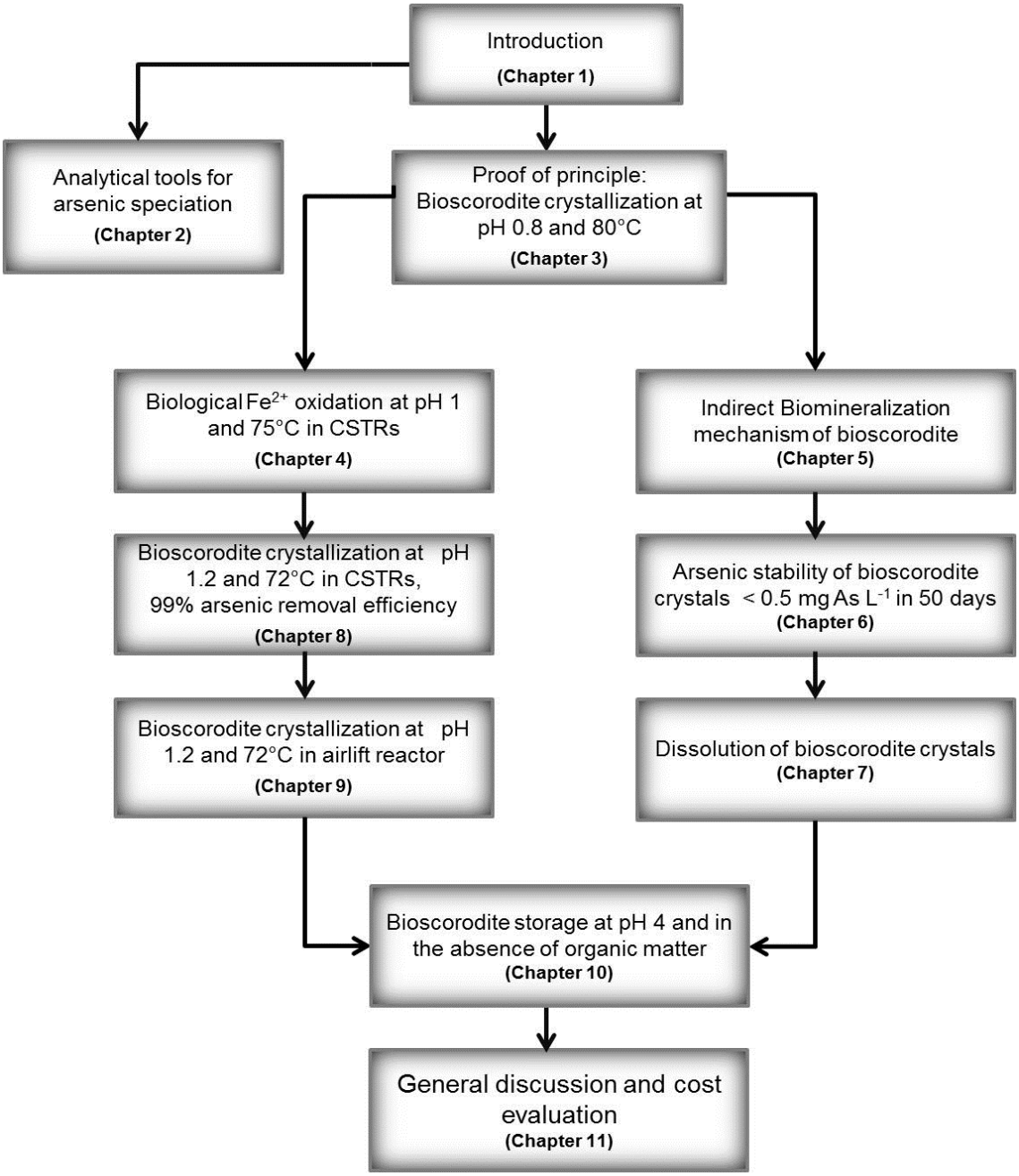

DIAGRAM. Overview and main outcome of this thesis.

NOMENCLATURE

As	total arsenic
As^{3+}-As(III)	arsenite
As^{5+}-As(V)	arsenate
D	Dilution rate
Fe	total iron
Fe^{2+}-Fe(II)	ferrous iron
Fe^{3+}-Fe(III)	ferric iron
J	joules
t	metric tonnes
kt	kilo tonnes
k_La	volumetric mass transfer coefficient
OTR	oxygen transfer rate
V	volume
V_G	gas superficial velocity
V_L	liquid superficial velocity
μ_{max}	Maximum specific growth rate

ABBREVIATIONS

AOs	arsenite-oxidizing prokaryotes
ATR	attenuated total reflectance
BDAT	best demonstrated available technology
BET	Brunauer-Emmett-Teller (BET) surface area analysis
CAOs	chemolithoautotrophic arsenite oxidizers
CCA	chromated copper arsenate
CSTR	continuously stirred tank reactor
DARPs	dissimilatory arsenate-reducing prokaryotes
DMA	dimethylarsinic acid
DTA	differential thermal analysis
EPA	US environmental protection agency
FTIR	Fourier-transform-infrared (spectroscopy)
HAOs	heterotrophic arsenite oxidizers
HRT	hydraulic retention time
IAP	ion activity product
ICP-OES	inductively coupled plasma optical emission spectrometry
MMA	monomethylarsonic acid
S	saturation level
Sb	saturation in bulk solution by primary nucleation
Sc	saturation on cell surface by secondary nucleation
Sb/2	saturation in bulk solution by secondary nucleation
SEM	scanning electron microscope
SPLP	synthetic precipitation leaching procedure
TCLP	toxicity characteristic leaching procedure
TGA	thermal gravimetric analysis
XRD	X-ray diffraction

LIST OF PUBLICATIONS FROM THIS THESIS

Gonzalez-Contreras, P.; Weijma, J, Buisman, C. J. N. Biological scorodite crystallization: Effect of high ferric concentration and foreign seeds. *Advanced Materials Research* **2009**, 71-73, 629-632.

Gonzalez-Contreras, P.; Weijma, J, Buisman, C. J. N. Biogenic scorodite crystallization by Acidianus sulfidivorans for arsenic removal. *Environmental Science and Technology* **2010**, 44, 675-680.

Gonzalez-Contreras, P; Gerrits-Benneheij, I, Weijma, J, Buisman, C.J.N. HPLC inorganic arsenic speciation analysis of samples containing high sulphuric acid and iron levels. *Toxicological and Environmental Chemistry* **2011**, 93 (3), pp. 415 - 423.

Gonzalez-Contreras, P; Weijma, J, Buisman, C. J. N., Kinetics of ferrous iron oxidation by batch and continuous cultures of thermoacidophilic Archaea at extremely low pH of 1.1-1.3. *Applied Microbiology and Biotechnology* **2012**, 93 (3), 1295-1303.

Gonzalez-Contreras, P; Weijma, J, Buisman, C. J. N., Arsenic removal in an airlift reactor for continuous bioscorodite production. *Crystal Growth & Design* **2012**, 12, 2699-2706.

Gonzalez-Contreras, P; Weijma, J, Buisman, C. J. N., Continuous bioscorodite crystallization in CSTRs for arsenic removal and disposal. *Submitted*.

Gonzalez-Contreras, P; Weijma, J, Buisman, C. J. N., Low arsenic leaching from biogenic scorodite crystals produced for arsenic immobilization and disposal. *Submitted*.

Gonzalez-Contreras, P; Weijma, J, Buisman, C. J. N., Facilitated biomineralization of bioscorodite and partial cell encrustation by thermoacidophilic archaeon. In preparation.

Gonzalez-Contreras, P; Weijma, J, Buisman, C. J. N., Structural changes of bioscorodite during long-term storage. In preparation.

Gonzalez-Contreras, P; Weijma, J, Buisman, C. J. N., Storage of bioscorodite crystals for arsenic immobilization. In preparation.

SELECTED ORAL PRESENTATIONS

Gonzalez-Contreras, P.A., Weijma, J., Buisman, C.J.N. Arsenic immobilization by bioscorodite crystallization: effect of foreign seeds addition. In: *Proceedings of 18th International Biohydrometallurgy Symposium*, September 13-17, **2009**, Bariloche, Argentina.

Gonzalez-Contreras, P.A., Weijma, J., Buisman, C.J.N. Molecular mechanism of bioscorodite formation mediated by thermoacidophilic archaea. In: *FIMIN Spring School: Iron in the Environment, from Nature to the Laboratory: Earth, Life and Fire*, March 7-11 **2011**, Cordoba, Spain.

Gonzalez-Contreras, P.A., Huisman, J., Weijma, J., Buisman, C.J.N. Bioscorodite crystallization for arsenic removal. In: *Proceedings of 6th European Metallurgical Conference*, June 26-29, **2011**, Düsseldorf, Germany.

Gonzalez-Contreras, P.A., Weijma, J., Buisman, C.J.N. Arsenic Biomineral Formation Leads to Partial Encrustation of Thermoacidophilic Archaeon. In: *Proceedings of Goldschmidt: Earth, Life and Fire,* August 14-19 **2011**, Prague, Czech Republic.

Huisman, J; Olde Weghuis, M, Gonzalez-Contreras, P.A. Biotechnology based processes for arsenic removal. In: *Proceedings of 9th international conference on clean technologies for the mining industry*, April 10-12 **2011**, Santiago, Chile.

AWARDS

2012 March. Water Business Challenge – Wetsus-Rabobank

2008 May. Granted for Ph.D. studies at Wageningen University.

Hiking in direction to the volcano Lonquimay at the Northern of Chilean Patagonia. At the back, "araucarias trees" rising high in the sky. This tree receives its name from the habitants of the zone: the Pehuenches. In Mapudungun (language of native indigenous inhabitants), *Pehuen* means Araucaria and *che* people.

ACKNOWLEDGEMENTS

At this part of the book everyone expects that I begin with the acknowledgment of institutions, supervisors and friends. I will attempt my acknowledgments by following chronological events. Why? Because the effort to complete this book is not only based on the last four years.

In the summer of 2006, I found myself in the Netherlands without speaking English and getting lost in Wageningen (yes, you can get lost). At that moment, I didn't evaluate the consequences of just following the way the wind blows. Luckily there were always friends supporting me. It is those friends that I would like to thank first: David J, Cecilia, Fer, the Bartacek family and from Chile Johana and Vivi. Also I would like to express my gratitude to Prof. Jules van Lier. You did trust me and supported me when I decided to become a researcher in the Netherlands. I enjoyed working with all those different topics and people. During the last period of 2007, Jules recommended me to Jan Weijma and that was the first time ever that I heard of scorodite. Jan's talk about the project sounded exciting but also very ambitious. I still remember that he said: "this is a very challenging project and if you manage to proof the principle of the bioscorodite process, then a project to do your Ph.D. research on may be available". With this message I locked myself in the lab and I didn't get out until I saw bioscorodite in my bottles.

In 2007, Wageningen University and CONICYT (Chile) signed an agreement to support Ph.D. studies in Wageningen. I am very glad to say that I was the first selected candidate. A year later Roberto arrived with Marcela. Therefore, I would like to thank the people who selected me and trusted me that I would carry out this Ph.D. thesis to a good end. After delivering the proof of principle of the bioscorodite process and being granted the Ph.D. research, everything came together and I became a Ph.D. student at ETE. This department represents a lot of things in my life, I grew up in this place, I made new friends, I lost my very blocked Chilean mind and I embraced all the changes that offered the way. Here it goes a big THANKS to all the ETE department!! Especially to Vinnie for all the safety support. I would like to also express my gratitude to Renata from ETE: you are a very nice lady that advised me when I most needed it! Thanks very much for that!

Today we will be calling each other "highly estimated" supervisor and candidate but allow me to say dear Cees and dear Jan. You both fully trusted me on my intuitions and capacities. I appreciate very much all the challenges that Cees put in my way and also all the corrections and sometimes difficult discussion that Jan put on the table (that happens when two "stubborn" persons meet). You both contributed enormously to my personal and professional growth. The InnoWator project was one instance more to learn. I am so glad that Paques and Nystar were part of this project. I enjoyed the discussions and meetings with all of you: Jacco, Henk, Martijn and Cris: dank jullie wel!!

I had wonderful times in Wageningen with the “Chileans”: Pame, Fran, Pablo, Roberto and Marce: muchas gracias!. Pia and Anita, thanks a lot for joining my running schedule. I also shared time in Wageningen with one of my best Chilean friends: Johana. What a time we had here eh?. Also my eternal Chilean friends: Ivan, Karlo, Mary, Pablo and Vivi, thank you very much for the chats! Rosario, who could predict that life will bring you to Spain. It is strange that during the exams in the high school I have you in the seat next to me, and now you will be in the aula supporting me.

In Wageningen I have met wonderful friends, Tania (my lost sister), Jarno (my personal advisor and pannenkoeken chef!) and Claudia (the best office –mate that you can get). Hey Clau, I cannot imagine a better companion in my office than you during these stressful and difficult months.

To the climbing people: you are very cool guys!!! Without knowing me too much you accepted me in the climbing weekends and afforded to understand my Dutch ☺. Some of you even taught me how to use the crampons for the first time and others gave me climbing tips. Thanks to all of you: David, Jantiene, Kirsten, Peter, Danny, Joost, Joris, Monique, Michiel (dancing M) and Roemert.

My paranymphs! These two wonderful friends, Tania and Simon, are from very different cultures but share similar professional excellence, good sense of humor and these two are such good human beings.

This time in the Netherlands changed everything that I felt comfortable with in Chile: language(s), food, tastes, music, people, culture etc. I couldn’t be successful in this personal aspect without the people that I am going to mention below:

Familie van den Bosch en Sinel. Dank u jullie allemaal voor de “gratis inburgering”. Lieve Ela, Bert en Hilke, dank jullie voor een plek in jullie familie en dat jullie je hart voor mij hebben geopend.

A mis padres: Papa, Maria y William. Gracias por permitirme volar tan lejos de ustedes para seguir mis instintos y encontrar mi vida. No ha sido facil pero estamos siempre conectados desde el corazon.

Life’s directions are difficult to understand or to predict but looking backwards, everything seems to happen in the right place. Now I think that was pretty clear, eh Pimba? Life put us together in the right time but also behind the right desks!!!. You became my friend, partner, climbing partner, runner partner, roller skating partner, English advisor ……etc. but also you have become my family. I do not need to write more words to express what you mean to me, you see it in my eyes every day.

Paula Andrea Gonzalez Contreras
Wageningen, June 2012

ABOUT THE AUTHOR

Paula Andrea Gonzalez Contreras was born on January 28, 1981 in San Felipe (Chile). In 2003 she obtained her Bachelor's degree in Bioprocess Engineering, at Pontificia Universidad Católica de Valparaíso, Chile. In 2007, she received her Master of Science degree in Biochemical Engineering, at the same university. For her thesis she worked at the Biochemical Engineering Department on anaerobic digestion and wetlands for the treatment of domestic wastewater at temperatures below 15°C. In 2006, she performed her internship at the Sub-department of Environmental Technology. Her work on the effects of high salinity on methanogenic sludge bed systems was published and supported the Ph.D. thesis of S. Ismail. During 2007, she worked as a researcher in the Ph.D. project of G. Kassab on simultaneous removal of carbon and nitrogen from domestic wastewater in UASB reactors. In the same year, she worked at Leaf (Lettinga associates foundation) on the urine harvesting project.

In May 2008 she started her Ph.D. research described in this thesis at the Sub-department of Environmental Technology of Wageningen University. She was awarded with a grant from Wageningen UR-CONICYT (Chile) agreement for her Ph.D. studies at Wageningen University. In March 2012, she won the "Wetsus-Rabobank Water Business Challenge".

From March, 2012 she is involved as post-doc researcher in identifying innovative metal extraction and recovery technologies within the Wageningen University–Wetsus framework.

Netherlands Research School for the
Socio-Economic and Natural Sciences of the Environment

C E R T I F I C A T E

The Netherlands Research School for the
Socio-Economic and Natural Sciences of the Environment
(SENSE), declares that

Paula Andrea Gonzalez Contreras

born on 28 January 1981 in San Felipe, Chile

has successfully fulfilled all requirements of the
Educational Programme of SENSE.

Wageningen, 22 June 2012

the Chairman of the SENSE board

Prof. dr. Rik Leemans

the SENSE Director of Education

Dr. Ad van Dommelen

The SENSE Research School has been accredited by the Royal Netherlands Academy of Arts and Sciences (KNAW)

KONINKLIJKE NEDERLANDSE
AKADEMIE VAN WETENSCHAPPEN

The SENSE Research School declares that **Ms. Gonzalez Contreras** has successfully fulfilled all requirements of the Educational PhD Programme of SENSE with a work load of 59 ECTS, including the following activities:

SENSE PhD courses

- Environmental Research in Context
- Research Context Activity: Organizing Conference on Novel Cost Effective Technologies for Waste Water Treatment and Bio-energy Production, 4-5 September 2008, Wageningen
- Speciation and Bioavailability
- Environmental Risk Assessment of Micropollutants

Other PhD courses

- Advance Course on Microbiology Physiology & Fermentation Technology
- 5th International Advanced Course on Bioreactor Design and Operation
- FIMIN Spring School "Iron in the Environment: From nature to the Laboratory
- Techniques for writing and presenting scientific papers

Didactic Skills Activities

- Supervision of laboratory practical's in the course Introduction Environmental Technology

Oral Presentations

- *Arsenic Immobilization by Biological Scorodite Crystallization.* Novel cost effective technologies for wastewater treatment and bio-energy production, September, 5, 2008, Wageningen, The Netherlands
- *Arsenic immobilization by bioscorodite crystallization: effect of foreign seeds.* 18th International Biohydrometallurgy Symposium , September 13-17, 2009, Bariloche, Argentina
- *Biotechnology-based processes for arsenic removal.* 9th International Conference on Clean Technologies for the Mining Industry, April 10-12, 2011, Santiago, Chile
- *Bioscorodite crystallization for Arsenic Removal.* European Metallurgical Conference, June 26-29, 2011, Dusseldorf, Germany
- *Arsenic Biomineral Formation Leads to Partial Encrustation of Thermoacidophilic Archaea.* Goldschmidt: Earth, Life and Fire, August 14-19, 2011, Prague, Czech Republic

SENSE Coordinator PhD Education and Research

Mr. Johan Feenstra

The research described in this thesis was financially supported by the Dutch Ministry of Economic Affairs/Agentschap NL through the INNOWator programme, Paques B.V (Balk, The Netherlands) and Nystar (Budel-Dorplein, The Netherlands).

Front cover thesis: Scanning electron microscopic picture of bioscorodite crystals produced in airlift reactors (modified from Fig.10.2, this thesis).
Back cover thesis (from left to right): scorodite mineral, CSTR systems and bioscorodite produced in CSTRs.

Printed by: Wöhrmann Print Service, Zutphen